Development of an innovative system for pollution abatement in the new natural gas vehicles

Acacio Miguel Nobre Mendes

Université Pierre et Marie Curie

Universidade de Lisboa

Ecole doctorale 391

Institut Jean Le Rond d'Alembert / Fluides Réactifs et Turbulence

Development of an innovative system for pollution abatement in the new natural gas vehicles

Par M. Acácio Miguel NOBRE MENDES

Thèse de doctorat de Génie des Procédés

Dirigée par M. Patrick DA COSTA et M. Carlos HENRIQUES

Présentée et soutenue publiquement le 30/11/2015

Devant un jury composé de :

M. Christophe DUJARDIN, Professeur, École Nationale Supérieure de Chimie de Lille, Université de Lille 1 – Sciences et Technologies, France (Rapporteur)

M. Patrick DA DOSTA, Professeur, Institut Jean le Rond d'Alembert, Université Pierre et Marie Curie, France (Directeur de Thèse)

M. Francisco LEMOS, Professor Catedrático, Instituto Superior Técnico, Universidade de Lisboa (Examinateur)

Mme. Isabel FONSECA, Professora Associada, Faculdade de Ciências e Tecnologia, Universidade Nova de Lisboa (Rapporteur)

M. Carlos HENRIQUES, Professor Associado, Instituto Superior Técnico, Universidade de Lisboa (Co-Directeur de Thèse)

Mme. Maria Elena GALVEZ-PARRUCA, Maître de Conférences, Institut Jean Le Rond d'Alembert, Université Pierre et Marie Curie, France (Examinatrice)

Université Pierre et Marie Curie
Universidade de Lisboa

Ecole doctorale 391

Institut Jean Le Rond d'Alembert / Fluides Réactifs et Turbulence

Development of an innovative system for pollution abatement in the new natural gas vehicles

Par M. Acácio Miguel NOBRE MENDES

Thèse de doctorat de Génie des Procédés

Dirigée par M. Patrick DA COSTA et M. Carlos HENRIQUES

Présentée et soutenue publiquement le 30/11/2015

Devant un jury composé de :

M. Christophe DUJARDIN, Professeur, École Nationale Supérieure de Chimie de Lille, Université de Lille 1 – Sciences et Technologies, France (Rapporteur)

M. Patrick DA DOSTA, Professeur, Institut Jean le Rond d'Alembert, Université Pierre et Marie Curie, France (Directeur de Thèse)

M. Francisco LEMOS, Professor Catedrático, Instituto Superior Técnico, Universidade de Lisboa (Examinateur)

Mme. Isabel FONSECA, Professora Associada, Faculdade de Ciências e Tecnologia, Universidade Nova de Lisboa (Rapporteur)

M. Carlos HENRIQUES, Professor Associado, Instituto Superior Técnico, Universidade de Lisboa (Co-Directeur de Thèse)

Mme. Maria Elena GALVEZ-PARRUCA, Maître de Conférences, Institut Jean Le Rond d'Alembert, Université Pierre et Marie Curie, France (Examinatrice)

Acknowledgements

Institutional acknowledgements are due to *Fundação para a Ciência e a Tecnologia* (FCT) for the financial support of my PhD thesis program between Portugal and France (grant number SFRH/BD/78639/2011), to *Conselho de Reitores das Universidades Portuguesas* and to *Campus France* for financing the mobility program *Ações Luso-Francesas/PAUILF 2013-2014* and to FCT and *Campus France* for financing the mobility program *PHC PESSOA 2014*.

Moreover, I would like to acknowledge the French company ENGIE (former GDF SUEZ), for financing the research collaboration project between IST/UPMC/ENGIE, in which framework this thesis was inserted. In particular, I thank to Dr. Sandra Capela and Eng. Miriam Eklo for their input as representatives of ENGIE in this project and for bringing an industrial point-of-view to this thesis. I am also grateful to Renault Trucks (Volvo group trucks technology), in particular to Eng. Vincent Lauga, for the interested shown in the work developed in this project and for the useful information provided, concerning the exhaust gases emissions of real heavy-duty engines.

I am thankful to Prof. Carlos Henriques, for convincing me to embrace this project in the first place, for all the opportunities he provided me in these years that made me grow further as a researcher, for all the advices, guidance and support.

I am grateful to Prof. Patrick Da Costa, for all the opportunities he provided me, for always pushing me further, for always believing in my qualities and for reminding me of them, for all the advices, guidance, support and friendship.

I am also thankful to Prof. Filipa Ribeiro, for her guidance and support, in particular, during the first years of my thesis.

A special thanks to Dr. Rui Bartolomeu, for all the support in the earlier stages of my thesis, for all the lessons that were crucial to my path during this thesis and for all the interesting discussions.

I want to thank to all other professors, researchers, engineers and technicians from both laboratories where I conducted my research activities and with who I had the privilege to work with, namely, Dr. Auguste Fernandes (IST), Prof. João Miguel Silva (IST), Prof. Carla Pinheiro (IST), Prof. José Madeira Lopes (IST) and Prof. Rosário Ribeiro (IST), Prof. Elena Galvez (UPMC), Allain Toullec (UPMC), Jérôme Bonnety (UPMC), Dominique Busquet (UPMC) and Jêrome Péquin (UPMC).

From LCS-ENSICAEN, I would like to express my gratitude to Professor Frédéric Thibault-Starzyk and to Dr. Vladimir L. Zholobenko, for giving me the opportunity to be a visiting student at LCS, for their willing to collaborate and for their precious insights on the characterisation of zeolites. I also thank to Eng. Valérie Ruaux for all the help during my staying in Caen.

To my colleagues in Lisbon - Suse, João, Inês, Luís, Ilona, Ana, Filipa, Liliana, Marta, Alexandre, Daniela, Telma, Márcia, André, Ana Elisa, Susana, Isabel, Tânia, Joana, Clara, Carina, Willem,

Ana Sofia, Beatriz, Cátia – I thank you for all the memories. To Raquel, thank you for all the moments we shared and for your friendship. To Pedro, thank you for the passionate discussions about catalysis, chemistry, politics and life, but mostly for your friendship. To Carminha, thank you for all the moments, for all the joy you brought into the lab every day, for all the help and support in the final stages of my thesis but, mostly, for being my confidant.

To my colleagues in Paris – Yiquan ”George”, Sandrine, Johnny, Radek, Monika, Annia, Jean-François, Diane, Evelyne, Guillaume, Hugo, Jean-Marie, Paulo, Magda – thank you for all the memories. To Cansu, thank you for all the “soirées chez Les Sciences” and for the moments we shared. To Elza, thank you for all the laughs and joy but, mostly, for your friendship. To Alexis, thank you for all the help and support in my research activities and for all the goods moments, the pizzas, the pints and tennis matches.

To Prof. Henrique Matos and Prof. Ana Carvalho, who walked me through my first steps in the research world and who never lost track of my activities, I thank you for your friendship.

Finally, to Joaquim, Alzira, Artur, Alzira Maria and Jacinto, for your eternal love and unconditional support. I dedicate this thesis to you.

Abstract

The selective catalytic reduction of nitrogen oxides, in lean-conditions, using methane as reductant (NO_x CH_4-SCR) over PdCe/zeolite-based catalysts was considered in this work.

Preparation method for Pd introduction, Pd/Ce loadings and metal introduction order were optimised for a formulation considering MOR zeolite as the catalytic support. The effect of different test conditions, namely [CH_4]/[NO] ratio and water presence in the reaction mixture was assessed.

The effect of the zeolite support in the stabilisation of Pd/Ce species was also evaluated by preparing a similar PdCe-BEA catalyst to the optimised PdCe-MOR catalyst, considering the same metal loadings and preparation methods. Both catalysts exhibited different metal species and different catalytic performances. Structure-reactivity relationships were drawn from the comparison of several characterisation techniques and catalytic test results for both catalysts. A synergic effect resulting from the use of both catalysts in a single bed application (mixed-bed and dual-bed configuration) is reported.

An innovative thermal treatment applied to PdCe-MOR catalyst during its preparation is reported. Under certain conditions, this treatment results in the enhancement of the catalytic performance, namely, in higher NO_x conversion into N_2 and CH_4 selectivity towards NO_x SCR.

Structured catalysts were prepared by washcoating of PdCe-MOR onto cordierite monoliths with different geometry (cpsi). Preparation parameters were evaluated through characterisation techniques and the catalytic performance was assessed in a synthetic gas bench plant.

Keywords: NO_x HC-SCR, methane, zeolites, palladium, cerium.

Résumé

Ce travail traite de la réduction catalytique sélective des oxydes d'azote en utilisant du méthane comme agent réducteur sur catalyseurs bimétalliques Pd/Ce/zéolithes.

Dans un premier temps, la méthode d'introduction du palladium, la teneur en palladium et cérium ainsi que l'ordre d'introduction des métaux ont été optimisés pour une formulation considérant une zéolithe MOR comme support catalytique. Puis, l'effet des différentes conditions opératoires ont été évalués.

L'effet du support catalytique a été également étudié en comparant un catalyseur PdCe-BEA au catalyseur PdCe-MOR résultant de l'optimisation effectuée. Il a été montré que les deux catalyseurs possèdent différentes espèces métalliques conduisant ainsi à différentes performances catalytiques. Des Relations structure/réactivité ont été établies par différentes techniques de caractérisation et des résultats des tests catalytiques. Il a été mis en évidence un effet synergique résultant de la combinaison de ces deux catalyseurs dans le même pot catalytique (configurations lit mélangé et lit double).

Un traitement thermique innovant appliqué au catalyseur PdCe-MOR, pendant sa préparation a été développé et optimisé. Dans certaines conditions, ce traitement conduit à l'amélioration de la performance catalytique, notamment, à une conversion de NO_x à N_2 et à une sélectivité de CH_4 pour la réaction NO_x RCS plus élevée.

Enfin, des catalyseurs structurés ont été préparés par "washcoating" de PdCe-MOR sur des monolithes de cordiérite possédant des géométries différentes. Les paramètres de préparation ont été ainsi évalués par des techniques de caractérisations et par des tests en banc de gaz.

Mots-clés: NO_x HC-RCS, méthane, zéolithes, palladium, cérium.

Index

Introduction

Over the last decades, developed countries have made an effort to mitigate the impact of air pollution from man-made activities. Nitrogen oxides (NO_x) are one of the chemical compounds associated to this type of pollution and road transportation sector is known to be one of the major contributors for total NO_x emissions. In particular for this sector, several directives have been published over the years, namely by EU, imposing increasingly restrictions on NO_x emissions. The most recent directive, known as EURO 6 standard, became effective on 1st September 2014 for the approval of vehicles, and from 1st January 2015 for the registration and sale of new types of cars. For positive-ignition engines (typically for gasoline-powered vehicles), a very effective after-treatment technology known as 3-way catalyst is capable to eliminate pollutants contained in the exhaust gases, namely NO_x. However, when considering compression-ignition engines (typically for diesel-powered vehicles), this technology is not able to remove NO_x, forcing the automobile constructors to find out other solutions to address this issue. However, alternative solutions still face some problems in fulfilling the NO_x emissions levels and the most recent scandal, already known as *Dieselgate* (in which Volkswagen installed a defeat device in some diesel vehicles capable to identity when the vehicles are being submitted to inspection tests, in order to activate measures to eliminate NO_x only during such tests, but not during on-road driving) brought this subject to the order of the day.

Moreover, it is expectable that natural gas vehicles (NGV) will increase in the next years, reason why the continuous study of after-treatment systems capable of mitigate the pollution of these vehicles, namely NO_x emissions, is pertinent and necessary. A promising technology to address this issue, in particular for heavy-duty vehicles where the combustion takes place in excess of oxygen (compression-ignition engines), consists in selective catalytic reduction of NO_x using as reductant the unburned hydrocarbons (HC) also present in the exhaust gases (NO_x HC-SCR). This technology allows to reduce NO_x into N_2, leading to simultaneously removal of NO_x and HC. For NGV, the most abundant hydrocarbon contained in the exhaust gases is CH_4. However, in order to successfully employ such after-treatment system into NGV, further technological improvements are still required in terms of the development of potential catalysts to be considered for this application, namely, concerning their activity and stability.

The main objective of this work is the further study Pd/zeolite-based catalysts suitable for NO_x CH_4-SCR in the presence of oxygen excess, which are known to be active materials for this reaction. Cerium has been reported as an adequate promotor capable of enhancing the catalytic performance of this system and, hence, it has been considered in this study as the promoter to be included in the catalyst. The methodology adopted for this work is developed in five chapters and consisted in the development of a catalytic system from the active site until its final application at pilot-scale.

Chapter I consists in bibliographical study, where the problematic of NO_x emissions is discussed, as well as an overview on the currently available technologies for exhaust gases after-treatment

systems. Moreover, an extensive literature review on the materials used for NO_x CH_4-SCR reaction is presented, particularly focused on the use of zeolite-based catalysts, namely, the ones containing palladium as active phase.

Chapter II is focused in the study of the PdCe-MOR catalyst. The optimisation of the catalyst preparation is presented, supported on several characterisation techniques employed to understand the role of the different Pd and Ce species on the NO_x SCR reaction (structure-reactivity study). The performance of the optimised catalysts tested in representative conditions of exhaust gases from a real heavy-duty engine, working in lean-gas conditions, is evaluated.

In Chapter III, the effect of the zeolite structure on the stabilisation of different metal species is assessed by comparing PdCe-MOR and PdCe-BEA catalysts. A dual-bed configuration approach based on the use of two different catalysts is explored, in order to achieve an enhancement of the catalytic performance of the after-treatment system.

Chapter IV concerns the further optimisation of PdCe-MOR catalyst by applying a thermal treatment to the catalyst, in the presence of water (steaming), as an additional operation unit to be performed during the preparation of the catalysts. The influence of several parameters involved in this treatment, namely temperature, amount of water in the gas feed and positioning of the steaming treatment in the catalysts preparation, are study and optimised.

Finally, Chapter V presents the development of a pilot-scale application of the powder formulations previously studied and optimised. Structured catalysts considering honeycomb monoliths were prepared through a washcoating technique. Several parameters involved in the preparation of such structured catalysts, namely, properties of the zeolite slurry used in the washcoating and the geometry (cells/in^2) of the monolith substrates used, are studied. Catalytic test results of the structured catalysts performed in a synthetic gas bench plant, simulating representative conditions of exhaust gases from a real heavy-duty engine, are presented and discussed.

This work was developed with the framework of a research collaboration project between Instituto Superior Técnico, Université Pierre et Marie Curie and ENGIE (former GDF SUEZ, French company) for the development of innovative depollution system suitable for the NGV engines. VOLVO group trucks technology (Renault TRUCKS) also collaborated as industrial partner.

Chapter I. Bibliographical Study

I.1. Introduction and Motivation

I.1.1. NO_x emissions – The issues and the numbers

The term NO_x is attributed to the group of nitrogen oxides gases. Commonly, NO_x is used to designate NO (nitrogen monoxide) and NO_2 (dinitrogen monoxide) but, in fact, other gases are also included in this group, such as nitrous acid and nitric acid.

Nitrogen oxides are toxic for human health and can be associated to respiratory diseases, such as asthma, emphysema and bronchitis [1]. However, one can say that the major concern of NO_x emissions is the direct impact on the environment through the possibility of generation of acid rains and all the indirect environmental and health issues related to this phenomenon, such as acidification, eutrophication, *etc*.

Nitrogen is an inert gas and does not react with the oxygen from the air at ambient temperature. However, when exposed to high temperatures this mixture tends to react, leading to the formation of NO, which can be oxidised to NO_2 due to the presence of oxygen. In the presence of water, NO_2 reacts and gives nitrous acid and nitric acid (equation (I-1)). The nitrous acid can also be decomposed to nitric acid (equation (I-2)).

$$2\,NO_2 + H_2O \rightarrow HNO_3 + HNO_2 \qquad \text{(I-1)}$$

$$3\,HNO_2 \rightarrow HNO_3 + 2\,NO + H_2O \qquad \text{(I-2)}$$

Nitrogen oxides also play a major role in the formation of tropospheric ozone [2], which is also toxic for human health.

NO_x emissions are related to the activity of several sectors. According to *Eurostat*, the total emission of these pollutants in the EU-27, in 2010, was higher than 9 millions of tonnes (Figure I-1). The road transportation sector appears as the sector with most impact on NO_x emission, being responsible for almost 42% of the total emissions.

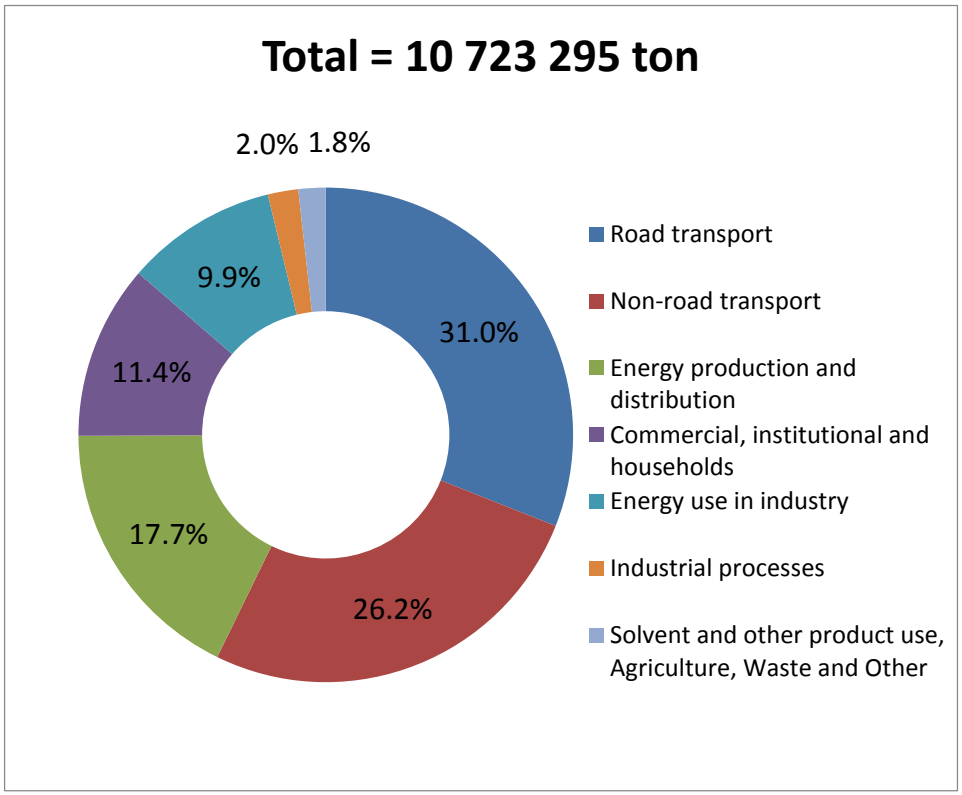

Figure I-1 – Emissions of NO_x by source sector in EU-28 (year 2012).

(Source: *Eurostat, update of 19/09/2014, accessed in 29/09/2014*)

It is worthwhile to notice that efforts have been made to reduce the nitrogen oxides emissions, namely in European Union. In 2001, the Directive 2001/81/EC (National Emission Ceilings - NEC) established upper limits to the NO_x emissions, among others, which state members should put in practice by 2010.

In 2014, the European Environment Agency published the *NEC Directive Status Report 2013*, containing the results regarding the emissions for 2013. Figure I-2 exhibits the deviations in NO_x emissions for each state member, regarding the values initially established in 2001.

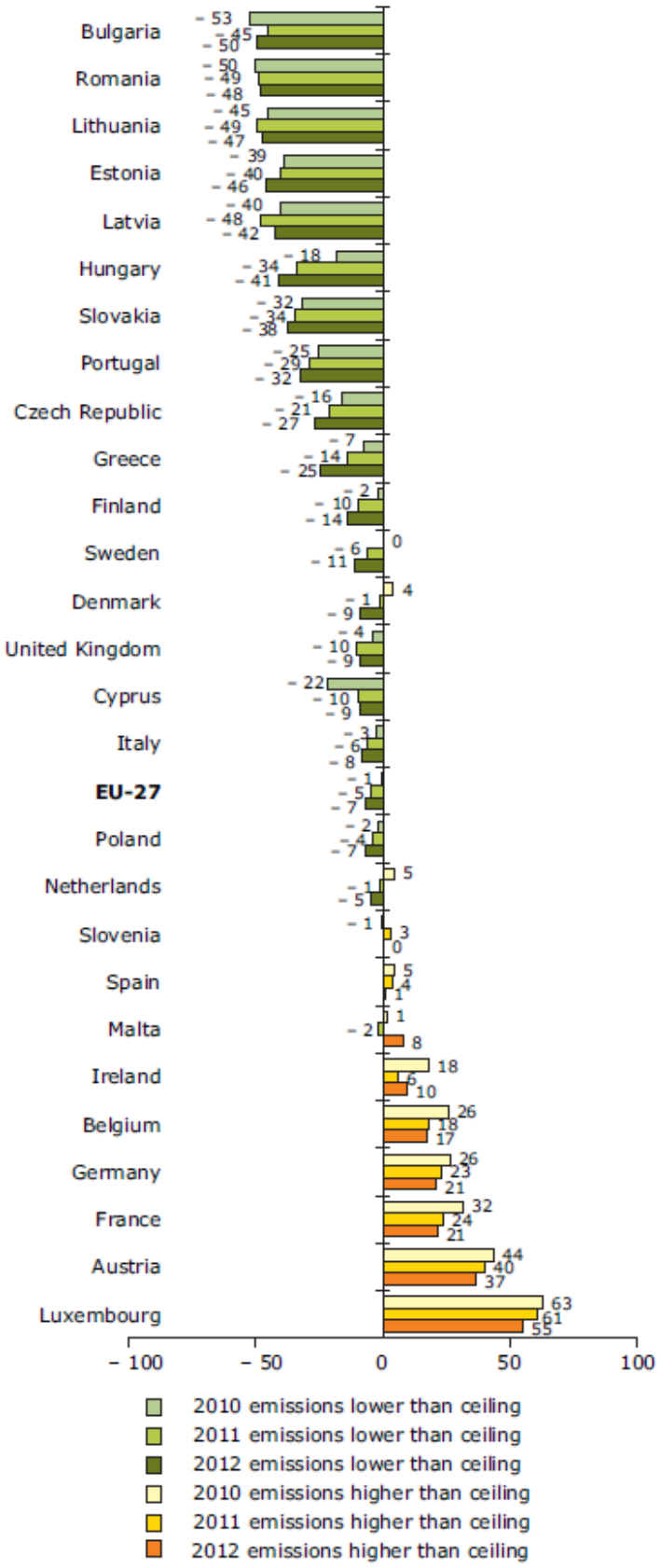

Figure I-2 – Distance (%) from the ceilings established in Directive 2001/81/EC for NO_x emissions in 2010, 2011 and 2012, for each state member (EU-28) [3].

The EU-28 has managed to reduce the NO_x emissions from 19,013,835 ton, in 1990, to 10,723,295 ton, in 2012 (Eurostat, update of 19/09/2014, accessed in 29/09/2014), which represents a reduction of about 44%.

I.1.2. European Union legislation on NO_x emissions

The first European Directive limiting the pollutants emitted by motor vehicles, namely for passenger cars, was published in 1991 (Directive 91/441/EEC, from 26 June 1991, that changes the directive 70/220/EEC), became effective on 1992 and known as Euro I standards. Since then, several directives have been published imposing harder restrictions on the allowed emission values. Current legislation on this matter is given by Euro VI (Directives EC 715/2007 from 20 June 2007, 692/2008 from 18 July 2008 and 595/2009 from 18 June 2009), which become effective on 2014. Euro I to VI define specific emissions for each type of vehicle, the conditions under which the tests should be performed, *etc*. Table I-1 summarises the values of HC and NO_x emissions for heavy duty and light passengers vehicles according to the different European Standards (from Euro I to Euro VI).

Table I-1 – HC and NO_x emissions for heavy duty and light passengers vehicles, from Euro I to Euro VI standards.

	Heavy duty		Light Passengers (Compression Ignition)		Light Passengers (Positive Ignition)		
	HC (g/kWh)	NO_x (g/kWh)	HC+NO_x (g/km)	NO_x (g/km)	HC (g/km)	HC+NO_x (g/km)	NO_x (g/km)
Euro I (1992)	1.1	8	0.97	-	-	0.97	-
Euro II (1996)	1.1	7	0.7	-	-	0.5	-
Euro III (2000)	0.66	5	0.56	0.5	0.2	-	0.15
Euro IV (2005)	0.46	3.5	0.3	0.25	0.1	-	0.08
Euro V (2009)	0.46	2	0.23	0.18	0.1	-	0.06
Euro VI (2014)	0.13	0.4	0.17	0.08	0.1	-	0.06

(Source: Adapted from DieselNet [4].)

I.2. The use of Natural Gas as an alternative mobile fuel

In the last decades, the use of natural gas as an alternative mobile fuel started to be seen as a feasible solution from technical, economic and environmental point of view. According to the International Association for Natural Gas Vehicles [5], the total number of natural gas vehicles (NGV) in the World increased from 415,855 in 1991 to 15,192,844 in 2011. It is estimated that this value corresponds to about 1.2% of the total worldwide fleet. The number of natural gas fuelling stations also increased from 11,107 in 2007 to 19,947 in 2011.

Natural gas is mainly composed by methane (about 90%) and it is available as a gas at ambient pressure and temperature. In order to be used as a transportation fuel, it is necessary to compress (CNG) or liquefy it (LNG). CNG is commonly more used than LNG for transport applications. However, the use of LNG is increasing [6]. Table I-2 summarises the advantages and disadvantages of both CNG and LNG as a fuel.

Table I-2 – Advantages and disadvantages of CNG and LNG use as a fuel.

	Advantages	Disadvantages
CNG	- Unlimited hold times with no fuel loss; - More mature technology; - Gas/vapour instead of cryogenic; - Simple fuel tanks and pressure management; - System design can be customised for application.	- Cost of compression – energy and maintenance with a compression station; - Size of storage tanks; - Possible weight disadvantage.
LNG	- Fewer tanks/ less space requirements; - Greater fuel density; - Lower weight storage.	- The complexity of tanks; - Pressure and temperature management of fuel to engine is more complex; - High maintenance cost of cryogenic parts; - The fuel is used or it is lost; - Reliability is challenging; - The life cycle fuel cost over CNG may be higher.

(Source: Agility Fuel Systems [7].)

There are several studies which highlight that the use of natural gas generates less pollutant emissions, compared to liquid fuels [8, 9]. For instance, it was shown that for similar models of diesel vehicles, NGV could result in reductions of 60-96% of PM emissions, 17-80% of NO_x emissions, 4-96% of NMHC emissions and 75-95% of CO emissions [8].

Despite the price of natural gas follows a similar trend the crude oil, statistical data shows that the price of natural gas is considerably lower when compared to oil-based fuels [8]. In 2007, the Energy Management Institute of USA concluded that natural gas was historically 48.6% less

expensive than gasoline/diesel between 2004 and 2007. In spite of this margin has decreased in the last years, values of April 2010 show that natural gas was 30% less expensive than diesel [8].

I.3. Exhaust gases after-treatment systems - NO_x removal techniques

There are several available technologies aiming to control/reduce the pollutant emissions from exhaust gases, which are can be identify as carbon monoxide (CO), unburned hydrocarbons (HC), nitrogen oxides (NO_x) and particulate matter (PM). Oxidation catalysts (also known as 2-way catalyst) can convert CO and HC to CO_2 and water. This system is suitable for lean conditions. Particulate filters are used to remove PM from exhaust gases though a physical filtration and are often used in diesel vehicles.

The NO_x removal possibilities can be summarised in 3 main technologies:

a. Non-selective catalytic reduction;
b. NO_x adsorption;
c. Selective catalytic reduction.

I.3.1. Non-selective catalytic reduction (3-way catalyst)

This technology consists in the simultaneously conversion of CO to CO_2, HC to CO_2 and water and NO_x to N_2 and O_2. Typically, the catalysts used in this technology are named as 3-way catalysts. These catalysts are commonly used in gasoline vehicles which work under stoichiometric conditions (*i.e.* air-fuel ratio around 1). In fact, this technology is very effective for air-fuel ratio slightly lower than 1 but for values significantly lower or higher than this, the conversion of CO, HC and NO_x is far from the desired (Figure I-3).

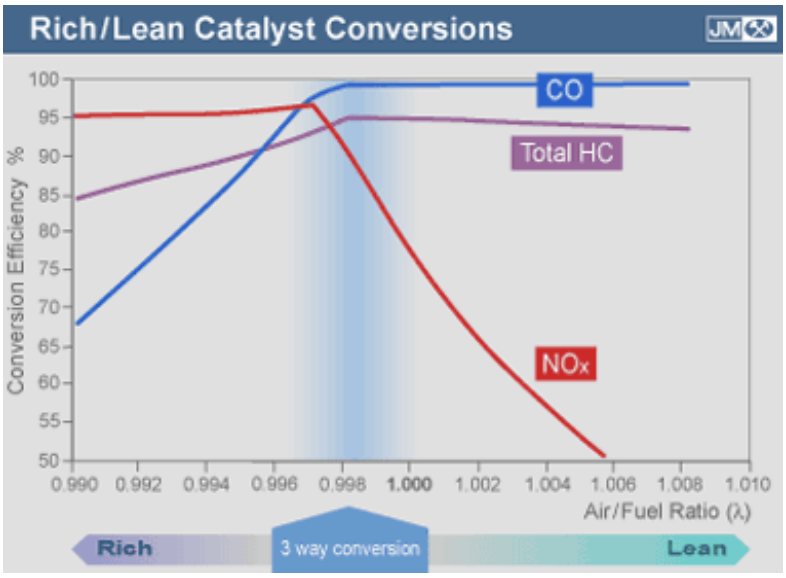

Figure I-3 – Conversion efficiency of CO, HC and NO_x of a 3-way catalyst depending on the air-fuel ratio [10].

I.3.2. NO_x adsorption

NO_x adsorption is a process that considers two steps for the removing of NO_x from the gas stream. Firstly, the chemical adsorption of NO_x takes place onto the appropriate active sites of the catalyst and it occurs during the regular operating conditions which are lean conditions (Figure I-4A). The NO_x remains stored in the sites but eventually, the storage capacity of the catalyst will be depleted due to saturation. The second step consists in changing the operating conditions during a small fraction of time to rich conditions. This changing results in the release of NO_x from the sites (regeneration) and reduction of NO_x to N_2 in a similar reaction that takes place in the 3-way catalysts (Figure I-4B).

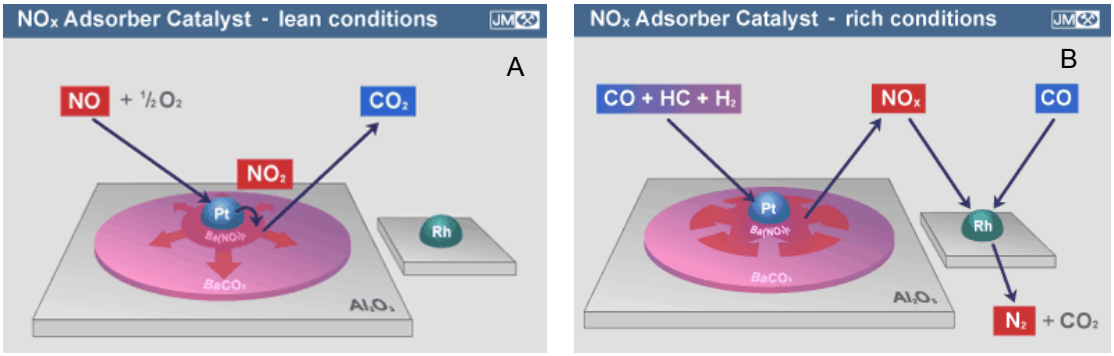

Figure I-4 – Schematic representation of NO_x adsorption technology: A – Adsorption of NO_x in lean conditions; B – Elimination of NO_x in rich conditions [10].

I.3.3. Selective catalytic reduction

The selective catalytic reduction (SCR) of NO_x is accomplished by using a reductant that enables this reaction. This technology can be grouped according to the type of reductant considered:

a) Selective catalytic reduction with ammonia;
b) Selective catalytic reduction with hydrocarbons.

I.3.3.1. NO_x selective catalytic reduction with ammonia (NH_3-SCR)

Lately, technical developments have been made in order to implement the use of ammonia as reducing agent in SCR systems, with particular focus on heavy-duty vehicles. The reaction follows three main pathways:

$$4\,NH_3 + 4\,NO + O_2 \rightarrow 4\,N_2 + 6\,H_2O \quad \text{(I-3)}$$

$$2\,NH_3 + NO + NO_2 \rightarrow 2\,N_2 + 3\,H_2O \quad \text{(I-4)}$$

$$8\,NH_3 + 6\,NO_2 \rightarrow 7\,N_2 + 12\,H_2O \qquad \text{(I-5)}$$

The use of ammonia in exhaust gases after-treatment systems is accomplished through the use of urea solution (32.5%) in water, also known as Diesel Exhaust Fluid (DEF) or Adblue®, which is stored in an additional tank in the vehicle (Figure I-5). This solution is then sprayed into the after-treatment system, where occurs the hydrolysation of urea into ammonia. The use of this solution should be 5-7% of the fuel consumption for a EURO V engine, which represents autonomy of 10,000 km per tank, for a truck [11]. Currently, this system (Figure I-5) is now being implemented in heavy-duty vehicles and it is available for commercialisation world-widely.

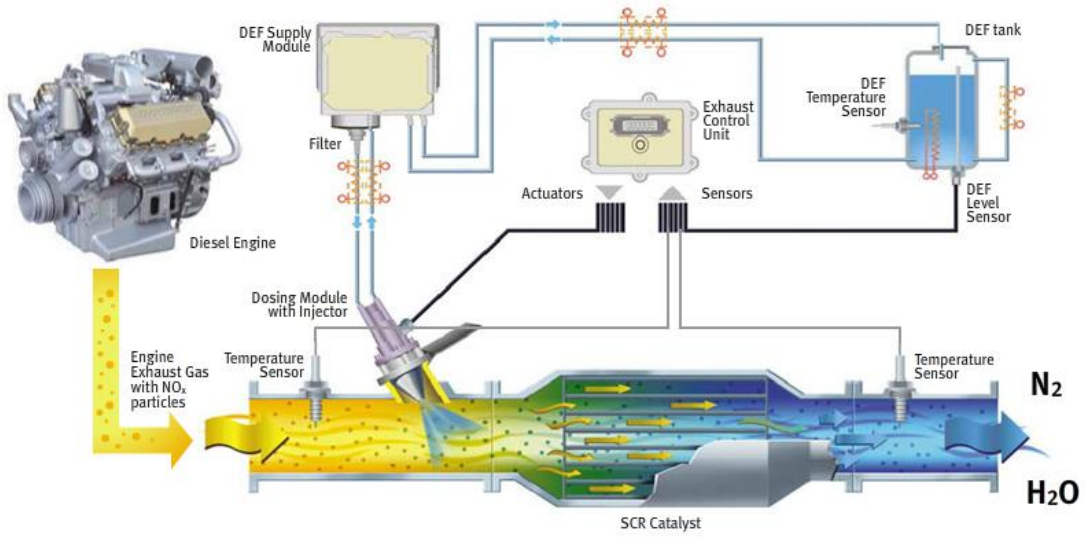

Figure I-5 – Schematic representation of a complete NH_3-SCR system [12].

I.3.3.2. NO_x selective catalytic reduction with hydrocarbons (HC-SCR)

Other promising technology regarding the selective catalytic reduction of NO_x is the hydrocarbon-SCR, where the unburned HC contained in the exhaust gases is the reducing agent. Hydrocarbons can also be added directly to the exhaust gas in order to perform the reduction of NO. Some advantages and disadvantages are associated to HC-SCR when compared to ammonia-SCR. An effective HC-SCR system would not require additional investment for tanks, pipes and control systems that are necessary for the ammonia-SCR. However, the currently available HC-SCR technology cannot offer the same performance of ammonia-SCR systems and further technological development is still required in order to the application of these type of catalysts become feasible.

Several attempts to understand the mechanism of the reaction of SCR of NO_x using hydrocarbons (HC) as reductant have been made in the last decades. However, this reaction is considerably complex and may involve the formation of many different intermediates. The study of this topic is

far from being trivial, but important developments have been accomplished so far in order to help to understand the possible mechanisms for this reaction.

Based on a literature review, Gorce *et al.* [13] have gathered several proposed mechanism, which are reproduced in Figure I-6.

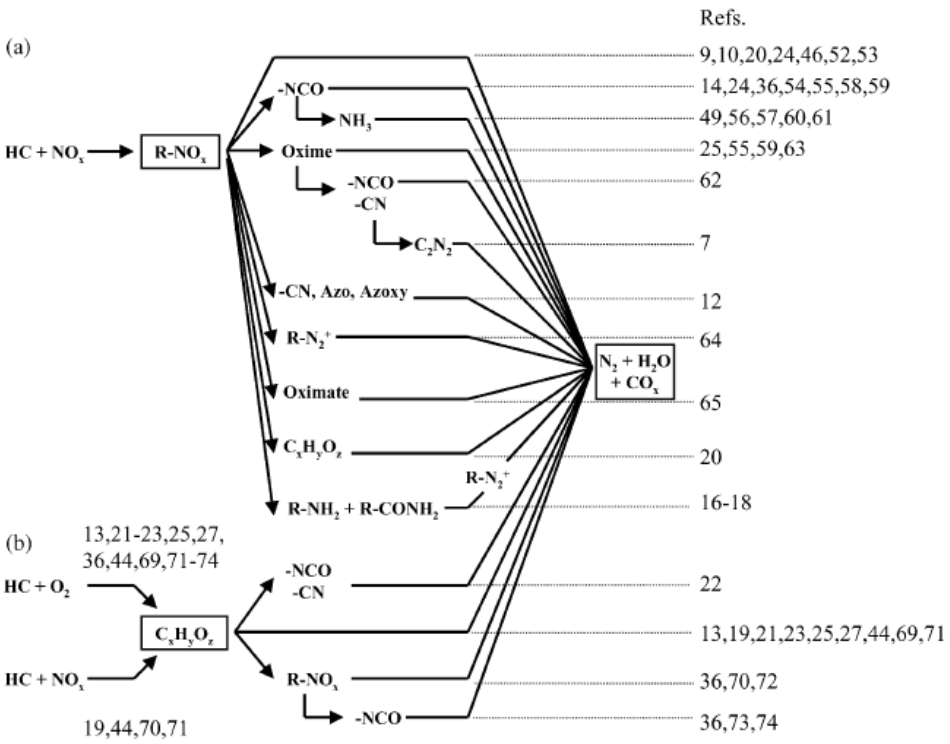

Figure I-6 – Reaction pathways involving organic species proposed in lean deNO$_x$ catalysis.

Many factors influence the mechanism involved in the reaction, namely the HC and the operating conditions considered. It is not necessary that there is a single pathway for each system. Djega-Mariadassou [14] proposed a mechanism based on three functions (steps) which would be required in order to accomplished the SCR of NO$_x$ with HC (Figure I-7).

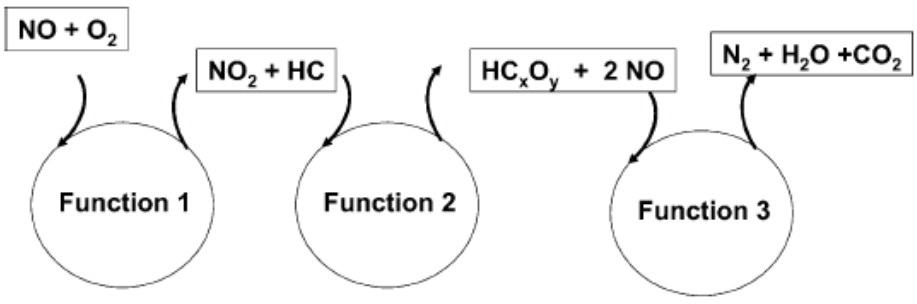

Figure I-7 – Simplified mechanism of SCR of NO$_x$ involving 3 functions.

Function 1 consists in the oxidation of NO to NO$_2$. As it is referred moreover, this is considered by many authors as a fundamental step for the SCR of NO$_x$ using methane as reductant. NO$_2$

would be more active to react with the reductant in order to form HC_xO_y intermediate compounds (Function 2). These compounds would be the effective reductant species, which would be responsible for regenerating (throughout oxidation) the active sites where the direct NO decomposition to N_2 take place (Function 3).

I.4. NO_x CH_4-SCR in lean conditions – Literature review

In this section, a literature review is performed concerning the state-of-art of catalytic systems for NO_x selective catalytic reduction using methane as reductant. Annex A describes the methodology used in the review herein presented

I.4.1. Monometallic catalysts

Traa *et al.* [15] presented, in 1999, a comprehensive review of the use of zeolite-based catalysts for the selective reduction of nitrogen oxides by hydrocarbons. In what concerns the use of methane as reductant, the authors identify important works and developments on the use of Co, Pd, In and Ga to generate active sites required for this reaction. The authors also referred that even in that time there was a trend towards the use non-zeolite structures, mainly due to deactivation problems of zeolite-based catalysts in the presence of water

In 2001, Fokema and Ying [16] have reviewed the use of metal oxide catalyst for the SCR of NO_x with CH_4, with particular emphasis on basic metals oxides (Group IIA, IIB and lanthanides) and supported gallium oxide catalysts. They concluded that Ga_2O_3-based catalysts are very selective but they suffer from deactivation in the presence of water. On the other, basic metals oxides present moderate activities but show tolerance to water and SO_2 presence.

In 2002, Burch *et al.* [17] critically reviewed the state-of-art regarding non-zeolite oxides and platinum group metal catalyst for SCR of NO_x with hydrocarbons. Though this work did not focus specifically in the use of CH_4 as reductant, important conclusions were highlighted by the authors regarding the difficulty of translating the laboratorial successful results to real exhaust systems.

One can say that monometallic catalyst (zeolite or non-zeolite) will definitely not be the catalyst to be employed for commercial purposes to accomplish effective NO_x CH_4-SCR. Nevertheless, the knowledge accumulated by scientific community over the past three decades regarding these materials is absolutely relevant to understand important factors such as nature of active sites, mechanism of reaction, preparations methods, *etc*.

I.4.1.1. Monometallic zeolite-based catalyst (other than Pd)

Back in the 90's, Li and Armor [18] discovered a family of catalyst that could effectively reduce NO_x with methane in the presence of excess oxygen. This catalysts consisted in zeolite structures (such as ZSM-5, mordenite and ferrierite) containing supported metals in the structure. In that time, several studies were published presenting the catalytic activity of several different combinations of metals and zeolite structures (monometallic).

From the several different works that can be found in the literature, one can say that ZSM-5 and MOR were the zeolite structures most considered and study for the SCR of NO_x with methane in lean conditions. A very extensive set of metals for this application was considered and reported in the literature, but it is possible to affirm that the monometallic zeolite-based catalysts presenting the best catalytic performance are the ones containing cobalt (usually around 2 - 5 wt.%), palladium (usually around 0.1 - 0.7 wt.%) and indium (usually around 4-8 wt.%). The preparation methods considered to prepare Pd or Co-based catalyst are typically ion exchange (liquid phase) and incipient wetness impregnation. A considerable number of works refer solid-state ion exchange as the best method to prepare indium-based zeolite systems. Nevertheless, the methods reported in the distinct works present several differences regarding technical parameters such as volume of solution / zeolite ratio, temperature of preparation, temperature of calcination, *etc*. Table I-3 summarises an extensive compilation of monometallic zeolite catalysts described in the literature.

Table I-3 – Summary of monometallic zeolite catalyst used for NO_x CH_4-SCR in lean conditions.

Ref.	Structure	Metal	Description	Main conclusions / Observations
[18]	MFI	Co	Influence of operating conditions on Co-ZSM-5 system.	Presence of O_2 enhances significantly the catalyst activity. The catalytic activity increases with the increase of CH_4 concentration.
[19]	MFI	Co	Effect of water vapour on SCR of NO with CH_4 on Co-ZSM-5 system.	Deactivation due to water is more significant at lower temperatures. The effect of water is proportional to a certain percentage of water, after which it becomes independent.
[20]	MFI	Co	Mechanism study of SCR of NO with CH_4 in Co-ZSM-5 system.	The rate-determining step in SCR reaction involves detachment of hydrogen from CH_4 by adsorbed nitrogen dioxide, forming a methyl species which will react with NO or O_2.
[21]	MFI	Co	Preparation methods of Co-MFI catalyst.	Sublimation of $CoBr_2$ onto HMFI generates an equally active catalyst (compared to other methods) but more stable, namely in the presence of water.

Ref.	Structure	Metal	Description	Main conclusions / Observations
[22]	MFI	Co	Role of Co species in the reaction.	The activity for SCR of NO with CH_4 is dependent of Co sites located in the zeolite cavities. The absence of acidic sites results in NO oxidation and CH_4 combustion but SCR of NO do not take place. Protonic sites should be involved in the formation of active intermediate or HC-adsorption.
[23]	MFI	Co	Study of actives sites of Co-H-MFI catalyst through FT-IR *in situ* and *operando*.	Co^{3+} species are located inside the channels, whereas Co^{2+} species are present in both external and internal surfaces. The former are largely present in active catalysts. Isocyanate and nitrate species appear to be the intermediates for the reaction.
[24]	MFI	Co	Characterisation of Co-MFI system. Adsorption of NO species.	Adsorbed NO species are not direct intermediates in the reaction that can activate CH_4, due to their low stability. The necessary species are formed when adsorption of NO_2 or $NO+O_2$ occurs in the Co sites. NO_2 is not essential to the formation of $-NO_y$ adsorbed species.
[25]	MFI	Co	Effect of extra-framework Al in monolith Co-ZSM-5 system.	When preparing monoliths, the presence of Al^{3+} and Co^{2+} in aqueous suspension originates new mixed oxides which are inactive for SCR of NO by methane.
[26]	MFI	Co	Co-ZSM-5 system is presented. Effect of CH_4/NO ratio is analysed, as well as Co loading. Mn, Cu, Ni, Cr, Ag, Rh are considered as doping metals.	Patent.
[27]	MFI	In	Effect of Si/Al ratio in In-H-ZSM5 system.	Introduction of In in zeolite decrease the concentration of Brønsted sites and produce new and stronger Lewis sites. Samples with the highest Lewis to Brønsted sites ratio was the one with highest activity for SCR of NO with CH_4.

Ref.	Structure	Metal	Description	Main conclusions / Observations
[28]	MFI	In	Characterisation of In sites. Effect of water presence.	Irreversible deactivation in presence of water causes conversion of $(InO)^+$ species into indium oxide species.
[29]	MFI	In	Effect of preparation method in catalytic activity. Characterisation of In species.	Intrazeolite indium oxo species are active sites. InO_x species enhance CH_4 combustion. Acidic sites are required for SCR of NO but not for direct CH_4 combustion. Physical mixtures of In_2O_3 with H-ZSM-5 allow to obtain similar activities to catalysts prepared by aqueous techniques.
[30]	MFI	In	In-H-ZSM-5 synthesis method by heating a mechanical mixture of In_2O_3 and ZSM-5 in the absence of O_2.	In introduced in the lattice of ZSM-5 can be oxidised to $(InO)^+$. Reversible change in the oxidation state of In sites (from $(InO)^+$ to In^+ and *vice-versa*) makes this type of catalyst a good candidate for this reaction, since both forms are active and they occur during reaction steps.
[31]	MFI	In	Cooperative effect of In_2O_3 and In-HZSM-5.	In_2O_3 promotes the NO oxidation to NO_2 and increased the formation of InO^+ active sites on In-HZSM-5.
[32]	MFI	Ag	Role of Ag species in the SCR of NO with CH_4. Mechanism.	Silver species are able to activate CH_4 and to lower the light-off temperatures for the reaction. In excess of O_2, nitrates are formed in silver sites which are effectively reduced by CH_4.
[33]	MFI	Ag	Effect of Ag loading in the reaction.	For loadings above 7 wt. %, activity is significantly enhanced due to the presence of nano-silver particles, which provide much stronger adsorption of nitrates species. However, the presence of isolated silver ions in the zeolite is inevitably necessary.
[34]	MFI	Ag	Effect of microstructural changes in the reaction.	Thermal pre-treatment in absence of O_2 leads to higher activity but lower activity. The opposite occurs if the treatment is performed in the presence of O_2. NO conversion increases in silver reduced species but direct CH_4 combustion as well. During reaction, those species are gradually oxidised.

Ref.	Structure	Metal	Description	Main conclusions / Observations
[35]	MFI	Ga	Study of Ga-ZSM-5 system for SCR of NO with methane.	Ga-H-ZSM-5 is active for SCR of NO with CH_4.
[36]	MFI	Ga	Revision on Ga-based catalyst.	Activity on gallium centres are drastically affected by water presence, which represent a major obstacle for its applications.
[37]	MFI	Mn	Study of chemistry of Mn sites in ZSM-5. Comparison of Mn-ZSM-5 with Co- and Cu-ZSM-5	Order of reaction is independent of Mn loading. Monodentate nitrate species plays a major role in the reaction.
[38]	MFI	Mn	Influence of preparation method. Effect of loading. Tolerance to the presence of SO_2.	Mn-ZSM-5 exhibits some tolerance to water and SO_2. MnO_x dispersed sites are responsible for catalytic activity.
[39]	MFI	Fe	Optimisation of Fe loading in ZSM-5 to obtain measurable activity for SCR of NO.	From 0.05-10% loading, the value 0.5% is the optimal.
[40]	MFI	CeO_2	Effect of CeO_2 precipitation and mechanical mixture with H-ZSM-5 in the reaction. Mechanism.	Oxidation of NO to NO_2 takes place over CeO_2 surface. CeO_2 also activates CH_4, possibly assisted by NO_2 adsorbed species (nitromethane or nitrosomethane as intermediate). Bifunctional interaction is not mediate by long distance transport step.
[41]	MFI	Several (In /Ga)	Effect of water in the catalytic activity of Ga and In/H-ZSM-5.	H_2O inhibits the NO oxidation that takes place in Lewis acid sites. The addition of additives (Pd, Rh and Ir) improves the catalytic activity.
[42]	MFI	Several (Rh /Pt /Co / Cu)	Effect of methane and ethane as reductant for SCR of NO.	Adsorbed NO_2 species play a major role in the reaction. Rh-ZSM5 is more active. Co-ZSM5 revealed to be quite stable under reaction conditions.
[43]	MFI	Several (Co /Cu)	Study of chemistry of Co and Cu sites in ZSM-5 in HC-SCR (methane and propane). Mechanism study: formation of NO-adsorbed species.	Nitrilo groups formed in Co sites are able to react with CH_4, which does not happen with nitrate and nitro species formed in Cu sites.

Ref.	Structure	Metal	Description	Main conclusions / Observations
[44]	MFI	Several (Co /Cu)	Comparison between CuZSM-5 and CoZSM-5.	CuZSM-5 possesses a larger fraction of Cu oxides than Cu ions, which promotes CH_4 combustion. The difference in the intrinsic ability of Co^{2+} and Cu^{2+} to activate NO_x to form adsorbed species, which react more easily with gaseous CH4, explains why CoZSM-5 is able to selectively reduce NO_x with CH_4.
[45]	MFI	Several (In /Ga /Co)	Catalytic performance of In-H-ZSM-5 than other systems.	Highly dispersed In centres are active for SCR of NO with CH_4 in excess of O_2. Acidity of structure is crucial to obtain catalytic activity.
[46]	MFI	Several (Co /Cu /Fe)	Mechanism study involving nitromethane as reductant.	Formation of HCN, NH_3 and HNCO suggested that there is not a single pathway to N_2 formation. Reaction study using $N^{15}O$ revealed that N_2 is generated from both CH_3NO_2 and NO_2 species.
[47]	MFI	Several (Zn /Cu)	Zn- and Cu-ZSM-5 systems is presented. Effect of CH_4 and O_2 concentrations.	Patent.
[48]	MOR	Co	Characterisation of Co sites of Co-MOR system.	Presence of oxides blocks some channels. Pre-treatment influences stabilisation of Co sites (He or H_2 generates less gas-accessible Y-Co sites and O_2 leads to stabilisation of Co in more accessible sites, α- and β-Co). Co_3O_4 negatively affects the NO to N_2 conversion and NO adsorption for all pre-treatments.
[49]	MOR	Co	Effect of the presence of acidic sites Co-MOR system.	Monodentate nitrate species are formed in Co^{2+} sites on Co-Na-MOR whereas NO^+ species are formed in Co^{2+} sites on Co-H-MOR. The former favours CH_4 combustion, which results in lower selectivity of the respective catalyst.

Ref.	Structure	Metal	Description	Main conclusions / Observations
[50]	MOR	Co	Effect of preparation method.	Impregnation leads to the formation of Co_3O_4 whereas ion-exchange results in the stabilisation of Co^{2+} and $[Co\text{-}O\text{-}Co]^{2+}$ ions. Co-MOR prepared by ion-exchange exhibit activity over a wide temperature region.
[51]	FER	Co	Influence of operating conditions on Co-FER system. Mechanism and kinetics.	Formation of adsorbed NO_2 species is a necessary step for NO reduction to N_2. The peak with volcano shape curve for T>500ºC is due to disappearance of such species and for lower temperatures is due to CH_4 combustion. H_2O physically occupies the actives sites, which diminishes NO and CH_4 conversion.
[52]	FER	Co	Influence of operating conditions on Co-FER system. Characterisation.	Valence state of Co is 2+ on Co-zeolites. In the presence of O_2, both mononitrosyl and dinitrosyl species can generate NO_2 adsorbed species, which are crucial to activation of methane.
[53]	FER	Co	Characterisation of Co sites distribution of Co-FER system.	β-Co is the predominate Co sites at all Co loadings. Ɣ-Co represents the minority of Co^{2+} ions and their population is higher for CoH- than CoNaK-FER. α-Co occupation increases with Co loading for CoH- and decreases for CoNaK-FER.
[54]	FER	Several (Co /Mn /Ni)	Study of Co-FER system and comparison with Co-ZSM-5.	Co-FER presents twice the conversion of Co-ZSM-5 at T>500ºC. Selectivity of CH_4 utilisation decreases with increasing of Co^{2+} loading. Optimal exchange level is situated in the range of 70-80%.
[55]	FER	Several (Cu /Co /Mn /Ni)	Effect of exchanged metal in FER system.	The type and quantity of cation introduced into the structure influences NO CH_4-SCR. Cu and Co were the most active metals.
[56]	BEA	Co	Activity and stability of Co-BEA system in the presence of SO_2.	The addition of 78 ppm of SO_2 generates reversible loss of NO conversion. Poison by SO_2 is irreversible for Co^{2+} ions but reversible for polynuclear and/or nano-sized Co oxide species.

Ref.	Structure	Metal	Description	Main conclusions / Observations
[57]	BEA	Co	Effect of C_1 and C_2 reducing agents in NO SCR.	Catalyst is more active when considering ethylene and ethanol reductants, compared to methane and methanol.
[58]	BEA	In	Influence of preparation methods on catalytic activity: Study of the In loading, type of precursor and nature of active sites.	Catalysts prepared by ion exchange in liquid phase present better catalytic performance compare to ion-exchange in solid state.
[59]	BEA	In	Study of In active sites.	Catalytic activity of In-BEA is attributed to $(InO)^+$ sites. NO_3^- and NO_2 adsorbed species are intermediates in the reaction.
[60]	BEA	Fe	Study of the interaction between Fe species and Al species from zeolite framework.	Al(III) and Fe(III) sites can act as Brønsted and Lewis acidic sites and they are responsible for catalytic behaviour.
[61]	FAU	Several (Co / Ag)	Dual-bed system catalyst comprising Co-NaX and Ag-NaX catalysts.	Pre-treatment of Co-Na-X catalyst with CO forms Co oxides, which are active for NO oxidation to NO_2. A second bed consists in a Ag-Na-X catalyst to convert NO_2 into N_2.
[62]	Several (MFI / FER)	Co	Effect of SO_2 and H_2O presence on catalytic activity.	The presence of SO_2 significantly enhances the NO conversion on Co-ZSM-5 for T > 500ºC, but the additional presence of water results in activity loss. Co-FER shows higher toleration to SO_2 and H_2O presence.
[63]	Several (MOR / FER)	Co	Characterisation of Co sites distribution of Co-FER, Co-ZSM-5 and Co-MOR.	Location of Co ions in the inner zeolite volume, their coordination and the distance between Co ions are important factors for SCR of NO with CH_4.
[64]	Several (MFI / MOR / FER / BEA / CHA)	Co	Effect of density of cation sites on total Co.	α-type Co^{2+} ions located in the main channels of MOR and FER exhibit the highest activity in these zeolites. β-type Co^{2+} located in the channel intersection of ZSM-5 in channels of BEA control the activity of these catalysts.

Ref.	Structure	Metal	Description	Main conclusions / Observations
[65]	Several (MFI / MOR)	Co	Role of acidity in Co-zeolites.	Prior to reduction to N_2, NO is oxidised to NO_2, catalysed by Co species (ions and oxides). N_2 formation occurs in the acid sites, where protonation of the reductant takes place.
[66]	Several (MFI / MOR)	Co	Characterisation of Co-MFI and Co-FER systems.	Acid strength of residual protonic sites is slightly increased by Co exchange. Cobalt ions act as medium-strength Lewis sites. It is proposed that NO reduction occurs via Co^{2+}/Co^{3+} redox couple mechanism and nitrate adsorbed species. Protonic sites are possibly involved in NO and CH_4 adsorption.
[67]	Several (MFI / MOR)	Co	Mechanism of NO-SCR by CH_4.	Bifunctional mechanism is proposed. NO_3^- /NO^+ species are intermediates. Co-oxide sites promote CH_4 combustion, decreasing both NO-SCR activity and selectivity.
[68]	Several (BEA /FAU)	Co	Co exchanged BEA/Y composite.	A new type of Co^{2+} sites can be obtained by growing a layer of BEA epitaxially to Y zeolite. More NO and NO_2 can be adsorbed in this composite. This material is also more resistant to water presence.
[69]	Several (BEA /MFI/MOR)	Co	Co exchanged BEA/MFI and BEA/MOR composites. Effect of metal additives.	The addition of Zn promotes better dispersion of Co, reducing the presence of Co oxides.
[70]	Several (MFI /MOR)	In	Study of chemistry of In sites in zeolite supports. Effect of thermal treatments on In dispersion.	Treatment under air at 500 ºC results in exchanged $(InO)^+$ species and highly dispersed In_xO_y species, which are active for the reaction.
[71]	Several (MFI /MOR)	Ga	Study of chemistry of Ga sites in ZSM-5. Comparison of Ga-ZSM-5 with Co-ZSM-5	Preparation method of Ga-H-ZSM-5 is not important to obtain catalytic activity. MOR and MFI are adequate supports but FAU is not. CH_4 is more selective for NO reduction in Ga-ZSM-5 then in Co-ZSM-5. However, the decrease in activity is more relevant in Ga-H-ZSM-5,

Ref.	Structure	Metal	Description	Main conclusions / Observations
[72]	Several (MFI / FAU)	Ni	Nature of Ni species supported in ZSM-5. Mechanism.	Formation of monodentate nitrates is a key step for the reaction and occurs in the Ni^{2+} sites. It is suggested that CH_x and NO_3^- species adsorb simultaneous in a single site, generating isocyanates and nitriles that will react with NO_x in the gas.
[73]	Several (MFI / MOR)	Several (Co / Cu / Mn / Ni)	Exploratory study regarding combination of metal-structure to obtain active catalyst	Variation of NO conversion follows volcano shape curves and the inversion in the trend is explained by the CH_4 combustion. NO conversion is proportional to exchange level of Co^{2+}, until a certain concentration. Cu^{2+} is not active for this reaction, neither Co-Y. Acidity and shape selectivity are not the important properties, but electronic influence of the cations by zeolites is.
[74]	Several (MFI / MOR / FER)	Several (Ga / In)	Exploratory study regarding combination of metal-structure to obtain active catalyst	Ga- and In-ZSM-5 is able to selectively reduce NO with CH_4. Oxidation of NO to NO_2 is an important step. Presence of water inhibits catalytic activity, but In-ZSM-5 presents moderate activity.

I.4.1.2. Monometallic zeolite-based catalyst only containing palladium

Nishizaka and Misono were the first to report the high activity of Pd-zeolite catalysts for the selective catalytic reduction (SCR) of NO using methane [75, 76], in particular the Pd-ZSM-5. Since then, several research groups including Misono's have made a significant progress in understanding this type of systems.

Nishizaka and Misono have concluded that the acidity of the catalytic support plays a major role in the reaction. This result was supported by experiments using Pd-ZSM-5 in protonic and sodic forms, which allowed to observe that the CH_4 conversion into CO_2 presented similar values for both catalysts but Na-Pd-ZSM-5 revealed to be inactive for the reduction of NO into N_2 [75-77]. It is believed that Brønsted acidity plays a major role and interferes directly in some reaction steps. On the other hand, palladium is involved in the CH_4 activation.

Uchida and co-workers studied the effect of the exchanged metal on mordenite [78]. It was found that the use of Pd presented the highest values of NO conversion into N_2, followed by Pt, Rh, Cu and Co. The effect of the reducing agent was also studied and it was found that, for the same C_1 concentration, methane was the best reducing agent when compared to ethane, propane and butane. This result is attributed to the readily combustion of the heavier hydrocarbons. It was verified that the increase of CH_4 concentration results in an increase of NO conversion and a decrease of CH_4 conversion.

It is worthy to mention that there is a patent regarding the use of Pd-zeolites (namely, Pd-ZSM-5) as NO_x CH_4-SCR technology [79]

Palladium species in the catalyst

Nishizaka and Misono [75] were the first to suggest that acidity might play a role in the stabilisation of palladium. In fact, Ali *et al*. [80] realised that palladium is stabilised in Pd^{2+} form when acid supports are used. Conversely, the use of other non-acid supports results in stabilisation of palladium as PdO. Other works also showed that acid supports result in high dispersion of palladium as Pd^{2+} [77, 81, 82]. The Pd^{2+} and PdO species were identified by many authors who performed characterisation studies of Pd-zeolites before and after being used in catalytic tests [81, 83-85].

It is wide accepted that dispersed Pd^{2+} promotes the selective reduction of NO, while PdO agglomerates promote the methane combustion and therefore, decreases the NO conversion to N_2. Ogura *et al.* [84] were able to verify, through NaCl elution and H_2-TPR, the presence of PdO in Pd-H-ZSM-5 samples, which is less active than Pd^{2+} to SCR of NO. Ohtsuka and Tabata were also able to verify the same, through NaCl elution and Raman spectroscopy [83]. Kikuchi and Ogura stated that for palladium loadings lower than 0.7%, the palladium is presented in the form of Pd^{2+} when supported in ZSM-5 [85].

Catalytic tests using Pd-H-MOR allowed to understand that the SCR of NO to N_2 occurs essentially in active sites were mononitrosyl species are formed [86]. These active sites consist in palladium in Pd^{2+} form, located at the main channels of mordenite. Palladium could also be stabilised in small cavities of the support which are characterised by the formation of dinitrosyl species. These sites are not active for the SCR and can be removed from the lattice by dealumination processes. The role of Pd sites where the formation of mononitrosyl species occurs was also highlighted for MFI support. Descorme *et al.* [87] realised that the ratio of NO conversion values of a Pd-H-ZSM-5 catalyst (Si/Al =25) and a Pd-H-Silicate (Si/Al = 131 but with the same MFI structure) were exactly the same as the ratio between the intensity of the mononitrosyl band in the FTIR spectra with NO adsorbed of these structures. This result shows a direct correlation between the existence of these sites and the catalytic activity for the reduction of NO with CH_4.

Ogura *et al.* [84] proposed a scheme for the state of palladium supported in ZSM-5, considering the different stages of its preparation and use. After the ion-exchange of palladium with NH_4-ZSM-5, the predominant form would be $Pd(NH_3)_4^{2+}$ which is converted to Pd^{2+} after the calcination procedure and, eventually, partially converted to PdO. After reaction of NO_2, CH_4 and O_2, the formation and then adsorption of water would convert the palladium in a palladium hydroxide cationic species $H^+[Pd^{2+}(OH)^-]^+$. By submitting the used catalyst to a new calcination, Pd^{2+} state could be reached again.

An interesting result regarding the state of palladium in ZSM-5 was obtained by Aylor *et al.* [81]. Through FTIR characterisation of fresh Pd-H-ZSM-5 samples with low (*ca.* 0.4%) and high (*ca.* 4%) loading of palladium, they realised that the amount of palladium supported in a highly dispersed state (*i.e.* Pd^{n+}, with n =1-3) is independent of the loading. The comparison of both IR spectra evidenced the existence of limited number of sites capable of stabilising palladium in the previous mentioned form. When this capacity is exceeded, the remaining palladium is stabilised as PdO.

The role of acidity in maintaining palladium dispersed as Pd^{2+} was mentioned before. Nevertheless, Adelman and Sachtler [88] presented another important function of protons in Pd/zeolite-based catalysts, namely in Pd-H-ZSM-5. Accordingly to the authors, these acid sites are responsible for a phenomenon named by them as *protonolysis* of large PdO particles, *i.e.* the conversion of PdO into Pd^{2+} in the presence of NO_x. Apparently, this phenomenon is the reason for the significant increase with time of NO_2 conversion to N_2, (from 20% to *ca.* 50%) in the catalytic test presented by the authors.

A similar conversion effect of conversion of PdO into Pd^{2+} over time of reaction was also reported by *Koyano et al.* [89]. They performed catalytic tests with Pd-H-ZSM-5 submitted to different ion-exchange sequence and oxidation/reduction pre-treatments before the reaction. It was concluded that after 14h of reaction, all different catalysts presented the same type of palladium species, Pd^{2+}, even when the pre-treatment generated different initial palladium species (PdO, Pd^0 or Pd^{2+}).

However, Okumura *et al.* [82] disagree with the previous groups on which state is the palladium stabilised in the support. They processed data obtained from EXAFS of a Pd-H-ZSM-5 catalyst and detected the presence of palladium metallic particles with a diameter range of 1.5 to 4 nm, after calcination of Pd-NH_4-ZSM-5 in the absence of O_2. This particles are larger than zeolites pores, suggesting that amine complex decomposed and Pd^0 was originated and agglomerated in the outer surface of the zeolite. By submetting the calcinated catalyst to an oxidation, PdO was formed. The same peaks corresponding to Pd-O (one peak) and Pd-Pd (two peaks) interactions were detected for a palladium oxide sample and Pd-Na-ZSM-5 sample spectra. These peaks are also present in Pd-H-ZSM-5 samples with high values of Si/Al ratio (namely, 19-37.5). However, the intensity of the Pd-Pd peaks decreases with the decreasing of Si/Al ratio, *i.e.* with the increasing of number of acid sites. The Pd-O peak, though, remains unchangeable and closely similar to the one present in the palladium oxide sample. This suggest that in lower acidity structures, large aglomerates of Pd^0 tend to be formed, whereas in high acidity structures (namely, H-ZSM-5 with Si/Al ratio of 12) the palladium tends to be stabilised as dispersed PdO.

These findings suggest that *protonolysis* hypothesis, proposed by Adelman and Sachtler [88], where the palladium would be stabilised by protonic sites, is inappropriate and instead, they suggest a model similar to the one proposed by Aylor *et al.* [81], where PdO is held by acid sites.

Despite the fact that Pd^{2+} is considered the adequate form for stabilising palladium in order to achieve better catalytic performances in the Pd-zeolite catalysts, some authors believe that PdO also plays a role in the SCR of NO with CH_4. Park *et al.* [90] proposed that the PdO at the outside surface of the zeolite could result in a synergic effect, along with Pd^{2+} and acidic sites, to enhance the catalytic performance of Pd-BEA. Wen, *et al.* [91] may be important to NO CH_4-SCR, by promoting the dissociation of C-H bonds.

Effect of Pd loading in catalytic performance

Ali *et al.* [80] have performed catalytic tests using several different structures such as ZSM-5, Silica, zeolite Y, mordenite and sulphated zirconia. Different amounts of Pd (0.1-1%) were stabilised in those structures and it was concluded that the best catalytic performance was achieved with Pd-H-MOR and Pd-H-ZSM-5, with 0.3 wt.% Pd. For higher loadings, PdO agglomerates were formed in higher amounts. These results are consistent with the ones previously reported by the same group, who have pointed out that not only activity but also selectivity finds a maximum value at 0.3 wt.% Pd with ZSM-5 [92]. A later study by this group reported again the value 0.3 wt.% of palladium as being the loading that correspond to maximum catalytic performance of Pd-H-MOR [93].

However, the studies performed by Misono and co-workers about the effect of the amount of Pd supported in ZSM-5 revealed that the activity increased with higher amounts of Pd, from 0.1 to

1.0 wt.%, being 1.0 wt.% Pd the ideal loading [75, 77]. For higher values, NO conversion became lower and CH_4 combustion of was favoured.

Ogura *et al.* [84] have also studied the effect of Pd loading in ZSM-5 in the reduction of NO_2 with CH_4. They concluded that the highest catalytic performance, *i.e.* the highest values of NO_2 conversion into N_2 were achieved with 0.7 wt.% Pd. They verified that below this loading, all palladium was stabilised as Pd^{2+} whereas above palladium started to be stabilised in other forms, namely PdO.

Mechanism of SCR of NO with methane over Pd-based catalysts

The mechanism of the SCR of NO with CH_4 over active palladium sites was also object of detailed study by several authors [92, 94].

Nishizaka and Misono realised that the acidity of the support was necessary to obtain interesting catalytic activity performance of Pd-based catalyst, namely Pd-H-ZSM-5, for the SCR of NO with CH_4 [75]. They verified that the CH_4 conversion into CO_2 had similar values when using an acidic support (such as H-ZSM-5) or a non-acidic support (such as Na-ZSM-5), but the same was not verified for the NO conversion into N_2, with the latter catalyst being inactive. They suggested that acidity should play a major role in the NO oxidation into NO_2. They also performed catalytic test using mixtures of NO-CH_4 and NO_2-CH_4, in presence (excess) and absence of oxygen and assessed NO conversion into NO_2 in Pd-H-ZSM-5, Pd-Na-ZSM-5 and H-ZSM-5 [76].

A three step bifunctional mechanism was then proposed [76]. The first step would be the oxidation of NO into NO_2, promoted by the acidity of the support. The second step should be the CH_4 activation, due to its interaction with palladium. Finally, CH_x species would react with NO_2 resulting in N_2 and CO_x which is promoted by the acidity of the support.

In a latter study, Misono's group realised that the dissociation of C-H bond in CH_4 to originate CH_x adsorbed species, which would then react in NO_2, is not the rate-determining step of the reaction. The results presented in their studied [95] suggested that this step is slow but there are also other slow steps in the SCR of NO with CH_4. This is not the case when Co-H-ZSM-5 is used for the same reaction [20]. Hence, it seems that the mechanism of this reaction using different metal-based catalyst, even with the same support structure, is not the same. Though, some similarities between the mechanisms of the reaction with different metal-based catalysts are also reported in the literature.

Loughran and Resasco [92] suggested that the reaction mechanism using Pd-H-ZSM-5 is similar to the bifunctional one proposed by Kikuchi and Yogo [74] for In-H-ZSM-5 and Ga-H-ZSM-5. The authors highlighted the importance of the NO oxidation into NO_2 as the first step of the reaction, being promoted by the protonic sites of the catalyst. Once formed, the NO_2 activates CH_4, originating a reaction intermediate and water. This intermediate then reacts with NO or NO_2 which

results in the formation of N_2, water and CO or CO_2, respectively. In this studied, it was evidenced that the effect of the metal is not the promotion of NO oxidation but, instead, the promotion of the NO_2-CH_4 reaction. These results are in agreement with the ones presented by Misono and co-workers.

Ogura *et al.* [96] suggested the role of zeolite might be slightly different when different metals are the active sites for the SCR of NO with CH_4. While on In-H-ZSM-5 the purpose of zeolite porosity is NO_2 species adsorbed near the $(InO)^+$ active sites, the ion-exchange capacity is required for Pd-H-ZSM-5 in order to provide Pd^{2+} in a highly dispersed state, so that NO can chemisorb efficiently.

Lobree *et al.* [94] realised that the state of palladium in ZSM-5 support is strongly dependent of operating conditions, namely temperature and presence of oxygen [94]. In the presence of oxygen (lean conditions), dispersed Pd ions remain in the same state and are not reduced. The NO adsorbs into the Pd ions, resulting in nitrosyl species. CH_4 reacts with these species resulting in CH_2NO that generates CN species by losing H_2O. Then, the O_2 in excess will react with the later specie, generating NO and CO. The Pd(H) resulted from the later reaction is regenerated by O_2 to Pd(OH). Metallic Pd can also be formed, which is oxidised by O_2 to PdO. Palladium oxide is very effective for CH_4 combustion, reducing the amount of CH_4 available for the SCR of NO.

Adelman and Sachtler also defended that the Pd-H-ZSM-5 catalyst acts as a bifunctional catalyst [88]. This idea is supported by the fact that acidity is necessary in order to accomplish the SCR of NO with CH_4. However, it seems that protons appear not to be involved in the CH_4 activation. Thus, they should be involved in subsequent steps. This hypothesis is consistent with the results obtain by Loughran and Resasco [92], who realised that mechanical mixtures of a non-acidic Pd-based catalyst (such as Pd-SiO_2) and an acidic support (such as sulphated zirconia) presented very interesting values of NO conversion into N_2, even comparable with the activity of high catalytic performance as Pd-H-ZSM-5.

A kinetic study of the SCR of NO with CH_4 over Pd-H-MOR (0.7% wt. Pd) was conducted by Shimizu *et al.* [97], by changing the concentration of NO, CH_4 and O_2 in the feed stream. The variation of NO (from 0 to 1250 ppm) showed that below 500 ppm the order of reaction was *ca.* 0.6 and for higher concentrations the order of reaction was near zero. This result supports the idea for concentration values above 500 ppm of NO, the active sites of the catalyst are covered with strongly adsorbed NO-derived species. Also, the increase of CH_4 in the stream results in an increase of NO conversion (from 0 to 2000 ppm), corresponding to an order of reaction of *ca.* 0.7. This evidences that weakly held CH_4-derived species are involved in the crucial steps of the reaction. Finally, variation of O_2 (from 0 to 10%) showed that the presence of oxygen is not essential to this system but slightly promotes the SCR of NO.

Based on IR, UV-VIS and kinetic results and considering previous literature results from other authors, Shimizu *et al.* proposed a reaction mechanism for the reduction of NO with CH_4 [97]. The formation of mononytrosil complex species in Pd^{2+} sites would be the first step. Methane would

also adsorbed on vacant Pd^{2+} sites, resulting in Pd^{2+}-CH_x species, which would react with the mononytrosil complex species, resulting in NCO and/or CN species. The formation of these species had been previously reported by Lobree *et al.* [94]. These species are easily hydrated to NH_3, which would migrate to acid sites to origin adsorbed NH_4^+ species together with CO_x. The NO_2 resulted from the oxidation of NO with O_2 would finally react with NH_4^+ species, resulting in N_2 and H_2O. The NH_4^+ species could also react with the mononytrosil complex species to give N_2 and H_2O.

Stability of catalysts

Despite the promising values of NO conversion into N_2 obtained in the SCR of NO with CH_4 on palladium-based catalysts, there is also a considerable number of results reported in the literature, by different authors, regarding some stability issues of these catalysts [78, 83, 88, 98].

Uchida and co-workers concluded that the NO conversion into N_2 values decreased with the increase of water concentration in the feed stream (until 9%), using a Pd-MOR catalyst [78]. However, they realised that by suppressing water, the conversion values returned to the initial ones obtained in its absence. Hence, it was suggested a competitive adsorption effect of NO and H_2O for Pd active sites. However, several studies indicate that irreversible deactivation, instead of inhibition, is likely to occur in the presence of water.

Ohtsuka and Tabata have reported irreversible deactivation of Pd-H-ZSM5 and Pd-H-MOR in the presence of water [98]. They have proposed that, in the presence of water, the migration of Pd^{2+} is energetically favoured by the formation of $Pd(OH)_2$ (Equation (I-6)) when compared with the formation of PdO in the absence of water (Equation (I-7)).

$$Z^- - Pd^{2+}(OH)^- + H_2O \rightarrow Z^-H^+ + Pd(OH)_2 \quad \text{(I-6)}$$

$$Z^- - Pd^{2+}(OH)^- \rightarrow Z^-H^+ + PdO \quad \text{(I-7)}$$

Adelman and Sachtler [88] proposed that, even in the absence of water in the feed stream, the deactivation of the catalyst could occur through the formation of PdO by the hydrolysis of Pd^{2+} with H_2O formed during CH_4 combustion (Equation (I-8)).

$$Pd^{2+} + H_2O \rightarrow 2H^+ + PdO \quad \text{(I-8)}$$

Other cause for the catalyst deactivation is pointed out by the same authors, as being the reduction of Pd^{2+} (Equation (I-9)) followed by oxidation (Equation (I-10)):

$$Pd^{2+} + \text{Hydrocarbon} \rightarrow Pd^0 + 2H^+ + ... \quad \text{(I-9)}$$

$$Pd^0 + ½\ O_2 \rightarrow PdO \quad \text{(I-10)}$$

H_2-TPR tests conducted in this study over Pd-H-ZSM-5 seem to support that the later mechanism is the prominent one in the presence of water.

The effects of water deactivation were also evidenced by Descorme, *et al.* [99], throughout a steam ageing performed at 800 ºC, in the presence of 10 vol.% H_2O for 6 h. Not only the Pd ions migrated into large metal Pd particles, but also the catalyst exhibit signs of severe delamination, being both effects responsible for the loss of activity. These effects can be seen as consequence of the exposure of Pd-catalysts to the prolonged catalytic test conditions. However, strategies have been reported in the literature to overcome the stability issues related to the water presence. Namely, in Pd-HZSM-5, Suzuki *et al.* [100] reported that the chemical vapour deposition of silica in the catalyst would decrease the water adsorption in the catalyst, mitigating the effect of water presence in the catalytic performance of NO_x CH_4-SCR. Other strategies involve the addition of a co-metal that stabilises palladium in the adequate positions of the zeolite framework, avoid its migration/aggregation. This topic is explored in the next section.

Interestingly, a single case of enhanced catalytic performance of Pd-MOR catalyst for SCR of NO with CH_4 due to the presence of water is reported by Descorme *et al*. [86]. This phenomenon is explained by the authors as being due to the interconversion process between dinitrosyl sites (non-active) and mononitrosyl sites (active). Nevertheless, it is worthwhile mention that this particular experiment was conducted in stoichiometric conditions.

I.4.1.3. Monometallic non-zeolite catalyst

Other family of catalyst adequate for the selective catalytic reduction of NO_x with methane in lean conditions consists in metal oxides. One can say that the most common oxides used for this application is alumina and zirconia. Commonly, these materials are sulphated in order to create acid sites in the structure, which are known to be required for NO_x SCR. Sulphate content varies from work to work, but usually is around 2-10 wt.%. The metals used in these systems are, in general, the same ones used in zeolite-based systems. One can say that palladium is one of the most considered and the content is also similar to the one considered for zeolites (typically around 0.1-0.5 wt.%). Table I-4 summarises the use of different these catalyst for this reaction.

Table I-4 – Summary of monometallic non-zeolite catalyst used for NO_x CH_4 -SCR in lean conditions.

Ref.	Structure	Metal	Description	Main conclusions
[101]	Al_2O_3	Pd	Effect of the palladium precursors and pre-treatment on preparation of alumina-based catalysts.	$Pd(NH_3)_4(NO_3)_2$ led to the most active and stable catalyst.
[102]	Al_2O_3	Pd	Alternative pre-treatment method using fluidised bed plasma reactor for treatment of alumina instead calcination.	Higher activity of catalyst is obtained through this method, compared to classical calcination, in particular for low range temperatures. Formation of Pd^{2+} surrounded by oxygen species is promoted, instead of PdO species.
[103]	Al_2O_3	Pt	Preparation of Pt nano particles-Y-Al_2O_3 using DEN as template agent	Highly effective surface area of Pt nanoparticles in Pt/Al_2O_3 catalyst enhanced overall NO_x reduction. Selectivity towards N_2O also decreases when compared to conventional preparation methods.
[104]	Al_2O_3	Pt	Preparation of Pt nano particles-Y-Al_2O_3 using different dendrimers (DEN) as template agent	The catalyst presented high-surface area and thermal resistance, exhibiting higher activity and stability when compared to a conventional Pd/Al_2O_3 catalyst.

Ref.	Structure	Metal	Description	Main conclusions
[105]	Al_2O_3	Pt	Effect of mixing α- and Ɣ-Al_2O_3 containing Pt.	Pt/α-Al_2O_3 shows excellent CH_4 adsorption properties and Pt/Ɣ-Al_2O_3 shows excellent NO adsorption characteristics. A mechanical mixture of both conducted to a new catalyst.
[106]	Al_2O_3	Cu	Novel method for Cu-Al_2O_3 synthesis.	Super-microporous structure and high exposure of active sites are the base of the catalytic improvement for NO CH_4-SCR, in particular, direct NO decomposition.
[107]	Al_2O_3	Ag	Study of Ag/Ɣ-Al_2O_3 system. Characterisation and mechanism.	Ionic silver bounded with alumina [Ag-O-Al] is responsible for catalytic activity towards N_2. CH_x species adsorb in these sites and react with NO_x adsorbed on alumina.
[108]	Al_2O_3 (S)	Pd	Proposal of Pd-SA as effective catalyst for SCR of NO with CH_4.	Sulphation increases the acidity which is essential for the reaction.
[109]	Al_2O_3 (S)	Pd	Study of catalytic behaviour of Pd-Ɣ-sulphated alumina monoliths at pilot plant scale level.	Palladium chloride was the most effective Pd precursor, due to successful stability of surface sulphates and the role that Cl^- ions have in the reaction.
[110]	Al_2O_3 (S)	Pd	Effect of sulphation on stabilisation of Pd species in alumina.	Palladium is stabilised as isolated Pd^{2+} ions in sulphated alumina, whereas in alumina it mainly exist as oxides. Partial oxidation or activation of CH_4 is a necessary step for reduction of NO.
[111]	Al_2O_3 /MgO	Ag	Synthesis of MgO-Al_2O_3 and impregnation with Ag.	MgO significantly decreases the active temperature window and confers resistance to SO_2 poisoning, which will adsorb in magnesia surface.

Ref.	Structure	Metal	Description	Main conclusions
[112]	Al_2O_3 /Ga_2O_3	-	Synthesis of γ-Ga_2O_3-Al_2O_3 active for SCR of NO with methane.	Spinel structure is obtained with Ga^{3+} and Al^{3+} occupying tetrahedral and octahedral sites, respectively. In Al^{3+} sites, surface nitrate species are formed and Ga^{3+} performs the CH_4 activation. Most important parameter is the proximity of these sites.
[113]	Al_2O_3 /Ga_2O_3	-	Treatment of γ-Ga_2O_3-Al_2O_3 with NH_3 for enhancing the catalytic performance.	By treating the catalyst with NH_3, a rearrangement of Ga^{3+} and Al^{3+} takes place, increasing the tetrahedral Ga^{3+} ions in the defective spinnel structure.
[114]	ZrO_2 (S)	Pd	Catalytic behaviour comparison between Pd-SZ and Pd-H-ZSM-5.	SZ offers more resistance to structural damage due to steaming than ZSM-5. Loss of sulphate occurs but remaining sulphate is able to provide the required acidity to the catalyst.
[115]	ZrO_2 (S)	Pd	Influence of sulphate content on catalytic performance of Pd-ZrO_2.	In a range of 1-7 wt. % of sulphate doping, the value of 4 wt. % revealed to be the optimum. This value influences the stabilisation and dispersion of Pd.
[116]	ZrO_2 (S)	Mn	Study of Mn-sulphated zirconia system and comparison with Mn-H-ZSM-5.	Mn-SZ presented better catalytic performance and toleration to water and SO_2 compared with Mn-H-ZSM-5. Sulphation process provides the required acidic sites and improves the dispersion of Mn species.
[117]	ZrO_2 /WO_3	Pd	Mechanism study of SCR of NO with CH_4 over tungstated zirconia with supported palladium.	Nitrates species are formed on Pd-TZ and decomposed to NO_2, initiating the formation of nitromethane. This compound will decompose through to cis-methyl nitrite and then to formates and NO adsorbed. $HCOO^-$ will reduce NO to N_2.

Ref.	Structure	Metal	Description	Main conclusions
[118]	ZrO_2 /WO_3	In	Promotional mechanism of tungstation for SCR of NO with CH_4.	In is presented as $(InO)^+$ and In_2O_3. Tungstation provides Brönsted acid sites which leads to the formation of $(InO)^+$ sites responsible for activating methane to $HCOO^-$, the actual reductant.
[119]	CeO_2 -ZrO_2 (S)	Pd	Nature of Pd species in sulphated ceria-zirconia	Brønsted acidity of sulphated support resulted in stabilisation of highly dispersed Pd species. Comparison of the results with Pd-SZ gives the idea that cerium sites act as a promoter of both SCR reaction and CH_4 combustion.
[120]	TiO_2	Pd	Study of Pd-TiO_2 system. Characterisation and mechanism.	Relative abundance of oxide and metallic sites of palladium determines the extension of each occurring reactions (SCR by CH_4, direct NO decomposition and CH_4 combustion).
[121]	TiO_2	Pt	UV photocatalytic reduction of NO with CH_4. Mechanism.	UV radiation promotes the formation of surface species that play a role in the NO SCR reaction.
[122]	SiO_2 / Al-SiO_2	Pd	Influence of synthesis parameters of Pd-SBA-15 / Pd-Al-SBA-15	Use of Pd amine precursor led to higher activities, compared to Pd nitrate. The highest NO_x reduction is observed in the catalyst prepared by incipient wetness impregnation.

Note

(S) after the structure indicates that the catalyst is sulphated.

I.4.2. Bimetallic catalysts

Bimetallic catalysts overcome to some extent the main problems presented by the monometallic catalysts. One can say that the second metal plays three major roles, which are not necessarily independent:

a. Improving the catalytic activity due to synergies generated between both metals;
b. Promoting stabilisation of other metal species which are active for the reaction. The co-cation occupies empty positions on the structure, usually not the ideal ones for the active metal to be stabilised in order to be involved in SCR reaction;
c. Attenuating deactivation effect in the presence of water (and SO_2) due to the fact that migration of active species is decrease by the positioning of co-cation as referred in the previous paragraph.

In this section, the state-of-art regarding bimetallic-based catalyst is presented. It is worthwhile to mention that an exhaustive literature review of such topic is hard to accomplish. Even in 1990, Traa *et al.* [15] referred that nearly all metals of periodic table were used as promoters for the selective catalytic reduction of NO_x with hydrocarbons. Nevertheless, since methane is a particular case of this group, the coverage of a more considerable group of studies in this case might be accomplished. It should be noted that there are some patents that consider the application of NO_x CH_4-SCR technology based on bimetallic formulations, PdCo-MOR [123] and PdCe-MOR [124], which may also indicate which are the pertinent formulations towards a commercial application.

In section I.4.2.1., the catalytic activity of bimetallic zeolite-based catalyst is target of a quantitative analysis, were values of conversion and catalytic test conditions were considered based on elements retrieved from the literature.

In section 0., the use of metals promoters (other than cobalt) in Pd-zeolite systems is considered in more detail and, for these systems, profiles of conversion over temperature and time are gathered and presented herein.

Section I.4.2.3 contains the summary of major bimetallic non-zeolite catalysts that can be found in the literature.

I.4.2.1. Bimetallic zeolite-based catalysts

In this section, it is performed a quantitative analysis of a considerable amount of literature elements regarding selective catalytic reduction of NO_x with methane. For this analysis, a total of 27 elements from literature (listed in Table I-5) were analysed in detailed. Information regarding catalytic test operating conditions and NO_x conversion to N_2 were compiled and are presented in this work.

Table I-5 – List of catalyst considered for the quantitative analysis of catalytic activity regarding bimetallic zeolite catalysts.

Reference	Catalyst	Si/Al	Metal 1	(wt.%)	Metal 2	(wt.%)
[125]	Pt-Pd-MOR	7	Pd	0.4%	Pt	0.4%
[126]	Co-Pd-MOR	6	Co	6.28%	Pd	0.15%
[127]	Co-Pd-MOR	10	Pd	0.40%	Co	2.20%
[128]	Ce-Pd-MOR	10	Pd	0.4%	Ce	2-4%
[129]	RE-Pd-MOR	12	Pd	0.3%	RE	1%
[130]	Pd-In-MOR	6.7	In	In/Al = 1/6	Pd	0.50%
[131]	Ce-Pd-MOR	5	Pd	0.2%	Ce	2%
[132]	Pd-In-MOR	6.7	In	6.8%	Pd	0.50%
[133]	Fe-In-MOR	10	Fe	n.a.	In	n.a.
[134]	Pt-Co-MOR	5.9	Pt	0.39%	Co	2.87%
[135]	Co-La-MOR	6.5	Co	1.69%	La	1.22%
[136]	Co-Pd-MFI	13	Pd	0.40%	Co	2.30%
[137]	Co-Pd-MFI	20.2	Co	3.30%	Pd	0.40%
[127]	Co-Pd-MFI	12	Pd	0.40%	Co	2.30%
[138]	In-Ir-MFI	11.9	In	4%	Ir	1%
[139]	In-Fe-MFI	12.5	In	5%	Fe_2O_3	20%
[140]	Ce-In-MFI	14	Ce	2%	In	2%
[141]	In-Ce-MFI	14	In	7%	Ce	9%
[142]	Co-In-MFI	33	In	1.70%	Co	0.34%
[143]	Zn-Co-MFI	12.5	Co	2%	Zn	2%
[144]	Ag-Co-MFI	n.a.	Co	3%	Ag	3%
[145]	Ce-Ag-MFI	14.05	Ce	Ce/Al=0.08	Ag	Ag/Al = 0.78
[127]	Co-Pd-FER	9	Pd	0.35%	Co	2.20%
[146]	Co-Pd-FER	9	Co	2.20%	Pd	0.15%
[147]	Pt-In-FER	8.8	Pt	0.50%	In	0.52%
[148]	In-Co-FER	8.8	Co	2.13%	In	3.28%
[149]	Mn-Co-FER	8.4	Mn	0.14%	Co	4.66%
[127]	Co-Pd-BEA	11	Pd	0.40%	Co	2.20%
[150]	Co-Pd-BEA	12.5	Co	2%	Pd	0.15%
[151]	Co-Pd-BEA	1000	Pd	0.15%	Co	3%

Figure I-8 illustrates the range of NO and methane concentrations considered for the inlet feed of the several catalytic tests showed in Table I-5. The points overlapped with the diagonal of the plot correspond to catalytic tests were $[CH_4]/[NO]$ ratio is equal to the unity. For points situated below, one can say that more severe catalytic operating conditions were considered.

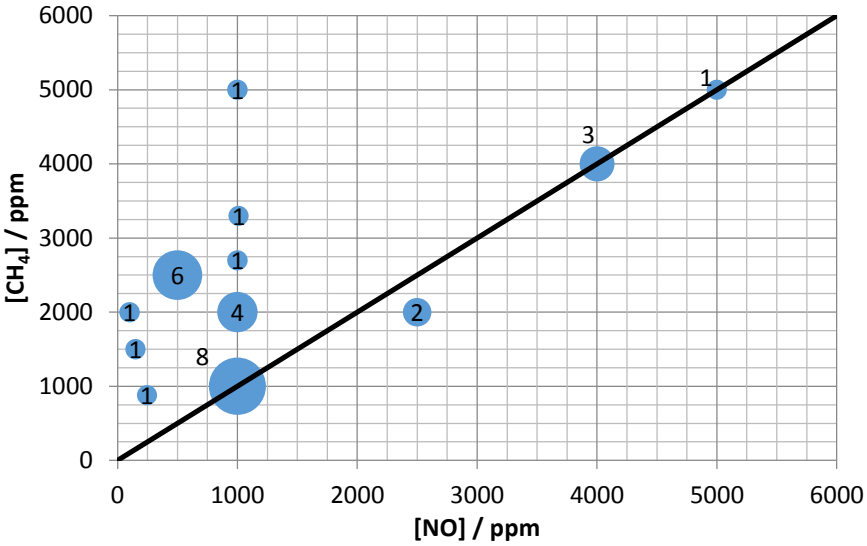

Figure I-8 – Distribution of NO and CH_4 concentration for the catalytic tests considered in Table I-5.

A compilation of gas hourly space velocity (GHSV) and flow rates values regarding the previous mention catalytic tests is also presented in Figure I-9. Only catalytic tests were the authors explicitly indicate these values are considered in this analysis (total of 14 literature elements). One can say that higher values of GHSV and flowrates are more likely to reproduce operating conditions of real exhaust gas system. On the other hand, it is known that the increase of GHSV tends to decrease catalytic activity.

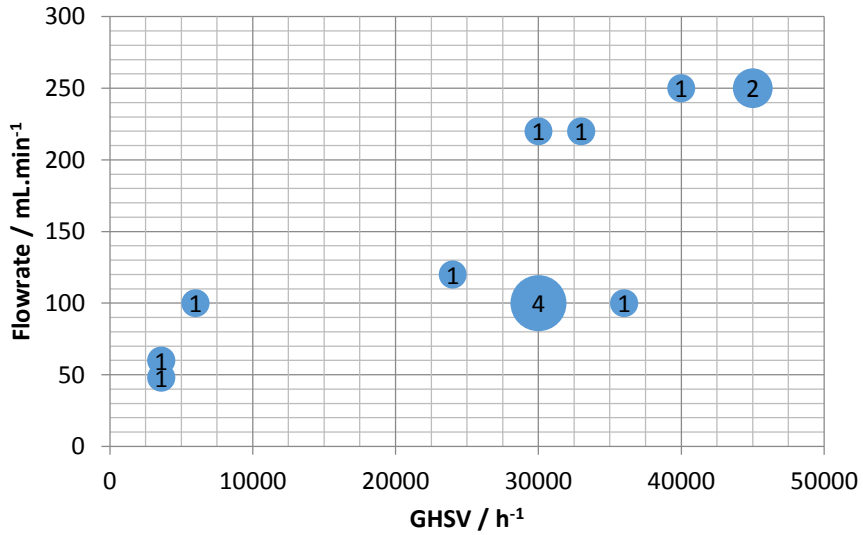

Figure I-9 – Distribution of GHSV and flowrate values for the catalytic tests considered in Table I-5.

Figure I-10 illustrates the window of conversion and maximum conversion values obtain for the several catalytic tests considered herein. For the purpose of this analysis, it was assumed that window of conversion only exists in cases were the NO conversion into N_2 was at least 50% (in the absence of water in the feed stream to the reactor). For this reason, only 18 elements are included in this analysis. All other elements can be found in Annex A.

Blue arrows on Figure I-10 illustrate the windows of conversion (*i.e.* the range of temperatures were NO conversion into N_2 is at least 50%) for the catalysts used in each respective catalytic test. The red dashes represent the maximum conversion temperatures for each catalyst. In the table contained in Figure I-10 it is possible to see which are the catalyst and the reference in literature that correspond to the respective result. It is also possible to observe that in some cases the blue arrow is missing and only a red dash is presented. This means that only for the temperature indicated by the red dash, a conversion equal or above 50% is registered, meaning that the window of conversion is very narrow (in the limit, it is a single point which coincides with the temperature of maximum conversion).

The interpretation of Figure I-10 leads to the conclusion that for bimetallic zeolite based catalysts, the window of conversion is typically between 350-500 ºC and the maximum conversion temperature is typically inside the range of 450-500 ºC. It is crucial to have this information in mind when the development of a zeolite-based technology is intended.

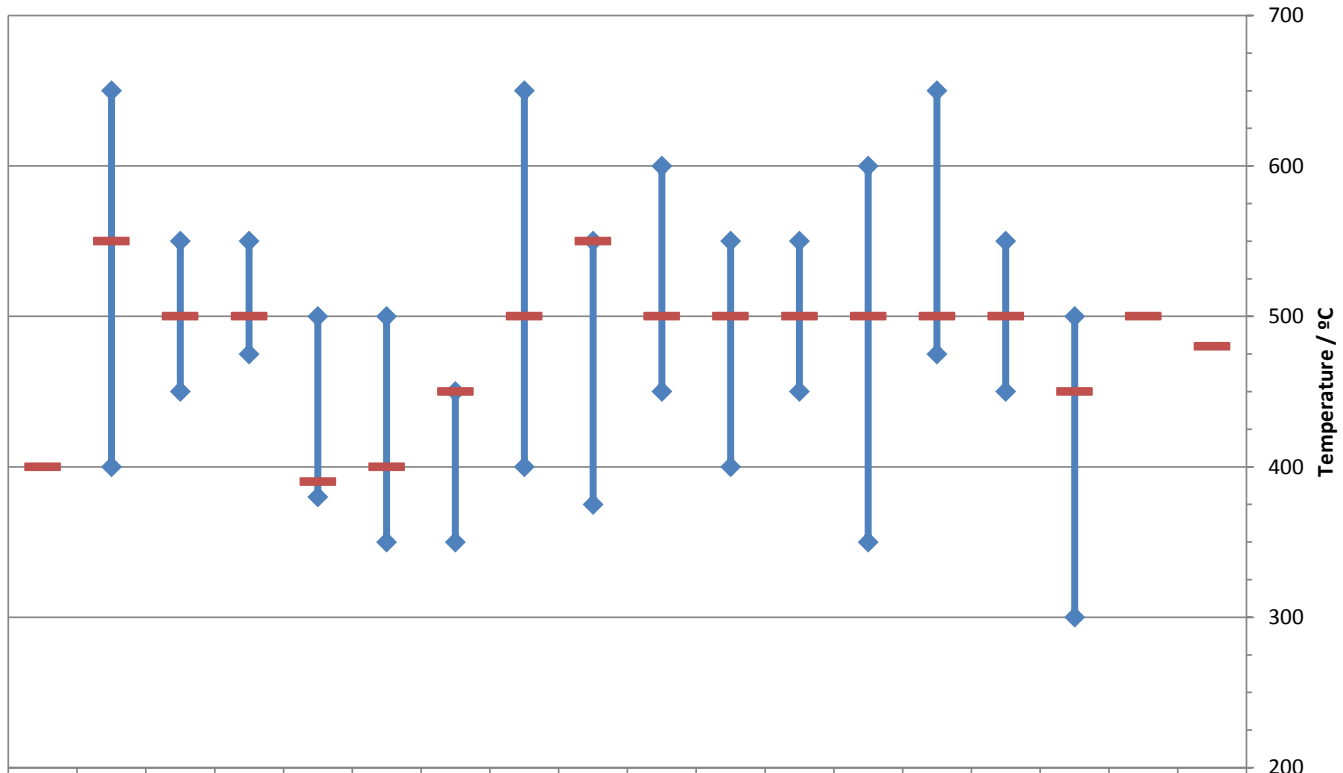

	Pd-In-MOR [129]	Ce-Pd-MOR [130]	Fe-In-MOR [132]	Pt-Co-MOR [133]	Co-Pd-MFI [135]	Co-Pd-MFI [136]	In-Ir-MFI [137]	In-Fe-MFI [138]	Ce-In-MFI [139]	In-Ce-MFI [140]	Co-In-MFI [141]	Zn-Co-MFI [142]	Ag-Co-MFI [143]	Ce-Ag-MFI [144]	Pt-In-FER [146]	In-Co-FER [147]	Mn-Co-FER [148]	Co-Pd-BEA [150]
Max. Conv.	55%	90%	57%	80%	98%	90%	90%	100%	85%	92%	85%	55%	98%	80%	82%	98%	51%	55%
T Max. Conv.	400	550	500	500	390	400	450	500	550	500	500	500	500	500	500	450	500	480
T window (upper)	400	650	550	550	500	500	450	650	550	600	550	550	600	650	550	500	500	480
T window (lower)	400	400	450	475	380	350	350	400	375	450	400	450	350	475	450	300	500	480

Figure I-10 – Window of conversion and temperature of maximum conversion for bimetallic zeolite-based catalyst.

As it is known and widely described in the literature, the presence of water causes loss of activity of zeolite-based systems for NO_x CH_4-SCR. In order to understand the impact of the presence of water in the catalytic behaviour of bimetallic zeolite catalysts, the data regarding catalytic tests performed in the presence and absence of water for the catalysts presented in Table I-5 was analysed.

Figure I-11 summarises the NO_x conversion into N_2 for the bimetallic catalysts considered in Table I-5 which references contain data regarding catalytic tests in the presence and absence of water in the feed stream.

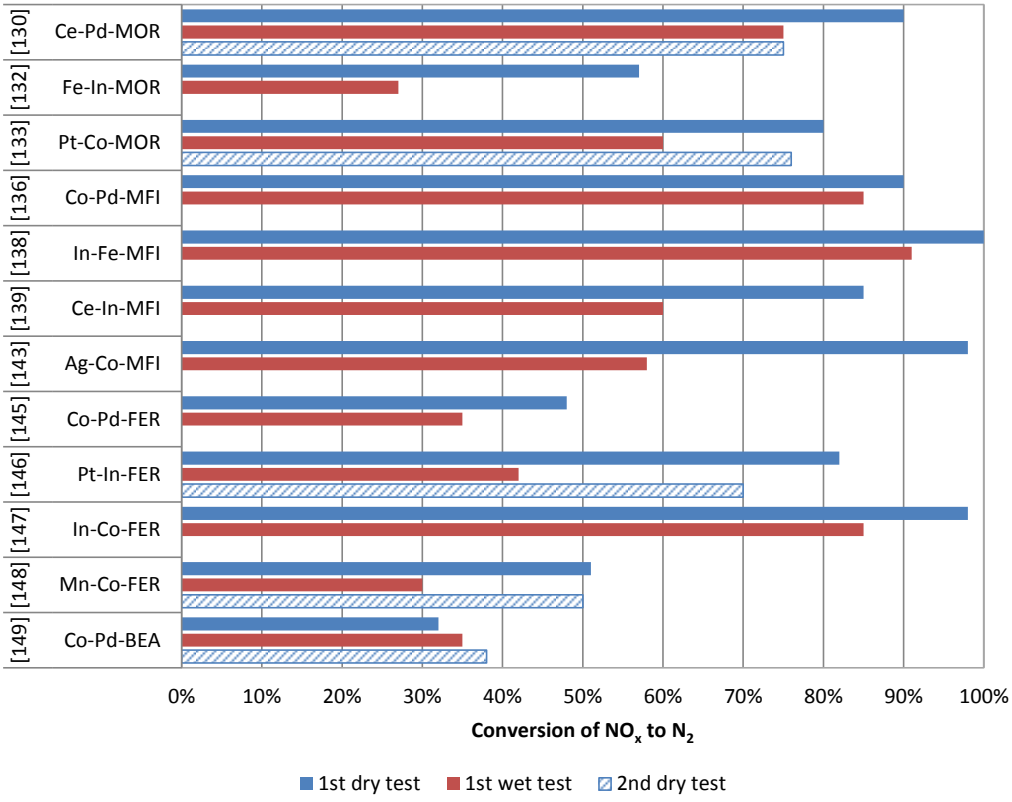

Figure I-11 – Effect of water presence in the maximum catalytic NO_x conversion into N_2 for bimetallic zeolite catalysts.

Detailed description of the catalysts and operating conditions of catalytic tests can be found in Annex A. In Figure I-11, the conversion values presented for the 1st dry test refer to the highest conversion value registered for each catalysts. The values of 1st wet test and 2nd dry test refer to the conversions registered at the same temperature corresponding to the conversion values presented for the 1st dry test.

The catalytic behaviour of these catalysts in the presence of water will depend from the operating conditions considered in the catalytic tests, in particular the water content in the feed stream. Hence, careful should be taken when attempting to compare the catalytic behaviour of the different systems. Nevertheless, results illustrated in Figure I-11 allow to realise that the presence

of water is responsible for deactivation of the catalyst and that this deactivation is, in general, irreversible, since the catalyst is unable to fully restore its catalytic activity once the water is removed from the feed stream. However, it is worthwhile to mention that there is a work where a catalytic activity enhancement is reported due to the presence of water in the feed stream [150]. It is the case Co-Pd-BEA catalysts. In this work, during the catalysts preparation, a heat treatment in the presence of water was performed (steaming). The authors believe that this treatment cause structural modifications in the catalyst and allowed the stabilisation of active metal species in a way that the system would not be affect by the presence of water.

I.4.2.2. Bimetallic Pd/zeolite-base catalysts (without cobalt)

Several authors observed that the presence of an additional metal (a co-cation) in a monometallic catalysts (*e.g.* palladium-based catalysts) could enhance their catalytic performance, resulting in more active and more stable catalytic systems.

De Correa and co-workers studied the catalytic performance of Pt-Pd-H-MOR [125]. They realised that there was a synergic effect of the two metallic species, supported by the fact that this catalyst was more active than Pt-H-MOR and Pd-H-MOR. They realised that the addition of platinum to Pd-H-MOR favoured the NO oxidation into NO_2, which would indirectly result in the increase of NO SCR. Besides, it was verified that the bimetallic catalyst was also more tolerant to the presence of water and SO_2.

Pieterse and co-workers realised that the addition of cerium as co-cation in Pd-zeolites, namely Pd-H-MOR, could generate a catalyst with similar high catalytic performances as the ones where cobalt is used as co-cation [128, 129, 152]. They focused their work in control pollution of stationary sources and realised that for a representative stream with 245 ppm of NO, 881 ppm of CH_4, 11.3 vol.% of water and 6.4 vol.% of O_2, at 385 ºC and with GHSV of 17,000 h^{-1}, a NO conversion into N_2 of *ca.* 60% was obtained, as well as a CH_4 conversion into CO_2 of *ca.* 21%. Durability catalytic tests were also performed and allowed to concluded that Pd-zeolites doped with cerium were able to maintain their activity over 100 h of test, which was not the case when cobalt was used as co-cation, in particular, when BEA, ZSM-5 and FER where used.

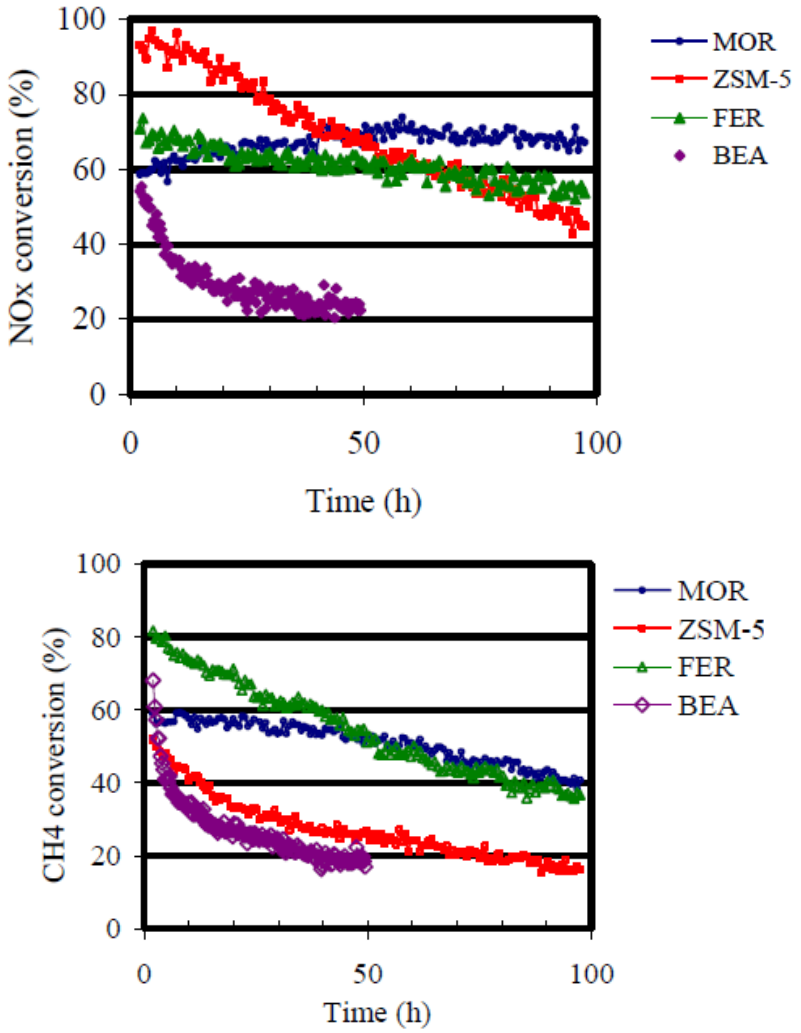

Figure I-12 – NO_x conversion into N_2 and CH_4 conversion over the time, for Co-Pd-zeolites. Inlet stream: 500 ppm of NO, 2,500 ppm of CH_4, 5% of O_2, 5% of H_2O, T = 450 ºC and GHSV – 20,000 h^{-1} (10,000 h^{-1} for FER).

(Source: [128])

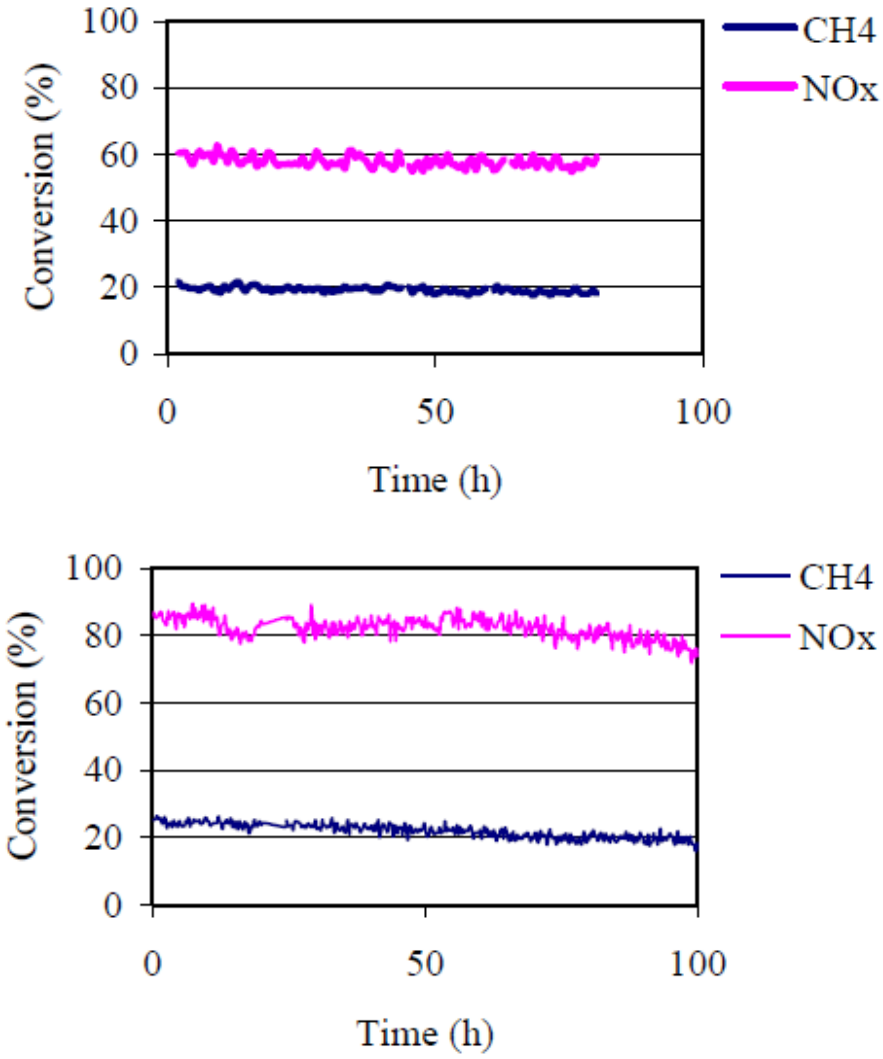

Figure I-13 - NO_x conversions into N_2 and CH_4 conversion over the time, for Ce-Pd-MOR. Inlet stream: 500 ppm of NO, 2,500 ppm of CH_4, 5% of O_2, 5% (up) or 11% (down) of H_2O, T = 375 ºC (up) or 400 ºC (down) and GHSV – 17,000 h^{-1} (up) or 15,000 h^{-1} (down).

(Source: [128])

Costilla *et al.* [131] studied the effect of adding Ce to Pd-H-MOR catalyst in the presence and absence of water. Pd(0.2%)-H-MOR and Ce(2%)-Pd(0.2%)-H-MOR, with Si/Al = 5, were tested with a mixture of NO (1010 ppm), CH_4 (3300 ppm), O_2 (4.1 vol.%) and H_2O (5 vol.%, when present) in a range of temperature from 300 to 650 ºC, first in the absence of water (dry cycle), then in the presence of water (wet cycle) and finally, in a second dry cycle.

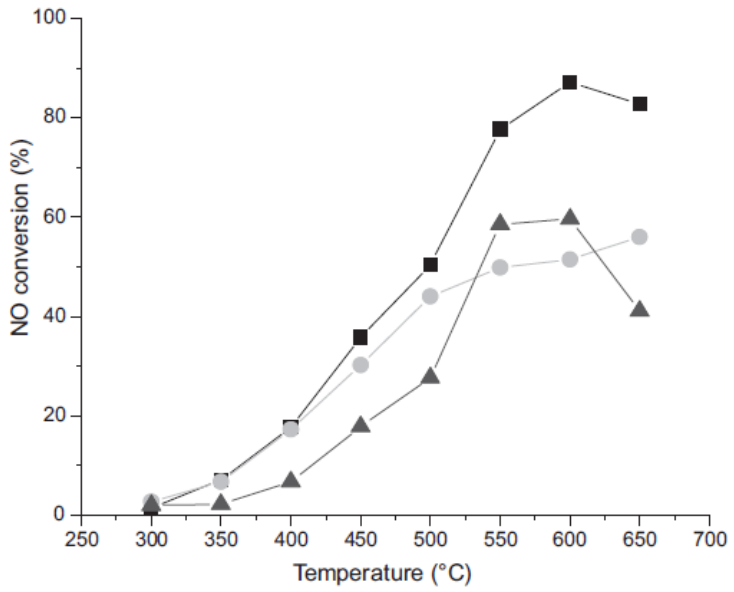

Figure I-14 – NO conversion vs. temperature on Pd-H-MOR:
(■) Dry feed; (▲) wet feed; (●) dry feed. Inlet stream: 1,010 ppm of NO, 3,300 ppm of CH_4, 4.1% of O_2, 5% of H_2O and GHSV of 33,000 h^{-1}).

(Source: [131])

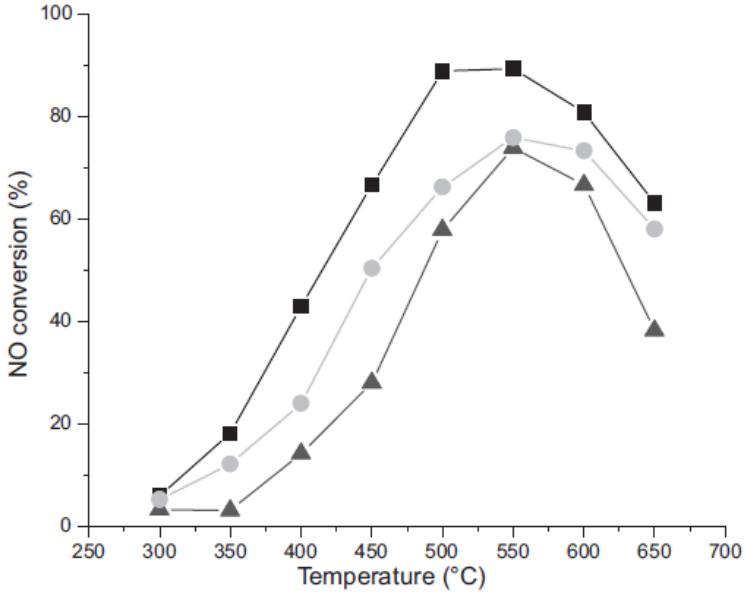

Figure I-15 – NO conversion vs. temperature on Ce-Pd-H-MOR.
(■) Dry feed; (▲) wet feed; (●) dry feed on sample exposed to water). Inlet stream: 1,010 ppm of NO, 3,300 ppm of CH_4, 4,1% of O_2, 5% of H_2O and GHSV of 33,000 h^{-1}).

(Source: [131])

In dry conditions, results show that it is possible to achieve interesting increases in NO conversion, from 400 to 500 ºC. For instance, the addition of cerium to Pd-H-MOR is responsible for the increasing in NO conversion from 19% to 41%. In the presence of water, this improvement is more evident for higher temperatures.

Results also show that the highest NO conversion into N_2 was obtained in the 1st dry cycle (*ca.* 90%). In the wet cycle, the conversion decreased to 75%, which was similar to the 2nd dry cycle. From this behaviour it is noticed an irreversible loss of conversion, which was similar to one verify for Pd-H-MOR. However, the maximum value of NO conversion was obtained at a lower temperature for Ce-Pd-H-MOR. Also, the irreversible loss of conversion was less in the bimetallic catalyst (from 90% in the 1st dry cycle to 75% in the 2nd dry cycle, compared to 90% to 50%, respectively, in Pd-H-MOR). Moreover, NO conversion into N_2 is partially recovered in Ce-Pd-H-MOR for lower temperatures, which is not the case form Pd-H-MOR.

By FTIR spectroscopy of fresh and used samples with CO adsorption, it was possible to verify the band corresponding to CO adsorbed in metallic palladium presented small changes, which reveals that Ce stabilises palladium as Pd^{2+} (otherwise, Pd metallic bands would increase significantly in the used samples spectrum).

Recently, Gutierrez's group reported the use of palladium as a co-cation, in order to improve the catalytic performance of indium zeolite catalysts [130, 132, 153]. According to these studies, palladium would increase the formation of NO_2, which has better potential for SCR, compared to NO. This effect would generate higher formation of indium nitrate ($In^+NO_3^-$), consider an important precursor for SCR. Also, it is believed that there is a synergetic effect of palladium and indium, that is attributed to the InO^+ species preventing the formation of nitrosyl species (generated in the Pd^{2+} sites) into more stable and less reactive species (nitrile and isocyanate). Gutierrez and co-workers reported an increase of NO conversion into N_2 from 16% with Pd-H-MOR to 55% with Pd-In-H-MOR, at 400 ºC (Figure I-16).

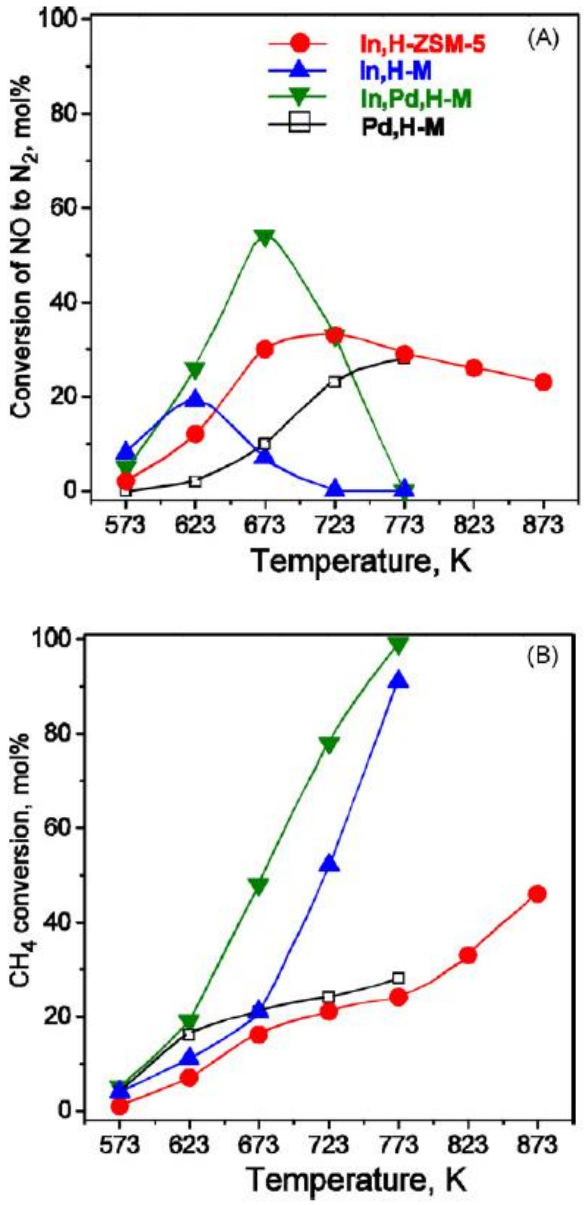

Figure I-16 – NO conversion into N_2 (A) and CH_4 conversion (B) over Pd/In-based catalysts. Inlet stream: 4,000 ppm of NO, 4,000 ppm of CH_4, 2% of O_2 and GHSV – 30,000 h^{-1}

(Source: [130])

I.4.2.3. Bimetallic non-zeolite catalysts

Table I-6 summarises the bimetallic non-zeolite catalysts that can be found in literature. Most of the studies reported in this table can be considered recent, compared to the ones about zeolite-based catalysts, they were published in the 2000's. Most of them were even published after 2010. Other important aspect is the fact that three of this publications [154-157] refer the use of dual-bed catalysts consisting in the combination of monometallic catalysts, instead of impregnated structures with two metals.

Table I-6 - Summary of bimetallic non-zeolite catalyst used for NO_x CH_4-SCR in lean conditions.

Ref	Structure	1st M.	2nd M.	Description	Main conclusions
[154]	ZrO_2 (S) /ZrO_2 (dual-bed)	Pd	Co	Dual-bed catalytic system composed by Pd-sulphated-ZrO_2 and Co-ZrO_2.	In simulated lean natural gas exhaust, N_2 yields were not inhibited and the dual-catalyst is also able to oxidise CO, C_3H_8 and CH_4.
[155]	ZrO_2 (S) /ZrO_2 (dual-bed)	Pd	Co	Dual-bed catalytic system composed by Pd-sulphated-ZrO_2 and Co-ZrO_2.	The proximity between Pd-SZ and Co-Z showed to offset the effect of water presence.
[156]	ZrO_2 (S) /ZrO_2 (dual-bed)	Pd	Co	Dual-bed catalytic system composed by Pd-sulphated-ZrO_2 and Co-ZrO_2.	Catalyst resists to water presence and it is able to perform the following three reactions: reduction of NO_x, combustion of unburned HC and CO oxidation.
[157]	ZrO_2 (S) /CeO_2 (dua-bed)	Pd	Co	Dual-bed catalytic system composed by Pd-sulphated-ZrO_2 and CoO_x-CeO_2.	Pd-sulfated zirconia is the reductant catalyst and CoO_x-ceria is the oxidation catalyst. It is evidenced the resistance to water presence.
[158]	ZrO_2 (S) /CeO_2 (dua-bed)	Pd	Co	Dual-bed catalytic system composed by Pd-sulphated-ZrO_2 and CoO_x-CeO_2.	Co loading in the oxidation catalyst is crucial for the overall performance of the dual-bed catalyst.
[159]	ZrO_2 (S)	In	Ce	Catalytic screening of SZ doped with Ni, Fe, In, Ca, Ce, Ga and In-Ce oxides.	Impregnation of both Ga and In results in the most active catalyst for SCR of NO with CH_4.
[160]	ZrO_2 (S)	In	Fe	Promotional effect of Fe addition to In-sulfated zirconia.	The addition of Fe to In-SZ increased the surface area and the amount of strong Brønsted sites, which helps in the dispersion of $(InO)^+$ species. Also, it increases the amount of Lewis sites responsible for activating methane.

Ref	Structure	1st M.	2nd M.	Description	Main conclusions
[161]	Al_2O_3	Ag	Cs	Study of the effect of Cs as promoter in Ag-Al_2O_3 system.	Addition of Cs as promoter resulted in samples with stronger NO adsorption properties and more stable Ag crystallisation.
[162]	Al_2O_3	Ag	Several (K /Cs /Na).	Effect of alkali promoters on Ag/Y-Al_2O_3 system.	The addition of alkali metals supresses the accumulation of sulphur compounds, which explains the improved catalytic performance in the presence of H_2O and SO_2. K and Cs revealed to be the best promoters.
[163]	Al_2O_3 (S)	Ag	K	Effect of sulphation in catalytic performance in Ag-K-Al_2O_3.	Sulphation contributes to improve the catalytic performance. During the reaction, desulphation takes place, redispersing the Ag clusters.
[164]	TiO_2	Pd	Gd	Role of lanthanide elements (Ce, Gd, La and Yb) as promoters of SCR of NO with CH_4 in Pd-TiO_2.	The use of Gd led to resistance of water presence over 18h and resistance to SO_2 over 6h. This element is the most effective promoter.
[165]	TiO_2	Pd	Several (Sm / Yb)	Promotional effect of Sm and Yb on Pd-TiO_2, introduced during synthesis, through the use of $(DMF)_{10}Ln_2[Pd(CN)_4]_3$ (Ln=Yb,Sm) precursor.	The novel selection of Yb and Sm precursor successfully enabled a uniform ratio of metals to be delivered in the support surface. Better catalytic performance was obtained when compared to conventional methods of impregnation.

Note:

(S) after the structure indicates that the catalyst is sulphated.

I.5. Conclusions

This chapter intends to draw a picture concerning the work already developed by scientific community regarding the selective catalytic reduction of nitrogen oxides with methane as reductant. One major conclusion is related to the type (nature) of the catalyst used for this reaction, which can be grouped in two major families: zeolite-based catalyst and non-zeolite based catalysts, in particular metal oxides.

In order to obtain an appropriated catalyst, active sites must be generated within the support structure. This process involves impregnation of metals, which can be successfully accomplished through the use of several techniques (e.g. liquid ion-exchange, incipient wetness impregnation, solid state ion-exchange) and many different precursors (e.g. oxides, nitrates, acetates). Pre-treatments (typically thermal treatments) are also employed in order to activate the catalysts. Different combination of structures, impregnation methods and treatments leads to different catalyst due to stabilisation of different active species in the structure.

It is widely accepted that the achievement of an active and stable catalyst with potential to be employed for commercialisation will necessarily involve the use of more than one single metal and, eventually, the combination of more than one structure. Data analysed in this review suggests that potential metal candidates are Pd, In, Co and Ce. Also, structures as MOR, ZSM-5, FER and sulphated alumina/zirconia should be considered.

The interpretation of this document (eventually complemented with other literature elements not considered in this document) and accumulated *know-how* established within CRERG-IST and IJLRDA-UPMC will be the base for the work preparation related to this project with GDF SUEZ, towards the development of a successful catalytic system for reducing nitrogen oxides contained exhaust gas emissions.

The results presented in this chapter were the base for the work preparation related to the research collaboration project between IST/UPMC/ENGIE aiming the development of a successful catalytic system for reducing nitrogen oxides contained in the exhaust gas of natural gas powered vehicles.

I.6. References

[1] United States Environmental Protection Agency (EPA), website, http://www.epa.gov/air/nitrogenoxides/health.html, accessed in 17/10/2012.

[2] D. Fowler, C. Flechard, U. Skiba, M. Coyle, J.N. Cape, New Phytologist, 139 (1998) 11-23.

[3] NEC Directive status report 2013, European Environment Agency, 2014.

[4] DieselNet, website, http://www.dieselnet.com/standards/#eu, accessed in 08/03/2013.

[5] NGV Global, website, Current Natural Gas Vehicle Statistics, http://www.iangv.org/current-ngv-stats/, accessed in June 2015.

[6] The International Association for Natural Gas Vehicles (IANGV), website, Natural Gas, http://www.iangv.org/natural-gas-vehicles/natural-gas/, accessed in 10/03/2013.

[7] Agility Fuel Systems, website, http://www.agilityfuelsystems.com/why-natural-gas/lng-vs-cng.html, accessed in 10/03/2013.

[8] M.R.S. Werpy, D.; Burnham, A.; Mintz, M., Natural Gas Vehicles: Status, Barriers, and Opportinities, Argonne, U.S.A, 2010.

[9] N.-O.E. Nylun, K.; Lappi, M.; Ikonen, M., Transit bus emission study: Comparison of emissions from diesel and natural gas buses, VTT Processes, 2004.

[10] Johnson Matthey Catalysts, website, http://ect.jmcatalysts.com/emission-control-technologies-three-way-catalysts, accessed in 31/05/2012.

[11] C.M. Favre, J.; Bosteels, D., Emissions control technologies to meet current and future european vehicle emissions legislation, Association for Emission Control by Catalyst, Belgium.

[12] Doosan, website, http://www.doosanequipment.com/dice/products/tier4/Tier+4+Technologies.page#, accessed in 27/06/2014.

[13] O. Gorce, F. Baudin, C. Thomas, P. Da Costa, G. Djega-Mariadassou, Appl. Catal., B, 54 (2004) 69-84.

[14] G. Djega-Mariadassou, Catal. Today, 90 (2004) 27-34.

[15] Y. Traa, B. Burger, J. Weitkamp, Micropor. Mesopor. Mat., 30 (1999) 3-41.

[16] M.D. Fokema, J.Y. Ying, Cat. Rev. - Sci. Eng., 43 (2001) 1-29.

[17] R. Burch, J.P. Breen, F.C. Meunier, Appl. Catal., B, 39 (2002) 283-303.

[18] Y.J. Li, J.N. Armor, Appl. Catal., B, 1 (1992) L31-L40.

[19] Y.J. Li, P.J. Battavio, J.N. Armor, J. Catal., 142 (1993) 561-571.

[20] A.D. Cowan, R. Dumpelmann, N.W. Cant, J. Catal., 151 (1995) 356-363.

[21] X. Wang, H.Y. Chen, W.M.H. Sachtler, Appl. Catal., B, 29 (2001) 47-60.

[22] G. Bagnasco, M. Turco, C. Resini, T. Montanari, M. Bevilacqua, G. Busca, J. Catal., 225 (2004) 536-540.

[23] T. Montanari, O. Marie, M. Daturi, G. Busca, Appl. Catal., B, 71 (2007) 216-222.

[24] J. Zhang, Y. Liu, W. Fan, Y. He, R. Li, Fuel, 86 (2007) 1577-1586.

[25] A.V. Boix, E.E. Miro, E.A. Lombardo, J.L.G. Fierro, Catal. Today, 133 (2008) 428-434.

[26] Y. Li, J.N. Armor, Patent, EP0525701A1 (1992).

[27] F.G. Requejo, J.M. Ramallo-Lopez, E.J. Lede, E.E. Miro, L.B. Pierella, O.A. Anunziata, Catal. Today, 54 (1999) 553-558.

[28] J.M. Ramallo-Lopez, L.B. Gutierrez, A.G. Bibiloni, F.G. Requejo, E.E. Miro, Catal. Lett., 82 (2002) 131-139.

[29] T. Sowade, C. Schmidt, F.W. Schutze, H. Berndt, W. Grunert, J. Catal., 214 (2003) 100-112.

[30] R.M. Mihalyi, Z. Schay, A. Szegedi, Catal. Today, 143 (2009) 253-260.

[31] L.L. Ren, J. Chem., Article ID 851605 (2014).

[32] C. Shi, M.J. Cheng, Z.P. Qu, X.F. Yang, X.H. Bao, Appl. Catal., B, 36 (2002) 173-182.

[33] C. Shi, M.J. Cheng, Z.P. Qu, X.H. Bao, Appl. Catal., B, 51 (2004) 171-181.

[34] C. Shi, M.J. Cheng, Z.P. Qu, X.H. Bao, J. Mol. Catal. A: Chem., 235 (2005) 35-43.

[35] K. Yogo, M. Ihara, I. Terasaki, E. Kikuchi, Chem. Lett., (1993) 229-232.

[36] J.N. Armor, Catal. Today, 31 (1996) 191-198.

[37] M.C. Campa, D. Pietrogiacomi, S. Tuti, G. Ferraris, V. Indovina, Appl. Catal., B, 18 (1998) 151-162.

[38] S. Chen, X. Yan, J. Chen, J. Ma, R. Li, Chin. J. Catal., 31 (2010) 1107-1114.

[39] L.L. Ren, T. Zhang, Chin. Chem. Lett., 21 (2010) 674-677.

[40] T. Liese, E. Loffler, W. Grunert, J. Catal., 197 (2001) 123-130.

[41] E. Kikuchi, M. Ogura, N. Aratani, Y. Sugiura, S. Hiromoto, K. Yogo, Catal. Today, 27 (1996) 35-40.

[42] R. Burch, S. Scire, Appl. Catal., B, 3 (1994) 295-318.

[43] B.J. Adelman, T. Beutel, G.D. Lei, W.M.H. Sachtler, J. Catal., 158 (1996) 327-335.

[44] A.J. Desai, V.I. Kovalchuk, E.A. Lombardo, J.L. d'Itri, J. Catal., 184 (1999) 396-405.

[45] X.J. Zhou, T. Zhang, Z.S. Xu, L.W. Lin, Catal. Lett., 40 (1996) 35-38.

[46] E.A. Lombardo, G.A. Sill, J.L. d'Itri, W.K. Hall, J. Catal., 173 (1998) 440-449.

[47] S.L. Hung, Patent, US5364606 (1994).

[48] L.B. Gutierrez, E.E. Miro, M.A. Ulla, Appl. Catal., A, 321 (2007) 7-16.

[49] D. Pietrogiacomi, M.C. Campa, V. Indovina, Catal. Today, 155 (2010) 192-198.

[50] B. Li, H. Wang, F.C. Ding, C.Q. Li, Y.J. Song, M. Ke, C.T. Ren, Acta Physico-Chimica Sinica, 29 (2013) 1289-1296.

[51] Y.J. Li, J.N. Armor, J. Catal., 150 (1994) 376-387.

[52] Y.J. Li, T.L. Slager, J.N. Armor, J. Catal., 150 (1994) 388-399.

[53] D. Kaucky, J.I. Dedecek, B. Wichterlova, Micropor. Mesopor. Mat., 31 (1999) 75-87.

[54] Y.J. Li, J.N. Armor, Appl. Catal., B, 2 (1993) 239-256.

[55] W. Cwikla-Bundyra, Pol. J. Chem. Tech., 15 (2013) 10-15.

[56] S. Chen, X. Yan, Y. Wang, J. Chen, D. Pan, J. Ma, R. Li, Catal. Today, 175 (2011) 12-17.

[57] J. Janas, W. Rojek, S. Dzwigaj, Catal. Today, 191 (2012) 32-37.

[58] O.A. Anunziata, A.R. Beltramone, F.G. Requejo, J. Mol. Catal. A: Chem., 267 (2007) 194-201.

[59] O.A. Anunziata, A.R. Beltramone, E.J. Lede, F.G. Requejo, J. Mol. Catal. A: Chem., 267 (2007) 272-279.

[60] J. Janas, S. Dzwigaj, Catal. Today, 176 (2011) 272-276.

[61] J.H. Lee, J.G. Kim, J.K. Lee, J.H. Kim, Catal. Today, 87 (2003) 35-42.

[62] Y.J. Li, J.N. Armor, Appl. Catal., B, 5 (1995) L257-L270.

[63] D. Kaucky, A. Vondrova, J. Dedecek, B. Wichterlova, J. Catal., 194 (2000) 318-329.

[64] J. Dedecek, D. Kaucky, B. Wichterlova, Top. Catal., 18 (2002) 283-290.

[65] J.T. Miller, E. Glusker, R. Peddi, T. Zheng, J.R. Regalbuto, Catal. Lett., 51 (1998) 15-22.

[66] C. Resini, T. Montanari, L. Nappi, G. Bagnasco, M. Turco, G. Busca, F. Bregani, M. Notaro, G. Rocchini, J. Catal., 214 (2003) 179-190.

[67] F. Lonyi, H.E. Solt, Z. Paszti, J. Valyon, Appl. Catal., B, 150 (2014) 218-229.

[68] J. Zhang, W. Fan, Y. Liu, R. Li, Appl. Catal., B, 76 (2007) 174-184.

[69] J.Q. Chen, S.W. Chen, R.F. Li, J.J. Zheng, Russ. J. Phys. Chem., A, 88 (2014) 1103-1112.

[70] H.P. Decolatti, A. Martinez-Hernandez, L.B. Gutierrez, G.A. Fuentes, J.M. Zamaro, Micropor. Mesopor. Mat., 145 (2011) 41-50.

[71] Y.J. Li, J.N. Armor, J. Catal., 145 (1994) 1-9.

[72] M. Mihaylov, K. Hadjiivanov, D. Panayotov, Appl. Catal., B, 51 (2004) 33-42.

[73] Y.J. Li, J.N. Armor, Appl. Catal., B, 3 (1993) L1-L11.

[74] E. Kikuchi, K. Yogo, Catal. Today, 22 (1994).

[75] Y. Nishizaka, M. Misono, Chem. Lett., 8 (1993) 1295-1298.

[76] Y. Nishizaka, M. Misono, Chem. Lett., 12 (1994) 2237-2240.

[77] M. Misono, Y. Nishizaka, M. Kawamoto, H. Kato, in: H. Chon, S.-K. Ihm, Y. S. Uh (Eds.) Stud. Surf. Sci. Catal., Elsevier, 1997, 105, 1469-1474

[78] H. Uchida, K. Yamaseki, I. Takahashi, Catal. Today, 29 (1996) 99-102.

[79] E. Garbowski, B. Pommier, M. Primet, Patent, EP0656810B1 (1994).

[80] A. Ali, W. Alvarez, C.J. Loughran, D.E. Resasco, Appl. Catal., B, 14 (1997) 13-22.

[81] A.W. Aylor, L.J. Lobree, J.A. Reimer, A.T. Bell, J. Catal., 172 (1997) 453-462.

[82] K. Okumura, J. Amano, N. Yasunobu, M. Niwa, J. Phys. Chem. B, 104 (2000) 1050-1057.

[83] H. Ohtsuka, T. Tabata, Appl. Catal., B, 26 (2000) 275-284.

[84] M. Ogura, M. Hayashi, S. Kage, M. Matsukata, E. Kikuchi, Appl. Catal., B, 23 (1999) 247-257.

[85] E. Kikuchi, M. Ogura, Res. Chem. Intermed., 26 (2000) 55-60.

[86] C. Descorme, P. Gélin, C. Lécuyer, M. Primet, J. Catal., 177 (1998) 352-362.

[87] C. Descorme, P. Gelin, C. Lecuyer, M. Primet, Appl. Catal., B, 13 (1997) 185-195.

[88] B.J. Adelman, W.M.H. Sachtler, Appl. Catal., B, 14 (1997).

[89] G. Koyano, S. Yokoyama, M. Misono, Appl. Catal., A, 188 (1999).

[90] Y.K. Park, J.W. Lee, C.W. Lee, S.E. Park, J. Mol. Catal. A: Chem., 158 (2000).

[91] B. Wen, Q. Sun, W.M.H. Sachtler, J. Catal., 204 (2001) 314-323.

[92] C.J. Loughran, D.E. Resasco, Appl. Catal., B, 7 (1995) 113-126.

[93] A. Ali, Y.H. Chin, D.E. Resasco, Catal. Lett., 56 (1998).

[94] L.J. Lobree, A.W. Aylor, J.A. Reimer, A.T. Bell, J. Catal., 181 (1999) 189-204.

[95] H. Kato, C. Yokoyama, M. Misono, Catal. Lett., 47 (1997).

[96] M. Ogura, M. Hayashi, E. Kikuchi, Catal. Today, 45 (1998) 139-145.

[97] K. Shimizu, F. Okada, Y. Nakamura, A. Satsuma, T. Hattori, J. Catal., 195 (2000).

[98] H. Ohtsuka, T. Tabata, Appl. Catal., B, 21 (1999) 133-139.

[99] C. Descorme, P. Gelin, M. Primet, C. Lecuyer, J. SaintJust, Zeolites: A Refined Tool for Designing Catalytic Sites, 97 (1995) 287-294.

[100] M. Suzuki, J. Amano, M. Miwa, Micropor. Mesopor. Mat., 21 (1998) 541-547.

[101] R. Marques, L. Mazri, S. Da Costa, F. Delacroix, G. Djega-Mariadassou, P. Da Costa, Catal. Today, 137 (2008) 179-184.

[102] M. Foix, C. Guyon, M. Tatoulian, P. Da Costa, Catal. Commun., 12 (2010) 20-24.

[103] P.A. Kumar, H.P. Ha, Catal. Lett., 136 (2010) 177-184.

[104] K.N. Rao, C.Y. Yu, H.P. Ha, Adv. Compos. Mater., 21 (2012) 123-131.

[105] S.S. Kim, S.H. Choi, S.M. Lee, S.C. Hong, J. Ind. Eng. Chem., 18 (2012) 272-276.

[106] Y.F. Li, J.J. Su, J.H. Ma, F. Yu, J.Q. Chen, R.F. Li, Catal. Commun., 65 (2015) 6-9.

[107] X. She, M. Flytzani-Stephanopoulos, J. Catal., 237 (2006) 79-93.

[108] N. Li, A.Q. Wang, W.L. Ren, M.Y. Zheng, X.D. Wang, T. Zhang, Top. Catal., 30-1 (2004) 103-105.

[109] J.C. Martin, S. Suarez, M. Yates, P. Avila, Chem. Eng. J., 150 (2009) 8-14.

[110] H.Y. Zhang, L. Li, N. Li, A.Q. Wang, X.D. Wang, T. Zhang, Appl. Catal., B, 110 (2011) 171-177.

[111] Y. Shi, H. Pan, Y.T. Zhang, W. Li, Catal. Commun., 9 (2008) 796-800.

[112] T. Nakatani, T. Watanabe, M. Takahashi, Y. Miyahara, H. Deguchi, S. Iwamoto, H. Kanai, M. Inoue, J. Phys. Chem. A, 113 (2009) 7021-7029.

[113] T. Watanabe, Y. Miki, Y. Miyahara, T. Masuda, H. Deguchi, H. Kanai, S. Hosokawa, K. Wada, M. Inoue, Catal. Lett., 141 (2011) 1338-1344.

[114] Y.H. Chin, A. Pisanu, L. Serventi, W.E. Alvarez, D.E. Resasco, Catal. Today, 54 (1999) 419-429.

[115] P. Bautista, M. Faraldos, M. Yates, A. Bahamonde, Appl. Catal., B, 71 (2007) 254-261.

[116] L. Ning, A.Q. Wang, X.D. Wang, M.Y. Zheng, R.H. Cheng, T. Zhang, Appl. Catal., B, 48 (2004) 259-265.

[117] M. Kantcheva, I. Cayirtepe, Catal. Lett., 115 (2007) 148-162.

[118] G.H. Jing, J.H. Li, D. Yang, J.M. Hao, Appl. Catal., B, 91 (2009) 123-134.

[119] B. Azambre, L. Zenboury, P. Da Costa, S. Capela, S. Carpentier, A. Westermann, Catal. Today, 176 (2011) 242-249.

[120] M.W. Kumthekar, U.S. Ozkan, J. Catal., 171 (1997) 45-53.

[121] Y.T. Wu, Y.H. Yu, V.H. Nguyen, J.C.S. Wu, Res. Chem. Intermed., 41 (2015) 2153-2164.

[122] M. Boutros, M.E. Galvez, T. Onfroy, P. Da Costa, Micropor. Mesopor. Mat., 183 (2014) 1-8.

[123] C. Hamon, O. Le Lamer, J. Saint-Just, Patent, WO15339 (1998).

[124] J.A.Z. Pieterse, R.W. Van den Brink, Patent, US0105902A1 (2006).

[125] C.M. de Correa, F. Córdoba C, F. Bustamante L, in: F.V.M.S.M. Avelino Corma, G.F. José Luis (Eds.) Stud. Surf. Sci. Catal., Elsevier, 2000, 130, 1469-1474.

[126] F. Bustamante, F. Cordoba, M. Yates, C.M. de Correa, Appl. Catal., A, 234 (2002) 127-136.

[127] J.A.Z. Pieterse, R.W. van den Brink, S. Booneveld, F.A. de Bruijn, Appl. Catal., B, 46 (2003) 239-250.

[128] J.A.Z. Pieterse, R.W. van den Brink, S. Booneveld, F.A. de Bruijn, in: E. VanSteen, M. Claeys, L.H. Callanan (Eds.) Recent Advances in the Science and Technology of Zeolites and Related Materials, 2004, pp. 2522-2526.

[129] J.A.Z. Pieterse, H. Top, F. Vollink, K. Hoving, R.W. van den Brink, Chem. Eng. J., 120 (2006) 17-23.

[130] F. Lonyi, H.E. Solt, J. Valyon, H. Decolatti, L.B. Gutierrez, E. Miro, Appl. Catal., B, 100 (2010) 133-142.

[131] I.O. Costilla, M.D. Sanchez, M. Alicia Volpe, C.E. Gigola, Catal. Today, 172 (2011) 84-89.

[132] H. Decolatti, H. Solt, F. Lonyi, J. Valyon, E. Miro, L. Gutierrez, Catal. Today, 172 (2011) 124-131.

[133] R. Serra, M.J. Vecchietti, E. Miro, A. Boix, Catal. Today, 133 (2008) 480-486.

[134] L. Gutierrez, A. Boix, J.O. Petunchi, J. Catal., 179 (1998) 179-191.

[135] L. Gutierrez, E.A. Lombardo, Appl. Catal., A, 360 (2009) 107-119.

[136] J.A.Z. Pieterse, R.W. van den Brink, S. Booneveld, F.A. de Bruijn, Appl. Catal., B, 39 (2002) 167-179.

[137] M. Ogura, Y. Sugiura, M. Hayashi, E. Kikuchi, Catal. Lett., 42 (1996) 185-189.

[138] M. Ogura, M. Hayashi, E. Kikuchi, Catal. Today, 42 (1998) 159-166.

[139] X.D. Wang, T. Zhang, X.Y. Sun, W. Guan, D.B. Liang, L.W. Lin, Appl. Catal., B, 24 (2000) 169-173.

[140] H. Berndt, F.W. Schutze, M. Richter, T. Sowade, W. Grunert, Appl. Catal., B, 40 (2003) 51-67.

[141] T. Sowade, T. Liese, C. Schmidt, F.W. Schutze, X. Yu, H. Berndt, W. Grunert, J. Catal., 225 (2004) 105-115.

[142] F. Lonyi, H.E. Solt, J. Valyon, A. Boix, L.B. Gutierrez, J. Mol. Catal. A: Chem., 345 (2011) 75-80.

[143] L.L. Ren, T. Zhang, D.B. Liang, C.H. Xu, J.W. Tang, L.W. Lin, Appl. Catal., B, 35 (2002) 317-321.

[144] X. Chen, A. Zhu, C.T. Au, C. Shi, Catal. Lett., 141 (2011) 207-212.

[145] Z.J. Li, M. Flytzani-Stephanopoulos, Appl. Catal., A, 165 (1997) 15-34.

[146] A.P. Ferreira, S. Capela, P. Da Costa, C. Henriques, M.F. Ribeiro, F.R. Ribeiro, Catal. Today, 119 (2007) 156-165.

[147] J.M. Ramallo-Lopez, F.G. Requejo, L.B. Gutierrez, E.E. Miro, Appl. Catal., B, 29 (2001) 35-46.

[148] A. Kubacka, J. Janas, B. Sulikowski, Appl. Catal., B, 69 (2006) 43-48.

[149] P. Ciambelli, D. Sannino, E. Palo, A. Ruggiero, Top. Catal., 42-43 (2007) 177-181.

[150] A.P. Ferreira, C. Henriques, M.F. Ribeiro, F.R. Ribeiro, Catal. Today, 107–108 (2005) 181-191.

[151] A. Rodrigues, P. da Costa, C. Methivier, S. Dzwigaj, Catal. Today, 176 (2011) 72-76.

[152] J.A.Z. Pieterse, S. Booneveld, Appl. Catal., B, 73 (2007) 327-335.

[153] L. Gutierrez, A. Boix, H. Decolatti, H. Solt, F. Lonyi, E. Miro, Micropor. Mesopor. Mat., 163 (2012) 307-320.

[154] E.M. Holmgreen, M.M. Yung, U.S. Ozkan, Appl. Catal., B, 74 (2007) 73-82.

[155] B. Mirkelamoglu, M.M. Liu, U.S. Ozkan, Catal. Today, 151 (2010) 386-394.

[156] B. Mirkelamoglu, U.S. Ozkan, Appl. Catal., B, 96 (2010) 421-433.

[157] P. Gawade, A.M.C. Alexander, R. Silver, U.S. Ozkan, Energy Fuels, 26 (2012) 7084-7091.

[158] P. Gawade, A.M.C. Alexander, R. Clark, U.S. Ozkan, Catal. Today, 197 (2012) 127-136.

[159] W. Suprun, K. Schaedlich, H. Papp, Chem. Eng. Technol., 28 (2005) 199-203.

[160] H.Y. Zhang, N. Li, L. Li, A.Q. Wang, X.D. Wang, T. Zhang, Catal. Lett., 141 (2011) 1491-1497.

[161] K.N. Rao, H.P. Ha, Catal. Sci. Technol., 2 (2012) 495-498.

[162] K.N. Rao, H.P. Ha, Appl. Catal., A, 433 (2012) 162-169.

[163] K.J. Lee, K.N. Rao, C.Y. Yu, S.I. Hong, H.P. Ha, Res. Chem. Intermed., 39 (2013) 1463-1479.

[164] J. Mitome, E. Aceves, U.S. Ozkan, Catal. Today, 53 (1999) 597-606.

[165] A. Rath, E. Aceves, J. Mitome, J. Liu, U.S. Ozkan, S.G. Shore, J. Mol. Catal. A: Chem., 165 (2001) 103-111.

Chapter II. Study of Pd/MOR-based system for NO_x CH_4-SCR

II.1. Introduction

From the bibliographic study presented in Chapter I, it became clear that zeolite-based catalysts containing different metals are active materials for the selective catalytic reduction of NO_x with methane (CH_4-SCR). Cobalt-based zeolites, which were firstly reported by Li and Armor as active materials for CH_4-SCR [1], have been widely study by scientific community. These studies have significantly contributed to a further understanding of the nature of the active species involved in this reaction, as well as the most important parameters that influence NO_x CH_4-SCR reaction, such as temperature, $[CH_4]/[NO]$ feed ratio, water feed content, among others. Moreover, it is known that the use of bimetallic formulations result in better catalytic performances. Many different studies involving bimetallic zeolite-based catalysts containing Co have been also conducted, mainly due to the promising results that can be obtained with this system [2-5].

However, the use of Co in a final product such as catalytic converter might be conditioned from the legal point of view. Cobalt dichloride, cobalt(II) carbonate, cobalt(II) diacetate, cobalt(II) dinitrate and cobalt(II) sulphate are chemical products which are included in the candidate list of substances of very high concern for authorisation (REACH regulation) [6]. Some of these compounds, namely cobalt(II) diacetate and cobalt(II) dinitrate, are commonly used in the preparation of Co-zeolite catalysts. Though their use is not forbidden, the EU suppliers of items that contain these substances in a concentration above 0.1 wt.% need to declare it to the appropriate authorities. This may discourage companies to invest in the development of this type of technology. Nevertheless, zeolites-based catalysts containing metals other than Co are also active NO_x CH_4-SCR, which is the case of Pd-zeolite catalysts.

Similarly to what happens with the Co-based catalysts, the use of a second metal in the Pd-based catalyst in order to enhance the catalytic performance has been widely reported. Examples of bimetallic Pd-based systems are Pd/Pt, Pd/In and Pd/Ce. Contrarily to platinum and indium, the use of cerium may represent an advantage from the economical point of view, despite the fact that this rare earth starts to present supplying limitations. Moreover, the results about Pd/Ce system presented elsewhere [7, 8] seem to be promising. Nevertheless, the role of the different Pd/Ce species in the NO_x CH_4-SCR is not yet entirely clear. The aim of the work presented in this chapter is precisely to bring further enlightening on the role of the metal species considered in this system, in particular, on the role of cerium as enhancing metal for Pd-zeolite catalysts.

Several zeolites have been reported in the literature as adequate supported for Pd-based catalysts for NO_x CH_4-SCR, namely, MOR, MFI and FER. When considering PdCe-zeolite formulations [7, 8], MOR zeolite has been shown to be a potential candidate to be considered in a commercial application, reason why it was chosen as support to be used in the present study.

In this chapter is presented a study of the preparation methods of PdCe-MOR system, including the optimisation of Pd loading, Pd introduction method, Ce loading and metal introduction method.

The addition of iron as a potential promoter of NO_x CH_4-SCR reaction for PdCe-MOR system was also considered.

Catalysts were characterised by H_2-TPR, DRS UV-Vis, PXRD, N_2 adsorption, FTIR-CO/pyridine and TEM/EDS, and their catalytic performance for NO_x CH_4-SCR was assessed using a lab-scale plant. Once optimised, the influence of catalytic tests conditions on the catalytic performance of PdCe-MOR catalyst was assessed, namely GHSV, $[CH_4]/[NO]$ ratio and water presence in the inlet feed. Finally, the optimised catalyst was test under representative conditions of a real lean-gas engine from a heavy-duty road vehicle.

II.2. Catalyst preparation

Catalysts Pd(x)-HMOR (x = 0.15, 0.5 and 0.7) and Pd(0.3)-HMOR(IE) were prepared by ion-exchange, using NH_4-MOR as starting material and following the procedure described in Annex A, section C.1.2. The same procedure was also followed in the preparation of Pd(0.3)-HMOR(IE80), but the ion-exchange temperature was 80 ºC (instead of room temperature) and the heating rate in calcination was 0.5 ºC/min (instead of 1 ºC/min). Pd(0.3)-HMOR(IWI) catalyst was prepared by incipient wetness impregnation (IWI), using NH_4-MOR as starting material and following the procedure described in Annex A, section C.1.2.

Catalysts Pd(0.3)Ce(x)-HMOR (x = 1, 2, 3, 5 and 10), Pd(y)Ce(2)-HMOR (y = 0.15, 0.3, 0.5 and 0.7) and Ce(2)-HMOR were obtained by introducing Ce by IWI, following the procedure described in Annex A, section C.1.3 and using as starting materials Pd(0.3)-HMOR(IE), Pd(y)-HMOR and NH_4-HMOR, respectively.

Ce(2)Pd(0.3)-HMOR was obtained by introducing Pd by ion-exchange (same procedure as for Pd(0.3)-HMOR), using Ce(2)-MOR as starting material.

Pd(0.3)/Ce(10)-HMOR was obtained by introducing Ce by mechanical mixture and co-grinding with CeO_2, following the procedure described in Annex A, section C.1.3 and using as starting material the Pd(0.3)-HMOR.

Table II-1 contains the chemical composition of all Pd/Ce-containing MOR catalysts considered in this chapter, obtained by ICP analysis.

Table II-1 – Chemical composition of the Pd/Ce-containing MOR catalysts obtained by ICP-OES analysis.

Catalyst	Al (wt.%)	Pd (wt.%)	Ce (wt.%)	ER_{Pd}* (%)	ER_{Ce}* (%)
Pd(0.15)-HMOR	3.3	0.16	-	2.4	-
Pd(0.3)-HMOR(IE80)	3.6	0.35	-	5.0	-
Pd(0.3)-HMOR(IE)	3.3	0.36	-	5.5	-
Pd(0.3)-HMOR(IWI)	3.1	0.30	-	4.8	-
Pd(0.5)-HMOR	3.3	0.55	-	8.4	-
Pd(0.7)-HMOR	3.3	0.75	-	11.7	-
Pd(0.3)Ce(1)-HMOR	3.3	0.35	0.8	5.4	13.7
Pd(0.3)Ce(2)-HMOR	3.4	0.29	1.9	4.3	32.2
Pd(0.3)Ce(3)-HMOR	3.5	0.39	2.8	5.6	46.0
Pd(0.3)Ce(5)-HMOR	2.9	0.27	4.8	4.8	97.1
Pd(0.3)Ce(10)-HMOR	2.8	0.27	9.1	4.8	185.3
Pd(0.15)Ce(2)-HMOR	3.2	0.15	1.8	2.4	32.9
Pd(0.5)Ce(2)-HMOR	3.3	0.52	1.7	7.9	29.6
Pd(0.7)Ce(2)-HMOR	3.2	0.70	1.9	11.3	35.0
Ce(2)-HMOR	3.3	-	2.1	-	36.6
Ce(2)Pd(0.3)-HMOR	3.2	0.42	1.8	6.8	33.6

*ER – Exchange Rate (Assuming 2+ and 3+ coordination for Pd and Ce, respectively).

II.3. Monometallic Pd-HMOR system

In this section, the optimisation of Pd-HMOR catalyst is presented based on the study of the effect of Pd loading and Pd introduction method. H_2-TPR, DRS UV-Vis and FTIR-CO were used to characterise the Pd species. Catalytic performance was assessed by steady-state tests.

II.3.1. Effect of Pd loading

Different studies were performed in order to identify the optimal metal loading on monometallic Pd-based catalysts for better NO_x CH_4-SCR performance. For instance, Ali *et al.* [9] concluded that, for Pd-HMFI and Pd-HMOR catalysts, the best performance was achieved with 0.3 wt.% Pd. However, Misono and co-workers reported that, with Pd-HMFI, the best performance was obtained with 1 wt.% Pd [10, 11]. Moreover, Ogura *et al.* [12] reported that the higher NO_2 conversion into N_2 could be over Pd-HMFI catalysts with 0.7 wt.% Pd.

It is worthy to mention that the optimal metal loading is likely to depend on the exhaust gas composition. Therefore, in this section, a detail study regarding the effect of Pd loading on mordenite is presented.

II.3.1.1. Temperature programmed reduction under H_2

H_2-TPR profiles of Pd(x)-HMOR catalysts (with x = 0, 0.15, 0.3, 0.5 and 0.7 wt.% Pd) are presented in Figure II-5. A single peak can be found between 80-180 ºC. According to literature, this peak is attributed to the reduction of Pd^{2+} in exchange position to Pd^0 [13-15]. Some authors also refer that the reduction of PdO species might take place at these temperatures [18]. However, the reduction of PdO particles in zeolites is commonly reported to occur at ambient temperature or even lower [13, 14, 20]. The integration of all peaks result in a H_2/Pd ratio close to unity (Table II-2), suggesting that practically all Pd is stabilised in the cationic form.

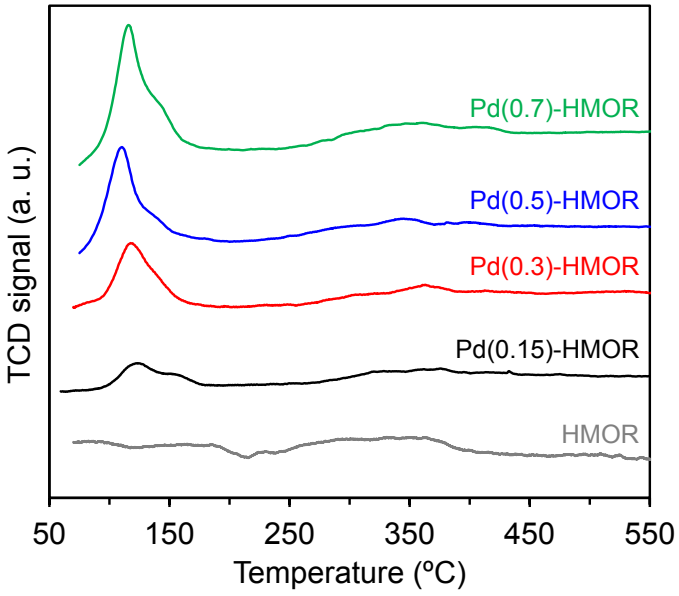

Figure II-1 – H_2-TPR profile of Pd(x)-HMOR catalysts with different Pd loadings.

Table II-2 – Quantification of H_2 consumption by peak integration of H_2-TPR profiles of Pd(x)-HMOR catalysts with different Pd loadings.

	T (ºC)	H_2/Pd	µmol H_2 /$g_{catal.}$
Pd(0.15)-HMOR	80-180	0.9	17
Pd(0.3)-HMOR	70-200	0.9	39
Pd(0.5)-HMOR	75-175	1.0	51
Pd(0.7)-HMOR	90-185	1.0	72

However, by observing in more detail the region between 80-180 ºC (Figure II-2), it is possible to realise that the reduction process can be decomposed into two different Gaussian peaks. The first peak is centred at temperatures below 125 ºC and the second one is centred at temperatures above 130 ºC.

One possible explanation for this phenomenon might be the stabilisation of Pd^{2+} ions in different exchange positions of MOR structure. Dedecek and Wichterlová [21] have conducted a detailed study regarding the nature of Co^{2+} ion sites and their occupation in a MOR structure. By using diffuse reflectance UV-Vis-NIR spectroscopy on Co-MOR samples, containing different amounts of Co introduced by ion-exchange, they managed to identify three different Co species (α, β and γ) corresponding to different three different spectral components of DRS-UV-Vis-NIR spectrum. These different Co^{2+} ions would be stabilised in specific ion-exchange sites corresponding, respectively to sites E, A and C according the nomenclature proposed by Mortier [22].

A density functional investigation conducted by Grybos *et al.* [23] focused on the stabilisation of Pd^{2+} ions in mordenite exchange positions corresponding to sites A, B, C, D and E proposed by Mortier [22]. The authors studied the role of Al distribution over the zeolite framework and concluded that, despite being more or less random, it has an effect on the stability of Pd^{2+} ions in each site, which is related to the number of bonds between Pd and O atoms directly connected to Al sites. Based on the calculation of the total energy associated to each configurations for Al ions distribution involved in the different sites, the authors concluded that, though Pd location in positions B, D and E do not represent a very large penalty in terms of total energy, positions A and C are the energetically most favourable locations for Pd^{2+} cations [23].

By H_2-TPR, it is not possible describe with the same precision the nature and location of the eventually different Pd^{2+} ions identified. Nevertheless, for each sample, the integration of the Gaussian peaks obtained allows to estimate the distribution of palladium as different Pd^{2+} ions (Figure II-2, Table II-3), even though the exact location and nature cannot be described.

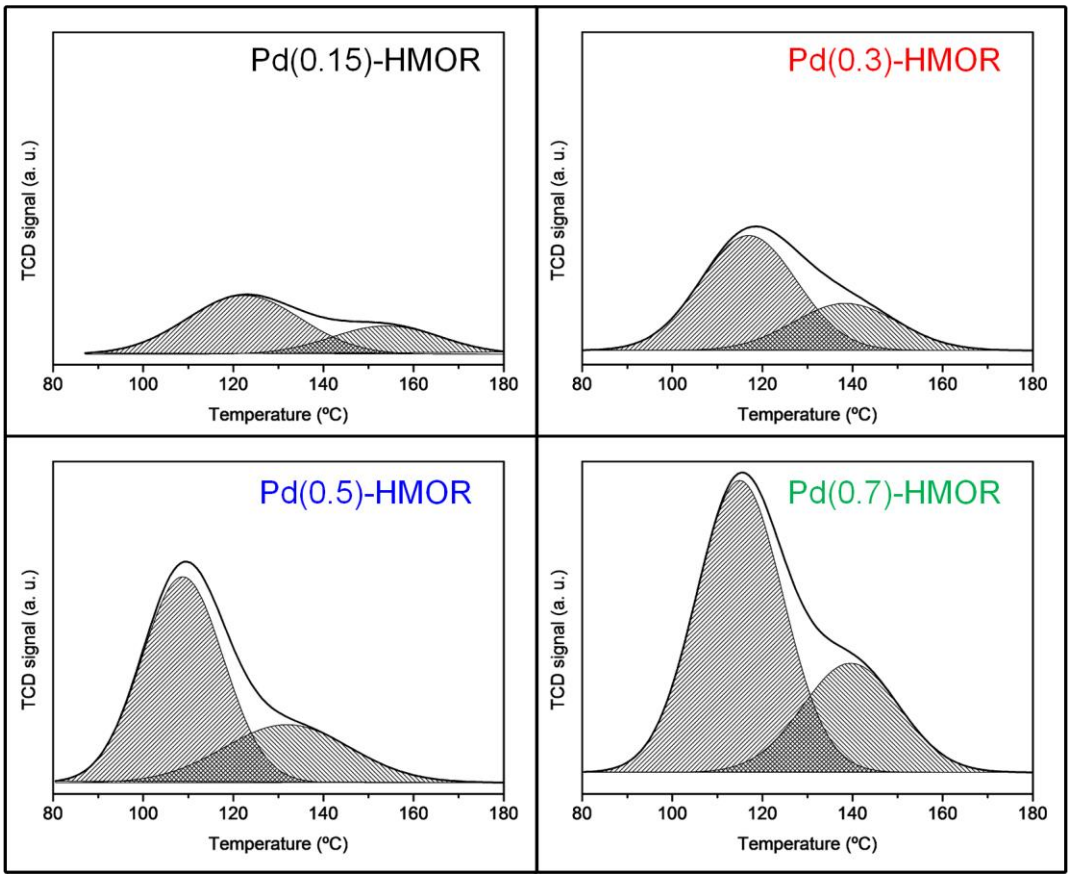

Figure II-2 – Gaussian peak fitting to H_2-TPR of Pd(x)-HMOR catalysts with different Pd loadings.

Table II-3 – Quantification of the relative amount of Pd^{2+} corresponding to both reduction process of Pd(x)-HMOR catalysts with different Pd loadings.

	Gaussian peak 1		Gaussian peak 2	
	T (ºC)	Amount of Pd^{2+}	T (ºC)	Amount of Pd^{2+}
Pd(0.15)-HMOR	121	68%	153	32%
Pd(0.3)-HMOR	118	69%	141	31%
Pd(0.5)-HMOR	109	70%	132	30%
Pd(0.7)-HMOR	114	71%	136	29%

The proportion of both species stabilised in the zeolite framework seems to be constant (approximately, 70%/30%), independently of the Pd loading. Hence, the increase of Pd loading results in an increase of both species proportionally and this could be related to the fact that, even with 0.7 wt.% Pd, the exchange rate is considerably low (11.7% - see Table II-1).

II.3.1.2. Diffuse reflectance UV-Vis spectroscopy (DRS UV-Vis)

In Figure II-3 are presented the DRS UV-Vis spectra of Pd(x)-catalysts (x = 0.15, 0.3, 0.5 and 0.7). All catalysts present bands around 300-450 nm. It is worthy to mention that for Pd(0.15)-HMOR, the band appears slightly blue shifted, around 375 nm. In this region, bands are attributed to d-d transitions of Pd^{2+} ions affected by different oxygen environments and/or presence of water (PdO, $Pd(H_2O)_4^{2+}$; $Pd(O_z)_n^{2+}$) [24]. For instance, a band around 390-410 nm has been assigned to $Pd(H_2O)_n^{2+}$ complex [25].

Also, for high Pd loadings (namely 0.7 wt.%) a band around 250 nm becomes visible. This band is attributed to charge transfer between oxygen of the support and Pd^{2+} (LMCT) [24], which intensity is also known to increase with the increase of Pd loading [25].

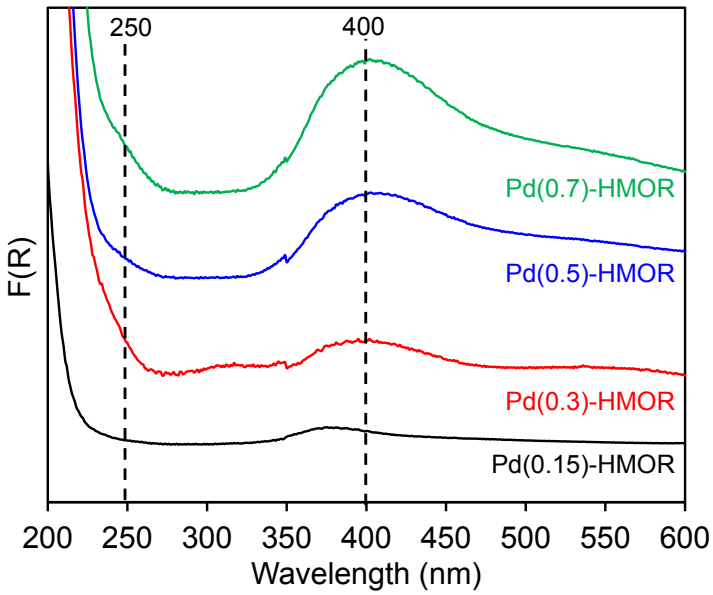

Figure II-3 – Diffuse Reflectance UV-Vis spectra of Pd(x)-HMOR catalysts with different Pd loadings.

II.3.1.3. CO adsorption followed by FTIR spectroscopy

Figure II-4 exhibits the FTIR spectra of the HMOR and Pd(x)-HMOR catalysts, containing different Pd loadings, after CO adsorption.

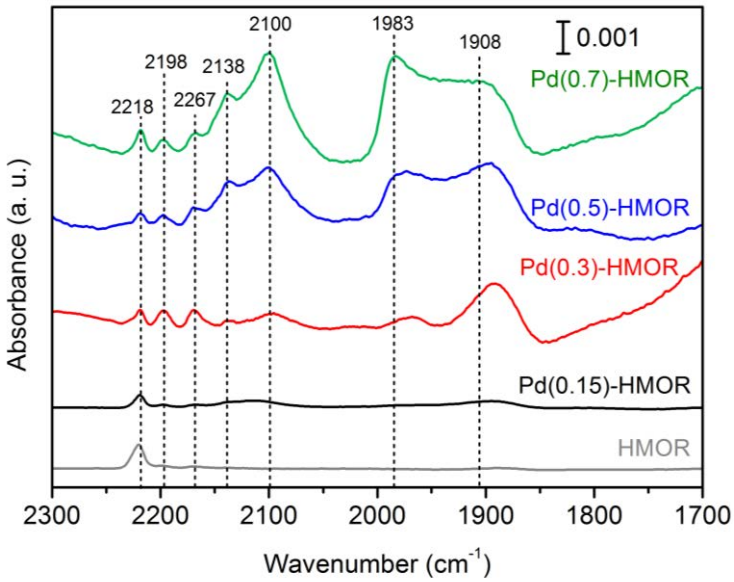

Figure II-4 – FTIR spectra of reduced catalysts at room temperature, after exposure to 5 torr of CO: HMOR and Pd(x)-HMOR catalysts with different Pd loadings.

In the Pd-free HMOR sample spectrum, it is possible to observe two bands, at 2220 and 2199 cm^{-1}, assigned to Al^{3+}-CO complexes [26-28]. Even at room temperature, these complexes are likely to be formed, resulting from the interaction of CO with extra-aluminium species (Lewis acid sites – LAS) [15, 29]. These bands are also observed in all Pd(x)-HMOR catalysts spectra.

For Pd(0.15)-HMOR, two additional bands of low intensity are observed at 2167 and 2140 cm^{-1}. According to Hadjiivanov and Vayssilov [26], IR bands in the 2215-2110 cm^{-1} spectral range have been attributed to linear Pd^{n+}-CO complexes. The band at 2167 cm^{-1} can be assigned to residual Pd cations, such as Pd^{2+} [26], or to Brønsted acid sites (BAS) [15, 29], whereas the band at 2140 cm^{-1} can be ascribed to Pd^{+}-CO or $Pd^{\delta+}$-CO complexes [15]. The presence of both bands suggest, hence, the existence of Pd cations or small positively charged Pd clusters, likely to be located in the vicinity of BAS, even after reducing the samples at 400 ºC. Bands below 2100 cm^{-1} are typical of CO interactions with metallic palladium species [26]. The band at 2114 cm^{-1} is assigned to linear Pd^{0}-CO complexes, though it appears slightly blue-shifted. The bands at 1954 and 1894 cm^{-1} are ascribed to bridging CO on Pd^{0} clusters (two-fold and three-fold co-ordinations, respectively). The fact that these three previously mentioned bands, typical from Pd^{0}-CO complexes, present a considerably low intensity is related to the also low content of palladium in the sample.

For Pd(0.3)-HMOR catalyst, all bands previously observed are also identified. Their intensity is significantly higher than the ones observed for Pd(0.15)-HMOR, which can be attributed to the higher loading of Pd in the sample. However, the band at 2221 cm^{-1}, characteristic from CO

complexes formed on LAS, also exhibits a significant increasing when compared to the one at 2219, from Pd(0.15)-HMOR. Hence, one cannot exclude the possibility of some contribution of Pd^{n+}-CO complexes (for instance, due to the presence of bulk carbonyls of Pd^{2+}), since this band appears within the spectral range of such species [26].

For Pd(0.5)-HMOR and Pd(0.7)-HMOR the same bands previously mentioned can be also observed in the spectra. For both catalysts, the bands near 2220 cm^{-1} are now considerably less intense when compared to the bands ascribed to Pd^0-CO complexes (around 2100 cm^{-1}, for linear CO complexes on Pd^0, and the other two bands at lower wavenumbers, for bridging CO-Pd^0 complexes). This is likely due to the higher contents of palladium in these samples which, once reduced, tend to form more metallic palladium species, leaving lower relative quantity of palladium as Pd^{n+} species in the zeolite. It is also worthy to mentioned that both bands ascribe to bridging CO-Pd^0 complexes are blue-shifted due to the increase of Pd, from 0.3 to 0.7 wt.% (two-fold coordination goes from 1949 to 1983 cm^{-1} and three-fold coordination goes from 1892 to 1908 cm^{-1}), which corresponds to the fact that these species are more stable in these catalysts.

II.3.1.4. Active species on Pd-HMOR for NO_x CH_4-SCR

The catalytic performance of Pd(x)-HMOR catalysts for NO_x CH_4-SCR was assessed in steady-state test conditions (Figure II-5). Between 300-450 ºC it is possible to observe that Pd(0.15)-HMOR presents slightly lower NO_x conversion values than the other catalysts, likely due to the low Pd loading in this catalyst (exchange rate = 2.4 %).

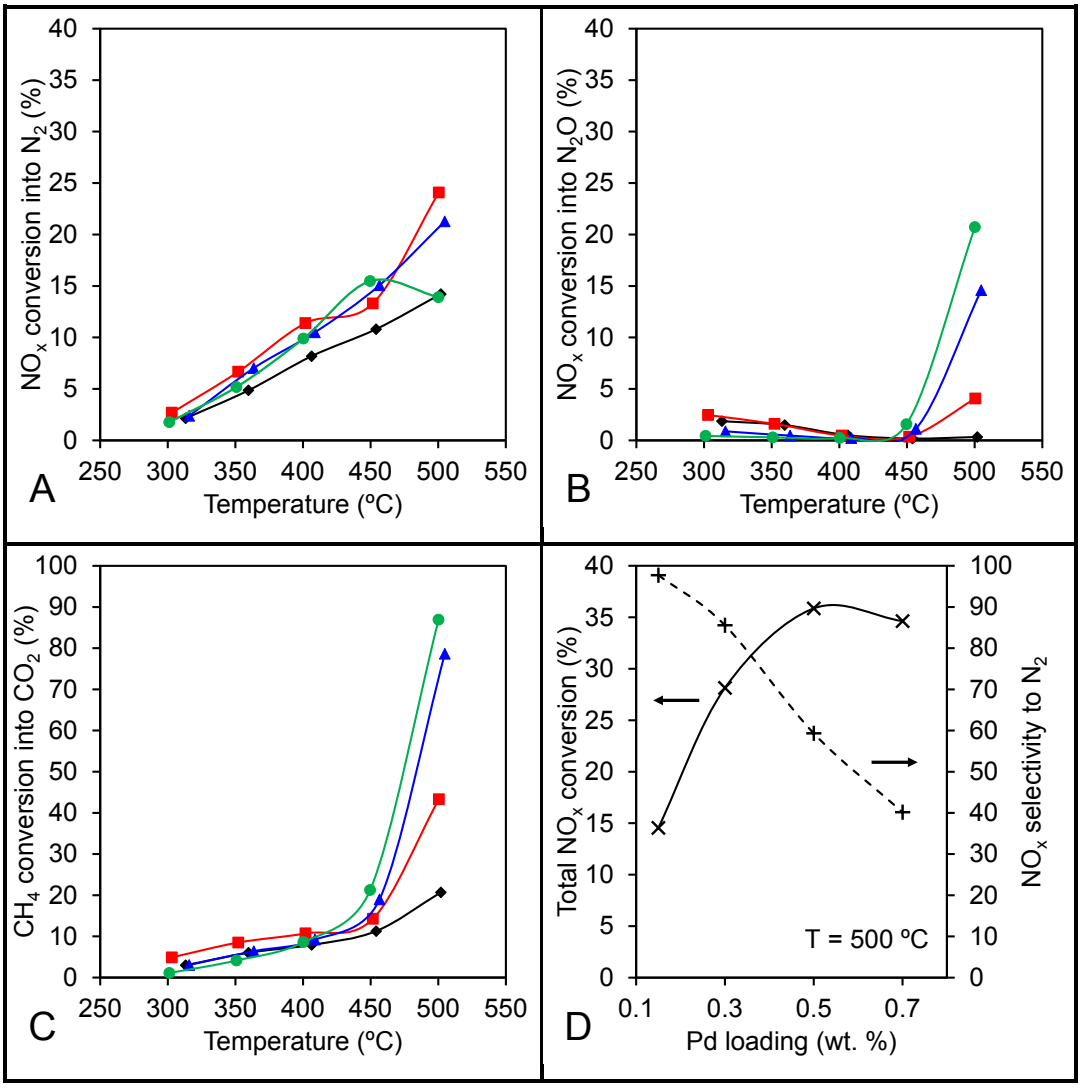

Figure II-5 – NO_x conversion into N_2 (A) and into N_2O (B), CH_4 conversion into CO_2 (C) and total NO_x conversion vs. NO_x selectivity to N_2 (D) for Pd(0.15)-HMOR (♦), Pd(0.3)-HMOR (■), Pd(0.5)-HMOR (▲) and Pd(0.7)-HMOR (●). Conditions: 1000 ppm NO, 1000 ppm CH_4, 7 vol.% O_2 and GHSV of 40000 h^{-1}.

For Pd loadings between 0.3-0.7 wt.%, all catalysts present similar values of NO_x and CH_4 conversion values, with practically no formation of N_2O. However, at 500 ºC, it is possible to observe a decrease on NO_x conversion to N_2 when the Pd loading increases from 0.3-0.7 wt.%, followed by both an increase of N_2O the formation and CH_4 conversion. NO_x selectivity to N_2, which is almost 100 % for Pd(0.15)-HMOR, is decreasing with the increase of Pd loading (Figure II-5D).

The best catalytic performance can be achieved by maximising both NO_x total conversion and NO_x selectivity to N_2. However, these two parameters evolve in opposite directions, when Pd loading is

increased. At 500 ºC, total NO_x conversion is being increased by the increase of Pd loading, but N_2O formation is being promoted instead of N_2. In fact, above 0.3 wt.% Pd, catalysts present lower NO_x conversion in N_2 than Pd(0.3)-HMOR. On the other hand, though Pd(0.15)-HMOR presents a very high NO_x selectivity to N_2, the conversion is considerably low when compared, for instance, with Pd(0.3)-HMOR. Based on these arguments, one can state the 0.3 wt.% Pd corresponds to optimal Pd loading.

From the combined analysis of the different characterisation results of the monometallic Pd-MOR catalysts, it was possible to conclude that all Pd dispersed as Pd^{2+} ions in exchange positions. Pd^{2+} ions have been identified as active species for NO_x CH_4-SCR in different Pd-based catalysts. For instance, Marques *et al.* [30] concluded that Pd^{2+} surrounded by oxygen atoms is the active phase for deNO_x process using CH_4 as reductant, when considering Pd/alumina catalysts. Even considering bimetallic formulations, namely Pd/Co/alumina, Pd^{2+} species are still the major active sites for the reaction [31].

Moreover, it seems to exist two different forms of Pd in cationic form, likely to correspond to Pd^{2+} in different exchange positions. The distribution of Pd^{2+} ions by these two different positions seems to be constant and independent of Pd loading, which is likely to be related to the low Pd exchange rate, even with 0.7 wt.% Pd. It is likely that such different type of cations have different activities and interact differently with the reactants. For instance, Kaucký *et al.* [32] concluded that cobalt cations located in different positions of the MOR and FER zeolites have different activity for NO_x CH_4-SCR. One cannot exclude a similar effect for the current system.

Palladium-loaded catalysts are also used as hydrocarbon oxidation catalysts [33, 34] and the increasing of Pd loading is known to promote CH_4 direct combustion. In this study, this was also observed (Figure II-5C). However, this increase in CH_4 conversion is often associated with the increase of PdO species, which is not the case of the studied catalysts. Instead, it is likely that one of the Pd species identified in the zeolite may play a role in the CH_4 direct combustion. Other possibility is that one of this species might be involved in the formation of N_2O, which can also be associated to the CH_4 direct combustion. Descorme, *et al.* [35] presented evidences of the existence of two different nitrosyl complexes formed with Pd cations in different locations of MOR zeolite. Pd mononitrosyl complexes would sit in the main channels of MOR and would play responsible for the NO_x SCR activity, whereas Pd dinitrosyl complexes, formed in the pocket sides of MOR, would be inactive for the reaction.

In summary, palladium is stabilised on Pd(x)-HMOR catalysts in the form of two distinguish cationic species, likely in different locations. Under the test conditions considered in this work, the best catalytic performance is achieved with 0.3 wt.% Pd.

II.3.2. Effect of Pd introduction method

Different methods can be employed in order to stabilise metal in the zeolite supports. When considering palladium, methods such as ion-exchange [10] of incipient wetness impregnation technique [9] can be used. In this section, the comparison between three different samples of Pd(0.3)-HMOR obtained by three different methods (ion-exchange at room temperature, ion-exchange at 80 ºC and incipient wetness impregnation) is performed.

II.3.2.1. Temperature programmed reduction under hydrogen (H_2-TPR)

H_2-TPR profiles of Pd-HMOR catalysts containing 0.3 wt.% of Pd, prepared by three different methods, are presented in Figure II-6.

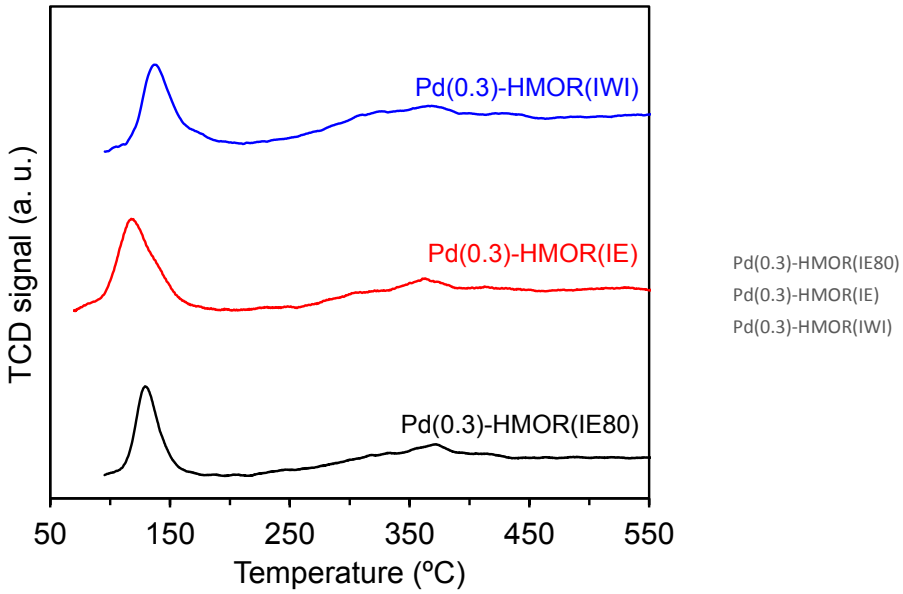

Figure II-6 – H_2-TPR profiles of Pd(0.3)-HMOR catalysts prepared by different methods.

In all profiles, it is possible to identify a single reduction peak between 70 - 200 ºC, corresponding to the reduction of Pd^{2+} in exchange position to Pd^0 [13-15].The integration of the peaks (Table II-4) shows an H_2/Pd ratio similar to the unity, which is consistent with approximately all Pd in the samples being presented as Pd^{2+} ions in exchange positions.

Table II-4 – Quantification of H_2 consumption by peak integration of H_2-TPR profiles of Pd(0.3)-HMOR prepared by different methods.

	T (ºC)	H_2/Pd	µmol H_2 /$g_{catal.}$
Pd(0.3)-HMOR(IE80)	85-180	0.8	26
Pd(0.3)-HMOR(IE)	70-200	0.9	39
Pd(0.3)-HMOR(IWI)	85-200	1.0	29

As it was shown before for Pd(x)-HMOR catalysts with different Pd loadings, the reduction peak at observed was actually composed by to different reduction processes (Gaussian peaks), likely to correspond to Pd^{2+} ions in different exchange positions. The same deconvolution procedure was applied to the H_2-TPR profiles presented on Figure II-6 and the relative distribution of Pd^{2+} ions are presented in Table II-5. It should be noted that the Pd(0.3)-HMOR(IWI) possesses a considerably higher amount of Pd^{2+} ions reducible at high temperature.

Table II-5 – Quantification of the relative amount of Pd^{2+} corresponding to both reduction process of Pd(0.3)-HMOR prepared by different methods.

	Gaussian peak 1		Gaussian peak 2	
	T (ºC)	Amount of Pd^{2+}	T (ºC)	Amount of Pd^{2+}
Pd(0.3)-HMOR(IE80)	129	78%	144	22%
Pd(0.3)-HMOR(IE)	118	69%	141	31%
Pd(0.3)-HMOR(IWI)	137	58%	152	42%

II.3.2.2. Diffuse reflectance UV-Vis spectroscopy (DRS UV-Vis)

Figure II-7 illustrates the DRS UV-Vis spectra of Pd-HMOR catalysts containing 0.3 wt.% Pd, prepared by the three different methods previously mentioned.

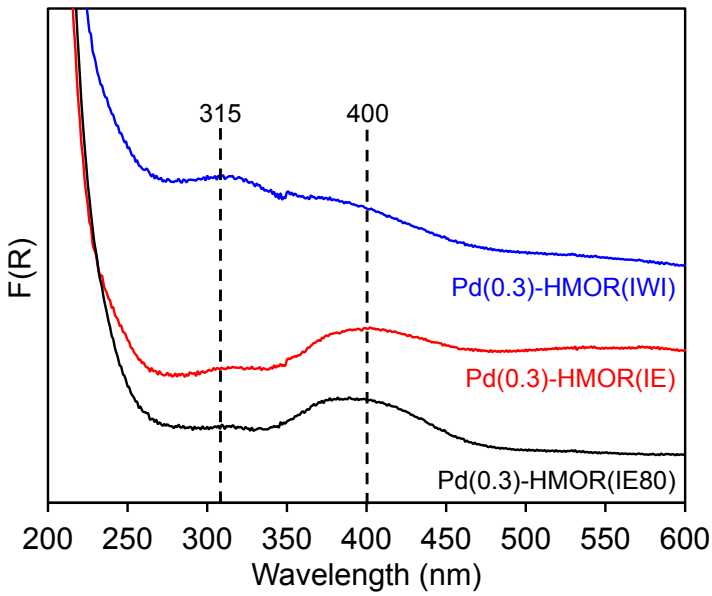

Figure II-7 – Diffuse Reflectance UV-Vis spectra of Pd(0.3)-HMOR catalysts prepared by different methods.

All catalysts present bands around 300-450 nm attributed to d-d transitions of Pd^{2+} ions [24, 25]. Both catalysts prepared by ion-exchange exhibit very similar spectra. However, the spectrum from Pd(0.3)-HMOR(IWI) presents a much pronounced band around 315 nm. This band might correspond to Pd^{2+} ions in different exchange positions from the ones characterised by the band at 400 nm, which is in agreement with the H_2-TPR characterisation.

II.3.2.3. NO_x CH_4-SCR

The catalytic performance for NO_x CH_4-SCR reaction of Pd(0.3)-HMOR catalysts prepared by different methods was assessed (Figure II-8).

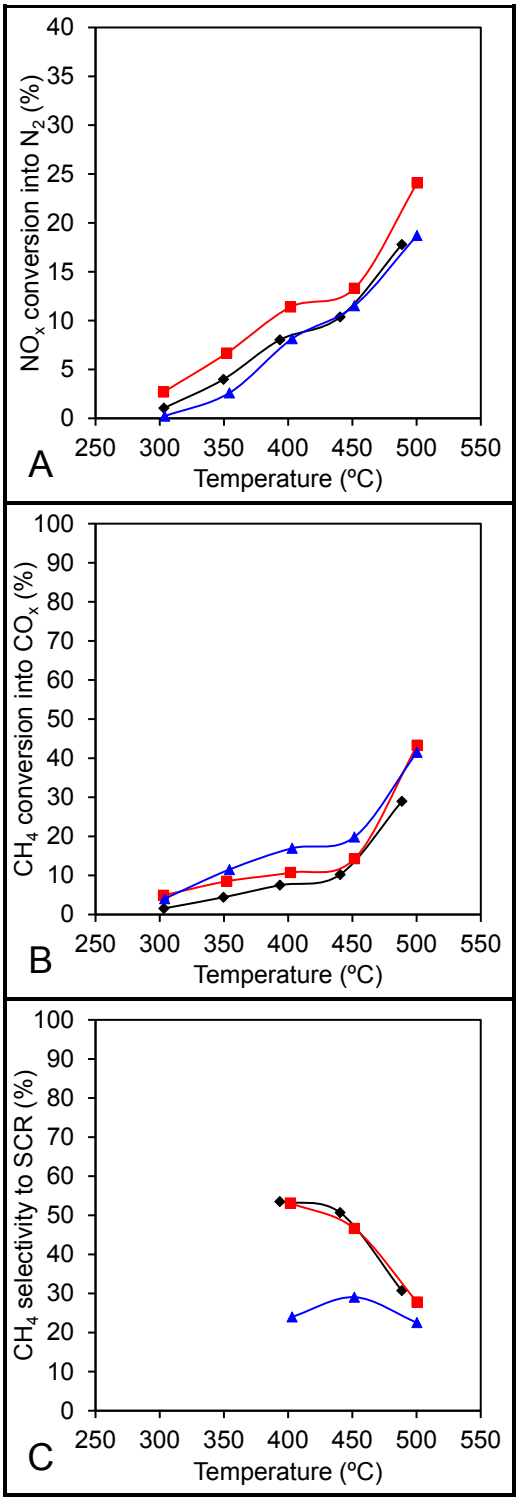

Figure II-8 – NO_x conversion into N_2 (A), CH_4 conversion into CO_x (B) and CH_4 selectivity to NO_x SCR reaction (C) over Pd(0.3)-HMOR catalysts prepared by different methods: Pd(0.3)-HMOR(IE80) (♦), Pd(0.3)-HMOR(IE) (■) and Pd(0.3)-HMOR(IWI) (▲). Conditions: 1000 ppm NO, 1000 ppm CH_4, 7 vol.% O_2 and GHSV of 40000 h^{-1}.

N_2O and CO formation are negligible (except at 500 ºC, where CH_4 conversion into CO is *ca.* 10% for all catalysts). The three catalysts exhibit NO_x conversion values very similar. However, Pd(0.3)-HMOR(IE) exhibits slightly higher values. Moreover, Pd(0.3)-HMOR(IWI) exhibits slightly higher CH_4 conversion values, when compared to the remaining catalysts. It should also be highlighted that Pd(0.3)-HMOR(IWI) exhibits a CH_4 selectivity towards SCR considerably lower than both catalysts prepared by ion-exchange – CH_4 selectivity towards SCR is only presented for temperatures above 350 ºC because the large error associated to the conversions at lower temperatures may result in a misrepresentation of the trend (all the CH_4 selectivity profiles hereafter will only be presented for temperatures higher than 350 ºC). This result might be explain due to the stabilisation of Pd^{2+} ions species in a specific position that might contribute to the direct CH_4 conversion instead of SCR, which is in agreement with the evidences obtained by H_2-TPR and DRS UV-Vis.

Previous works have shown the importance of the preparation methods in the catalytic performance of Pd-based catalysts for NO_x SCR. For instance, Marques *et al.* [30] concluded that the use of $Pd(NH_3)_4(NO_3)_2$ precursor in the preparation of a Al_2O_3-supported palladium catalysts leads to catalysts more active for NO_x CH_4-SCR, when compared to the use of other Pd precursors. In the present study, it is shown that the method chosen for the introduction of Pd is also an important parameter to take into consideration, when preparing active catalysts for NO_x SCR, namely zeolite-based catalysts.

In summary, the preparation method can influence the distribution of Pd^{2+} species in mordenite and consequently, the catalytic performance. By introducing palladium through ion-exchange (namely at room temperature), a better catalytic performance is obtained.

In the next section, the effect of cerium as co-metal in bimetallic Pd-based formulations is addressed. The monometallic Pd-MOR catalysts in base of such study were prepared by considering the inputs from the optimisation resulted from the study of Pd loading and Pd introduction method.

II.4. The enhancing effect of Cerium on Pd-MOR system

The use of a second metal in bimetallic Pd-based zeolite formulations is known to enhance the catalytic performance for NO_x CH_4-SCR [4, 7, 8, 29]. Particularly, the use of cerium has been reported as capable of promoting the activity and stability of Pd-MOR catalysts [7, 8]. This section is dedicated to the study of the effect of Ce as co-metal in Pd-MOR system, in order to further understand its role in NO_x CH_4-SCR reaction.

II.4.1. Effect of Ce loading

Though cerium is known to promote NO_x CH_4-SCR reaction over Pd-MOR catalysts, the effect of its loading in the system was not yet reported. This section addresses this point.

II.4.1.1. Temperature programmed reduction under H_2 (H_2-TPR)

In Figure II-9 are presented the H_2-TPR profiles of Pd(0.3)-HMOR and Pd(0.3)Ce(x)-HMOR catalysts with different Ce loadings.

For the catalysts containing 1, 2 and 3 wt.% Ce, in the region 70-220 ºC, it is possible to observe the existence of a peak composed by two reduction processes, one centred at *ca.* 120 ºC and another more close to 150 ºC. Similarly to Pd(x)-HMOR catalysts, one could say that both peaks correspond to Pd^{2+} ions in different exchange positions. However, for Pd(0.3)Ce(2)-HMOR, the integration of the peaks in the region 70-220 ºC corresponds to H_2/Pd higher than one. This can be explained by the presence of surface Ce^{4+} species, which are known to be reduced at this temperatures [36]. Hence, for these catalysts, it is likely that the second reduction process at low temperature correspond to the presence of surface Ce^{4+} species.

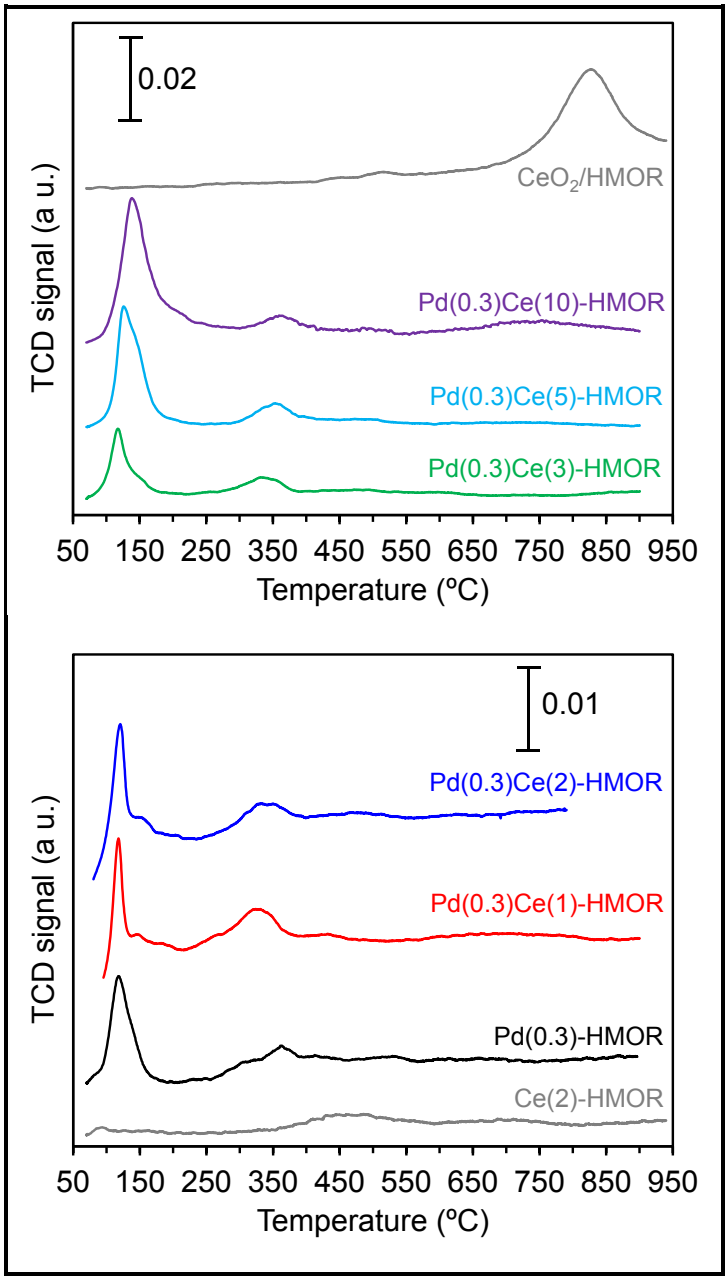

Figure II-9 – H_2-TPR profile of Pd(0.3)Ce(x)-HMOR catalysts with different Ce loadings, Ce(2)-HMOR, Pd(0.3)-HMOR and CeO_2/HMOR.

For Pd(0.3)Ce(5)-HMOR, it is possible to observe that this second reduction process is more intense and appears more overlapped with the first reduction process, which is explained by the increase of Ce loading. It is worthy to mention that the profile of Pd(0.3)Ce(10)-HMOR exhibits the reduction peak attributed to Ce^{4+} species at slightly higher temperature, closest to 200 ºC.

A second reduction peak can be identified between 225-560 ºC in all catalysts containing Ce. This peak is attributed to the reduction of CeO_2 species in interaction with Pd [17]. This interaction between species is typical from ceria, which is known to form “bronzes” with noble metals, namely with Pd [36].

In the reduction profile of Pd(0.3)Ce(10)-HMOR, it is also possible to observe a third wide reduction peak at 560-920 ºC. This peak is attributed to the reduction of bulk oxygen of CeO_2 [36]. In this case, the existence of higher amounts of CeO_2 species can be explained by the high loading of Ce. The reduction peaks corresponding to this species can be clearly observed in the reduction profile of CeO_2/HMOR sample, obtained by mechanical mixture of bulk CeO_2 with HMOR zeolite in proportion 1:2.

Table II-6 – Quantification of H_2 consumption by peak integration of H_2-TPR profiles of Pd(0.3)Ce(x)-HMOR catalysts with different Ce loadings.

	Peak 1			Peak 2			Peak 3		
	T (ºC)	H_2/Pd	µmol H_2 /$g_{catal.}$	T (ºC)	H_2/Ce	µmol H_2 /g_{catal}	T (ºC)	H_2/Ce	µmol H_2 /g_{catal}
Pd(0.3)Ce(1) -HMOR	100-210	1.0	32	250-560	0.39	22	-	-	-
Pd(0.3)Ce(2) -HMOR	95-215	1.4	39	240-560	0.27	37	-	-	-
Pd(0.3)Ce(3) -HMOR	70-220	1.4	50	225-560	0.14	29	-	-	-
Pd(0.3)Ce(5) -HMOR	75-220	4.1	103	250-560	0.10	35	-	-	-
Pd(0.3)Ce(10) -HMOR	70-270	6.0	152	290-560	0.02	15	560-920	0.06	41

In summary, the increasing of cerium loading results in an increasing of surface Ce^{4+} species, the relative amount of CeO_2 species (from the total Ce species) interacting with palladium (peak 2) decreases.

II.4.1.2. Diffuse reflectance UV-Vis spectroscopy (DRS UV-Vis)

Figure II-10 illustrates the DRS UV-Vis spectra of the Pd(0.3)-HMOR and Pd(0.3)Ce(x)-HMOR catalysts with different Ce loadings.

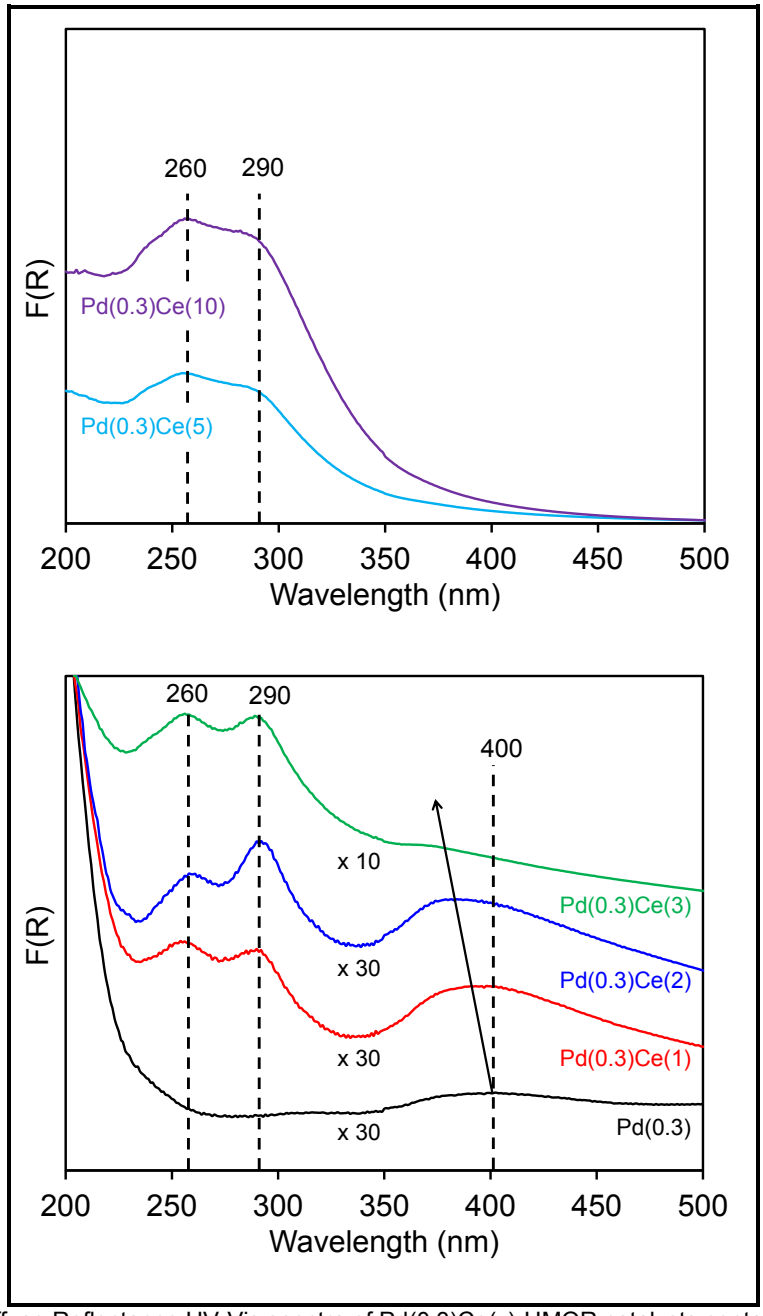

Figure II-10 – Diffuse Reflectance UV-Vis spectra of Pd(0.3)Ce(x)-HMOR catalysts containing different Ce loadings.

For the bimetallic catalysts, two additional bands can be identified in the spectra when compared to the Pd(x)-HMOR catalysts spectra. The first band, at 260 nm, corresponds to the transition 4f-5d of Ce^{3+} species [37, 38]. The second band, at 290 nm, is characteristic of the charge transfer from O^{2-} to Ce^{4+} in CeO_2 clusters [38]. It is possible observe that the increase of Ce loading causes a blue-shift in the band around 400 nm, attributed to the Pd^{2+} species – for Pd(0.3)Ce(3)-HMOR

the band is centred at *ca.* 380 nm. This behaviour might be related to the existence of an interaction between Pd and Ce species, which increases with the Ce loading. Evidences of this interaction were already observed by H_2-TPR. For Ce loadings above 5 wt.%, the bands corresponding to Ce species become so intense that it is not possible to clearly observe the band around 400 nm anymore.

II.4.1.3. Transmission electron microscopy (TEM/EDS)

H_2-TPR and DRS UV-Vis results previously presented evidenced an interaction between CeO_2 and Pd species. An attempt to understand if such interaction is likely to be related to the proximity of such species, TEM/EDS analyses were performed on Pd(0.3)-HMOR, Pd(0.3)Ce(2)-HMOR and Ce(2)-HMOR catalysts. Images are exhibited in Figure II-11.

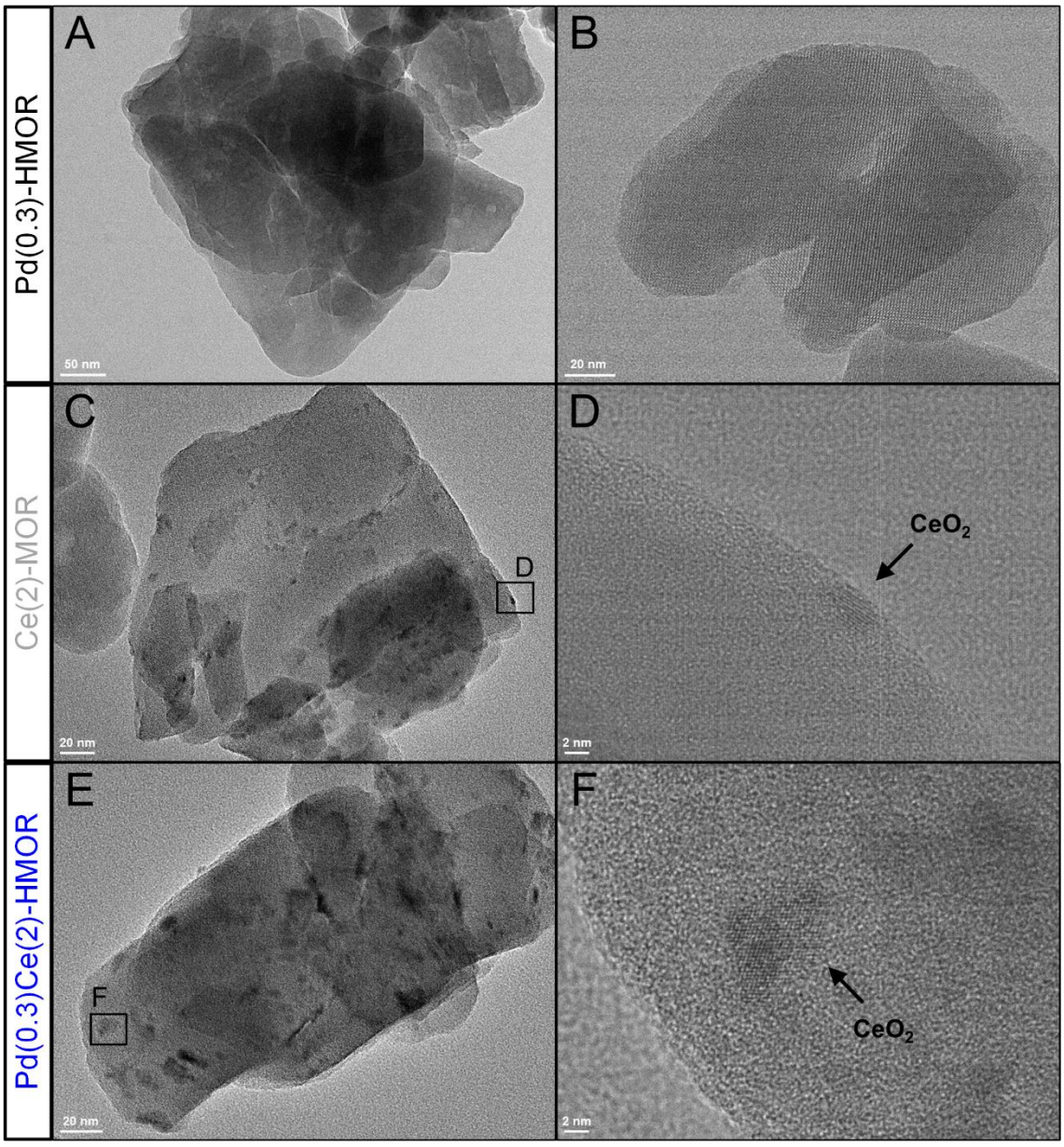

Figure II-11 – TEM images: Pd(0.3)-HMOR (A, B), Ce(2)-HMOR (C, D) and Pd(0.3)Ce(2)-HMOR (E, F).

For Pd(0.3)-HMOR, no metal particles were observed in the TEM images collected (Figure II-11A, B). Additionally, energy-dispersive X-ray spectroscopy (EDS) analyses did not detect Pd in the sample. Since it is known that Pd is actually present in the sample, the fact that it was not observed by TEM/EDS is likely to be related with the limit detection of this technique that does not allow to detect low amounts of Pd in samples where it is well dispersed.

For Ce(2)-HMOR, several metal clusters can be observed in TEM images (Figure II-11C). This clusters present an irregular shape, making difficult the quantification of their size. Nevertheless, one can note that the order of magnitude of such clusters (~10^1 nm) is clearly lower than the order of magnitude of the zeolite particle size (~10^2 nm). EDS analyses confirmed these are cerium clusters and, by using high resolution TEM (HRTEM), it was possible to quantify the distance between lattice planes in 2.7 and 3.1 Å, typical from CeO_2 (ICDD 00-034-0394).

Finally, for Pd(0.3)Ce(2)-HMOR, similar metal clusters observed in Ce(2)-HMOR were also present. EDS analyses allow to confirm these are also cerium clusters. Moreover, like in Pd(0.3)-HMOR, Pd was not identified by EDS.

Results were not able to confirm any evidence of possible interactions between CeO_2 and Pd species. Moreover, no differences were detected on CeO_2 distribution between Ce(2)-HMOR and Pd(0.3)Ce(2)-HMOR.

II.4.1.4. Quantification of acid sites by pyridine-FTIR spectroscopy

The role of acidity, namely Brønsted acid sites (BAS), in zeolites-based catalysts for NO_x CH_4-SCR have been widely studied and reported in literature [39-42]. In order to understand the eventual impact of metal introduction in the acidity, pyridine adsorption and consecutive thermodesorption was performed in Pd(0.3)-HMOR and Pd(0.3)Ce(2)-HMOR, follow by *in situ* FTIR.

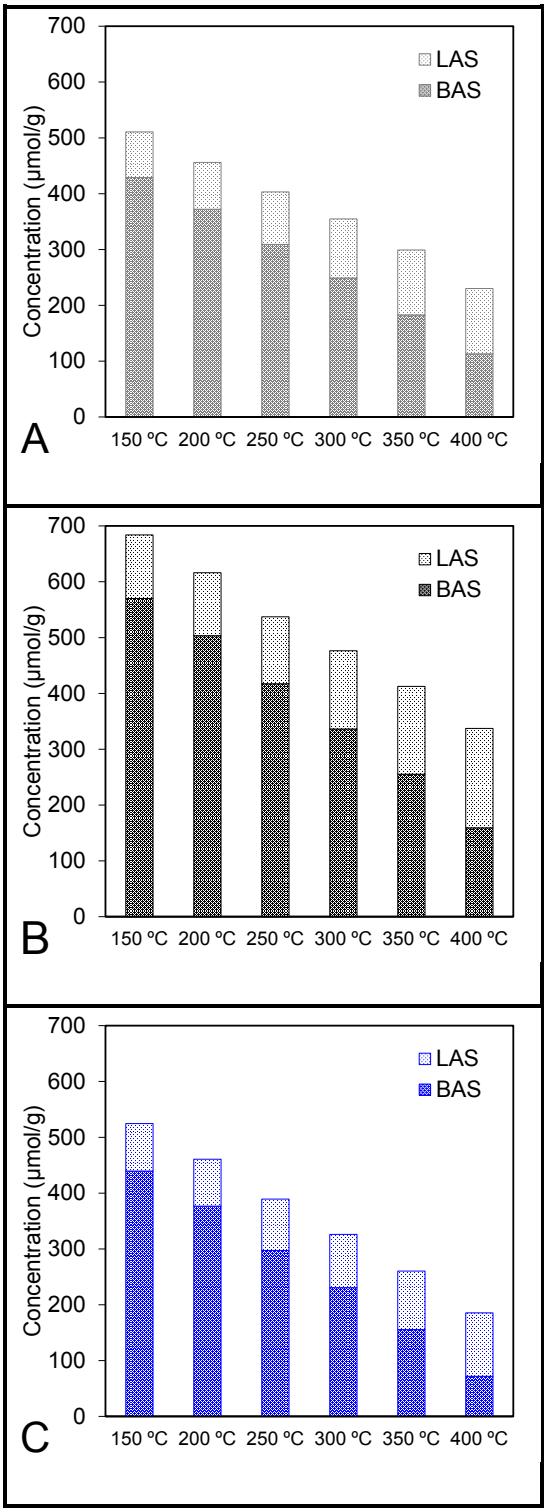

Figure II-12 – Quantification of acid sites of HMOR (A), Pd(0.3)-HMOR (B) and Pd(0.3)Ce(2)-HMOR (C) by pyridine thermodesorption followed by FTIR.

The quantification of total number of BAS and Lewis acid sites (LAS) was performed through the integration of IR bands around 1545 and 1455 cm^{-1}, respectively, and considering the molar extinction coefficients reported elsewhere [43]. The results are presented in Figure II-12, together in the quantification of the acids sites of a metal free HMOR sample, obtained by applying the same calcination procedure considered for PdCe-HMOR samples, after cerium introduction (see experimental part – Annex A, section C.1.3).

It is possible to observe that Pd(0.3)-HMOR exhibits significantly higher amount of BAS (503 μmol/g, 200 ºC) compared to HMOR (372 μmol/g, 200 ºC), when it should have lower (due to stabilisation of Pd^{2+} ions that represents a loss of H^+). However, it should be highlighted that, when performing the calcination procedure to obtain HMOR (8h, at 500 ºC), it is likely that part of -OH groups were removed in further extent comparing to the calcination of Pd(0.3)-HMOR (1h, at 500 ºC). Notwithstanding, Pd(0.3)Ce(2)-HMOR exhibits an amount of BAS (377 μmol/g, 200 ºC) similar to the one of HMOR (within the experimental error). Assuming that all palladium is stabilised as Pd^{2+} ions in exchange positions (which is supported by H_2-TPR), only a slight loss of acidity would be due to the Pd introduction since the maximum exchange rate of Pd in Pd(0.3)Ce(2)-HMOR is less than 4% (Table II-1). If a considerable part of cerium was likely to be stabilised as Ce^{3+} in exchange, one would expect a significant decrease on acidity, since the maximum exchange rate of Ce in Pd(0.3)Ce(2)-HMOR is around 30%. Hence, the fact that HMOR and Pd(0.3)Ce(2)-HMOR present similar amounts of BAS suggests that Ce^{3+} ions are definitely not the predominant Ce species that is stabilised in the zeolite framework but, instead, cerium oxides (as evidenced by TEM).

In summary, one can say that few modifications are verified in the acidity strength of the zeolite framework, due to the addition of both metals, mainly due to the low content of Pd added and to the fact that cerium is more likely to be stabilised as cerium oxide species.

II.4.1.5. Powder X-ray diffraction (PXRD)

Since the preparation of metal-containing zeolites involves several steps that might damage the structure, it is important to have an idea of the crystallinity of the material after the metal introduction, which can be assessed by the analysis of the PXRD patterns. Moreover, PXRD can be useful in the identification of some metal species, in particular to metal oxides and metallic particles. In the case of Pd and Ce species, these can be CeO_2 [44, 45], PdO or Pd^0 [46]. Figure II-13 illustrates the PXRD patterns collected for HMOR, Pd(0.3)-HMOR and Pd(0.3)Ce(2)-HMOR.

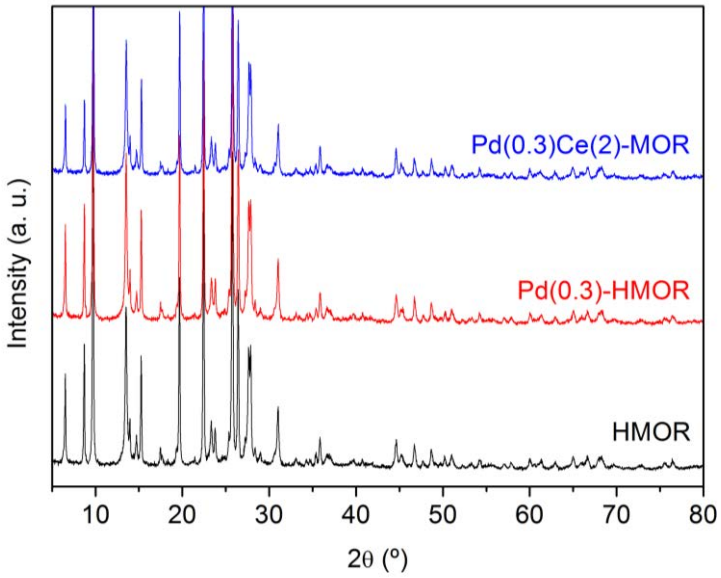

Figure II-13 – PXRD patterns of HMOR, Pd(0.3)-HMOR and Pd(0.3)Ce(2)-HMOR catalysts.

All peaks presented in the diffractograms correspond to MOR structure and no peaks from Pd/Ce species are visible. The absence of Pd^0 was expected since the quantification of H_2 consumption in H_2-TPR profile for Pd(0.3)-HMOR is close the unity (see Figure II-6, section II.3.1.1), . Likely in TEM/EDS analysis, PdO was not identify in the Pd-based catalysts. Though this can be explained by all Pd being dispersed as Pd^{2+} ions in exchange position, it should be noted that the lower Pd loading (0.3 wt.%) makes it unlikely to detect PdO species by XRD. Finally, no diffraction peaks correspond to CeO_2 are observed in the XRD pattern of Pd(0.3)Ce(2)-HMOR, though it has been clearly identified by TEM/EDS analysis (see Figure II-11E, section II.4.1.3). In fact, TEM showed that the CeO_2 particles presented in the zeolite are about one order of magnitude smaller than the zeolite particles. It is been reported in the literature that when CeO_2 is well dispersed in zeolites, no diffraction peaks are observed [47], which could be the case.

The crystallinity of the metal-containing catalysts was estimated through the integration of diffractograms between 16-30 º. The value obtained for HMOR was assumed to be 100% and it was used as reference in the calculation of the crystallinity (Table II-7).

Table II-7 – Crystallinity of Pd(0.3)-HMOR and Pd(0.3)Ce(2)-HMOR catalysts (reference – HMOR).

Sample	Crystallinity (%)
Pd(0.3)-HMOR	95
Pd(0.3)Ce(2)-HMOR	97

In summary, no Pd/Ce are evidenced by PXRD. Also, no loss of crystallinity due to the metals introduction is reported.

II.4.1.6. Nitrogen adsorption

Textural parameters, namely, porous volume (V_p) and external surface area (S_{ext} - not corresponding to the micropores) of HMOR, Pd(0.3)-HMOR and Pd(0.3)Ce(x)-HMOR catalysts were estimated through N_2 adsorption (not corresponding to the micropores), by applying the t-plot method, considering the reference isotherm Harkins-Jura [48]. Surface area estimated by Brunauer-Emmett-Teller (BET) method is also presented as indicative value.

Table II-8 – Textural parameters of HMOR, Pd(0.3)-HMOR and Pd(0.3)Ce(x)-HMOR.

	$V_{p,\ micro}$ (cm^3/g)	$V_{p,\ meso}$ (cm^3/g)	S_{ext} (m^2/g)	S_{BET} (m^2/g)
HMOR	0.207	0.081	29	470
Pd(0.3)-HMOR	0.215	0.074	27	507
Pd(0.3)Ce(2)-HMOR	0.203	0.086	31	486
Pd(0.3)Ce(5)-HMOR	0.186	0.072	24	440
Pd(0.3)Ce(10)-HMOR	0.173	0.067	21	408

It is possible to observed that the introduction of palladium and cerium (up to 2 wt.%) does not cause significant textural modifications. However, for cerium loadings higher than 5 wt.%, the micro and mesoporous volume decreases, which suggest blockage probably related to the formation of CeO_2 particles.

II.4.1.7. CO adsorption followed by FTIR spectroscopy

In Figure II-14 the CO-FTIR spectra of HMOR and Pd(0.3)-HMOR previously show in Figure II-4 are compared in the ones from Pd(0.3)Ce(2)-HMOR and Ce(2)-HMOR.

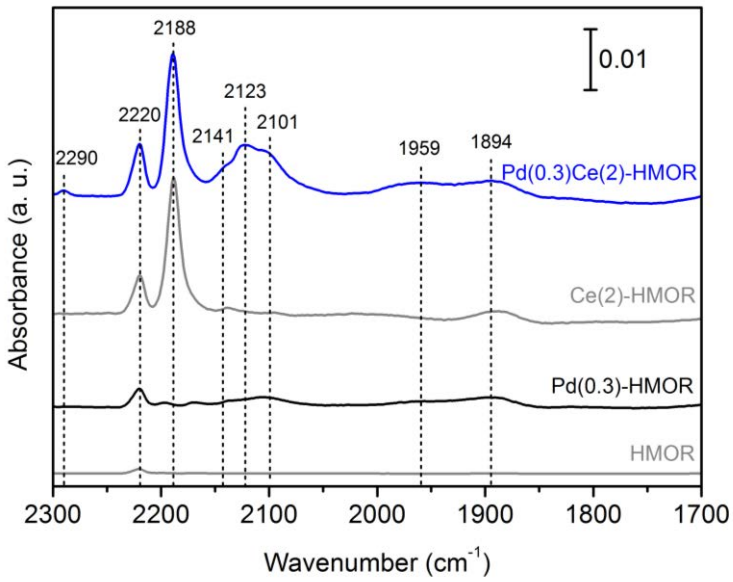

Figure II-14 – FTIR spectra of reduced catalysts at room temperature, after CO exposure to 5 torr: HMOR, Pd(0.3)-HMOR, Pd(0.3)Ce(2)-HMOR and Ce(2)-HMOR.

When observing the Pd(0.3)Ce(2)-HMOR spectrum, it is possible to observe that a new intense band, not presented in Pd(0.3)-HMOR, appears at 2188 cm^{-1}. This band is also observed in Ce(2)-HMOR and it is within the spectral region of carbonyls formed with cerium ions, 2190-2110 cm^{-1} [26]. Hence, it can be ascribed to Ce^{n+}-CO complexes (Ce^{3+} or Ce^{4+}). It should be noted that the presence of both Ce species in Pd(0.3)Ce(x)-HMOR catalysts was identified by DRS UV-Vis spectroscopy. An additional band is also observed at 2123 cm^{-1}, which is not observed neither in the Pd(0.3)-HMOR nor in the Ce(2)-HMOR. This band appears in both spectral range of Ce^{n+}-CO and Pd^{n+}-CO (2215-2110 cm^{-1}) [26], so it could be attributed to a Ce or Pd species, not present in the monometallic catalysts, eventually resulting from a interaction between both metals.

The band at 2290 cm^{-1} is ascribed to CO_2 complexes formed due to CO oxidation, and appears together with an intense at 2355 cm^{-1} attributed to linear CO_2 [49] (not shown). It is worthwhile mentioning these bands only appear in the bimetallic catalyst, which means that the CO oxidation seems to require the presence of both Pd and Ce species.

Finally, it should be mentioned that the band at 2138 cm^{-1}, in Ce(2)-HMOR is also ascribed to Ce^{n+}-CO complexes, since this is a Pd-free catalysts and, hence, such band does not corresponds to Pd^{n+}-CO complexes. Likewise, the band at 1888 cm^{-1} is likely to be related to the formation of some carbonate species.

II.4.1.8. NO oxidation

NO oxidation to NO_2 is considered to be a first key step in the NO_x SCR reaction involving hydrocarbons as reductant [50-52]. NO_2 plays an important role in the partial oxidation of the unburned hydrocarbon present in the exhausts gases, resulting $C_xH_yO_z$ intermediate species that will be act as effective reductants. Figure II-15 illustrates NO oxidation to NO_2 under similar conditions considered in this work to evaluate the NO_x SCR reaction, in this case without reductant in the inlet stream.

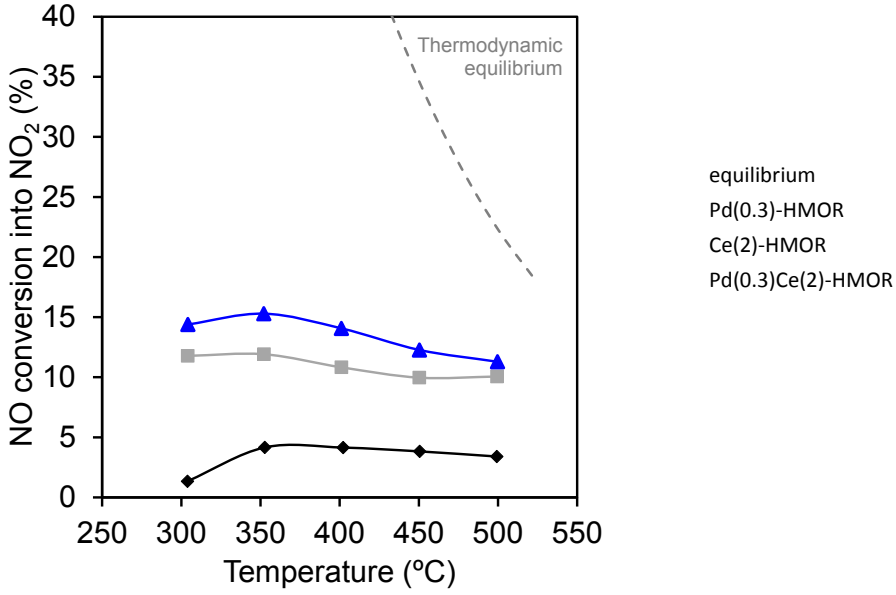

Figure II-15 – NO conversion into NO_2 for Pd(0.3)-HMOR (♦), Ce(2)-HMOR (■) and Pd(0.3)Ce(2)-HMOR (▲). Conditions: 1000 ppm NO, 7 vol.% O_2 and GHSV of 40000 h^{-1}.

As it is possible to observe, Pd(0.3)-HMOR presents low NO oxidation performance. Ce(2)-HMOR exhibits higher conversions values and Pd(0.3)Ce(2)-HMOR even higher, compared to Pd(0.3)-HMOR. This suggests that Ce species are responsible for promoting NO conversion in Pd(0.3)Ce(2)-HMOR which confirms that one of the roles of Ce, as enhancer of Pd(0.3)-HMOR catalytic performance for NO_x CH_4-SCR, is to oxidise NO to NO_2 [7]. The role of Ce as oxidation promoter was also observed by FTIR-CO, where it was evidenced the formation of CO_2 complexes on Pd(0.3)Ce(2)-HMOR, resulting from the CO oxidation. However, this phenomenon has not been observed for Ce(2)-HMOR, which suggests that the CO and NO oxidation mechanisms may involve different cerium species or follow different reaction paths.

II.4.1.9. Active species on Pd/Ce-HMOR for NO_x CH_4-SCR

The enhancing effect of Ce on NO_x CH_4-SCR was assessed by testing the Pd(0.3)Ce(x)-HMOR catalysts and comparing to Pd(0.3)-HMOR and Ce(2)-HMOR. The results are presented in Figure II-16 (N_2O and CO formation are negligible).

Ce(2)-HMOR reveals to be practically inactive for the NO_x CH_4-SCR reaction, in the entire range of temperatures tested and even CH_4 conversion is practically inexistent. Though Ce(2)-HMOR exhibit a NO conversion into NO_2 comparable to Pd(0.3)Ce(2)-HMOR (Figure II-16), it is clear that this catalysts is not active for deNO_x reaction. This is only accomplished in the presence of Pd species.

At low temperatures, 300-350 ºC, all Pd-based catalysts present similar NO_x and CH_4 conversion. However, for temperatures above 350 ºC, it is possible to observe that, by adding 1-5 wt.% Ce, NO_x conversion into N_2 becomes higher than the one observed for Pd(0.3)-HMOR. For Ce loadings of 1 and 2 wt.%, one can see that NO_x conversion increases with the temperature. However, for 3 and 5 wt.%, maximum NO_x conversion is reached at 450 ºC, starting to decrease afterwards. This behaviour can be explained due to the lack of reductant (CH_4), since its conversion reaches values of more than 80 %.

An important parameter to take into account when comparing the catalytic performance of the catalysts is the CH_4 selectivity to NO_x SCR, which gives an indication on how much reductant is effectively being used to reduce NO_x instead of being directly burned (Figure II-16C). It is possible to see than when 1 wt.% Ce is added to Pd(0.3)-HMOR, CH_4 selectivity is increased. For higher Ce loadings, the selectivity becomes lower than the one registered for Pd(0.3)-HMOR. Though with 2 wt.% Ce, the selectivity is lower than with 1 wt.% Ce, it is important to consider that there is also a significant difference in the NO_x conversion to N_2. Therefore, both parameters need to be taken into account looking for the best catalytic performance.

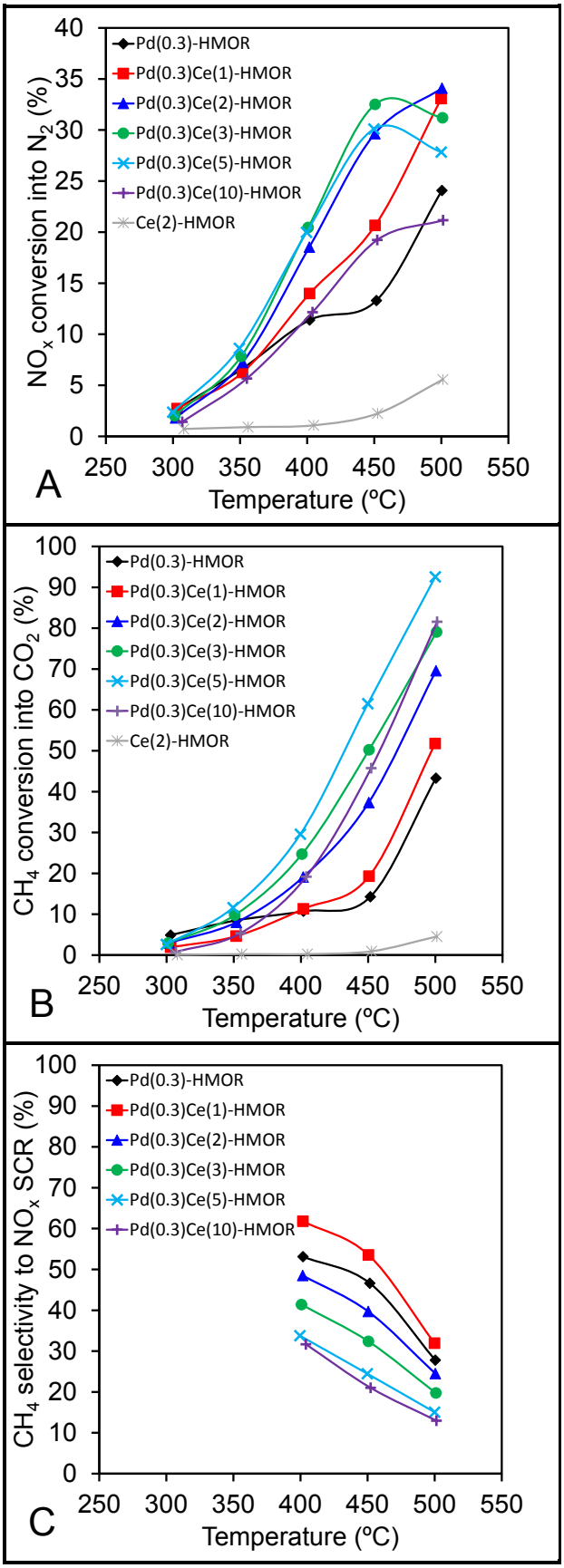

Figure II-16 – NO_x conversion into N_2 (A), CH_4 conversion into CO_2 (B) and CH_4 selectivity to NO_x SCR reaction (C) for Ce(2)-HMOR, Pd(0.3)-HMOR and Pd(0.3)Ce(x)-HMOR catalysts containing different Ce loadings. Conditions: 1000 ppm NO, 1000 ppm CH_4, 7 vol.% O_2 and GHSV of 40000 h^{-1}.

When considering 10 wt.% of Ce, catalytic behaviour changes completely. NO_x conversion of Pd(0.3)Ce(10)-HMOR becomes lower than Pd(0.3)Ce(1)-HMOR and CH_4 conversion, that one would expected to be the highest of all catalysts, becomes lower than Pd(0.3)Ce(5)-HMOR. The reason behind this catalytic behaviour might be the inexistence of the necessary interaction between Ce and Pd species, likely due to the difficulty to obtain CeO_2 species correctly dispersed in the zeolite structure. When comparing the catalytic performance of Pd(0.3)Ce(10)-HMOR with a sample of Pd(0.3)-HMOR that was mechanical mixed with bulk CeO_2 in order to obtain a similar Ce loading in the sample, *ca.* 10 wt.% - Pd(0.3)Ce(10)-HMOR(MM) (Figure II-17) - it is possible to see that NO_x conversion values are similar for both catalysts. In Pd(0.3)Ce(10)-HMOR(MM) catalyst, it is not expectable to obtain a good CeO_2 dispersion. Hence, one would expect larger CeO_2 particles in the external surface of the zeolite. Figure II-18 exhibits the H_2-TPR profile of Pd(0.3)/Ce(10)-HMOR(MM), where a reduction process of bulk CeO_2 is clear observed at high temperature.

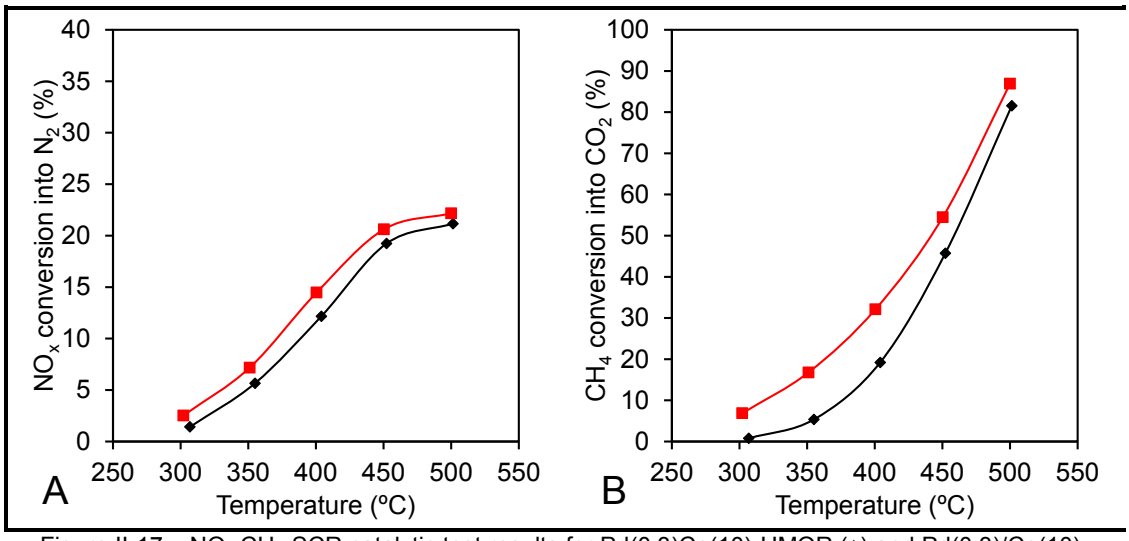

Figure II-17 – NO_x CH_4-SCR catalytic test results for Pd(0.3)Ce(10)-HMOR (♦) and Pd(0.3)/Ce(10)-HMOR(MM) (■): NO_x conversion into N_2 (A) and CH_4 conversion into CO_2 (B). Conditions: 1000 ppm NO, 1000 ppm CH_4, 7 vol.% O_2 and GHSV of 40000 h^{-1}.

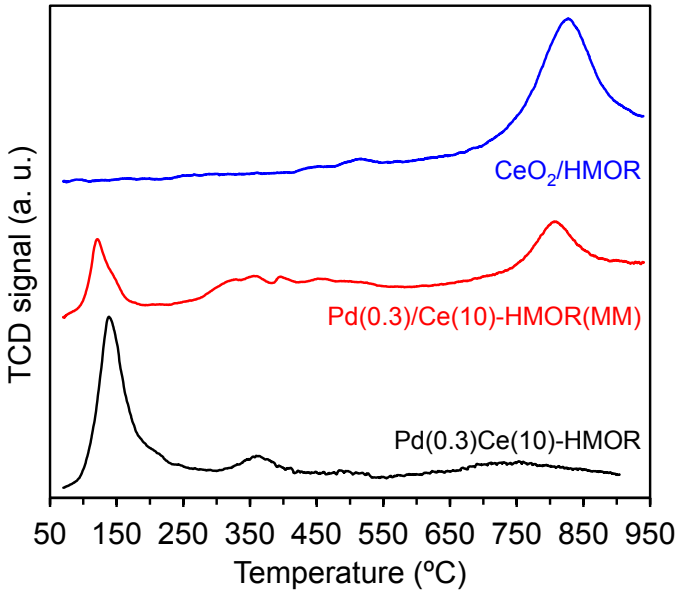

Figure II-18 – H_2-TPR profiles of Pd(0.3)Ce(10)-HMOR, Pd(0.3)/Ce(10)-HMOR and CeO_2-HMOR.

Ce(2)-HMOR revealed to be practically inactive for NO_x CH_4-SCR reaction and even for CH_4 direct combustion, which is likely to be associated to the lack of active species for deNO_x process, namely, Pd^{2+} ions in exchange position. However, this catalyst exhibits moderate conversion values for NO oxidation to NO_2 and significantly higher than the ones from Pd(0.3)-HMOR. It is clear that one of the roles of cerium species are, therefore, the promotion of NO oxidation, which is in agreement with other results previously reported in the literature [7, 53]. Several mechanism have been proposed in the literature for the HC-SCR reaction and some of them differ on the intermediate species involved and the reaction paths [51]. Notwithstanding, it seems to be clearly established that NO oxidation to NO_2 is a first key step in NO_x HC-SCR reaction.

In this study, further details can be provided regarding the Ce species that promote NO oxidation over zeolite-based catalysts. TEM/EDS evidenced that these are CeO_2 oxide species, disposed in small clusters (in comparison with the zeolite particle size). Moreover, the absence of reduction of peaks in H_2-TPR profiles, at high temperatures (< 700 ºC), characteristic of the reduction of bulk oxygen in CeO_2, evidences that these are mostly superficial clusters.

When looking at the catalytic performance of Pd(0.3)Ce(1)-HMOR, one can see than NO_x conversion increases but so does CH_4 selectivity to SCR. The increase of NO_2 formation due to cerium addition is likely to promote the formation of intermediate species involved the HC-SCR reaction [51, 54, 55] . However, the increase of CH_4 selectivity to SCR indicates that the catalyst is using the reductant more efficiently, when compared to the monometallic formulation. H_2-TPR, DRS UV-Vis and FTIR-CO evidenced the existence of an interaction between Pd/Ce species and this might be the key for the promotion of deNO_x process.

It is intriguing to observe that, for Pd(0.3)Ce(x)-HMOR catalysts, the quantification of the second reduction peak in H_2-TPR profiles results in a higher H_2/Ce ratio for Pd(0.3)Ce(1)-HMOR and that

the CH_4 selectivity towards SCR follows the same trend of this ratio. This ratio can be seen as an indicator of the relative amount of cerium species interacting with palladium species whereas the amount of total H_2 consumed in the corresponding reduction process is directly related to the absolute amount of Ce species in interaction with Pd species. The decreasing of the previous mentioned ratio with the increasing of Ce loading represents, therefore, an increasing of Ce species not interacting with Pd. Since CeO_2 species have an oxidative nature, it is expectable that they might be able to favour CH_4 direct combustion or eventual intermediates species formed. Pd(0.3)Ce(2)-HMOR exhibits a significant increase of the absolute amount of CeO_2 species in interaction with Pd, likely to compensate the increase of CeO_2 species not interacting with Pd (1 vs. 2 wt.%: H_2/Ce = 0.39 vs. 0.27; H_2 consumption of 22 vs. 37 $\mu mol/g_{catal.}$). For higher loadings, not only the CeO_2 species not in interaction increase, but also the interacting CeO_2 species decrease.

It is, then, possible to conclude that the equilibrium between the amount of CeO_2 species interacting and not interacting with Pd species play a crucial role in the catalytic performance of PdCe-HMOR for NO_x CH_4-SCR. By considering 0.3 wt.% Pd and 2 wt.% Ce, an optimal Pd/Ce species distribution is obtained, resulting in the better catalytic performance. The apparent energy activation for the NO_x CH_4-SCR reaction was calculated for the conditions tests considered herein (see Annex A).

II.4.2. Effect of Pd loading on PdCe-HMOR system

The effect of Pd loading have been previously study, in section II.3.1, for monometallic catalysts. Herein, a similar study in conducted for bimetallic formulations containing 2 wt.% of cerium, corresponding to the loading that allowed to obtain better results.

II.4.2.1. Temperature programmed reduction under hydrogen (H_2-TPR)

H_2-TPR profiles of Pd(x)Ce(2)-HMOR catalysts with different Pd loading are presented in Figure II-19.

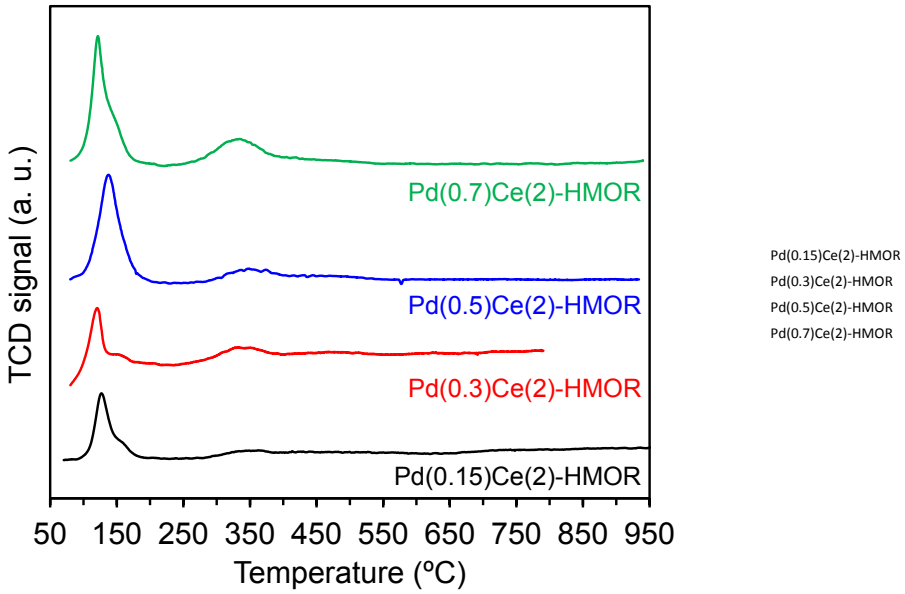

Figure II-19 – H_2-TPR profiles of Pd(x)Ce(2)-HMOR catalysts containing different Pd loadings.

A similar reduction peak to the ones observed in H_2-TPR profiles of monometallic Pd catalysts previously presented is also observed in these bimetallic catalysts. Moreover, the quantification of the H_2 consumption in this region (Table II-9) leads to a H_2/Pd higher than the unity for all catalysts. As it was described before for Pd(0.3)Ce(x)-HMOR catalysts with different Ce loading, this is related to the presence of surface Ce^{4+} species, which reduction is known to occur in the same range of temperatures [36].

Table II-9 – Quantification of H_2 consumption by peak integration of H_2-TPR profiles of Pd(x)Ce(2)-HMOR catalysts containing different Pd loadings.

	Peak 1			Peak 2		
	T (ºC)	H_2/Pd	μmol H_2 /$g_{catal.}$	T (ºC)	H_2/Ce	μmol H_2 /$g_{catal.}$
Pd(0.15)Ce(2)-HMOR	80-190	2.8	40	265-600	0.15	19
Pd(0.3)Ce(2)-HMOR	95-215	1.4	39	240-560	0.28	37
Pd(0.5)Ce(2)-HMOR	80-220	1.6	80	260-555	0.24	29
Pd(0.7)Ce(2)-HMOR	75-190	1.3	88	240-540	0.38	51

The higher H_2/Pd ratio was obtained for Pd(0.15)Ce(2)-HMOR, which means that a considerable amount of H_2 consumption is due to the presence of surface Ce^{4+} species. For 0.3 wt.% Pd, the ratio decreases significantly but the H_2 consumption is practically the same. Hence, this catalyst presents less surface Ce^{4+} species than the previous one. With 0.5 wt.% Pd, H_2/Pd ratio increases suggesting the formation of more Ce^{4+} species but with 0.7 wt.% Pd, the ratio decreases again. It is not possible, then, to obtain a correlation between the increasing of Ce^{4+} species with the increasing of Pd loading, which suggests that the formation of these species seems not to be dependent of Pd loading.

A second reduction peak in H_2-TPR profile of Pd(0.3)Ce(x)-HMOR catalysts previously shown, between 240-600 ºC, has been ascribed to the reduction of CeO_2 species in interaction with palladium species. For the Pd(x)Ce(2)-HMOR catalysts considered in this study, H_2/Ce ratio resulting from the quantification of the previous mentioned peak seems also to be independent from Pd loading (it increases from 0.15 to 0.3 wt.% Pd, then decreases from 0.3 to 0.5 wt.% Pd and increases again from 0.5 to 0.7 wt.% Pd). Notwithstanding, it is interesting to notice that the stabilisation of CeO_2 species in interaction with Pd species follows an opposite trend to the one verified for surface Ce^{4+} species, *i. e.*, when H_2/Ce ratio of CeO_2 interacting species increase, H_2/Pd decreases, and *vice versa*.

II.4.2.2. Diffuse reflectance UV-Vis spectroscopy (DRS UV-Vis)

Figure II-20 exhibits the DRS UV-Vis spectra of Pd(x)Ce(2)-HMOR catalysts considered in this work.

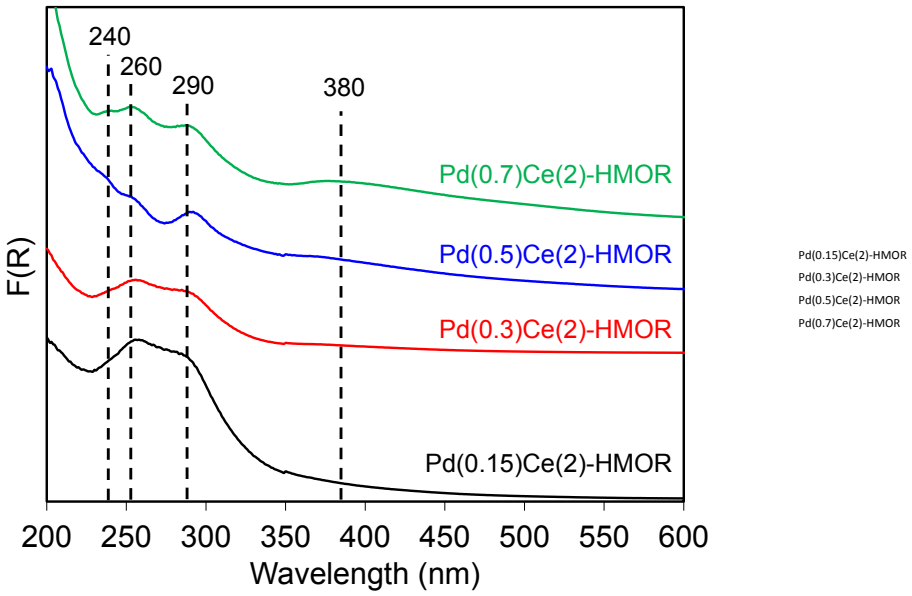

Figure II-20 – Diffuse Reflectance UV-Vis spectra of Pd(x)Ce(2)-HMOR catalysts containing different Pd loadings.

As previously identified for the monometallic Pd catalysts, the bands near 380 nm correspond are characteristic of Pd^{2+} species. The fact that it appears slightly blue-shifted, may be due to the presence of Ce (see Figure II-10, page 83). The bands at 260 and 290 are ascribed to transition 4f-5d of Ce^{3+} and to charge transfer from O^{2-} to Ce^{4+} in CeO_2 clusters Ce^{4+} species, respectively [37, 38]. The band at 240 nm is ascribed to the change transfer Pd→O [56].

From the spectra analysis, it is possible to observe that the band at 240 nm becomes more pronounced in the increasing of Pd loading, which is expectable. A similar increase in the band around 380 nm would be also expected, though not observed. The reason might be the interference of cerium characteristics bands.

II.4.2.3. NO_x CH_4-SCR

Steady-state test results obtained for Pd(x)Ce(2)-HMOR catalysts are exhibited in Figure II-21 (CO conversion is negligible).

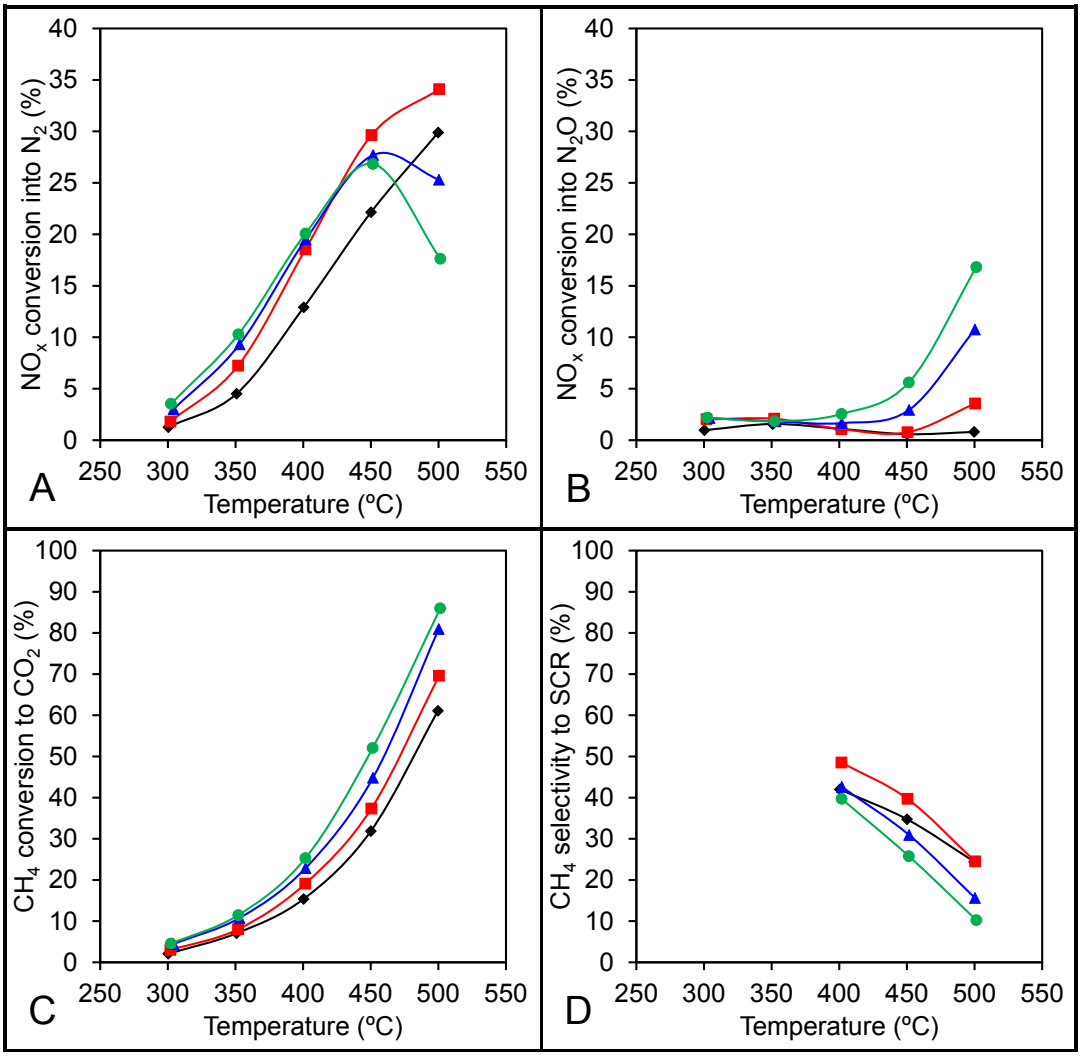

Figure II-21 – NO_x conversion into N_2 (A) and into N_2O (B), CH_4 conversion into CO_2 (C) and CH4 selectivity to SCR (D) over Pd(x)Ce(2)-HMOR catalysts containing different Pd loadings: Pd(0.15)Ce(2)-HMOR (♦), Pd(0.3)Ce(2)-HMOR (■), Pd(0.5)Ce(2)-HMOR (▲) and Pd(0.7)Ce(2)-HMOR (●). Conditions: 1000 ppm NO, 1000 ppm CH_4, 7 vol.% O_2 and GHSV of 40000 h^{-1}.

For temperatures below 450 ºC, NO_x conversion values are very similar for Pd loadings of 0.3-0.7 wt.%. Only for 0.15 wt.% Pd, NO_x conversion is significantly lower in practically the entire range of temperature. As it was previously presented for the optimisation of Pd loading in the monometallic catalysts, Pd(0.15)-HMOR also presented lower conversion values, when compared to Pd(x)-HMOR monometallic catalysts with 0.3-0.7 wt.% Pd. This behaviour was attributed to the low content of Pd, namely Pd^{2+} ions, which are known to be active species for the NO_x CH_4-SCR [31] and this is likely to be the explanation for the lower activity of Pd(0.15)Ce(2)-HMOR, when compared to the other catalysts.

Similarly to what was reported for the monometallic Pd(x)-HMOR catalysts, the increase of the Pd loading in bimetallic PdCe-HMOR catalysts also decreases the NO_x conversion into N_2 and promotes N_2O formation instead. This findings suggest, then, that Pd species are the ones directly related to the selectivity of NO_x towards N_2 and that cerium species do not determine this parameter.

As well as for monometallic Pd-MOR catalysts, CH_4 direct combustion of Pd(x)Ce(2)-HMOR catalysts increases with the increase of Pd loading. Palladium-loaded catalysts are also used as hydrocarbon oxidation catalysts [33, 34]. Hence, it is also likely that Pd species, together with CeO_2 species known for having oxidative properties, play a role in the CH_4 direct combustion.

Based on the catalytic test results obtained, it is possible to conclude that Pd(0.3)Ce(2)-HMOR is the catalyst that presents the better performance for NO_x CH_4-SCR in the conditions considered in this study, since it is the one that allows to obtain higher NO_x conversion into N_2 values using CH_4 more efficiently, as reductant (*i.e.* higher CH_4 selectivity towards NO_x SCR reaction). This better performance is attributed to stabilisation of palladium as Pd^{2+} ions in exchange position and an optimal balance between surface Ce^{4+} species and CeO_2 species interacting with Pd.

II.4.3. Effect of metal introduction order

As it was previous shown, metal loadings are a key parameter for the catalytic performance of Pd/Ce-MOR catalysts for NO_x CH_4-SCR. Another important parameter was proven to be the metal introduction order. For instance, Ferreira *et al.* [5] studied the influence of this parameter in the preparation of Pd/Co-FER catalysts and verified that, by changing the metal introduction order, different types and quantities of metal species were stabilised in different locations within the zeolite support. In this section, the effect of metal introduction order is investigated.

II.4.3.1. Temperature programmed reduction under hydrogen (H_2-TPR)

Figure II-22 illustrates the H_2-TPR profiles of Pd(0.3)Ce(2)-HMOR and Ce(2)Pd(0.3)-HMOR, both containing 0.3 wt.% Pd and 2 wt.% Ce, where metals were introduced in different order. The quantification of H_2 consumption can be found in Table II-10.

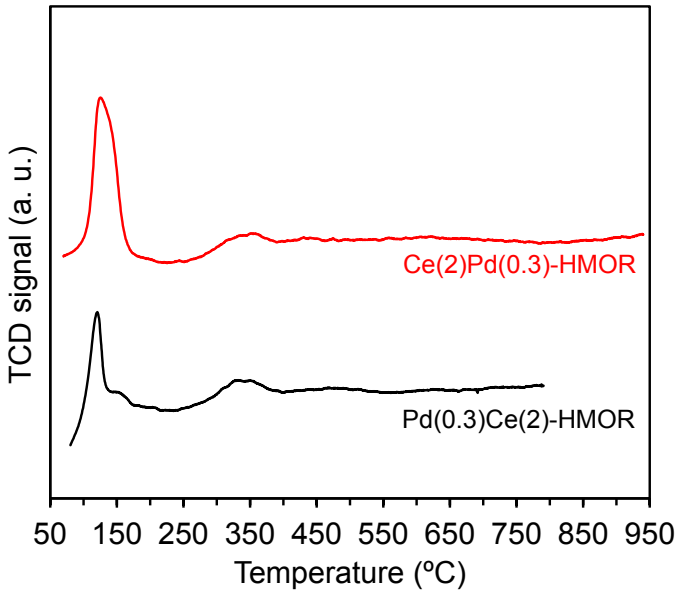

Figure II-22 - H_2-TPR profiles of Pd(0.3)Ce(2)-HMOR and Ce(2)Pd(0.3)-HMOR, both containing 0.3 wt.% Pd and 2 wt.% Ce, introduced in different order.

Table II-10 – Peak integration of H_2-TPR profiles of Pd(0.3)Ce(2)-HMOR and Ce(2)Pd(0.3)-HMOR, both containing 0.3 wt.% Pd and 2 wt.% Ce.

	Peak 1			Peak 2		
	T (ºC)	H_2/Pd	µmol H_2 /$g_{catal.}$	T (ºC)	H_2/Ce	µmol H_2 /$g_{catal.}$
Pd(0.3)Ce(2)-HMOR	95-215	1.4	39	240-560	0.28	37
Ce(2)Pd(0.3)-HMOR	70-190	1.9	74	240-560	0.22	29

The results show, on one hand, that when cerium is introduced before palladium (Ce(2)Pd(0.3)-HMOR), the H_2 consumption corresponding to low temperature reduction processes (< 215 ºC) increases, which means that the amount of surface Ce^{4+} species increases. On the other hand, H_2 consumption in the region 240-560 ºC decreases, meaning that the amount of CeO_2 species interacting with palladium also decrease.

II.4.3.2. Diffuse reflectance UV-Vis spectroscopy (DRS UV-Vis)

Figure II-23 exhibits the spectra of Pd(0.3)Ce(2)-HMOR and Ce(2)Pd(0.3)-HMOR, both containing 0.3 wt.% Pd and 2 wt.% Ce, where metals were introduced in different order.

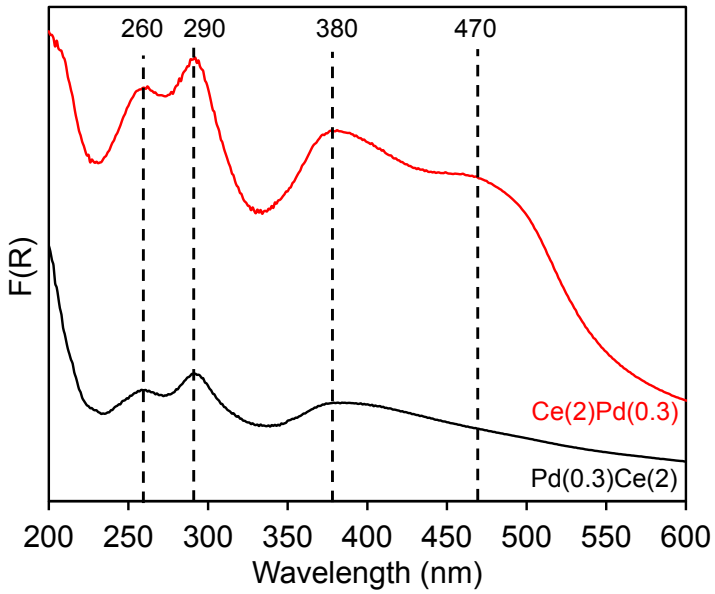

Figure II-23 – Diffuse Reflectance UV-Vis spectra of Pd(0.3)Ce(2)-HMOR and Ce(2)Pd(0.3)-HMOR, both containing 0.3 wt.% Pd and 2 wt.% Ce, introduced in different order.

Both spectra exhibit three similar bands at 260, 290 and 380 nm attributed to Ce^{3+}, Ce^{4+} and Pd^{2+} species, respectively. However, a forth band at 470 nm is shown in the Ce(2)Pd(0.3)-HMOR spectrum. As it was already mentioned, bands in this zone are characteristic of d-d transition of Pd^{2+} ions affected by different oxygen environments. In this case, there is evidence of the existence of two different Pd^{2+} species, which might be a result of the presence of Ce, when Pd was introduced.

II.4.3.3. NO_x CH_4-SCR

Figure II-24 compares the catalytic test results of Pd(0.3)Ce(2)-HMOR and Ce(2)Pd(0.3)-HMOR, both containing 0.3 wt.% Pd and 2 wt.% Ce, where metals were introduced in different order (N_2O and CO conversions are negligible).

In the entire range of temperature, Ce(2)Pd(0.3)-HMOR (Ce introduced first) presents higher CH_4 conversion values than Pd(0.3)Ce(2)-HMOR. For temperature below 450 ºC, the NO_x conversions are practically the same. In fact, it is possible to observe that CH_4 selectivity towards NO_x SCR of Ce(2)Pd(0.3)-HMOR is significantly lower than Pd(0.3)Ce(2)-HMOR. A 500 ºC, NO_x conversion for Ce(2)Pd(0.3)-HMOR decreases and becomes significant lower than Pd(0.3)Ce(2)-HMOR, which can be explained due to the lack of reductant available for the reaction.

Characterisation of Ce(2)Pd(0.3)-HMOR show evidence of the existence of different Pd species, compared to Pd(0.3)Ce(2)-HMOR. Though the analysis of H_2-TPR profile in the low temperature region does not allow to obtain a distribution of Pd^{2+} species as it was previously presented for the monometallic catalysts (due to the presence of Ce^{4+} species), one cannot exclude that a changing in the Pd species distributions when Ce has been already introduced. Likewise, the contribution of Ce^{4+} species for CH_4 direct oxidation cannot be excluded. Finally, it should be noted that CeO_2 species in interaction with Pd species seem to be less when Ce is introduced first. As previously mentioned, these species might be important for the NO_x CH_4-SCR. Hence, it is likely that their decreasing can also contribute to the worsen of catalytic performance of Ce(2)Pd(0.3)-HMOR.

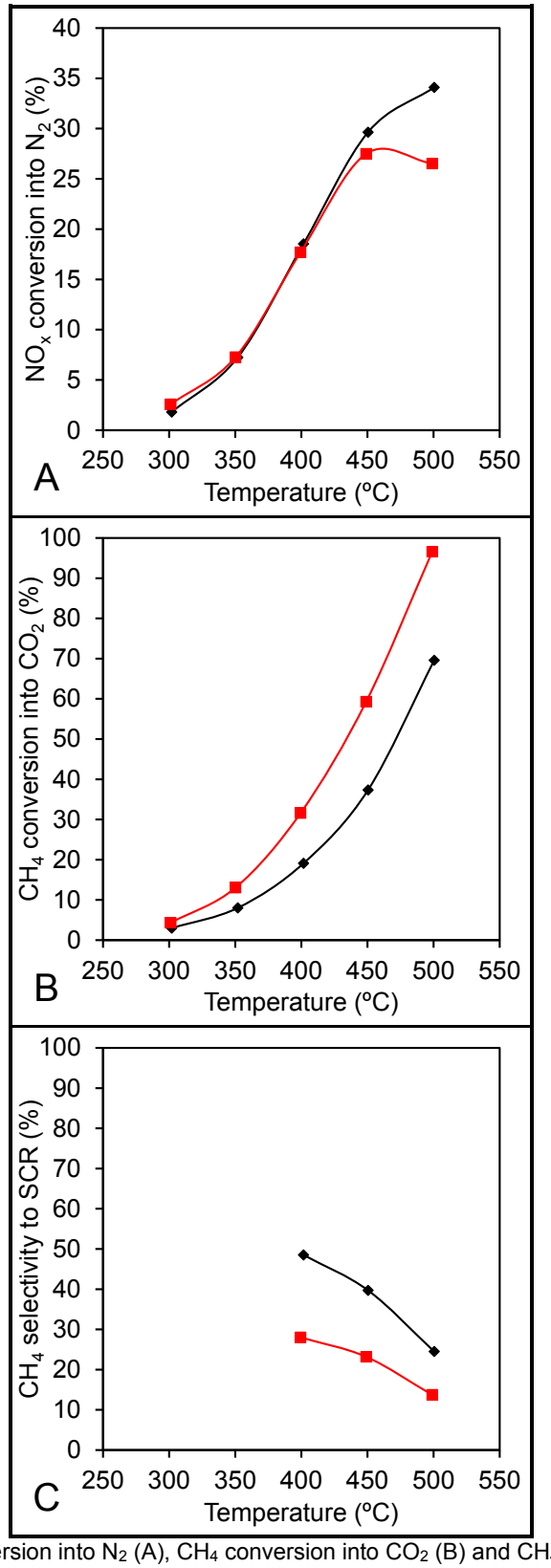

Figure II-24 – NO_x conversion into N_2 (A), CH_4 conversion into CO_2 (B) and CH_4 selectivity to NO_x SCR reaction of Pd(0.3)Ce(2)-HMOR (♦) and Ce(2)Pd(0.3)-HMOR (■), both containing 0.3 wt.% Pd and 2 wt.% Ce, introduced in different order. Conditions: 1000 ppm NO, 1000 ppm CH_4, 7 vol.% O_2 and GHSV of 40000 h^{-1}.

II.5. Three-metal formulation: Iron as promoter

In this section, the study of iron as co-promoting metal to be added to PdCe-HMOR is presented. Fe-based catalysts are known to be capable of catalyse the methanol production from methane. According to some authors, HC-SCR mechanism contemplates the formation of oxygenated hydrocarbon species ($C_xH_yO_z$) as an important step in NO_x SCR reaction [51]. $C_xH_yO_z$ species are responsible for regenerating the active sites where NO decomposition to N_2 takes place. When using methane as a reductant, previous works have shown that methanol can be the intermediary oxygenated hydrocarbon species [55, 57].

On the other hand, iron as being reported in the literature as a successful promoter of zeolite-based catalysts for NO_x SCR with methane, namely, in catalysts containing indium [58, 59]. Hence, the study of its incorporation in Pd-based catalysts is considered pertinent.

II.5.1. Catalysts preparation

Figure II-25 summarises the preparation sequence of the catalysts studied in this section.

Pd(0.3)Fe(2)-HMOR and Fe(2)-HMOR were obtain by introducing Fe in Pd(0.3)-HMOR and NH_4MOR, respectively, by incipient wetness impregnation technique, following the procedure described in Annex A, section C.1.4.

PdCeFe-HMOR$_{mix1}$ and PdCeFe-HMOR$_{mix2}$ were prepared by mixing and co-grinding Pd(0.3)Ce(2)-HMOR with Fe(2)-HMOR and Pd(0.3)Fe(2)-HMOR, respectively, in a proportion of 2:1.

Pd(0.3)Ce(2)Fe(2)-HMOR(IWI) was obtained by introducing Fe in Pd(0.3)Ce(2)-HMOR by incipient wetness impregnation technique, following the procedure described in Annex A, section C.1.4.

Finally, Pd(0.3)Ce(2)/Fe(2)-HMOR(MM) was obtained by introducing Fe by mechanical mixture with Fe_2O_3 following the procedure described in Annex A, section C.1.4.

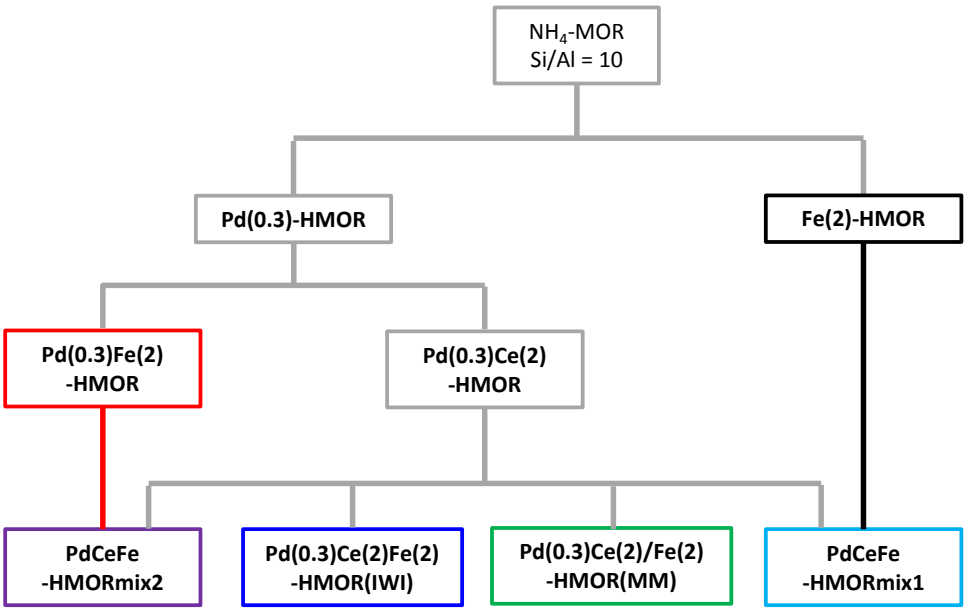

Figure II-25 – Summary of MOR considered for the study of Fe as promoter.

II.5.2. Characterisation

II.5.2.1. Temperature programmed reduction under hydrogen (H_2-TPR)

Figure II-26 exhibits the H_2-TPR profiles of Fe-containing catalysts, where Fe was introduced by incipient wetness impregnation. Pd(0.3)-HMOR and Pd(0.3)Ce(2)-HMOR are also presented to allow the comparison.

For Fe(2)-HMOR catalyst, it is possible to identify a wide reduction zone between 200-700 ºC, corresponding to the reduction of Fe^{3+} (ferric) to Fe^{2+} (ferrous) [60-62]. It is also possible to observe that the reduction profile of iron species seems to be composed by several overlapped peaks between 200-700 ºC which might be attributed to the reduction of several iron oxides with different sizes and locations.

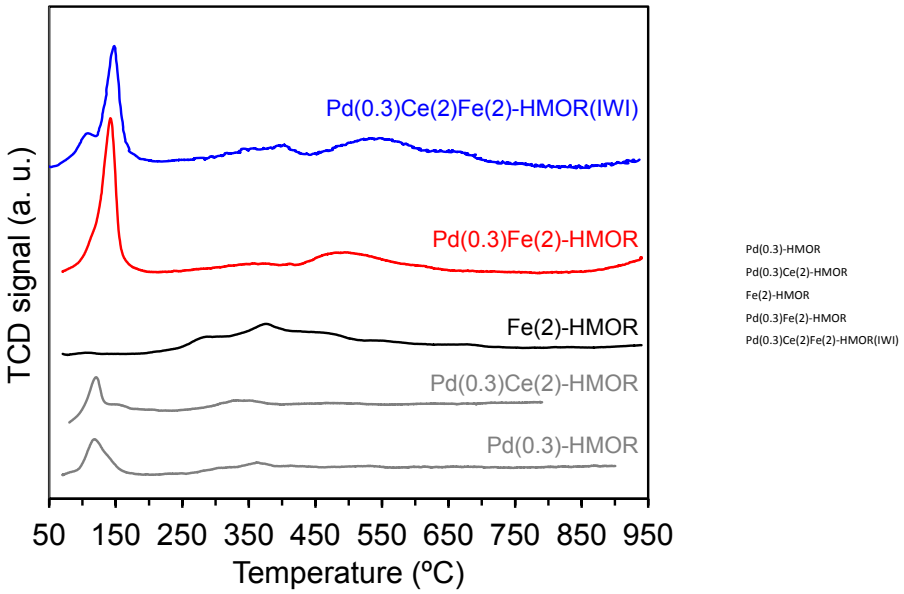

Figure II-26 – H_2-TPR profile of Fe-containing MOR catalyst, Pd(0.3)-HMOR and Pd(0.3)Ce(2)-HMOR.

Table II-11 – Peak integration of H_2-TPR profiles of Pd(0.3)-HMOR, Fe(2)-HMOR and Pd(0.3)Fe(2)-HMOR.

-HMOR	Peak 1				Peak 2				Peak 3		
	T (ºC)	H_2/Fe	H_2/Pd	µmol H_2 /$g_{catal.}$	T (ºC)	H_2/Fe	H_2/Ce	µmol H_2 /$g_{catal.}$	T (ºC)	H_2/Fe	µmol H_2 /$g_{catal.}$
Fe(2)	170 -720	0.37	-	143	-	-	-	-	-	-	-
Pd(0.3)Fe(2)	70 -200	-	5.1	145	200 -420	0.02	-	10	420 -660	0.13	55
Pd(0.3)Ce(2)	95 -215	-	1.4	39	240-560	-	0.28	37	-	-	-
Pd(0.3)Ce(2) Fe(2)	60 -210	-	4.3	122	265 -440	0.07	0.18	25	455 -735	0.22	80

Below 700 ºC, Fe^{2+} cannot be further reduced to Fe^{0} [60]. This means that, assuming all iron is in ferric form, the maximum H_2/Fe ratio would be 0.5, corresponding to the reduction of all iron to ferrous form. The integration of the peak from 200-700 ºC (Table II-11) leads to a H_2/Fe ratio of 0.37. This mean that about 26% of iron is in ferrous form.

After introducing 2 wt.% Fe in Pd(0.3)-HMOR it is possible to see that the Pd peak increased significantly its intensity and the corresponding H_2 consumption is significantly higher to the hydrogen required to reduce all palladium in the sample. On the other hand, the H_2/Fe ratio corresponding to the Fe^{3+} species peaks also decreased. This might indicate that some iron oxides may became now more easily reduced due to the presence of Pd. Moreover, it is possible to observe that the reduction zone between 200-700 ºC exhibits now a less complex profile, only composed by two wide peaks, suggesting that the distribution of iron oxides became affected.

II.5.2.2. Diffuse reflectance UV-Vis spectroscopy (DRS UV-Vis)

In Figure II-27 are presented the DRS UV-Vis spectra of Fe-containing catalysts considered in this section (the spectrum of Pd(0.3)Ce(2)-HMOR is also exhibit for comparison).

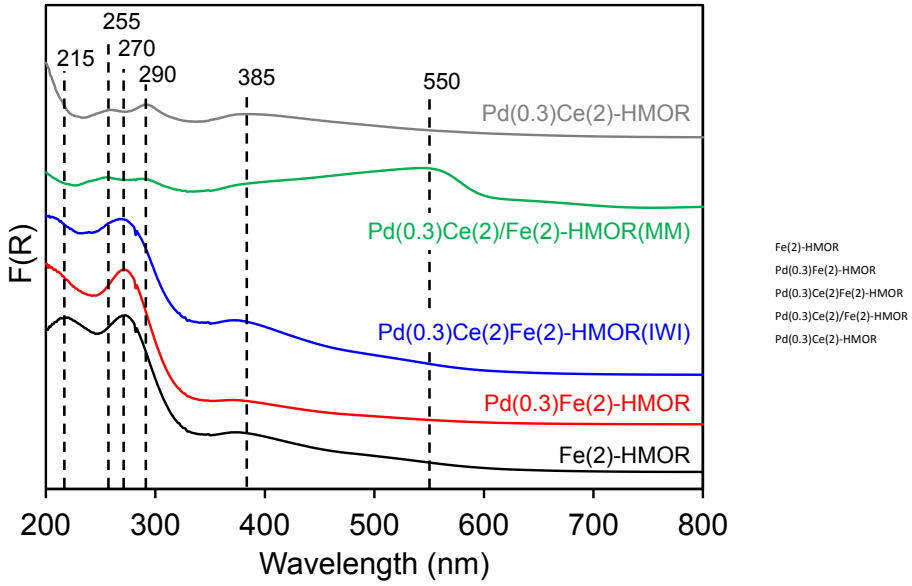

Figure II-27 – Diffuse Reflectance UV-Vis spectra of Fe-containing MOR catalysts and Pd(0.3)Ce(2)-HMOR.

In Fe(2)-HMOR spectrum, it is possible to observe four different bands. Two are clearly distinguished at 215 and 270 nm. Bands below 300 nm have been ascribed to isolated Fe^{3+} species [63-65]. The band at 215 nm is likely to be associated with to Fe^{3+} ions coordinated tetrahedral coordination [66], whereas the band at 270 nm are most likely due to the Fe^{3+} ions with higher coordination [67]. A third band can also be seen around 385 nm, within the region 300-400 nm,

where bands are typically ascribed to oligomeric Fe_xO_y clusters with octahedral coordination [63, 65, 66]. Around 500 nm, a wide absorption band (not very intense) can be observed. Bands above 400 nm are assigned to larger Fe_2O_3 [63, 66], which means that Fe(2)-HMOR also contains some large Fe oxide particles.

When observing Pd(0.3)Fe(2)-HMOR spectrum, some changes can be noticed, namely the band at 215 nm at 500 nm. It is possible that the presence of palladium affected than the formation of tetrahedral Fe^{3+} ions and Fe_2O_3 clusters.

For the Pd(0.3)Ce(2)Fe(2)-HMOR(IWI), the correct interpretation of each band observed becomes more difficult, since Ce bands appear overlapped the ones characteristic of Fe species. However, it should be noted that the band at 290 nm assigned to Ce^{4+} in Pd(0.3)Ce(2)-HMOR is not identified. It is possible that the addition of iron have changed the nature of Ce species. For instance, H_2/Ce quantification obtained from the H_2 consumption of the second peak in Pd(0.3)Ce(2)-HMOR H_2-TPR profile is lower than Pd(0.3)Ce(2)Fe(2)-HMOR(IWI) (0.25 *vs.* 0.18), which means that the change the previous band might be related to this species.

Though the analysis of Pd(0.3)Ce(2)Fe(2)-HMOR(IWI) spectrum in the low wavelength region is more difficult, it is possible to see that, above 400 nm, it is quite similar to the one of Fe(2)-HMOR. One could expected that, due to the higher metal loading, larger Fe particles would be formed, since Fe was the last metal to be introduced. However, this seems not to be the case. On the contrary, for Pd(0.3)Ce(2)Fe(2)-HMOR(MM), it is clear the presence of large Fe_2O_3 particles, since a very intense band at 550 nm can be observed. This was expected since this catalyst was prepared by mixing and co-grinding Pd(0.3)Ce(2)-HMOR with iron oxide.

II.5.2.3. NO_x CH_4-SCR

Fe-containing catalysts were tested in the same conditions and as PdCe-MOR catalysts. In Figure II-28, the catalytic performance of three-metal formulations is assessed and compared with bimetallic ones, as well as Fe(2)-HMOR.

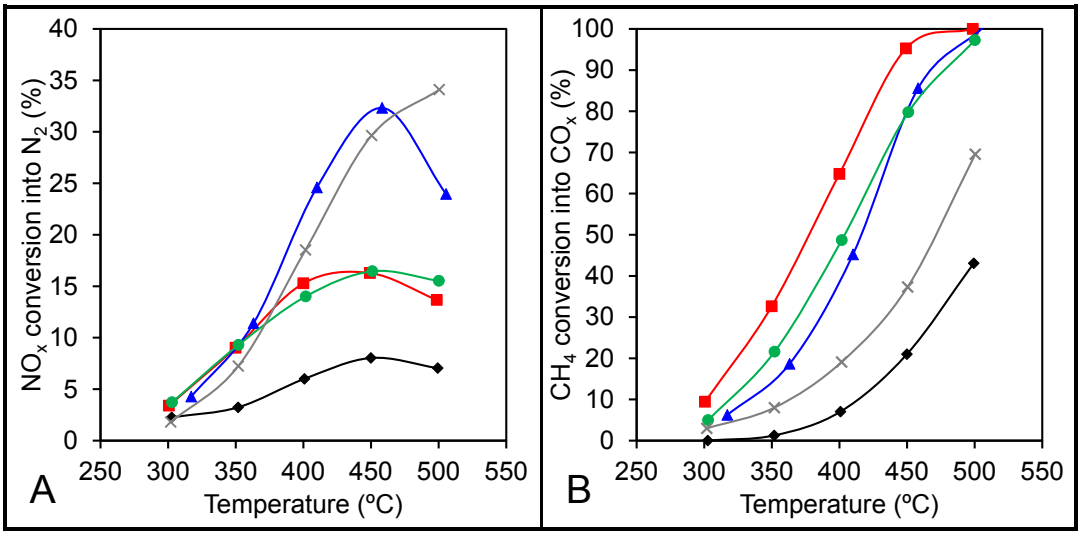

Figure II-28 – NO_x conversion into N_2 (A) and CH_4 conversion into CO_x (B) over Fe(2)-HMOR (♦), Pd(0.3)Fe(2)-HMOR (■), Pd(0.3)Ce(2)/Fe(2)-HMOR(MM) (▲) and Pd(0.3)Ce(2)Fe(2)-HMOR(IWI) (●) and Pd(0.3)Ce(2)-HMOR (x). Conditions: 1000 ppm NO, 1000 ppm CH_4, 7 vol.% O_2 and GHSV of 40000 h^{-1}.

Fe(2)-HMOR exhibits very low NO_x conversion values. Some deNO_x activity have been attributed to Fe isolated sites [68], which were identified in this catalyst (DRS UV-Vis) and can explain the existence of some activity. Moreover, CH_4 conversion is considerable (*ca.* 40% at 500 ºC), which means that Fe species are able to activate CH_4. In fact, Fe_2O_3 clusters have been identified in this catalyst and this species is known to cause non selective oxidation of several reductants [66], from which likely CH_4. It should be highlighted that, contrarily to other catalysts, some formation of CO was detected for Fe(2)-HMOR (CH_4 conversion into CO of 6 and 10%, at 450 ºC and 500 ºC, respectively).

Pd(0.3)Fe(2)-HMOR presents higher NO_x conversion values than Fe(2)-HMOR, which can be attributed to the presence of Pd^{2+} ions in exchange position. However, CH_4 direct combustion is also much higher. In fact, after the 400 ºC, its conversions is higher than 90% and the lack of reductant can explain the stabilisation of NO_x conversion values around 15%. The DRS UV-Vis spectrum and H_2-TPR profile of this catalyst did not allow to identify the significant changes in Fe species, in comparison with Fe(2)-HMOR (for instance, formation of Fe_2O_3 clusters or even large particles). However, it is likely that the presence of Pd affects the catalytic performance, since Pd is also known to be active for CH_4 oxidation.

When comparing Pd(0.3)Ce(2)Fe(2)-HMOR(IWI) with Pd(0.3)Ce(2)-HMOR, one can observed that the introduction of Fe by incipient wetness impregnation significantly worsens the catalytic performance. Though CH_4 direct combustion is not as high as Pd(0.3)Fe(2)-HMOR, it is significant higher than Pd(0.3)Ce(2)-HMOR, which can be related to the presence of Fe_2O_3 species previously mentioned. Moreover, the quantification of H_2 consumption of the peak associated to CeO_2 species in interaction Pd species results in a lower H_2/Ce ratio. It seems that the presence of iron supresses, somehow, the interaction between Pd and Ce species. Assuming that this species might play an

important role in the NO_x CH_4-SCR, the decreasing of NO_x conversion is understandable. This does not seem the case where Fe is added to Pd(0.3)Ce(2)-HMOR by mechanical mixture with Fe_2O_3. CH_4 conversion into CO_2 is also high for Pd(0.3)Ce(2)/Fe(2)-HMOR(MM), but NO_x conversion is slightly better than Pd(0.3)Ce(2)-HMOR (for T < 450 ºC). This might indicate that NO_x SCR is not affected by the presence of Fe_2O_3, likely because the interaction between Pd and Ce species is kept. Nevertheless, this catalyst significantly promotes the CH_4 direct combustion and, at 500 ºC, the sharp decrease in the NO_x conversion can be attribute to the lack of reductant, which is directly oxidised in Fe_2O_3 species.

Figure II-29 illustrates the catalytic performance of Fe(2)-HMOR, Pd(0.3)Ce(2)-HMOR, Pd(0.3)Fe(2)-HMOR and mixtures of catalysts containing palladium, cerium and iron.

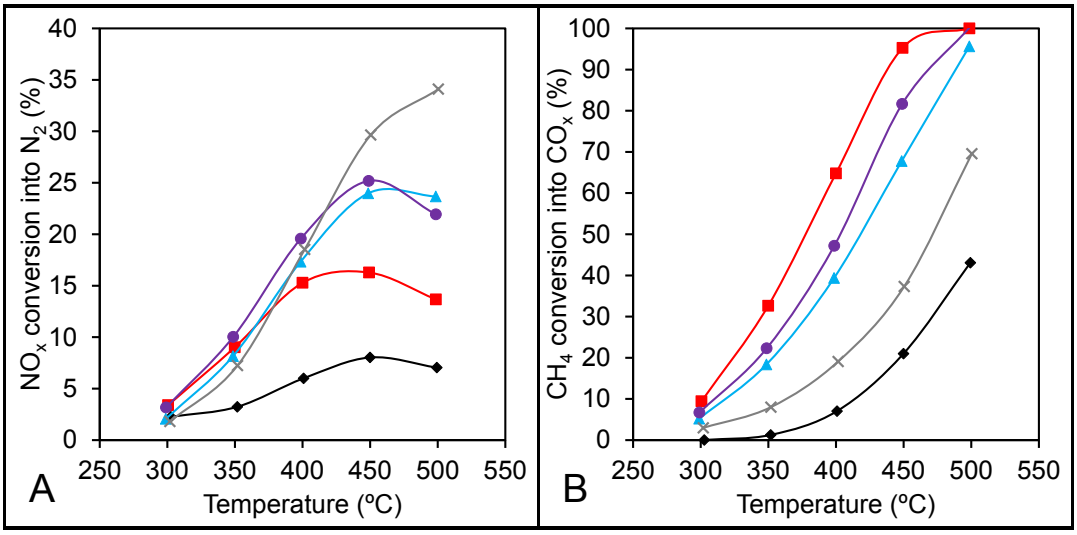

Figure II-29 – NO_x conversion into N_2 (A) and CH_4 conversion into CO_x (B) of Fe(2)-HMOR (♦), Pd(0.3)Fe(2)-HMOR (■), PdCeFe-HMOR$_{mix1}$ (▲), PdCeFe-HMOR$_{mix2}$ (●) and Pd(0.3)Ce(2)-HMOR (x). Condition: 1000 ppm NO, 1000 ppm CH_4, 7 vol.% O_2 and GHSV of 40000 h^{-1}.

PdCeFe-HMOR$_{mix1}$ was obtained by mixing Pd(0.3)Ce(2)-HMOR with Fe(2)-HMOR in a proportion of 2:1. In this case, it is possible to see NO_x conversion is higher than Pd(0.3)Fe(2)-HMOR but it is still lower than Pd(0.3)Ce(2)-HMOR. This supports the idea of the inexistence of synergies between this structures and the lower conversion than Pd(0.3)Ce(2)-HMOR can be explained by a dilution effect of this catalyst in the catalytic bed. Also, the lack of reductant might also explain this behaviour, since PdCeFe-HMOR$_{mix1}$ converts more CH_4.

To prepare PdCeFe-HMOR$_{mix2}$, Pd(0.3)Ce(2)-HMOR was mixed with Pd(0.3)Fe(2)-HMOR. In this case, it is possible to observe that the catalytic performance is similar to PdCeFe-HMOR$_{mix1}$, except that CH_4 conversion is now slightly higher, which might be explained by the presence of Pd in the Pd(0.3)Fe(2)-HMOR.

In summary, the use of iron as a third-metal promoter capable of enhancing the catalytic performance of NO_x CH_4-SCR was not successful. The presence of iron resulted in the increase of CH_4 direct combustion leaving less reductant available for the SCR reaction. Pd(0.3)Ce(2)-HMOR

was, thus, the best catalyst resulting from the optimisation performed and it will be the catalyst considered as reference for the next studies.

II.6. From laboratory scale to industrial conditions

The optimisation of PdCe-MOR system presented so far was supported based on catalytic tests performed at laboratory scale. The industrial conditions corresponding to real applications of this type of catalysts as an after-treatment system is far more complex and involves many factors not considered in the studies previously presented. In this section, such factors are gradually introduced and considered in the assessment of the catalytic performance of the optimised PdCe-MOR formulation.

II.6.1. Effect of catalytic test conditions

Due to the dynamic behaviour of a road vehicle, the real exhaust gases at the engine's outlet are never constant. Hence, it is crucial to understand the catalytic performance of the system when dealing with different inlet feed conditions. In the present section, the effect of important parameters in the catalytic performance of Pd(0.3)Ce(2)-HMOR are considered, namely, the effect of gas hourly space velocity (GHSV), the effect of $[CH_4]/[NO]$ ratio in the inlet gas feed and the effect of water presence.

II.6.1.1. Gas hourly space velocity (GHSV)

GHSV effect in NO_x SCR reaction was assessed in a range of 20000-60000 h^{-1}, by testing Pd(0.3)Ce(2)-HMOR catalyst, at 500 ºC (maximum conversion temperature). Results are presented in Figure II-30.

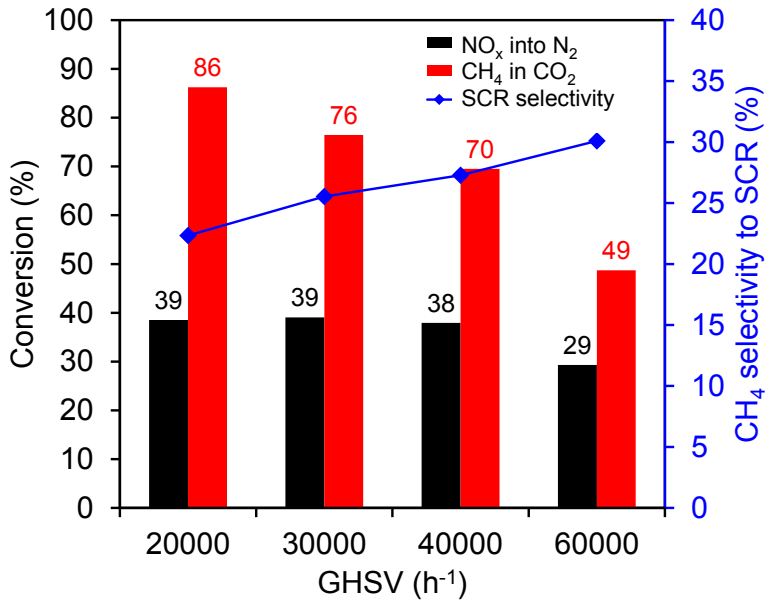

Figure II-30 – Steady-state test results for Pd(0.3)Ce(2)-HMOR with different GHSV. Conditions: 1000 ppm NO, 1000 ppm CH_4, 7 vol.% O_2, T = 500 ºC.

It is possible to observe that CH_4 conversion decreases with the increasing of GHSV, which was expectable due to the decrease of the contact time between the reaction mixture and the catalyst. However, NO_x conversion remains the same between 20000-40000 h^{-1}. This means that in this range of contact times, only CH_4 direct combustion is being affected, not NO_x SCR reaction. Only at 60000 h^{-1} the NO_x conversion value becomes lower, which suggest that for this GHSV value the NO_x adsorption might become affected. Notwithstanding, it is intriguing to observe that CH_4 selectivity to SCR increases with GHSV. One possible explanation could be, again, the decreasing of CH_4 contact time with the catalyst, which decreases the direct combustion. This could be an evidence that the formation of eventual intermediate species is easier than the direct oxidation of CH_4.

II.6.1.2. <u>CH_4/NO inlet feed ratio</u>

Figure II-31 illustrates the steady-state test results (performed at maximum conversion temperature) when considering different [CH_4]/[NO] ratios in the inlet feed (1000 ppm NO, 7 vol.% O_2, T = 500 ºC, GHSV = 40000 h^{-1}).

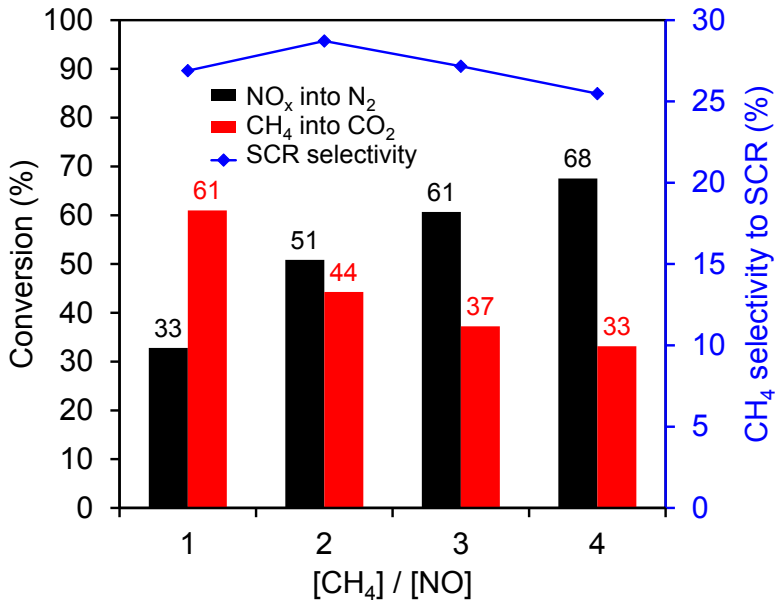

Figure II-31 – Steady-state test results for Pd(0.3)Ce(2)-HMOR with different inlet feed mixtures considering different $[CH_4]/[NO]$ ratios. Conditions: 1000 ppm NO, 7 vol.% O_2, T = 500 ºC, GHSV = 40000 h^{-1}.

It is possible to observe that NO_x conversion into N_2 increases with the increasing amount of reductant in the inlet stream. However, it should be noted that, independently the $[CH_4]/[NO]$ ratio considered in the inlet stream, the CH_4 selectivity towards SCR reaction is kept practically constant, between 25-27%. Based on these results, one can say that SCR selectivity is a crucial parameter to take into account when designing a NO_x CH_4-SCR catalyst. Hence, strategies for increasing this parameter shall be considered in the optimisation of catalyst formulation towards a commercial application.

II.6.1.3. Effect of water

Water is naturally present in the exhaust gases due to the combustion of the fuel that occurs in the motor. In order to assess the effect of water presence in the catalytic activity, tests were also performed in the same conditions previously described, now including 2 vol.% H_2O in the inlet feed. It is know that exposure to water may cause several modifications in the zeolite-based catalyst containing metals, namely the migration of species, which may result in partial deactivation. Consequently, in order to understand the effect of water exposure, a sequence of dry/wet/dry tests was also performed in Pd(0.3)Ce(2)-HMOR (Figure II-32).

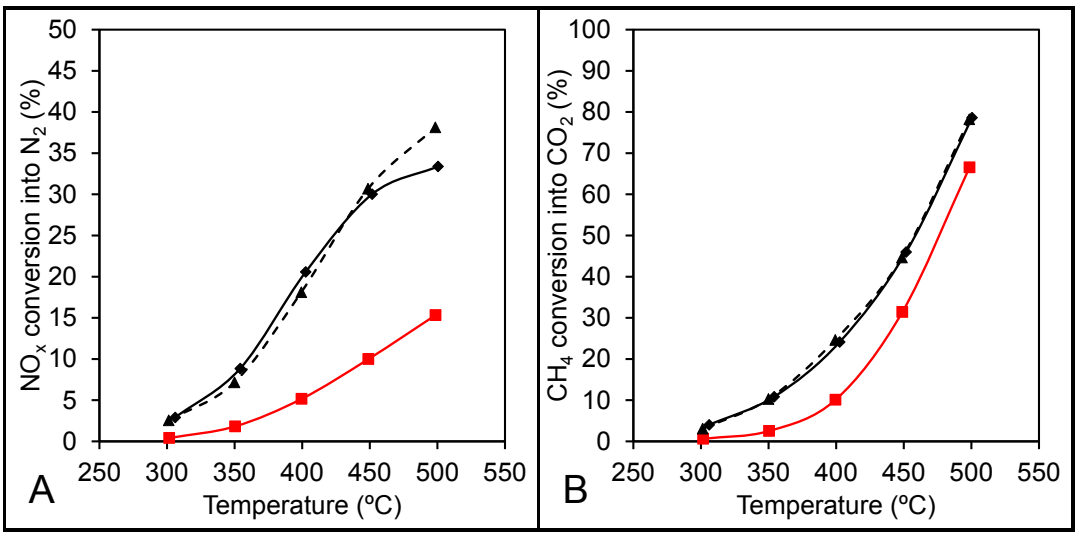

Figure II-32 – NO conversion into N_2 (A), CH_4 conversion into CO_2 (B) and CH_4 selectivity to SCR (C) of Pd(0.3)Ce(2)-HBEA: 1st dry test (♦), wet test (■) and 2nd dry test (▲). Conditions: 1000 ppm NO, 1000 ppm CH_4, 7 vol.% O_2, 2 (or 0) vol.% H_2O and GHSV = 40000 h^{-1}.

As it was expected, once water is added to the inlet stream (wet test), a drastic decrease of NO_x conversion is observed, as well as the decrease in the CH_4 conversion. This can be explain by the fact that water competitively adsorbs in the actives sites of the catalysts, causing an inhibition effect. However, after removing the water from the inlet stream (2nd dry test), the catalyst totally recover its NO_x and CH_4 conversion, which suggest that the presence of water did not irreversibly deactivate the catalyst. In order to try to understand if significant changes occurred in the active phases, H_2-TPR and DRS UV-Vis were performed on a fresh and used sample, the later one consisting in a sample obtained after a dry/wet/dry cycle.

Figure II-33 illustrates H_2-TPR profiles of both fresh and used samples of Pd(0.3)Ce(2)-HMOR. It is possible to notice changes in both reduction peaks at T< 215 ºC (corresponding to Pd^{2+} in exchange positions and surface Ce^{4+} species) and at T > 230 ºC (corresponding to CeO_2 in interaction with Pd species).

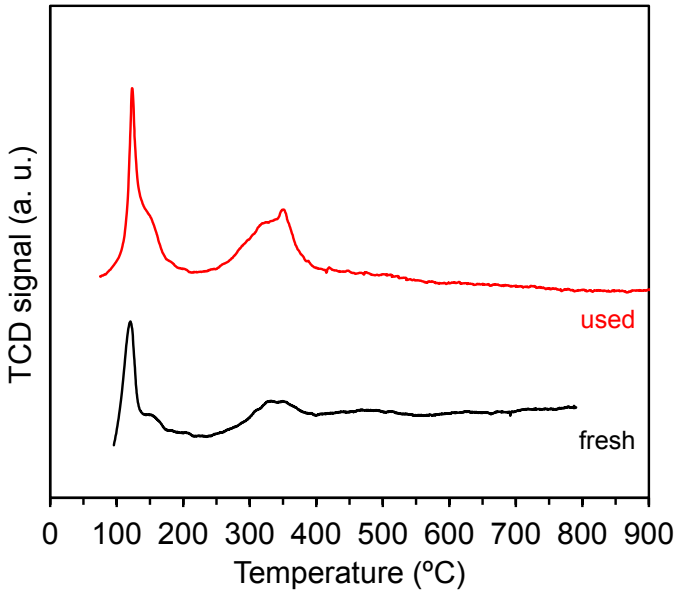

Figure II-33 – H_2-TPR profile of Pd(0.3)Ce(2)-HMOR, fresh and used.

The quantification of H_2 consumption is presented in Table II-12. It is possible to notice that H_2 consumption is higher, for both peaks, in the used catalyst. This suggests that some changes on Ce species might have occurred, namely stabilisation of more Ce^{4+} species, as well as the increasing of CeO_2 species interacting with Pd species.

Table II-12 – Quantification of H_2 consumption by peak integration of H_2-TPR profiles of Pd(0.3)Ce(2)-HMOR, fresh and used.

	Peak 1			Peak 2		
	T (ºC)	H_2/Pd	µmol H_2 /$g_{catal.}$	T (ºC)	H_2/Ce	µmol H_2 /$g_{catal.}$
fresh	95-215	1.4	39	240-560	0.28	37
used	70-215	2.2	61	230-560	0.41	56

DRS UV-Vis spectra of both fresh and used samples of Pd(0.3)Ce(2)-HMOR are presented in Figure II-34.

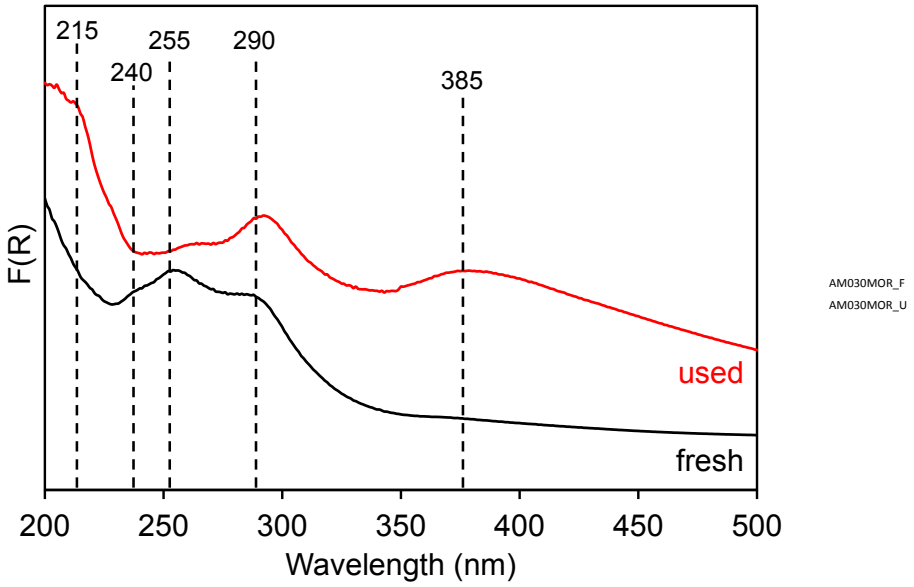

Figure II-34 – Diffuse Reflectance UV-Vis spectra of Pd(0.3)Ce(2)-HMOR, fresh and used.

One can observed that, for the used sample, the intensity of the band at 290 nm, corresponding to Ce^{4+} species, increased relatively to the band 255 nm, corresponding to Ce^{3+} species. This is in agreement with the H_2-TPR results that support the idea that Ce^{4+} species increased after test. Moreover, the band at 385 nm (corresponding to d-d transition of Pd^{2+} ions in exchange position) also increased intensity relatively to other bands, which could be related to interaction of CeO_2 species with Pd species. The bands at 215 and 240 nm, corresponding to Pd species, are also different in both samples, which evidences that some changes might have occurred with Pd species. Nevertheless, these are not likely to be significant, since after water expose, the catalyst continues to be active. In fact, it is likely that a significant part of Pd^{2+} ions in exchange position stayed unchanged, which explains the restore in conversion after removing water from the inlet feed.

II.6.2. Representative conditions of real lean-gas engine

The catalytic performance of the catalyst considered in this study was also assessed by considering inlet gas feed mixture (Mix 4, Table II-13) representative of real exhaust gases of a heavy duty vehicle's engine (Volvo engine MG9 in lean-gas burn conditions).

In order to assess the role of CO and H_2 as possible reductants in the NO_x SCR reaction, a reference mixture containing only CH_4, NO and O_2 (Mix 1) was considered. Mix 2 results from the addition of CO to Mix 1 and Mix 3 results from the addition of both CO and H_2. The steady-state test results are illustrated in Figure II-35.

Table II-13 – Inlet gas feed mixtures corresponding to Volvo engine MG9 exhaust gases (lean-burn conditions).

	Mix 1	**Mix 2**	**Mix 3**	**Mix 4**
[NO] / ppm	400	400	400	400
[CH_4] / ppm	1600	1600	1600	1600
[O_2] / %	7	7	7	7
[CO] / ppm	-	650	650	650
[H_2] / ppm	-	-	500	500
[H_2O] / %	-	-	-	2
GHSV / h^{-1}	40000	40000	40000	40000

II.6.2.1. Steady-state tests

When considering Mix 1 to 3 as inlet gas feed, NO_x conversion into N_2 is practically the same. The results show that the presence of CO and H_2 do not contribute to the NO_x SCR in the range of temperatures were NO_x conversion is pertinent (300-500 ºC) since these reducing agents are already completely consumed at 300°C in lean conditions (see next section).

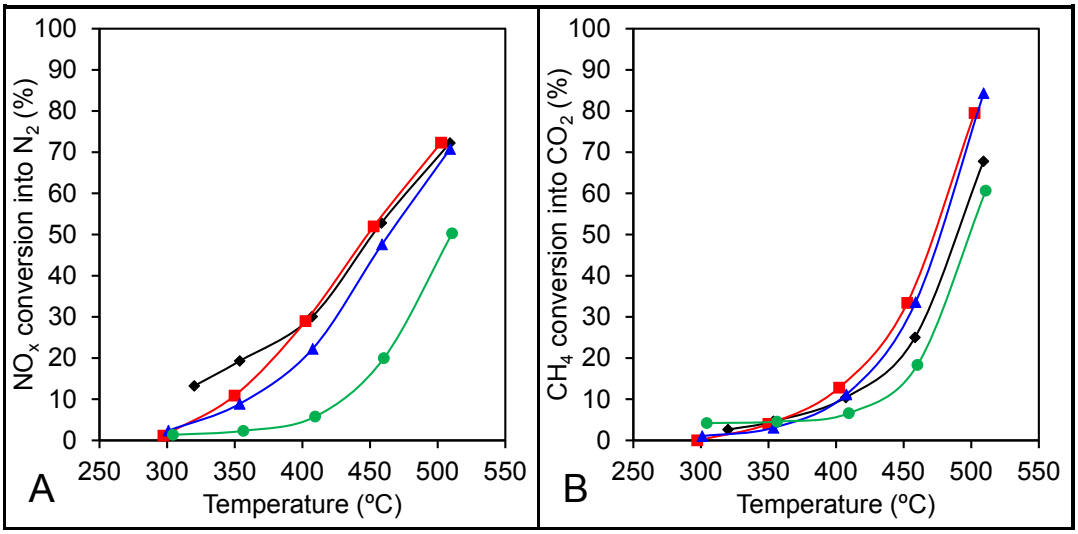

Figure II-35 – Steady-state test results with different inlet feed mixtures corresponding to Volvo engine MG9 exhaust gases (lean-burn conditions): Mix 1 (♦), Mix 2 (■), Mix 3 (▲) and Mix 4 (●):

The maximum NO_x conversion in obtained at 500 ºC and it is significantly higher than the one obtained when considering 1000 ppm NO / 1000 ppm CH_4 in the inlet feed (*ca.* 70% vs. 34%), which is naturally related to the presence of more reductant relatively to NO. In fact, the conversion obtain with Mix 1-3 is practically the same previously obtained with 1000 ppm NO / 4000 ppm CH_4, where the $[CH_4]/[NO]$ ratio in the inlet feed was also 4 (*ca.* 68%, at 500 ºC - Figure II-31, page 116).

As expected, when considering water in the inlet gas feed, both conversions decrease due to the competitive adsorption between water and the reactants. Notwithstanding, it should be mentioned that, when considering the representative conditions of real exhaust gases, NO_x conversion is much higher than when considering 1000 ppm NO / 1000 ppm CH_4 (*ca.* 50% vs. 16%, at 500 ºC).

II.6.2.2. Temperature programmed surface reaction (TPSR) tests

H_2 and CO are known to potentiate the NO_x CH_4-SCR reactions over Pd-MOR catalysts, especially at low temperatures (below 250 ºC) [7]. In order to further understand the roles of the different reducing agents in the NO_x SCR reaction, TPSR tests were performed and are analysed herein. Figure II-36 illustrates the results obtained using Mix 1 as inlet feed (CH_4+NO+O_2).

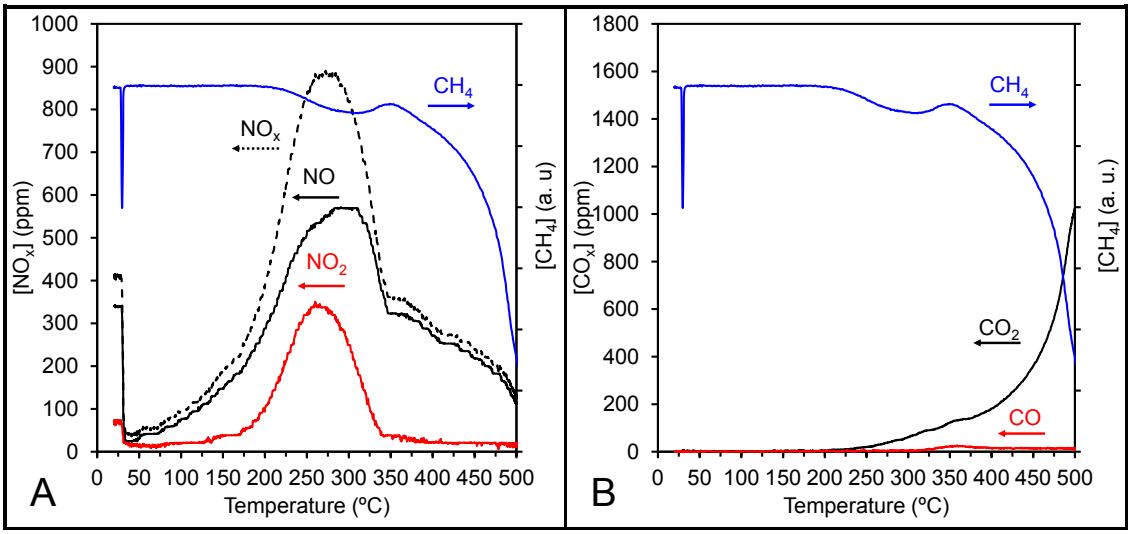

Figure II-36 – TPSR test results for Pd(0.3)Ce(2)-HMOR with Mix 1 inlet feed corresponding to Volvo engine MG9 exhaust gases (lean-burn conditions): NO_x (A) and CO_x (B) profiles.

It is possible to observe that CH_4 signal starts to decrease at *ca.* 200 ºC, same temperature where the NO_2 formation starts to take place. Several HC-SCR mechanisms consider the interaction of NO_2 and CH_4 to give intermediate species that participate in the reaction, such as $C_xH_yO_z$ or R-NO_x adsorbed species [51], which explains the results. Nevertheless, deNO_x activity is only registered after 340 ºC, temperature above which NO_x concentration becomes lower than 400 ppm.

In Figure II-37 are presented the test results considering Mix 2 as inlet feed (CH_4+NO+O_2+CO).

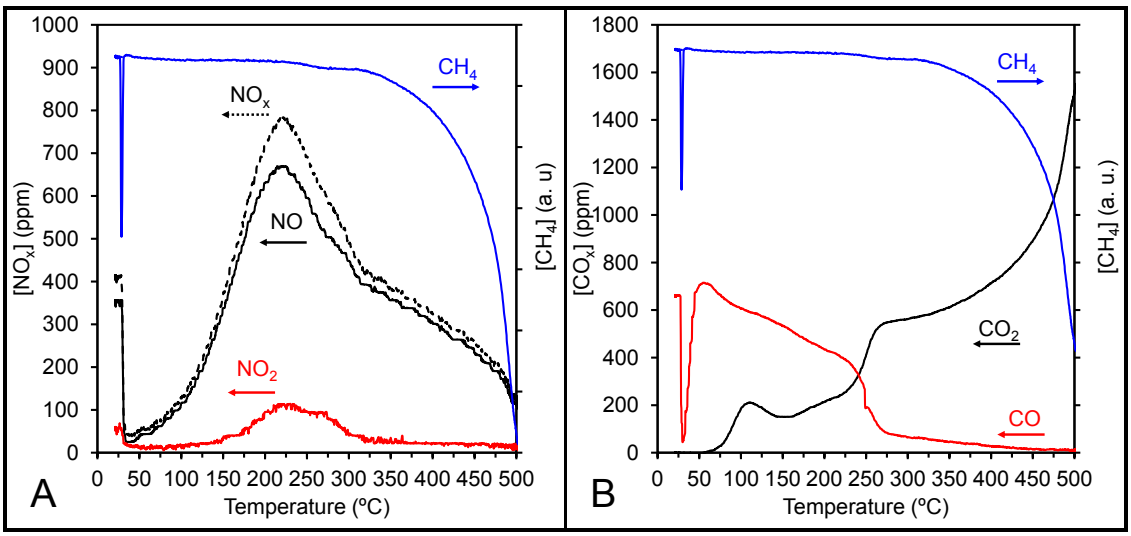

Figure II-37 – TPSR test results for Pd(0.3)Ce(2)-HMOR with Mix 2 inlet feed corresponding to Volvo engine MG9 exhaust gases (lean-burn conditions): NO_x (A) and CO_x (B) profiles.

Around 100 ºC, it is possible to observe a peak of CO_2 formation likely to be associated to the oxidation of CO that adsorbed at lower temperatures. Nevertheless, CO concentration starts to decrease after 50 ºC, which suggests it becomes oxidised at lower temperatures as well. CH_4 signal only starts to decrease at 250 ºC, when almost half of CO has already reacted. It seems that a competitive adsorption effect by CO occurs in the same sites where the formation of intermediate species from NO_2 and CH_4 takes place. With Mix 2, deNO_x activity is observed around the same temperature as with Mix 1, *ca.* 340 ºC.

The results obtained considering Mix 3 (CH_4+NO+O_2+CO+H_2) as inlet feed are presented in Figure II-38.

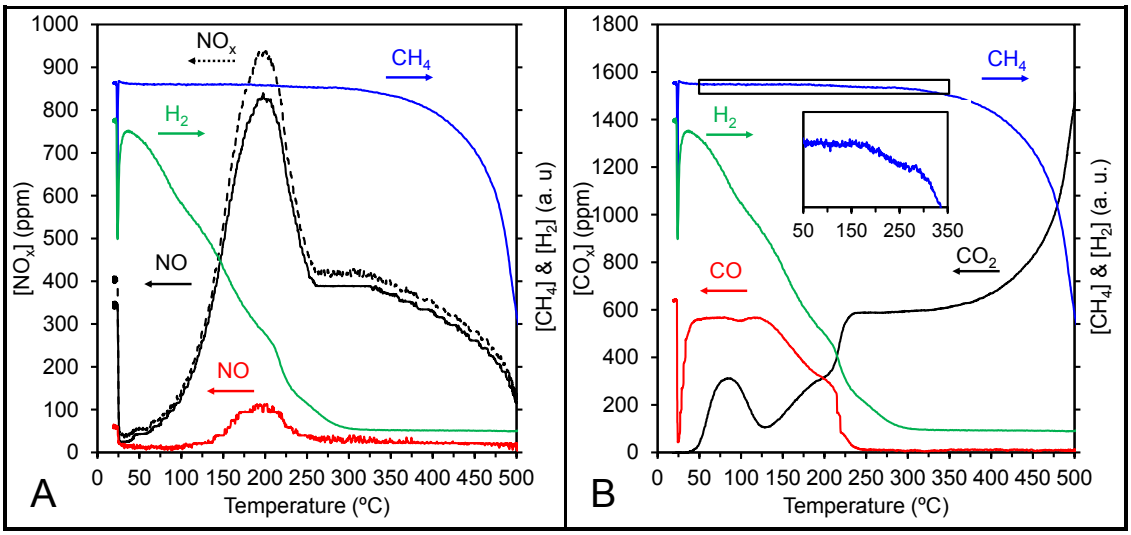

Figure II-38 – TPSR test results for Pd(0.3)Ce(2)-HMOR with Mix 3 inlet feed corresponding to Volvo engine MG9 exhaust gases (lean-burn conditions): NO_x (A) and CO_x (B) profiles.

It is possible to see that CO concentration remains stable until 130 ºC. However, from *ca.* 50 to 80 ºC, one can observe an increase of CO_2 associated to the oxidation of adsorbed CO. Between 80 and 130 ºC, CO_2 concentration decreases. Additionally, until 130 ºC, H_2 concentration decreases and no water formation is observed in MS, *i.e.* H_2 is not being oxidised. Pieterse, *et al.* [7] suggested that the formation adsorbed NCO species would occur after the adsorption of NO, H_2 and CO, consecutively. This species would be involved in the CO/H_2-SCR mechanism reaction.

At 130 ºC, CO concentration starts to decrease and CO_2 increases again, which coincides with the beginning of NO_2 desorption process. Above 170 ºC, water formation is observed in the MS, suggesting that H_2 oxidation starts to take place. CH_4 only starts to decrease at 190 ºC, precisely at the same temperature where NO_2 concentration is maximal. It is worthy to mention that CO is totally oxidised above 250 ºC and H_2 above 300 ºC, which mean they do not participate in the deNO_x process from 300-500 ºC.

Figure II-39 illustrates the results obtained considering Mix 4 as inlet feed (CH_4+NO+O_2+CO+H_2+H_2O)

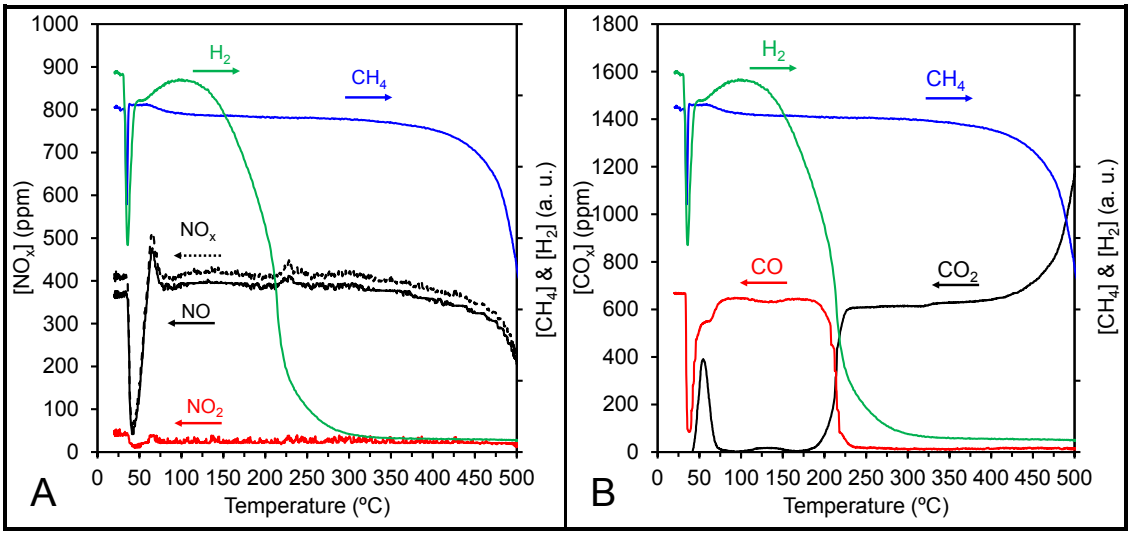

Figure II-39 – TPSR test results for Pd(0.3)Ce(2)-HMOR with Mix 4 inlet feed corresponding to Volvo engine MG9 exhaust gases (lean-burn conditions): NO_x (A) and CO_x (B) profiles.

The competitive adsorption effect of water can be clearly observed. Contrarily to what happen with Mix 3, the CO oxidation to CO_2 between 80-130ºC does not take place (CO_2 desorption peak between 45 and 75 ºC is likely due to some CO adsorption that might have occurred in the initial moments that the mixture contacted the catalyst). Moreover, H_2 and CO concentrations at *ca.* 150 ºC are similar to the ones observed in by-pass. Only above this temperature H_2 starts to decrease, likely due to oxidation, whereas CO is kept practically constant. Hence, the formation of NCO adsorbed species is not expected to occur. Moreover, the NO_x desorption peak below 250 ºC are also not observed.

II.7. Conclusions

In this chapter, important insights on the preparation of PdCe-MOR catalysts, active for NO_x selective catalytic reduction using methane as reductant (NO_x CH_4-SCR) were presented.

Previous studies show that are several parameters concerning the catalysts preparation that influence their catalytic performance for NO_x CH_4-SCR, namely, the palladium precursor [30]. In this work, it was shown that palladium introduction method also influences the catalytic performance of Pd/zeolite-based catalysts. When Pd is introduce by ion-exchange, better catalytic performance are achieved. Several studies reported in the literature reported the effect of Pd loading on zeolite-based catalysts, showing for instance that values between 0.7-1 wt.% Pd resulted in the better NO_x CH_4-SCR performance over Pd-MFI catalysts [11, 12]. In this work, it was verified that the increase of palladium loading in Pd-HMOR results in a decrease of NO_x selectivity towards N_2, favouring N_2O formation. Above 0.3 wt.% Pd, CH_4 conversion increases with the Pd loading, whereas total NO_x conversion is kept constant. The best catalytic performance for NO_x CH_4-SCR is achieved with 0.3 wt.% Pd, which is in agreement with other results, previously reported in the literature [41, 69].

The addition of cerium to Pd-HMOR is known to enhance the catalytic performance for NO_x CH_4-SCR [7, 8], though the effect of Ce loading has never been reported. The results obtained within this work show that, by adding 1 wt.% Ce, both NO_x conversion into N_2 and CH_4 selectivity towards SCR reaction are increased. However, for Ce loading above 3 wt.%, CH_4 direct combustion becomes highly favoured, in particular at high temperatures, resulting a worst NO_x CH_4-SCR performance. Pd^{2+} ions in exchange position are active species for deNO_x process. CeO_2 species play an important role in the NO oxidation to NO_2, which is considered a first key step in the HC-SCR reaction. For PdCe-HMOR system, the existence CeO_2 in interaction with Pd species are responsible for enhancing the catalytic performance. Moreover, it seems that the balance between CeO_2 species in interaction with Pd and CeO_2 species not in interaction stabilised in the MOR zeolite is an important parameter that influences the capacity of PdCe-HMOR catalysts for effectively using CH_4 as reductant in deNO_x process or promoting its direct combustion instead.

The influence of Pd loading in bimetallic PdCe-HMOR system was also assessed. It was shown that Pd loading does not influence the stabilisation of Ce species. However, it was observed that, when Pd is introduced before Ce, a better catalytic performance can be achieved. When Ce is introduced first, more Ce^{4+} species are stabilised and less CeO_2 species in interaction with Pd are present in the catalyst, which results a lower CH_4 selectivity towards SCR.

Regarding the effect of test conditions, it was shown that the increase of GHSV has a considerable effect in the CH_4 interaction with the support, decreasing CH_4 direct combustion. However, NO_x conversion is significantly less affected, which suggests that NO_x adsorption is likely not to be as affected as CH_4 interaction with the catalyst. Moreover, NO_x conversion can be increased by increasing the $[CH_4]/[NO]$ ratio in the inlet gas feed. However, independently of the $[CH_4]/[NO]$ ratio

considered, CH_4 selectivity towards NO_x SCR reaction remains practically constant. The improvement of this parameter is likely to be the key in order to obtain a better catalytic performance. Also, the presence of water in the inlet gas feed significantly decreases both NO_x and CH_4 conversions. Though some changes on Ce species were observed after water exposure, the main deNO_x active species (Pd^{2+} ions) are likely not to be affected, reason why water seems not to cause a deactivation effect, but an inhibition instead.

H_2 and CO are known to potentiate the NO_x CH_4-SCR reactions over Pd-MOR catalysts, especially at low temperatures (below 250 ºC) [7]. In this work, tests performed under representative conditions of real exhaust gases from heavy duty vehicle's engine revealed (TPSR tests) that CO and H_2 do not play a role in the NO_x SCR in the range of temperature where NO_x conversion is pertinent (300-500 ºC), being directly oxidised to CO_2 and H_2O.

A possible strategy to enhance the catalytic performance of this catalytic system shall consider the stabilisation of metal species capable of effectively promote the formation of intermediary species, from CO and H_2, in order to promote NO_x SCR at low temperatures (< 300 ºC), making possible to enlarge the conversion window and, thus, to enhance the catalytic performance.

II.8. References

[1] Y.J. Li, J.N. Armor, Appl. Catal., B, 1 (1992) L31-L40.

[2] L. Gutierrez, A. Boix, J.O. Petunchi, J. Catal., 179 (1998) 179-191.

[3] A. Kubacka, J. Janas, B. Sulikowski, Appl. Catal., B, 69 (2006) 43-48.

[4] M. Ogura, Y. Sugiura, M. Hayashi, E. Kikuchi, Catal. Lett., 42 (1996) 185-189.

[5] A.P. Ferreira, S. Capela, P. Da Costa, C. Henriques, M.F. Ribeiro, F.R. Ribeiro, Catal. Today, 119 (2007) 156-165.

[6] European Chemicals Agency, website, Candidate List of Substances of Very High Concern for Authorisation, http://echa.europa.eu/candidate-list-table, accessed in June 2015.

[7] J.A.Z. Pieterse, S. Booneveld, Appl. Catal., B, 73 (2007) 327-335.

[8] I.O. Costilla, M.D. Sanchez, M. Alicia Volpe, C.E. Gigola, Catal. Today, 172 (2011) 84-89.

[9] A. Ali, W. Alvarez, C.J. Loughran, D.E. Resasco, Appl. Catal., B, 14 (1997) 13-22.

[10] Y. Nishizaka, M. Misono, Chem. Lett., 8 (1993) 1295-1298.

[11] M. Misono, Y. Nishizaka, M. Kawamoto, H. Kato, in: H. Chon, S.-K. Ihm, Y. S. Uh (Eds.) Stud. Surf. Sci. Catal., Elsevier, 1997, 105, 1469-1474

[12] M. Ogura, M. Hayashi, S. Kage, M. Matsukata, E. Kikuchi, Appl. Catal., B, 23 (1999) 247-257.

[13] S.T. Homeyer, W.M.H. Sachtler, Appl. Catal., 54 (1989) 189-202.

[14] B.J. Adelman, W.M.H. Sachtler, Appl. Catal., B, 14 (1997).

[15] S.N. Reifsnyder, M.M. Otten, H.H. Lamb, Catal. Today, 39 (1998) 317-328.

[16] A.P. Ferreira, Redução Catalítica Selectiva de NOx com Metano sobre Zeólitos com Cobalto e Paládio, PhD Thesis, Universidade Técnica de Lisboa - Instituto Superior Técnico, Lisboa, 2006.

[17] Y.-S. Bi, G.-Y. Dang, X.-H. Zhao, X.-F. Meng, H.-J. Lu, J.-T. Jin, J. Hazard. Mater., 229–230 (2012) 245-250.

[18] E.M. Alayon, M. Nachtegaal, M. Ranocchiari, J.A. van Bokhoven, Chem. Commun., 48 (2012) 404-406.

[19] H.L. Tidahy, S. Siffert, J.F. Lamonier, R. Cousin, E.A. Zhilinskaya, A. Aboukais, B.L. Su, X. Canet, G. De Weireld, A. Frere, J.M. Giraudon, G. Leclercq, Appl. Catal., B, 70 (2007) 377-383.

[20] B. Wen, Q. Sun, W.M.H. Sachtler, J. Catal., 204 (2001) 314-323.

[21] J. Dedecek, B. Wichterlova, J. Phys. Chem. B, 103 (1999) 1462-1476.

[22] W.J. Mortier, Compilation of Extra Framework Sites in Zeolites, Butterworth Scientific Limited, 1982.

[23] R. Grybos, J. Hafner, L. Benco, H. Toulhoat, J. Phys. Chem. C, 111 (2007) 6454-6464.

[24] A.M. De Oliveira, I. Costilla, C. Gigola, I.M. Baibich, V.T. da Silva, S.B.C. Pergher, Catal. Lett., 136 (2010) 185-191.

[25] K. Shimizu, F. Okada, Y. Nakamura, A. Satsuma, T. Hattori, J. Catal., 195 (2000) 151-160.

[26] K.I. Hadjiivanov, G.N. Vayssilov, Adv. Catal., 47 (2002) 307-511.

[27] V. Gruver, J.J. Fripiat, J. Phys. Chem., 98 (1994) 8549-8554.

[28] M. Armandi, B. Bonelli, E. Garrone, M. Ardizzi, F. Cavani, L. Dal Pozzo, L. Maselli, R. Mezzogori, G. Calestani, Appl. Catal., B, 70 (2007) 585-596.

[29] H. Decolatti, H. Solt, F. Lonyi, J. Valyon, E. Miro, L. Gutierrez, Catal. Today, 172 (2011) 124-131.

[30] R. Marques, L. Mazri, S. Da Costa, F. Delacroix, G. Djega-Mariadassou, P. Da Costa, Catal. Today, 137 (2008) 179-184.

[31] R. Marques, L. Mazri, S. Da Costa, F. Delacroix, G. Djega-Mariadassou, P. Da Costa, Catal. Today, 137 (2008) 185-190.

[32] D. Kaucky, A. Vondrova, J. Dedecek, B. Wichterlova, J. Catal., 194 (2000) 318-329.

[33] P. Gelin, M. Primet, Appl. Catal., B, 39 (2002) 1-37.

[34] Y.J. Li, J.N. Armor, Appl. Catal., B, 3 (1994) 275-282.

[35] C. Descorme, P. Gélin, C. Lécuyer, M. Primet, J. Catal., 177 (1998) 352-362.

[36] A. Trovarelli, Cat. Rev. - Sci. Eng., 38 (1996) 439-520.

[37] L.F. Cordoba, M. Flytzani-Stephanopoulos, C.M. de Correa, Appl. Catal., B, 33 (2001) 25-33.

[38] Z.J. Li, M. Flytzani-Stephanopoulos, J. Catal., 182 (1999) 313-327.

[39] J.T. Miller, E. Glusker, R. Peddi, T. Zheng, J.R. Regalbuto, Catal. Lett., 51 (1998) 15-22.

[40] B.J. Adelman, W.M.H. Sachtler, Appl. Catal., B, 14 (1997) 1-11.

[41] C.J. Loughran, D.E. Resasco, Appl. Catal., B, 7 (1995) 113-126.

[42] Y. Nishizaka, M. Misono, Chem. Lett., 12 (1994) 2237-2240.

[43] C.A. Emeis, J. Catal., 141 (1993) 347-354.

[44] I. Graça, L.V. González, M.C. Bacariza, A. Fernandes, C. Henriques, J.M. Lopes, M.F. Ribeiro, Appl. Catal., B, 147 (2014) 101-110.

[45] Q.Q. Huang, X.M. Xue, R.X. Zhou, J. Mol. Catal. A: Chem., 331 (2010) 130-136.

[46] J.B. Miller, M. Malatpure, Appl. Catal., A, 495 (2015) 54-62.

[47] F.A.C. Garcia, D.R. Araujo, J.C.M. Silva, J.L. de Macedo, G.F. Ghesti, S.C.L. Dias, J.A. Dias, G.N.R. Filho, J. Brazil. Chem. Soc., 22 (2011) 1894-1902.

[48] G. Leofanti, M. Padovan, G. Tozzola, B. Venturelli, Catal. Today, 41 (1998) 207-219.

[49] M. Daturi, C. Binet, J.C. Lavalley, A. Galtayries, R. Sporken, Phys. Chem. Chem. Phys., 1 (1999) 5717-5724.

[50] G. Djega-Mariadassou, Catal. Today, 90 (2004) 27-34.

[51] O. Gorce, F. Baudin, C. Thomas, P. Da Costa, G. Djega-Mariadassou, Appl. Catal., B, 54 (2004) 69-84.

[52] A. Lamacz, A. Krzton, G. Djega-Mariadassou, Appl. Catal., B, 142 (2013) 268-277.

[53] T. Liese, E. Loffler, W. Grunert, J. Catal., 197 (2001) 123-130.

[54] S. Capela, R. Catalao, P. Da Costa, G. Djega-Mariadassou, F.R. Ribeiro, F. Ribeiro, C. Henriques, in: A.M.P.B.F. Gedeon (Ed.) Zeolites and Related Materials: Trends, Targets and Challenges, Proceedings of the 4th International Feza Conference, 2008, pp. 1033-1038.

[55] S. Capela, R. Catalao, M.F. Ribeiro, P. Da Costa, G. Djega-Mariadassou, F.R. Ribeiro, C. Henriques, Catal. Today, 137 (2008) 157-161.

[56] A.B. Gaspar, L.C. Dieguez, Appl. Catal., A, 201 (2000) 241-251.

[57] S. Capela, Estudo Mecanístico do Processo DeNOx: Activação do Metano com NO2 sobre Pd-Co-Ferrierite, PhD Thesis, Universidade Técnica de Lisboa - Instituto Superior Técnico, Lisboa, 2009.

[58] R. Serra, M.J. Vecchietti, E. Miro, A. Boix, Catal. Today, 133 (2008) 480-486.

[59] X.D. Wang, T. Zhang, X.Y. Sun, W. Guan, D.B. Liang, L.W. Lin, Appl. Catal., B, 24 (2000) 169-173.

[60] R.Q. Long, R.T. Yang, J. Catal., 207 (2002) 274-285.

[61] G. Delahay, D. Valade, A. Guzman-Vargas, B. Coq, Appl. Catal., B, 55 (2005) 149-155.

[62] F. Hamidi, C. Petitto, C. Signorile, G. Delahay, A. Bengueddach, React. Kinet. Mech. Cat., 104 (2011) 429-436.

[63] S.A. Skarlis, D. Berthout, A. Nicolle, C. Dujardin, P. Granger, J. Phys. Chem. C, 117 (2013) 7154-7169.

[64] S. Bordiga, R. Buzzoni, F. Geobaldo, C. Lamberti, E. Giamello, A. Zecchina, G. Leofanti, G. Petrini, G. Tozzola, G. Vlaic, J. Catal., 158 (1996) 486-501.

[65] J. Perez-Ramirez, J. Catal., 227 (2004) 512-522.

[66] M.S. Kumar, M. Schwidder, W. Grunert, A. Bruckner, J. Catal., 227 (2004) 384-397.

[67] J.Y. Wang, H.A. Xia, X.H. Ju, F.T. Fan, Z.C. Feng, C. Li, Chin. J. Catal., 34 (2013) 876-888.

[68] L.L. Ren, T. Zhang, Chin. Chem. Lett., 21 (2010) 674-677.

[69] A. Ali, Y.H. Chin, D.E. Resasco, Catal. Lett., 56 (1998).

Chapter III. Potential synergic effect between BEA and MOR zeolites in NO_x CH_4-SCR.

III.1. Introduction

Despite the fact that MOR, MFI and FER zeolites represent the frameworks that allow to obtain better catalytic performance of metal-containing zeolite-based catalysts for NO_x selective catalytic reduction using methane as reductant (NO_x CH_4-SCR), other zeolites have been also considered in some studies, namely BEA zeolite, but in a considerably lower number [1-6] . Notwithstanding, according to literature, BEA zeolite was the only support that allowed to obtain a catalyst that, once exposed to water, improved its catalytic performance for NO_x CH_4-SCR [2], more precisely, a Co-Pd-BEA formulation. The use of this metal combination was widely reported in the literature (see Chapter I), but never an effect as the previously mentioned one have been observed when using other supports, which is likely to suggest that this may be a unique feature of this structure. Since real exhaust gases necessarily contain water in their composition (as a result of the fuel combustion that takes place in the engine), an attempt to reproduce this results, even with different metal formulations, might be a key point in the development of this technology towards a commercial application. This was the main motivation for the study of PdCe-BEA system, herein presented.

Moreover, different authors have reported the benefits of combining different catalyst for deNO_x technologies, both zeolite-based catalysts for HC-SCR [7, 8] and even some examples are reported for NO_x CH_4-SCR technology [9, 10]. In this section, a combination of MOR- and BEA-based catalysts was also considered.

III.2. Pd/Ce-BEA system

III.2.1. Catalyst preparation

Both Pd(0.3)-HBEA and Pd(0.3)Ce(2)-HBEA catalyst were prepared by following the same procedure used in the preparation of Pd(0.3)-HMOR and Pd(0.3)Ce(2)-HMOR (see Annex A, sections C.1.2 and C.1.3), using NH_4BEA as starting material (Si/Al = 12.5). Table II-1 contains the chemical composition of both Pd/Ce-containing BEA catalysts considered in this chapter, obtained by ICP analysis.

Table III-1 – Chemical composition of the Pd/Ce-containing BEA catalysts obtained by ICP analysis.

Catalyst	Al (wt.%)	Pd (wt.%)	Ce (wt.%)	ER_{Pd}* (%)	ER_{Ce}* (%)
Pd(0.3)-HBEA	2.66	0.29	-	5.5	-
Pd(0.3)Ce(2)-HBEA	2.49	0.24	1.4	4.9	32.5

*ER – Exchange Rate (Assuming 2+ and 3+ coordination for Pd and Ce, respectively).

III.2.2. Temperature programmed reduction under hydrogen (H_2-TPR)

Figure III-1 illustrates the H_2-TPR profiles of Pd(0.3)-HBEA and Pd(0.3)Ce(2)-BEA catalysts.

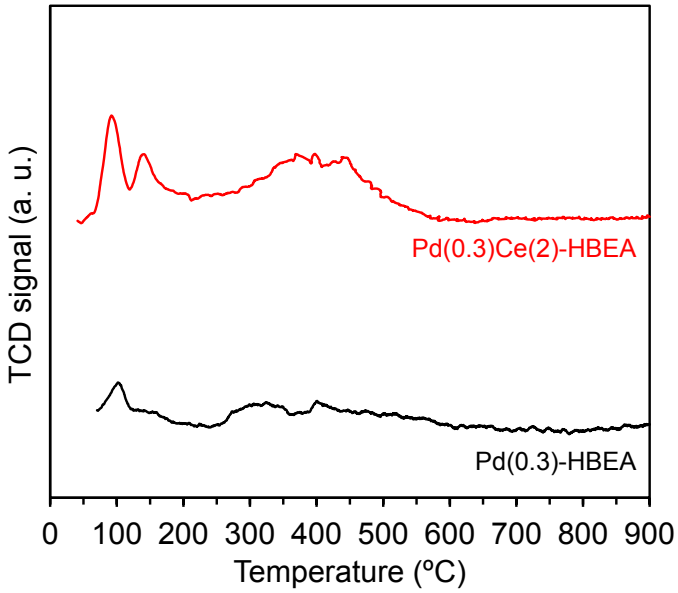

Figure III-1 – H_2-TPR profiles of Pd(0.3)-HBEA and Pd(0.3)Ce(2)-HBEA catalysts.

Conversely to what happens for Pd(0.3)-HMOR (see Chapter II, section II.3.1.1), in Pd(0.3)-HBEA the reduction peak corresponding to Pd^{2+} species (65-215 ºC) is much less intense. This might lead to the conclusion that palladium could be stabilised in this structure in its reduced form. However, there is evidence in the literature that, in fact, palladium species (namely PdO) in BEA zeolites are reduced at much lower temperature that in MOR, namely at from -20 to 25 ºC, as reported elsewhere [11]. This means that during the stabilisation of TCD signal, when the sample is put in contact with H_2/Ar stream at room temperature, it is likely that Pd species become reduced.

When cerium is added to Pd(0.3)-HBEA, the previously mentioned reduction peak becomes more intense and a second reduction peak can be clearly distinguished from the first one, between 120-205 ºC. This later one is likely to correspond to the reduction of surface Ce^{4+} species [12] and the fact that it does not appear overlapped with reduction peak corresponding to Pd^{2+} species, like in Pd(0.3)Ce(2)-HMOR catalyst, might be explained due to the lower amount of Pd^{2+} species.

From the quantification of H_2 consumption from H_2-TPR profiles of both BEA catalysts (Figure II-12), one can observed that H_2/Pd ratio corresponding to the first reduction peak slightly increases for Pd(0.3)Ce(2)-HBEA. It is possible that the presence of Ce may promote the stabilisation of part of the palladium as Pd^{2+} ions in exchange position or, eventually, to contribute for a more difficult reduction (*i. e.* at higher temperature) of part of the PdO.

Table III-2 – Peak integration of H_2-TPR profiles of Pd(0.3)-HBEA and Pd(0.3)Ce(2)-HBEA.

	Peak 1				Peak 2				Peak 3		
	T (ºC)	H_2/Pd	H_2/Ce	µmol H_2 /$g_{catal.}$	T (ºC)	H_2/Pd	H_2/Ce	µmol H_2 /g_{catal}	T (ºC)	H_2/Ce	µmol H_2 /g_{catal}
Pd(0.3) -HBEA	60-215	0.41	-	11	-	-	-	-	-	-	-
Pd(0.3)Ce(2) -HBEA	65-120	0.48	0.11	11	120-205	0.22	0.05	5	215-580	0.45	45

For Pd(0.3)Ce(2)-HBEA, it is also possible to observe a third reduction process, that takes place between 215-580 ºC, like to correspond to the reduction of surface capping oxygen from CeO_2 in interaction with Pd species [12], similarly to Pd(0.3)Ce(2)-HMOR. It is worthwhile mentioning that, for Pd(0.3)Ce(2)-HBEA, H_2/Ce ratio of this species is significantly higher than the one for Pd(0.3)Ce(2)-HMOR (*ca.* 0.45 against 0.27).

In summary, palladium is likely to be stabilised as PdO in BEA catalyst, which is reduced at lower temperatures than Pd^{2+} ions in MOR catalysts. In the presence of cerium, part of this palladium becomes more hardly reduced.

III.2.3. Diffuse reflectance UV-Vis spectroscopy (DRS UV-Vis)

DRS UV-Vis spectra of Pd(0.3)-HBEA and Pd(0.3)Ce(2)-HBEA are presented in Figure III-2.

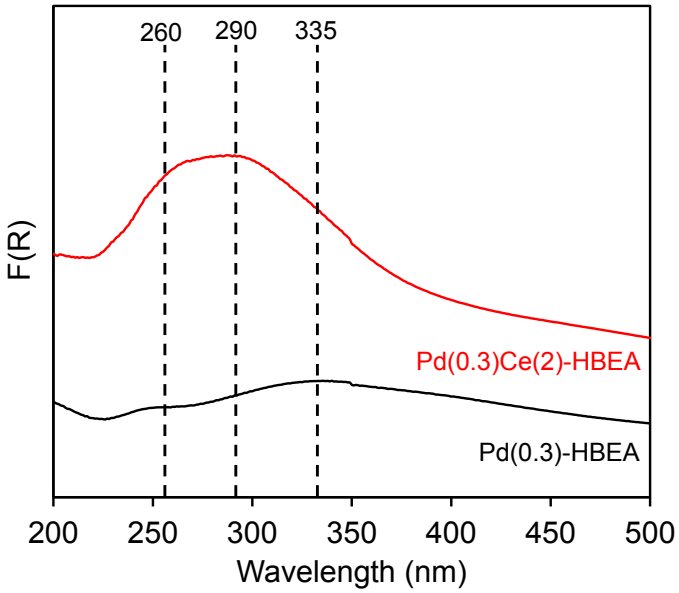

Figure III-2 – DRS UV-Vis spectra of Pd(0.3)-HBEA and Pd(0.3)Ce(2)-HBEA catalysts.

Pd(0.3)-HBEA exhibits a broad band at 335 nm, ascribed to charge transfer Pd→O [13]. It should be noted that, conversely to what was observed in DRS UV-Vis spectrum of Pd(0.3)-HMOR, a band around 400 nm corresponding to d-d transitions of Pd^{2+} species is not observed.

For Pd(0.3)Ce(2)-HBEA, two additional bands at 260 and 290 nm appear overlapped with the previous mentioned band. These two bands are the same ones observed for Pd(0.3)Ce(2)-HMOR, previously ascribed to Ce^{3+} and Ce^{4+} species, respectively (see Chapter II, section II.4.1.2).

III.2.4. Transmission electron microscopy (TEM/EDS)

TEM images of Pd(0.3)-HBEA and Pd(0.3)Ce(2)-HBEA are presented in Figure III-3. For the sake of comparison, Ce(2)-HBEA images are also shown.

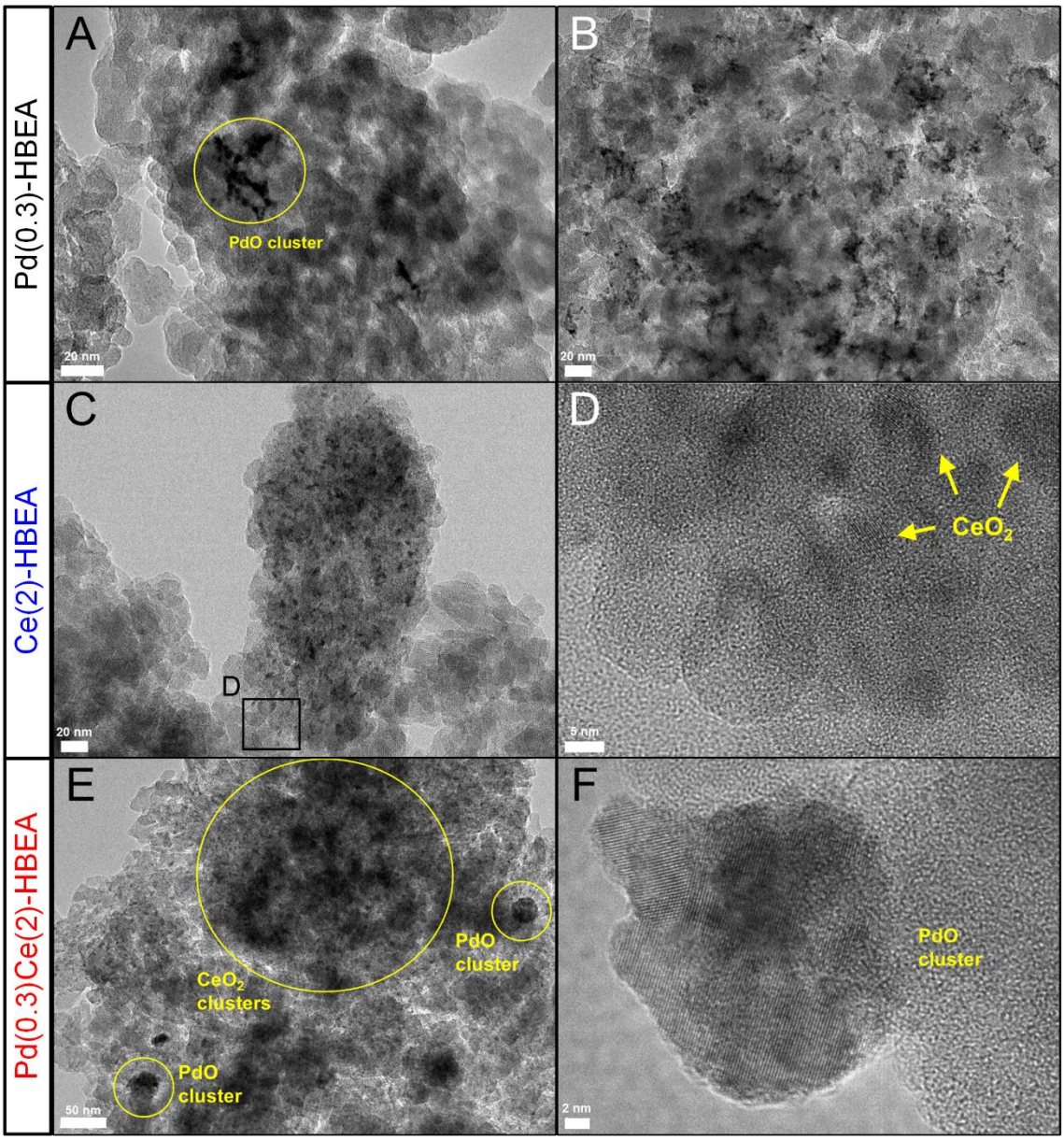

Figure III-3 – TEM images of Pd(0.3)-HMOR (A, B), Ce(2)-HBEA (C, D) and Pd(0.3)Ce(2)-HBEA (E, F).

Contrarily to Pd(0.3)-HMOR (see Chapter II, section II.4.1.3), TEM images of Pd(0.3)-HBEA reveal the existence of metal clusters in the external surface of the BEA zeolite particles (Figure III-3A,B). Energy-dispersive X-ray spectroscopy (EDS) analyses confirmed that these are, indeed, palladium clusters and HRTEM allowed the quantification of the distance between lattice planes in 2.6 Å, typical from PdO (ICDD 00-041-1107) – for further details on TEM/EDS analyses, please see Annex A.

For Ce(2)-HBEA, several metal particles can be observed in TEM images. EDS analyses confirmed these are cerium particles and, by using high resolution TEM (HRTEM), it was possible to quantify the distance between lattice planes in 2.7 and 3.1 Å, typical from CeO_2 (ICDD 00-034-0394). Like it was observed for Ce(2)-HMOR, these particles are very irregular which difficult the measurement of their size. Nevertheless, from the qualitative point of view, from the observation of the images it resembles that its concentration on the surface of zeolite particles is higher than the one observed for Ce(2)-HMOR.

TEM images of Pd(0.3)Ce(2)-HBEA show the presence two different type of clusters, which EDS analyses confirmed to be Pd and Ce clusters, more precisely, PdO and CeO_2 (HRTEM). From the comparison of Figure III-3C and E, it is possible to concluded that Ce clusters on Pd(0.3)Ce(2)-HBEA seem to be larger the ones observed on Ce(2)-HBEA. The same is applied to the PdO clusters from Pd(0.3)Ce(2)-HBEA, compared to the ones observed on Pd(0.3)-HBEA.

III.2.5. Quantification of acid sites by pyridine-FTIR spectroscopy

Figure II-12 illustrates the quantification of Brønsted acid sites (BAS) and Lewis acid sites (LAS) of Pd(0.3)-HBEA and Pd(0.3)Ce(2)-HBEA, obtained by pyridine adsorption and consecutive thermodesorption, followed by *in situ* FTIR (procedure as described in Annex A, section C.2.5). The quantification of the acids sites of a metal free HBEA sample, obtained by applying the same calcination procedure considered for Pd(0.3)Ce(2)-HBEA samples after cerium introduction was also performed (see Annex A, section C.1.3 – Catalyst preparation).

It is possible to observe that Pd(0.3)-HBEA exhibits practically the same amount of BAS (240 μmol/g, 200 ºC) compared to HBEA (227 μmol/g, 200 ºC). The fact that the value is slightly higher may be related to the calcination procedure performed to obtain HBEA (8h, at 500 ºC), which is likely to have removed part of -OH groups in further extension, compared to the calcination of Pd(0.3)-HBEA (1h, at 500 ºC). The same effect have been previously observed for MOR series catalysts (Chapter II, section II.4.1.4). Notwithstanding, it seems that HBEA exhibits more resistance to the loss of –OH groups, compared to HMOR.

Pd(0.3)Ce(2)-HBEA exhibits an amount of BAS (222 μmol/g, 200 ºC) similar to the one of HBEA, which means that the loss of H^+ due to the stabilisation of Pd and Ce species in exchange positions shall be minimal. This is in agreement with the stabilisation of the metals as PdO and CeO_2 (as evidenced by TEM) instead of Pd^{2+} and Ce^{3+} ions.

When comparing the acidity of BEA catalysts presented herein with the one from MOR catalysts (Chapter II, section II.4.1.4), it is possible to observe that the amount of BAS sites are lower for BEA catalysts (Pd(0.3)Ce(2)-HMOR: 377 μmol/g; Pd(0.3)Ce(2)-HBEA: 222 μmol/g; 200 ºC), whereas the amount of LAS is greater (Pd(0.3)Ce(2)-HMOR: 84 μmol/g; Pd(0.3)Ce(2)-HBEA: 378 μmol/g; 200 ºC). Though several studies report that the acid supports are required in order to obtain NO_x CH_4-SCR activity, it lacks studies that connect the quantification of acid sites with the activity. Moreover, it is not entirely clear if LAS play a significant role in this reaction. Nevertheless, the difference in the Pd and Ce species are likely to be more important in determining the catalytic performance of the catalysts.

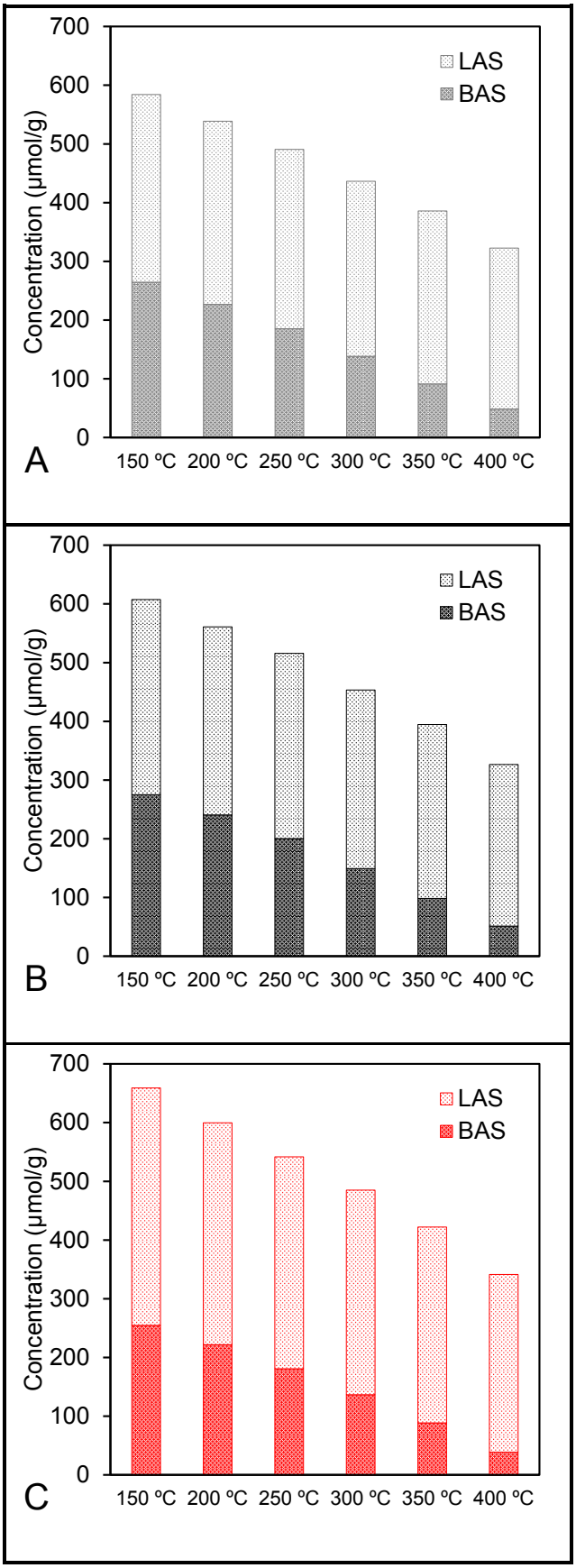

Figure III-4 – Quantification of acid sites of HBEA (A), Pd(0.3)-HBEA (B) and Pd(0.3)Ce(2)-HBEA (C) by pyridine thermodesorption followed by FTIR.

The quantification of acid sites in BEA catalysts revealed that metal introduction does not affect significantly the acidity.

III.2.6. Powder X-ray diffraction (PXRD)

Figure II-13 illustrates the PXRD patterns collected for HBEA, Pd(0.3)-HBEA and Pd(0.3)Ce(2)-HBEA samples.

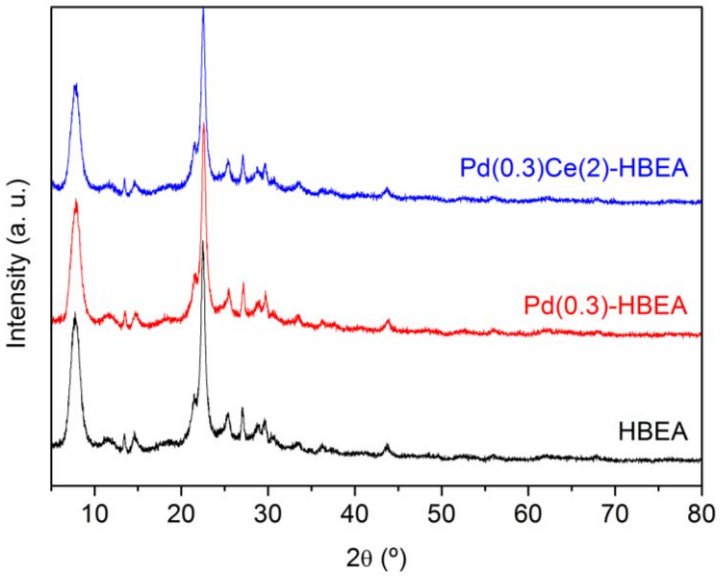

Figure III-5 – PXRD patterns of HMOR, Pd(0.3)-HBEA and Pd(0.3)Ce(2)-HBEA catalysts.

All peaks presented in the diffractograms correspond to BEA structure and no peaks from Pd/Ce species are visible. Despite TEM/EDS analyses revealed the presence of PdO in both Pd(0.3)-HBEA and Pd(0.3)Ce(2)-HBEA (Figure III-3, section III.2.4), the low Pd loading in both catalysts (0.3 wt.%) is likely to be the cause for the absence of evidence of this species in the PXRD patterns. Regarding cerium species, TEM/EDS analyses also revealed the presence of CeO_2 clusters in Pd(0.3)Ce(2)-HBEA, namely, with larger dimensions than the CeO_2 particles previously identified in Pd(0.3)Ce(2)-HMOR (Chapter II, section II.4.1.3). However, the dispersion of CeO_2 over BEA zeolite is still high enough to avoid its detection by PXRD.

The crystallinity of the metal-containing catalysts was estimated through the integration of diffractograms between 16-30 º. The value obtained for HBEA was assumed to be 100% and it was used as reference in the calculation of the crystallinity (Table II-7).

Table III-3 – Crystallinity of Pd(0.3)-HBEA and Pd(0.3)Ce(2)-HBEA catalysts (reference – HBEA).

Sample	Crystallinity (%)
Pd(0.3)-HBEA	82
Pd(0.3)Ce(2)-HBEA	84

Compared to the MOR-based catalysts (Chapter II, section II.4.1.5), BEA-based catalysts exhibit some loss of crystallinity after the introduction of metals. This is likely to be related with the nature

of BEA zeolite, which possess larger pores than MOR zeolite. Nevertheless, both metals still exhibit a high crystallinity.

III.2.7. CO adsorption followed by FTIR spectroscopy

Figure III-6 shows the FTIR spectra of Pd(0.3)-HBEA and Pd(0.3)Ce(2)-HBEA following CO adsorption.

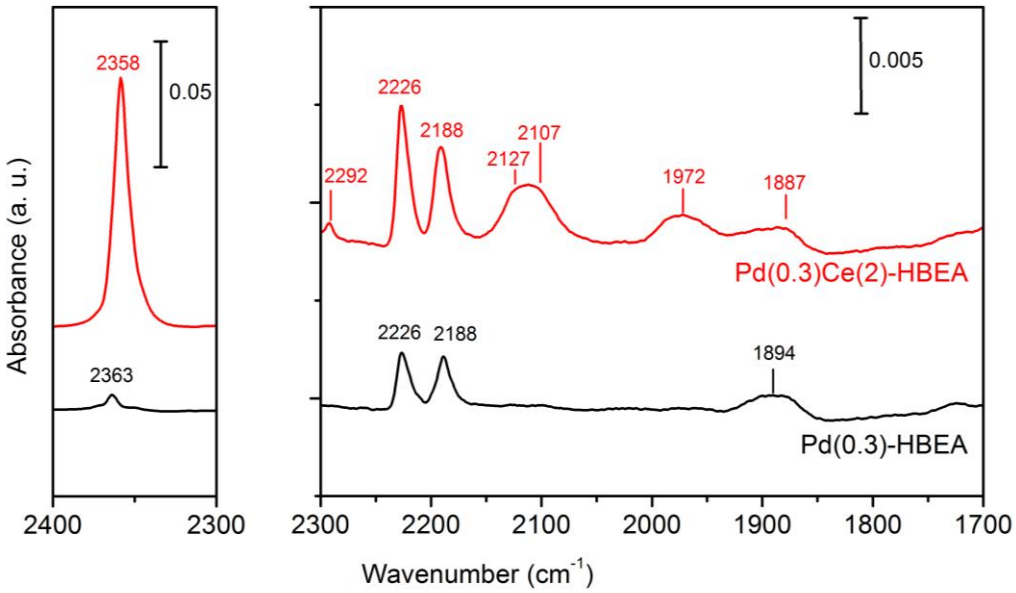

Figure III-6 – FTIR spectra of reduced Pd(0.3)-HBEA and Pd(0.3)Ce(2)-HBEA catalysts at room temperature, after 5 torr CO exposure.

For the reduced Pd(0.3)-HBEA catalyst, two bands at 2226 and 2188 cm^{-1}, can be observed in the CO spectrum, which are attributed to LAS of BEA zeolite [14, 15], similarly to what was observed for Pd(0.3)-HMOR (Chapter II, section II.4.1.7). In addition, for Pd(0.3)-HBEA, the bands attributed to Pd^{n+}-CO complexes are not observed. For metallic Pd species, typical bands of linear Pd^0-CO complexes (around 2100 cm^{-1}) are not visible, and only a band characteristic of bridging CO in Pd clusters is observed at 1894 cm^{-1}. This result supports the idea that, conversely to Pd(0.3)-HMOR, Pd is less well dispersed in the BEA structure, resulting in the formation of larger Pd^0 species. This in agreement with the TEM/EDS data, which confirms the presence of PdO clusters (before reduction). In Pd(0.3)-HBEA spectrum, a low intensity band at 2363 cm^{-1} is observed, which could be ascribed to CO_2 complexes. One can speculate that part of Pd^0 clusters might have been re-oxidised leading to the formation PdO, which would be responsible for CO oxidation to CO_2.

In the spectrum of Pd(0.3)Ce(2)-HBEA the bands at 2226 and 2188 cm^{-1} are more intense than those previously observed in Pd(0.3)-HBEA. This could be due to a higher number of LAS in this catalyst after the introduction of cerium (320 µmol/g against 378 µmol/g, at 200 ºC). Alternatively, the increase in intensity of the 2188 cm^{-1} band could be related to the presence of Ce^{n+} or Pd^{n+} species. In fact, an additional band is observed at 2127 cm^{-1} which could be attributed to Pd^{+}-CO

complexes. Moreover, unlike for Pd(0.3)-HBEA, bands at 2107 and 1972 cm^{-1} are observed in Pd(0.3)Ce(2)-HBEA, which suggests the existence of an higher relative amount of metallic palladium in smaller clusters allowing linear and two-fold bridging coordination. These results indicate that the presence of cerium oxide may promote the re-dispersion of Pd in BEA structure. Finally, the band at 2358 cm^{-1} is assigned to linear CO_2, which is in agreement with the observation for Pd(0.3)Ce(2)-HMOR.

III.2.8. NO oxidation into NO_2

It is well known that NO oxidation is part of NO_x CH_4-SCR mechanism [16-18]. The results from the NO oxidation into NO_2 for Pd(0.3)-HBEA and Pd(0.3)Ce(2)-HBEA is presented in Figure III-7.

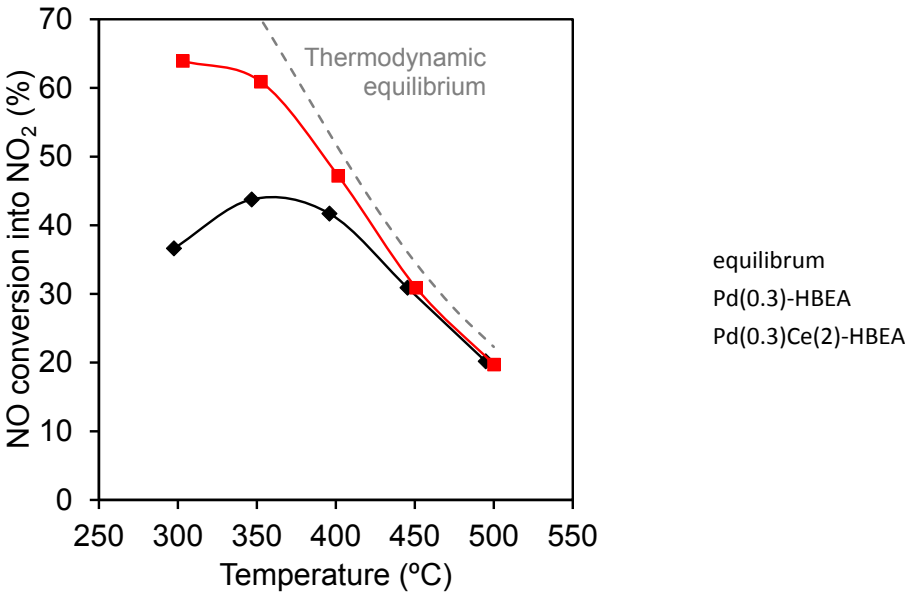

Figure III-7 – NO conversion into NO_2 of Pd(0.3)-HBEA (♦) and Pd(0.3)Ce(2)-HBEA (■). Conditions: 1000 ppm NO, 7 vol.% O_2 and GHSV = 40000 h^{-1}.

As it was previously presented in Chapter II (section II.4.1.8), Pd(0.3)-HMOR shows a poor activity for NO oxidation and even Pd(0.3)Ce(2)-HMOR exhibits a modest activity for NO oxidation. However, Pd(0.3)-HBEA revealed to be considerably active for this reaction. It is clear that the nature of Pd species influences the NO oxidation performance. H_2-TPR and TEM/EDS revealed the presence of PdO clusters. This species is known for its oxidative properties, namely CH_4 oxidation [19, 20], which may explain the good performance of Pd(0.3)-HBEA for NO oxidation.

Pd(0.3)Ce(2)-HBEA shows to be very effective in oxidising NO to NO_2, with the conversion values very close to the thermodynamic equilibrium in practically the entire range of tested temperatures. Cerium is well known to catalyse NO oxidation [21]. In fact, FTIR-CO spectrum of Pd(0.3)Ce(2)-HBEA exhibit very intense bands attributed to the formation of CO_2 complexes that resulted from CO oxidation (Figure III-6), like it was previously observed for Pd(0.3)-HBEA. The presence of cerium in the bimetallic formulation explains the higher NO oxidation compared to the monometallic formulation, not only for MOR-based catalysts (as previously shown in Chapter II, section II.4.1.8), but also for BEA-based catalysts.

III.2.9. NO_x CH_4-SCR

Figure III-8 exhibits the steady-state test results of Pd(0.3)-HBEA and Pd(0.3)Ce(2)-HBEA for NO_x CH_4-SCR.

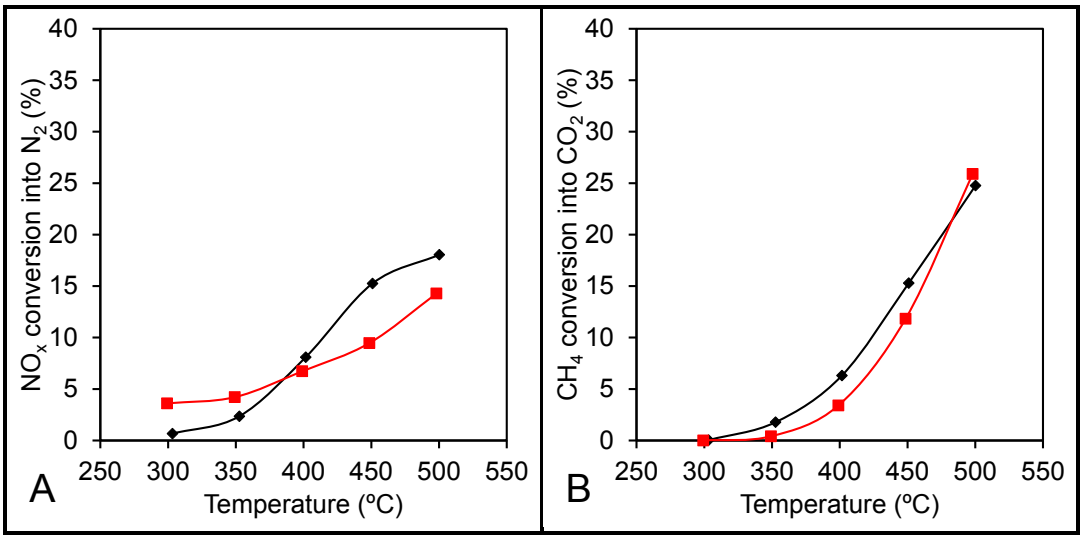

Figure III-8 – NO conversion into N_2 (A) and CH_4 conversion into CO2 (B) of Pd(0.3)-HBEA (♦) and Pd(0.3)Ce(2)-HBEA (■). Conditions: 1000 ppm NO, 1000 ppm CH_4, 7 vol.% O_2 and GHSV = 40000 h^{-1}.

Pd(0.3)-HBEA is significantly less active for NO_x SCR reaction when compared to Pd(0.3)-MOR - at 500 ºC (maximum conversion temperature), NO_x conversion into N_2 is only 18% (against 24%, see Chapter II, section II.3.1.4). At the first glance, this result seems to be quite unexpected considering the very high activity for NO oxidation, observed for Pd(0.3)-HBEA, which is known to be a first key step in the HC-SCR mechanism [16, 17]. Active Pd-zeolites are known to lose activity when, under certain conditions, Pd tends to agglomerate into large PdO clusters, *i. e.*, due to loss of Pd dispersion [22, 23]. The fact that Pd is stabilised as Pd^{2+} in exchange positions in Pd(0.3)-HMOR and as PdO clusters in Pd(0.3)-HBEA, might explain the differences on the catalytic behaviour. Also, the fact that this latter catalyst presents a notable performance for NO oxidation but very poor activity for NO_x SCR, reinforces the idea that the presence of Pd^{2+} ions in exchange positions is crucial for this reaction.

It is also intriguing the fact that CH_4 conversion is lower of Pd(0.3)-HBEA is significantly lower than Pd(0.3)-HMOR (25% against 43%, at 500 ºC). As it was previously mentioned, PdO is known to catalyse CH_4 direct combustion. However, it is possible that CH_4 is not able to contact PdO, due to competitive adsorption of NO.

Another interesting result relies on the fact that, when cerium is added to Pd(0.3)-HBEA, no enhancing effect is observed in the catalytic performance. Actually, NO_x conversion into N_2 is even lower for Pd(0.3)Ce(2)-HBEA. The quantification of H_2 consumption of the reduction peak in H_2-TPR profile corresponding to CeO_2 species in interaction with Pd resulted in a higher H_2/Ce ratio for Pd(0.3)Ce(2)-HBEA, in comparison with Pd(0.3)Ce(2)-HMOR (0.45 against 0.27). Considering that these species have an important role in the enhancement of NO_x SCR catalytic performance,

one would expect an improvement on the catalytic performance more significant for Pd(0.3)Ce(2)-HBEA. Since this is not the case, it seems then that the pertinent interaction between Ce and Pd, from the NO_x SCR point of view, needs, necessarily, to involve Pd^{2+} ions instead PdO clusters.

III.2.10. On the effect of water presence

Similar to what was presented in Chapter II (section II.6.1.3) for PdCe-HMOR system, the effect of water on the catalytic performance of Pd(0.3)Ce(2)-HBEA catalysts was also conducted by performing a sequence of dry/wet/dry tests, by adding 2 vol.% H_2O in the inlet feed considered in the wet test (Figure III-9).

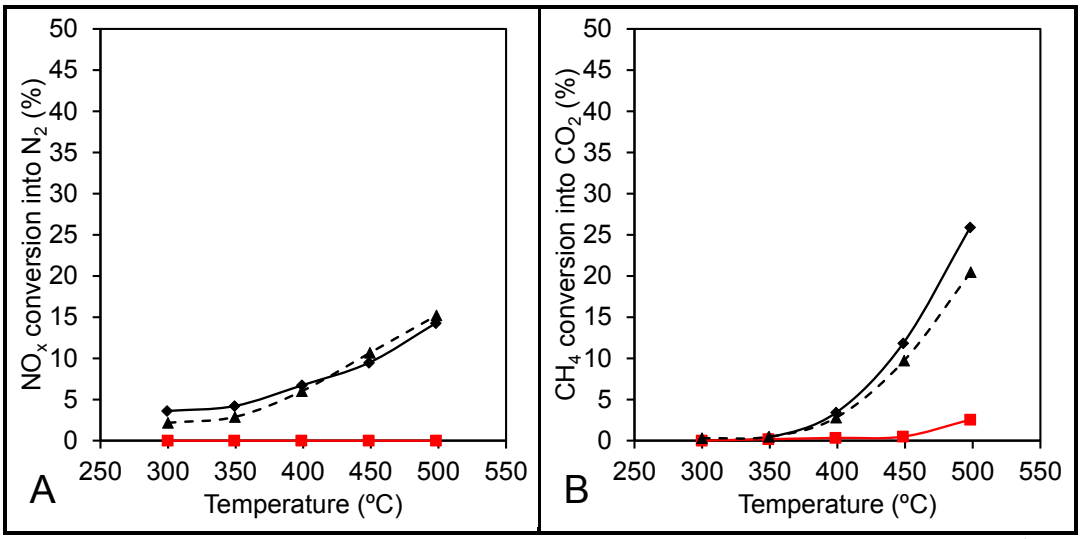

Figure III-9 – NO conversion into N_2 (A) and CH_4 conversion into CO_2 (B) of Pd(0.3)Ce(2)-HBEA: 1st dry test (♦), wet test (■) and 2nd dry test (▲). Conditions: 1000 ppm NO, 1000 ppm CH_4, 7 vol.% O_2, 2 (or 0) vol.% H_2O and GHSV = 40000 h^{-1}.

For Pd(0.3)Ce(2)-HBEA, the presence of water in the inlet gas feed has a drastic effect on NO_x conversion, with the catalyst being completely inactive in the entire range of temperature (for Pd(0.3)Ce(2)-HMOR, the catalyst presented a NO_x conversion into N_2 of 16%, at 500 ºC, considering the same test conditions). However, on the 2nd dry test, the catalyst is able to recover its catalytic performance, suggesting that, similar to what was verified for Pd(0.3)Ce(2)-HMOR, water possesses an inhibiting effect.

III.3. Combination of MOR and BEA catalysts

III.3.1. Strategy

By analysing the catalytic performance of both bimetallic formulation already presented herein and in Chapter II, one can observe that these catalysts seem to have a complementary performance. Pd(0.3)Ce(2)-HMOR shows poor NO oxidation activity but it is active for NO_x SCR, whereas Pd(0.3)Ce(2)-HBEA exhibits high NO oxidation activity but exhibits a low activity for NO_x SCR.

Only few studies can be found in the literature describing the combination of different catalysts in dual-catalysts systems as a possible solution for HC-SCR. For instance, Chen, *et al.* have reported the existence of synergies between different zeolites (namely, Fe-MFI and Fe-FER) for NO_x SCR with iso-butane [7]. Fe-FER presents lower activity NO_x SCR because the small pores of FER structure become blocked by nitrogen-containing compounds formed from the interaction between the hydrocarbons and NO_x. However, NO_2 is smaller enough to pass through the channels. On the other hand, Fe-MFI deactivates over time due to the formation of a deposit that blocks the sites responsible for the NO oxidation to NO_2, which is considered to be a first key step in the HC-SCR mechanism [17]. By mixing Fe-FER with Fe-MFI, the NO_2 formed in Fe-FER is able to interact with the active groups of the deposit on Fe-MFI and a resulting enhancement on catalytic performance is foreseen.

Holmgreen, *et al.*, have also studied the use of a dual-catalyst system for HC-SCR in lean-burn conditions, namely using methane as reductant [9]. They observed an enhancing effect on NO_x SCR performance of Pd-supported sulphated zirconia (reduction catalyst), when mixed with an oxidation catalyst, such as Co impregnated on zirconia (with low activity for NO_x SCR but high activity for NO oxidation to NO_2).

Due to the complementary catalytic performances of Pd(0.3)Ce(2)-HMOR and Pd(0.3)Ce(2)-HBEA, the combination of both catalyst in a catalytic bed was considered in this work. Since NO oxidation to NO_2 is considered a first key step of the NO_x HC-SCR mechanism, a chosen configuration consisted in a dual-bed catalyst, where the inlet gases would contact first with Pd(0.3)Ce(2)-HBEA (catalyst with the better NO oxidation performance). A second configuration, consisting in a mechanical mixture between Pd(0.3)Ce(2)-HBEA and Pd(0.3)Ce(2)-HMOR was also considered. For both dual-catalyst configurations, equal masses of both catalyst were used, each one corresponding to half of the mass considered for the tests with only one catalyst.

A schematic representation of the dual-catalyst systems considered herein is presented in Figure III-10.

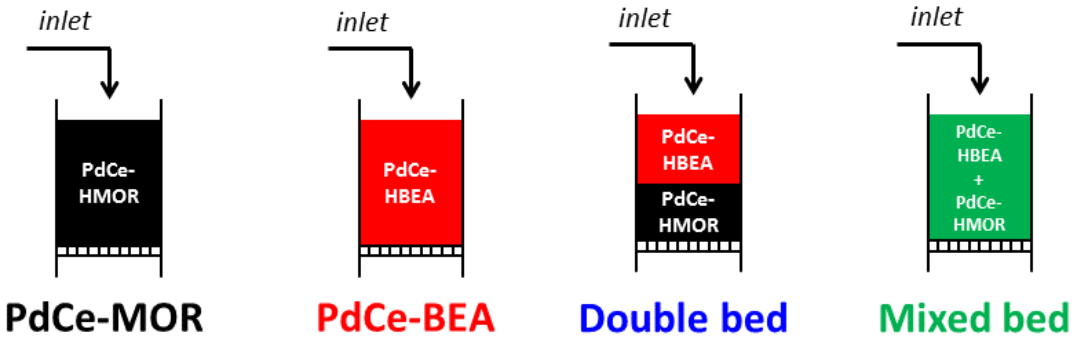

Figure III-10 – Schematic representation of catalytic bed considered for the dual-catalyst configurations.

For both dual-catalyst configurations previously considered, catalysts were tested in steady-state conditions, in a sequence of dry/wet/dry tests like previously described for Pd(0.3)-HMOR (Chapter II, section II.6.1.3) and Pd(0.3)-HBEA (section III.2.10).

III.3.2. Catalytic performance for NO_x CH_4-SCR

The results from the steady-state tests performed in 1st dry test, wet test and 2nd dry conditions for are illustrated in Figure III-11, Figure III-12 and Figure III-13, respectively, for Pd(0.3)Ce(2)-HMOR, Pd(0.3)Ce(2)-HBEA and both dual-catalyst configurations.

In the 1st dry test (Figure III-11) it is possible to see that NO_x conversion into N_2 for both dual-catalyst configurations (dual bed and mixed bed) is between the values registered for Pd(0.3)Ce(2)-HMOR and Pd(0.3)Ce(2)-HBEA standalone. This is likely due to the dilution effect of MOR-based catalyst (which is the most active for NO_x SCR) in the catalytic bed, which means that no synergic effect is observed with the dual configuration. CH_4 selectivity to NO_x SCR reaction is also worst for the dual-catalysts configuration, when compared to standalone catalysts.

When considering the presence of water in the inlet gas feed, *i.e.* representative conditions of real exhaust gases (Figure III-12), both dual-catalysts configurations exhibit higher NO_x conversion into N_2 when compared to Pd(0.3)Ce(2)-HMOR. With these conditions, instead of a decrease in the catalytic performance previously observed, due to dilution effect, a synergic effect is observed. Moreover, both dual bed and mixed bed catalyst exhibit higher CH_4 selectivity to NO_x SCR reaction, which means that CH_4 is being more effectively used as a reductant, instead of being directly oxidised to CO_2 (combustion).

The interpretation of the results suggests that a low performance of Pd(0.3)Ce(2)-HMOR for NO oxidation is limiting, up to some extent, its NO_x SCR performance. In the dual bed configuration, where the inlet gas mixture first contacts with Pd(0.3)Ce(2)-HBEA, a high amount of NO_2 is expected to be formed. Then, when it reaches Pd(0.3)Ce(2)-HMOR, it is likely that intermediate products resulting from the interaction of NO_2 and CH_4 can be produced (R-NO_x species/$C_xH_yO_z$), which would promote the global reaction.

It is interesting to notice that even with the mix bed configuration the NO_x conversion values are also improved. A possible explanation for this phenomenon might be the fact that, due to the high NO oxidation performance of Pd(0.3)Ce(2)-HBEA, only a fraction of this catalyst in the initial part of the catalytic bed can be enough for providing enough NO_2 to promote the formation of intermediate species.

Finally, when a 2rd dry test is performed (Figure III-13), after water exposure, the catalytic performance of both dual bed and mixed bed configurations resembles the one observed in the 1st dry test. This was already expected since the same was observed when both Pd(0.3)Ce(2)-HMOR and Pd(0.3)Ce(2)-HBEA where tested stand alone.

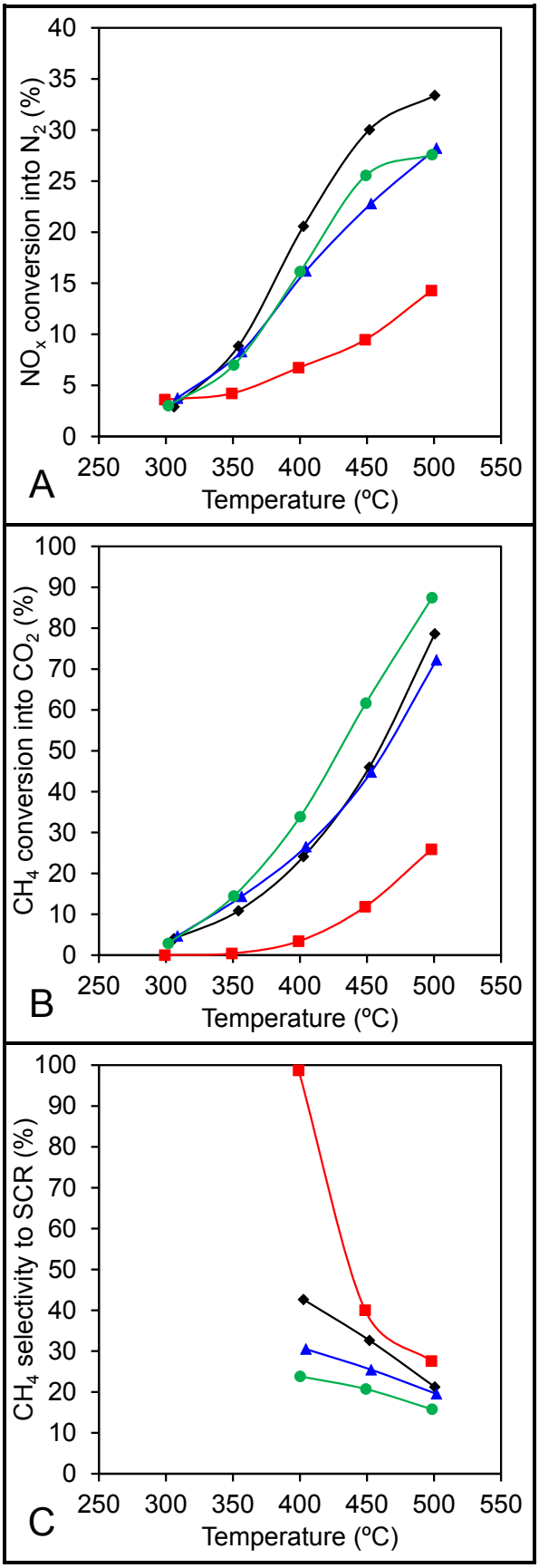

Figure III-11 – NO conversion into N_2 (A), CH_4 conversion into CO_2 (B) and CH_4 selectivity to SCR of Pd(0.3)Ce(2)-HMOR (♦) , Pd(0.3)Ce(2)-HBEA (■), dual bed (▲) and mixed bed (●). Conditions: 1000 ppm NO, 1000 ppm CH_4, 7 vol.% O_2 and GHSV = 40000 h^{-1} (1^{st} dry test).

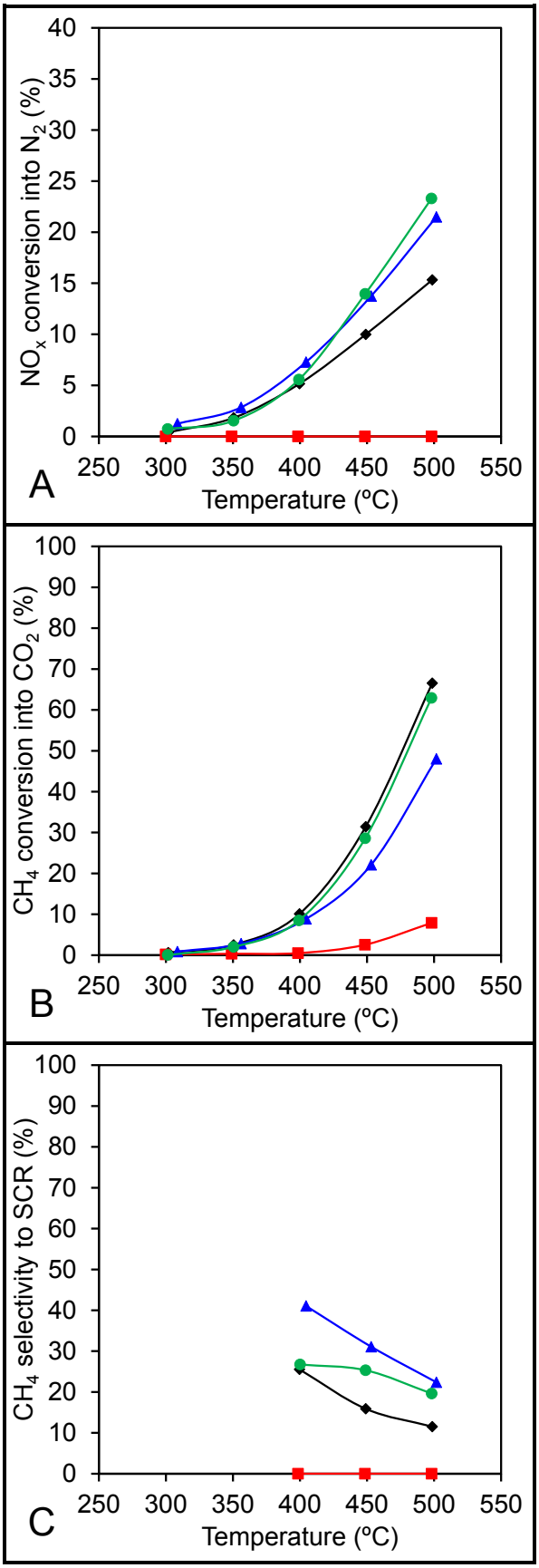

Figure III-12 – NO conversion into N_2 (A), CH_4 conversion into CO_2 (B) and CH_4 selectivity to SCR of Pd(0.3)Ce(2)-HMOR (♦) , Pd(0.3)Ce(2)-HBEA (■), dual bed (▲) and mixed bed (●). Conditions: 1000 ppm NO, 1000 ppm CH_4, 7 vol.% O_2, 2 vol.% of H_2O and GHSV = 40000 h^{-1} (wet test).

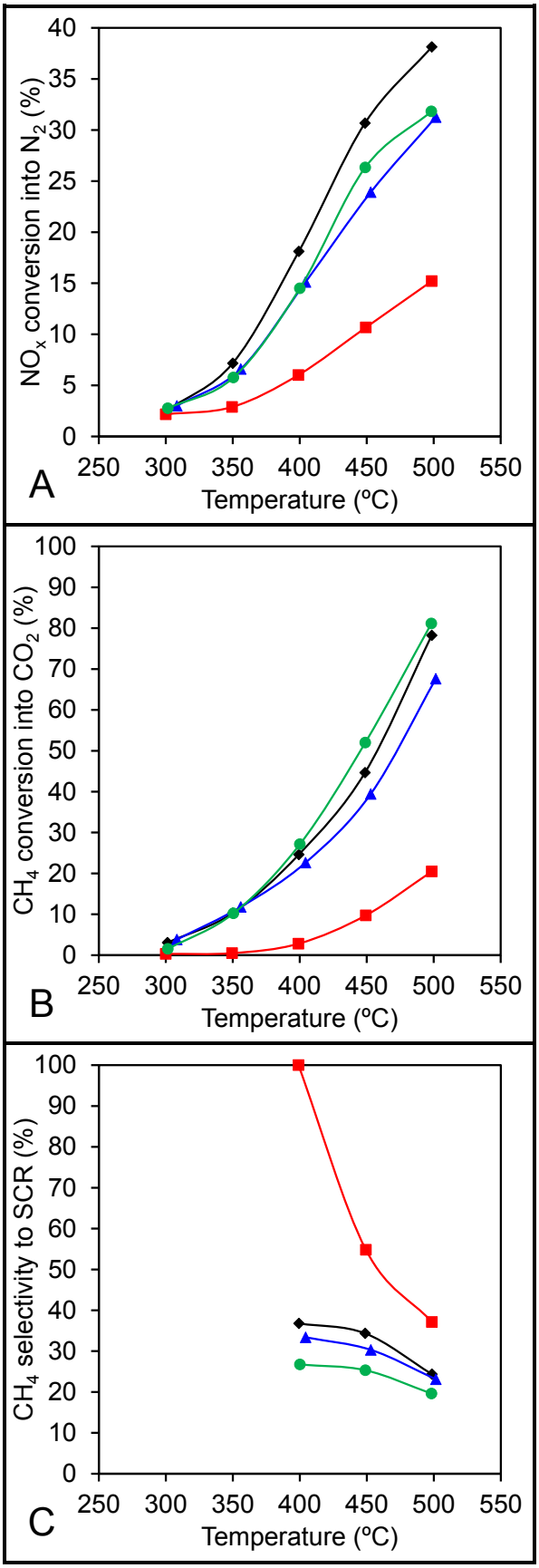

Figure III-13 – NO conversion into N_2 (A), CH_4 conversion into CO_2 (B) and CH_4 selectivity to SCR of Pd(0.3)Ce(2)-HMOR (♦) , Pd(0.3)Ce(2)-HBEA (■), dual bed (▲) and mixed bed (●). Conditions: 1000 ppm NO, 1000 ppm CH_4, 7 vol.% O_2 and GHSV = 40000 h^{-1} (2^{nd} dry test).

Figure III-14 illustrates the steady-state test results previous mentioned at 500 ºC, where it is possible to clearly observe the differences between all the configurations considered.

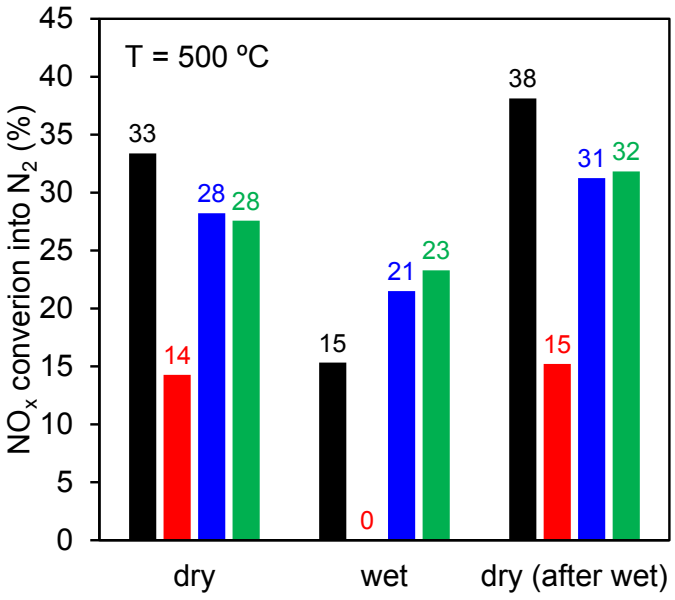

Figure III-14 – NO conversion into N_2 of Pd(0.3)Ce(2)-HMOR (■), Pd(0.3)Ce(2)-HBEA (■), dual bed (■) and mixed bed (■) in 1st dry, wet and 2nd dry steady-state test. Conditions: 1000 ppm NO, 1000 ppm CH_4, 7 vol.% O_2, 2 (or 0) vol.% H_2O, T = 500 ºC and GHSV = 40000 h^{-1}.

III.4. Conclusions

Contrarily to what happens in Pd-MOR system, the addition of cerium to Pd-BEA system does not result in an enhancing effect of the catalytic performance for NO_x CH_4-SCR. In fact, the use of different zeolites (BEA and MOR) in the preparation of bimetallic catalysts, containing similar amounts of metal, by addition of cerium to Pd-based catalyst resulted in two catalysts with completely different catalytic performances. Pd(0.3)Ce(2)-HBEA has shown to be very effective in oxidising NO to NO_2 and significantly better than Pd(0.3)Ce(2)-HMOR. This reaction is considered to be a first key step on the NO_x SCR mechanism using hydrocarbons (HC-SCR). However, Pd(0.3)Ce(2)-HMOR revealed to be significantly more active for NO_x CH_4-SCR, when compared to Pd(0.3)Ce(2)-HBEA.

Whereas in the MOR-based catalysts palladium is stabilised as Pd^{2+} ions in exchange positions, in BEA-based catalysts, a significant part of palladium is stabilised as PdO. Also, for BEA-based catalysts, CeO_2 is presented as metal clusters of higher dimensions which, together with the presence of PdO, explains the high NO oxidation performance. The lack of Pd^{2+} explains the low activity of BEA catalysts for NO_x SCR reaction.

A synergic effect was observed in the NO_x SCR performance when both bimetallic catalysts were tested in dual-catalyst configurations (dual bed and mixed bed). This synergy can be explained by the complementary catalytic behaviour of both catalysts in performing the different functions of HC-SCR mechanism.

III.5. References

[1] S. Chen, X. Yan, Y. Wang, J. Chen, D. Pan, J. Ma, R. Li, Catal. Today, 175 (2011) 12-17.

[2] A.P. Ferreira, C. Henriques, M.F. Ribeiro, F.R. Ribeiro, Catal. Today, 107–108 (2005) 181-191.

[3] J. Janas, W. Rojek, S. Dzwigaj, Catal. Today, 191 (2012) 32-37.

[4] O.A. Anunziata, A.R. Beltramone, F.G. Requejo, J. Mol. Catal. A: Chem., 267 (2007) 194-201.

[5] J. Janas, S. Dzwigaj, Catal. Today, 176 (2011) 272-276.

[6] Y.K. Park, J.W. Lee, C.W. Lee, S.E. Park, J. Mol. Catal. A: Chem., 158 (2000).

[7] H.Y. Chen, X. Wang, W.M.H. Sachtler, Appl. Catal., A, 194 (2000) 159-168.

[8] J.H. Lee, J.G. Kim, J.K. Lee, J.H. Kim, Catal. Today, 87 (2003) 35-42.

[9] E.M. Holmgreen, M.M. Yung, U.S. Ozkan, Appl. Catal., B, 74 (2007) 73-82.

[10] P. Gawade, A.M.C. Alexander, R. Clark, U.S. Ozkan, Catal. Today, 197 (2012) 127-136.

[11] H.L. Tidahy, S. Siffert, J.F. Lamonier, R. Cousin, E.A. Zhilinskaya, A. Aboukais, B.L. Su, X. Canet, G. De Weireld, A. Frere, J.M. Giraudon, G. Leclercq, Appl. Catal., B, 70 (2007) 377-383.

[12] A. Trovarelli, Cat. Rev. - Sci. Eng., 38 (1996) 439-520.

[13] A.B. Gaspar, L.C. Dieguez, Appl. Catal., A, 201 (2000) 241-251.

[14] P.S.F. Mendes, G. Lapisardi, C. Bouchy, M. Rivallan, J.M. Silva, M.F. Ribeiro, Appl. Catal., A, 504 (2015) 17-28.

[15] P. Li, Y. Xiang, V.H. Grassian, S.C. Larsen, J. Phys. Chem. B, 103 (1999) 5058-5062.

[16] G. Djega-Mariadassou, Catal. Today, 90 (2004) 27-34.

[17] O. Gorce, F. Baudin, C. Thomas, P. Da Costa, G. Djega-Mariadassou, Appl. Catal., B, 54 (2004) 69-84.

[18] A. Lamacz, A. Krzton, G. Djega-Mariadassou, Appl. Catal., B, 142 (2013) 268-277.

[19] P. Gelin, M. Primet, Appl. Catal., B, 39 (2002) 1-37.

[20] Y.J. Li, J.N. Armor, Appl. Catal., B, 3 (1994) 275-282.

[21] J.A.Z. Pieterse, S. Booneveld, Appl. Catal., B, 73 (2007) 327-335.

[22] I.O. Costilla, M.D. Sanchez, M. Alicia Volpe, C.E. Gigola, Catal. Today, 172 (2011) 84-89.

[23] H. Ohtsuka, T. Tabata, Appl. Catal., B, 21 (1999) 133-139.

Chapter IV. Optimisation of catalytic formulation of PdCe-MOR system by steaming treatments

IV.1. Introduction

Due to the fuel combustion reaction that takes place in the vehicle's engine, the presence of water in the exhaust gases is always inevitable. Water plays has an inhibition effect in the performance of the catalytic after-treatment system, namely NO_x CH_4-SCR catalysts, due to its competitive adsorption with the reactants for the active sites of the catalysts. This inhibition effect causes a significant decrease in the NO_x and CH_4 conversion values, which is clearly shown in Chapter II and Chapter III, and this has been widely reported in literature for the several combinations of supports/active phases. Moreover, there are several documented cases where water was proved to cause deactivation of zeolite-based catalysts, mainly due to migration of activity species, *i. e.* loss of dispersion [1, 2], often associated to the loss of integrity of the zeolite framework, in particular, dealumination [3-5].

Nevertheless, has it was stated in the literature review presented in Chapter II, there is one case (a CoPd-BEA catalyst) where the catalytic performance has improved in a 2nd dry test, after performing a test in the presence of water (dry/wet/dry cycle), presented by Ferreira *et al.* [6]. Moreover, the authors submitted the catalyst to a thermal treatment, consisting in a calcination under air containing water (steaming treatment) and realised that the catalytic performance of the steamed catalyst was not only higher than the non-steamed catalyst, in all three tests of the dry/wet/dry cycle, but also that the performance got better from 1st dry test to wet test. According to the study, the exposure to water caused structural modifications and stabilisation of active species that resulted in a better catalytic performance.

Though the previous mentioned work considered a significantly different system than the one within this study (CoPd-BEA *vs.* PdCe-MOR), a similar test methodology have been already applied to a PdCe-MOR catalyst by Costilla *et al.* [7], where the authors presented its catalytic performance in dry/wet/dry cycle. As expected, results show that, from 1st dry test to wet test, conversion values decrease due to the presence of water. On the 2nd dry test, the catalyst was able to partially recover NO_x and CH_4 conversion values but these became lower than the ones registered on the 1st dry test. This deactivation effect was attributed to the decrease of active Pd^{2+} species and consequently formation of Pd particles that favour CH_4 combustion over NO_x SCR.

Previously, in Chapter II (section II.6.1.3), results of catalytic tests performed by following the same methodology dry/wet/dry cycle were presented for Pd(0.3)Ce(2)-HMOR catalyst and revealed to be quite promising when compared to the ones obtained by Costilla *et al*. [7]. Not only the catalyst was able to totally recover the NO_x and CH_4 conversion values, but inclusively exhibit slightly higher NO_x conversion into N_2, at 500 ºC. Characterisation performed revealed that after exposed to water, the catalyst exhibited higher surface Ce^{4+} species and more CeO_2 species interacting with palladium, as well as some changes in the Pd^{2+} species. Based on these results and ones previously described by Ferreira *et al.* [6], the following question was naturally raised: *Is it possible to improve the catalytic performance of PdCe-MOR system by performing a steaming treatment?*

The challenge of finding an answer for this question was the motivation for the work herein presented.

IV.2. Effect of steaming parameters – water content and temperature

IV.2.1. Catalyst preparation

The steaming treatment considered in this studied was applied to the bimetallic Pd(0.3)Ce(2)-HMOR catalyst, previously described in Chapter II (Figure IV-1).

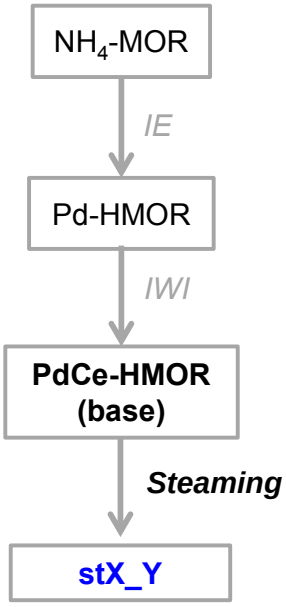

Figure IV-1 – Schematic representation of steamed catalyst preparation.

The catalyst was submitted to a thermal treatment, consisting in a calcination procedure under air flow, at a given temperature (heating rate of 5 ºC/min). Once this temperature was reached, a liquid water flow was fed to the reactor, together in the air flow, corresponding to a certain water content, for 3 h. After this period, water flow was stopped and the temperature was kept for an additional hour. Steamed catalysts were named as stX_Y, were X is the temperature (in ºC) and Y is the water content (in vol. %), according to the description presented in Table IV-1

Table IV-1 – Summary of steamed catalyst, obtained by considering different water content and temperature.

% H_2O / T (ºC)	450	500	550
5	-	st500_05	-
10	st450_10	st500_10	st550_10
20	-	st500_20	-

IV.2.2. Characterisation

IV.2.2.1. Powder X-ray diffraction (PXRD)

Steaming treatments are known to potentially cause loss of crystallinity of zeolites, due to dealumination of the framework [8, 9]. The loss of crystallinity may result in the migration of active metal species, which can affect the catalytic performance. Hence, in order to assess the effect of steaming treatment on the zeolite framework, PXRD patterns were collect for every sample (Figure IV-2).

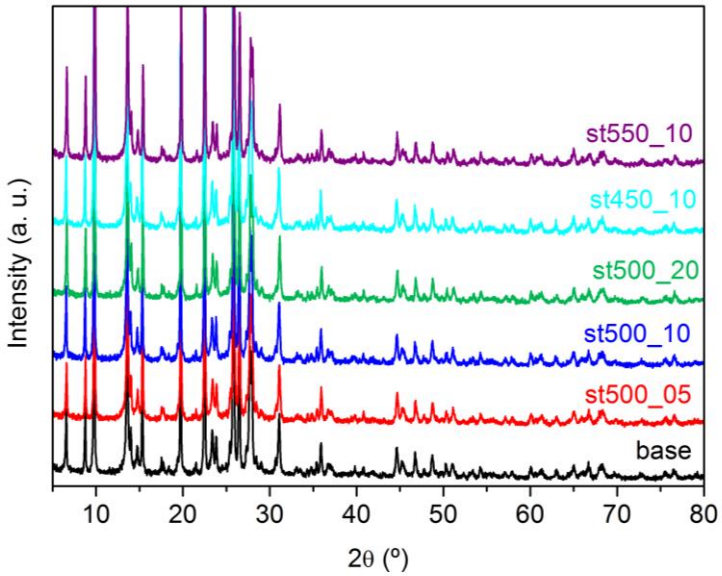

Figure IV-2 – PXRD patterns of Pd(0.3)Ce(2)-HMOR catalysts before and after steaming under different conditions.

All peaks presented in the diffractograms correspond to MOR structure. By comparing the diffractogram of base catalyst with the ones from steamed catalysts, no significant differences are found. Eventual agglomeration of metal species (for instance, PdO, Pd^0 or CeO_2) were not identify by PXRD.

The crystallinity of each sample was estimated through the integration of diffractograms between 16-30 º. The value obtained for the base catalyst was assumed to be 100% and it was used as reference in the calculation of the crystallinity of steamed samples (Table IV-2).

Table IV-2 – Crystallinity of Pd(0.3)Ce(2)-HMOR catalysts before and after steaming under different conditions (reference – base).

Sample	Crystallinity (%)
st500_05	95
st500_10	97
st500_20	91
st450_10	99
st550_10	94

The crystallinity of all steamed samples is higher than 90% (compared to base catalyst) and, consequently, no evidence of structural changes on the catalysts due to steaming are observed by PXRD.

IV.2.2.2. Temperature programmed reduction under hydrogen (H_2-TPR)

H_2-TPR profiles of base and steamed catalysts are illustrated in Figure IV-3 and the quantification of H_2 consumption of the reduction peaks of the respective profiles is presented in Table IV-3.

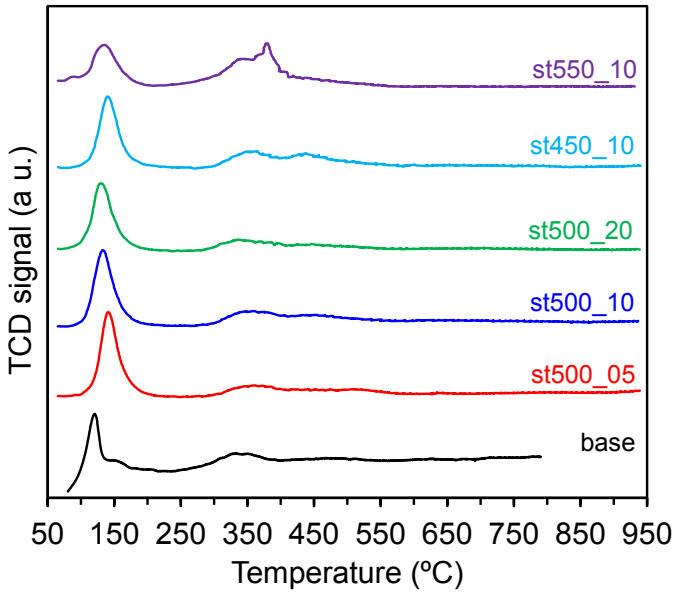

Figure IV-3 – H_2-TPR profile of Pd(0.3)Ce(2)-HMOR catalysts before and after steaming under different conditions.

Table IV-3 – Quantification of H_2 consumption by peak integration of H_2-TPR profiles Pd(0.3)Ce(2)-HMOR catalysts before and after steaming under different conditions.

	Peak 1			Peak 2		
	T (ºC)	H_2/Pd	µmol H_2 /$g_{catal.}$	T (ºC)	H_2/Ce	µmol H_2 /g_{catal}
base	95-215	1.4	39	240-560	0.27	37
st500_05	70-220	2.1	56	260-600	0.22	29
st500_10	85-210	2.0	54	275-565	0.24	33
st500_20	70-220	1.8	49	250-580	0.19	25
st450_10	75-220	1.8	50	275-590	0.32	43
st550_10	70-200	1.2	33	220-580	0.52	71

When performing the steaming treatment at 450 and 500 ºC, the catalysts exhibit and H_2-TPR profiles very similar between them. However, H_2 quantification of the reduction processes reveals some differences. For 500 ºC, H_2 consumptions are not particularly different when 5 and 10 vol.% H_2O are used in the steaming process. When comparing to the base catalyst, it seems that surface Ce^{4+} species (peak 1) tend to increase and CeO_2 species in interaction with Pd species (peak 2) tend to slightly decrease. With 20 vol.% H_2O, the decrease of this later species becomes more pronounced.

When considering 450 ºC, the same conclusion can be drawn for surface Ce^{4+} species, but CeO_2 species in interaction with Pd species seem to slightly increase. However, for 550 ºC, H_2-TPR profile becomes considerably different. In fact, H_2/Pd consumption decreases significantly (1.2 compared to *ca.* 2 for the other steamed catalysts) and H_2/Ce of the second reduction peak becomes closer to 0.5, which would correspond to have all Ce^{4+} being reduced to Ce^{3+} at this temperature. The reduction of surface Ce^{4+} species could result in an agglomeration of CeO_2 species, which would explain the increase of higher temperature reduction peak (peak 2). Nevertheless, eventually agglomerates formed to the steaming treatment at 550 ºC are likely not be large, since the reduction of bulk oxygen in CeO_2 occurs at high temperatures (> 700 ºC) and such reduction process is not observe. Notwithstanding, one cannot exclude the migration of Pd^{2+} species for other positions or the formation of PdO agglomerates, which may occur due to water exposure [1, 4, 7].

IV.2.2.3. *Diffuse reflectance UV-Vis spectroscopy (DRS UV-Vis)*

Figure IV-4 illustrates the DRS UV-Vis spectra of base and steamed catalysts.

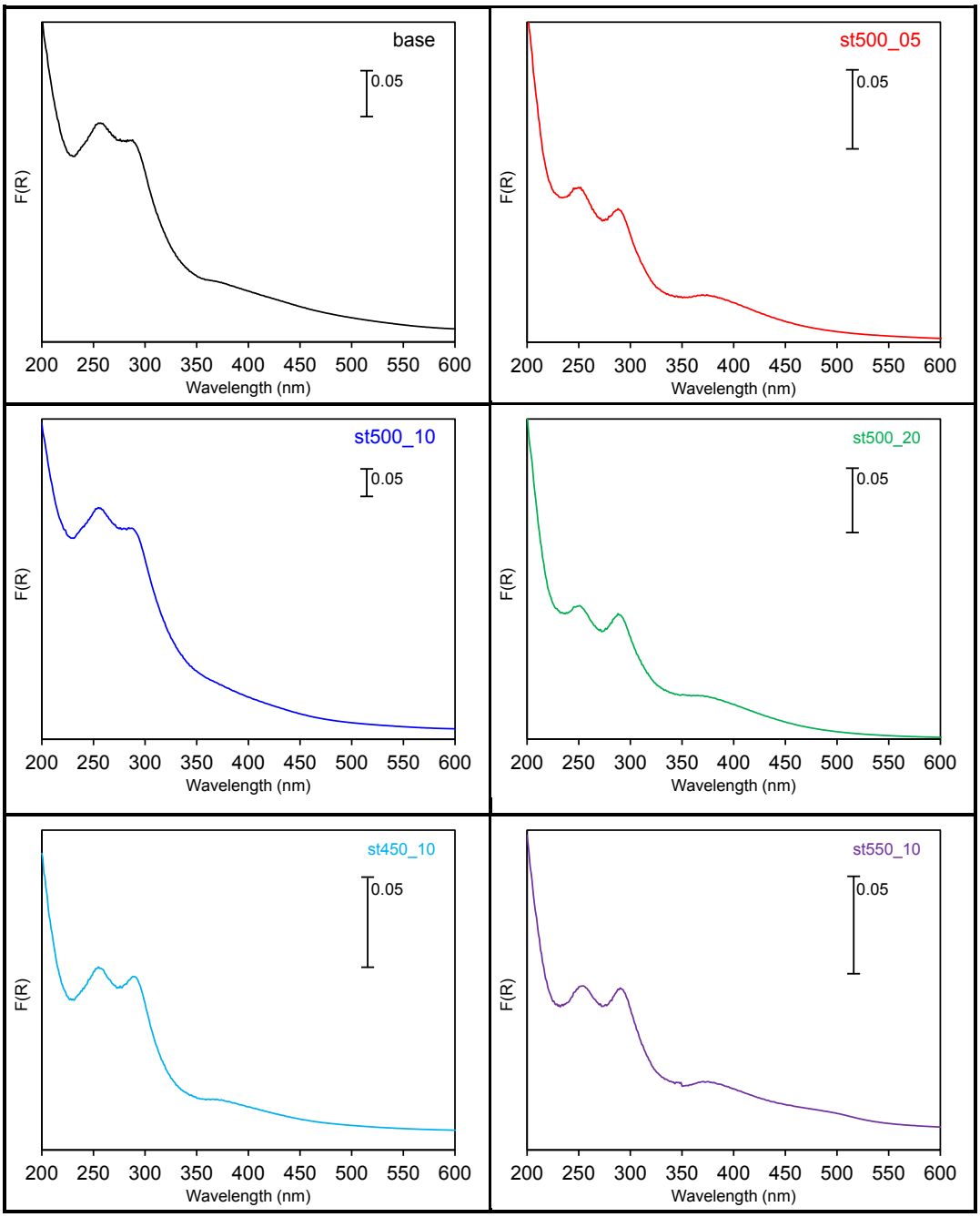

Figure IV-4 – Diffuse Reflectance UV-Vis spectra of Pd(0.3)Ce(2)-HMOR catalysts before and after steaming under different conditions.

In a general way, all catalysts exhibit the same absorption bands around 260, 290 and 385, which are ascribed to Ce^{3+}, Ce^{4+} and Pd^{2+} species, respectively, as already detailed in Chapter II, II.4.1.2. A quantitative analysis related to eventual changes in these species is not straightforward but, qualitatively speaking, it seems that the relative intensity of the band at 290 nm is always higher than 260 nm. Notwithstanding, a difference worthy to be mentioned is observed in the spectrum of st550_10, in which it is possible to observed a forth band around 500 nm. A similar band have been

previously identified in Chapter II (section II.4.3.2) for Ce(2)Pd(0.3)-HMOR, which was ascribed to a possible Pd^{2+} species in different location than the ones corresponding to the band at 385 nm. This is an evidence that the steaming treatment might have caused some changes in the distribution of Pd species.

IV.2.2.4. Transmission electron microscopy (TEM/EDS)

TEM images of st500_10 are presented in Figure IV-5.

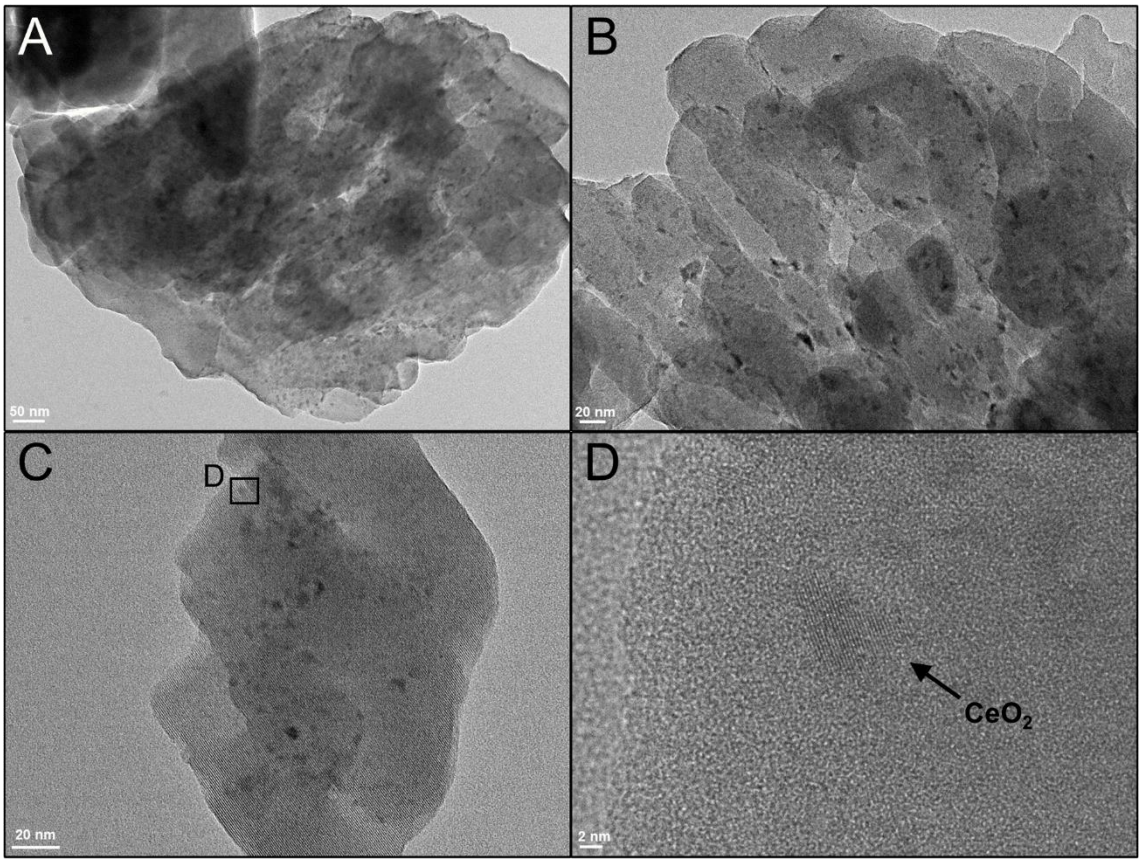

Figure IV-5 – TEM images of st500_10 catalyst.

The same features previously observed in TEM images of Pd(0.3)Ce(2)-HMOR (see Chapter II, section II.4.1.3) are also observed for st500_10. Small metal clusters (order of magnitude $\approx 10^1$ nm), with irregular shape, can be observed in the surface of the zeolite particles (Figure IV-5A, B and C). Energy-dispersive X-ray spectroscopy analyses confirmed that these are cerium clusters (palladium was not detected). Using high resolution TEM (HRTEM - Figure IV-5D) it was possible to quantify the distance between lattice planes in 2.7 and 3.1 Å, typical from CeO_2 (ICDD 00-034-0394).

In summary, no evidences of particular changes are observed by TEM/EDS between Pd(0.3)Ce(2)-HMOR and st500_10.

IV.2.2.5. *Quantification of acid sites by pyridine-FTIR spectroscopy*

Figure IV-6 shows the quantification of total number of BAS and Lewis acid sites (LAS) of Pd(0.3)Ce(2)-HMOR before and after steaming treatment (st500_10, st500_20 and st550_10). Samples were adsorbed with pyridine and, then, consecutive thermodesorption was performed and followed by *in situ* FTIR. The quantification of total number of BAS and Lewis acid sites (LAS) was performed through the integration of IR bands around 1545 and 1455 cm^{-1}.

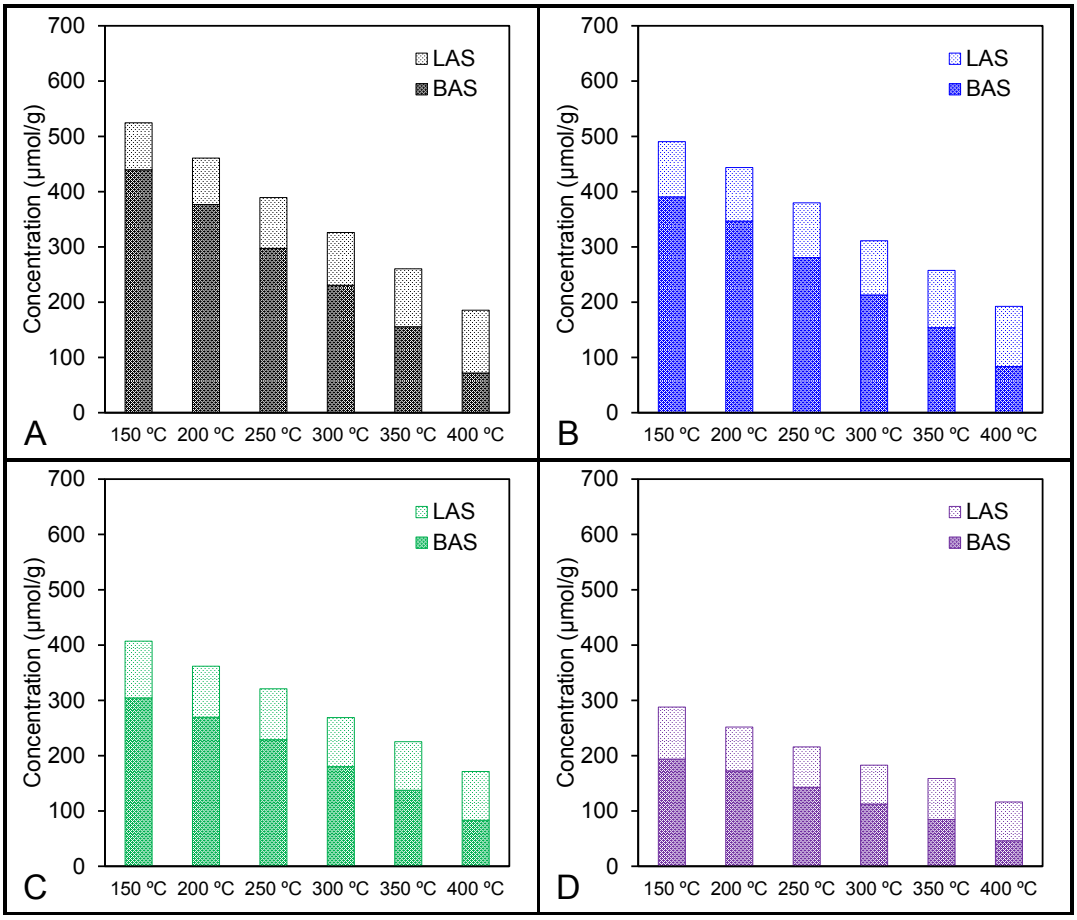

Figure IV-6 – Quantification of acid sites of base (A), st500_10 (B), st500_20 (C) and st550_10 by pyridine thermodesorption followed by FTIR.

Generically, it is possible to observe that steaming treatments cause a decrease on the number of BAS. For instance, st500_10 exhibits BAS concentration of 347 µmol/g (at 200 ºC) against 377 µmol/g for the base catalyst. This loss of acidity is more pronounced when considering more severe steaming conditions. For a water content of 20 vol. %, the steamed catalyst exhibits a BAS concentration of 270 µmol/g and when the steaming treatment is performed at 550 ºC, BAS concentration becomes 173 µmol/g.

It is known that, by performing thermal treatments on zeolites in the presence of water, dealumination of the structure can be accomplished, which generates extra-framework aluminium (EFAL) species [8, 9]. The migration of Al species from the framework represents the loss of

exchange positions and, hence, the loss of H^+. In fact, by observing the OH region of the spectra of Pd(0.3)Ce(2)-HMOR catalysts before and after steaming, prior to pyridine adsorption (Figure IV-7), one can see that for steamed catalysts (st500_10, st500_20 and st550_10) a new band around 3660 cm^{-1} appears.

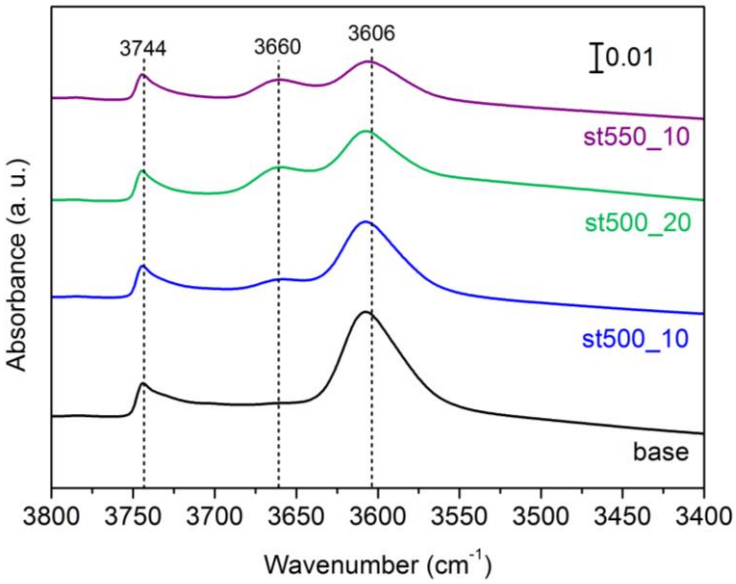

Figure IV-7 – FTIR spectra of OH groups of Pd(0.3)Ce(2)-HMOR catalysts before and after steaming under different conditions, after evacuation 673 K.

The previous mentioned band is ascribed to OH on extra-framework Al^{3+} (EFAL) species [10] and it is not observed on the spectrum of base catalyst. Only two bands at 3608 cm^{-1} and 3744 cm^{-1} are observed for this sample, ascribed to terminal silanols [10] and bridging Si-OH-Al groups [11], respectively. In fact, the quantification of maximum intensity of the band at 3608 cm^{-1} decreases from 0.36 (base) to 0.27 (st500_10). Moreover, the ratio between intensities I_{3658}/I_{3608} increases from 0.29 (st500_10) to 0.48 and 0.54 (st500_20 and st550_10, respectively), which clearly shows that by performing the steaming treatment under more severe conditions (higher water content and temperature), one promotes the relative increase of EFAL species.

IV.2.2.6. *CO adsorption followed by FTIR spectroscopy*

In Figure III-6, the CO-FTIR spectra of Pd(0.3)Ce(2)-HMOR before (base) and after steaming treatment (st500_10, st500_20 and st550_10) are presented.

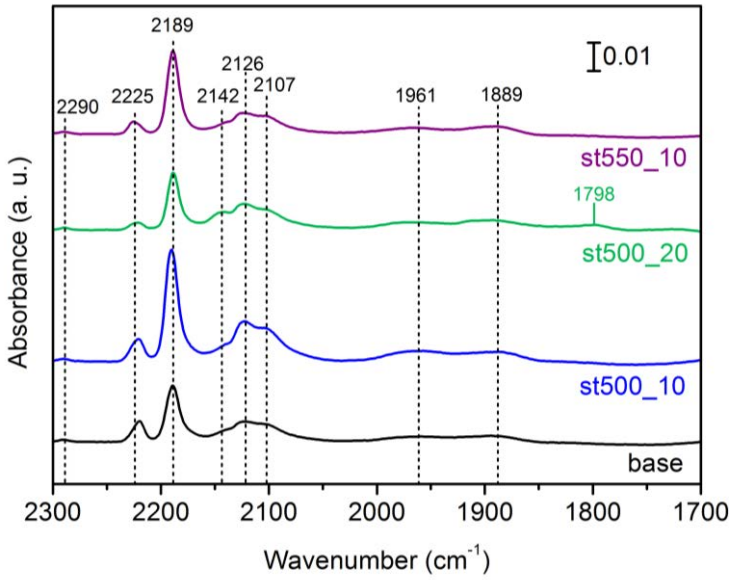

Figure IV-8 – FTIR spectra of reduced Pd(0.3)Ce(2)-HMOR catalysts before and after steaming under different conditions.

In general, the same species identified for the base catalyst are also presented in the steamed catalysts. However, for st500_10, it is possible to observe that the relative intensity of the band at 2190 cm^{-1} becomes higher than in the base case (when compared, for instance, with the intensity of the band at 2220 cm^{-1}). This band appears in the spectral region of carbonyls formed with cerium ions, 2190-2110 cm^{-1} [12], ascribed to Ce^{n+}-CO complexes (Ce^{3+} or Ce^{4+}). It suggests, hence, that an increase of this species is likely to occur, which is in agreement in results from H_2-TPR, where it was observed an increase of H_2 consumption at low temperature ascribed to the increase of surface Ce^{4+} after the steaming (see Figure IV-3, page 168). Also, for st500_10, the band at 2125 cm^{-1} exhibits a higher relative intensity. This band appears in the spectral range of both Ce^{n+}-CO and Pd^{n+}-CO (2215-2110 cm^{-1}) [12] and has been previously ascribed to Ce or Pd species in interaction. This increase may be an evidence of a promotion of the interaction between species, due to the steaming treatment.

It should be mentioned that, in st500_20 spectrum, an additional band at 1798 cm^{-1} can be observed. This band might correspond, eventually, to a different coordination of bridging CO on Pd^0 clusters, not identified for the other catalysts.

IV.2.2.7. *Nitrogen adsorption*

Textural parameters, namely, porous volume (V_p) and external surface area (S_{ext} - not corresponding to the micropores) of base and steamed catalysts were estimated through N_2 adsorption, by applying the t-plot method, considering the reference isotherm Harkins-Jura [13]. Surface area estimated by Brunauer-Emmett-Teller (BET) method is also presented as indicative value.

Table IV-4 – Textural parameters of Pd(0.3)Ce(2)-HMOR before and after steaming.

	$V_{p,\ micro}$ (cm^3/g)	$V_{p,\ meso}$ (cm^3/g)	S_{ext} (m^2/g)	S_{BET} (m^2/g)
base	0.203	0.086	31	486
st500_05	0.195	0.084	22	402
st500_10	0.243	0.109	31	504
st500_20	0.199	0.086	24	413
st450_10	0.194	0.082	23	401
st550_10	0.204	0.087	25	422

For all the steamed catalysts (except st500_10) textural properties seem to be kept constant. However, when steaming is performed at 500 ºC under 10 vol.% H_2O, both micro and mesoporous volumes are increased. In fact, from the interpretation of FTIR spectra in the OH region, it has been concluded that mild dealumination took place due to the steaming treatment. It might be the case, for st500_10, that this dealumination is related to the migration of the Al in the ring of the small cavities, which would explain the increase of the porosity.

IV.2.3. Catalytic performance NO_x CH_4-SCR

Figure IV-9 compares the catalytic performance of Pd(0.3)Ce(2)-HMOR before (base) and after steaming treatment, according to nomenclature previously presented in Table IV-1.

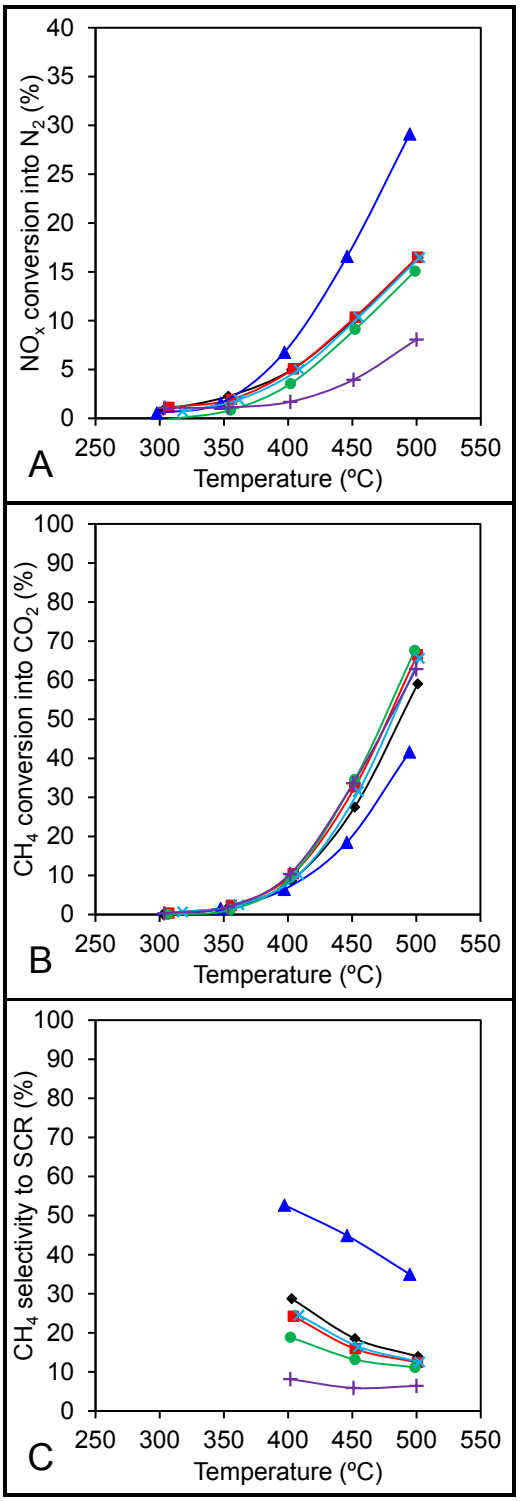

Figure IV-9 – NO_x conversion into N_2 (A), CH_4 conversion into CO_2 (B) and CH_4 selectivity to NO_x SCR reaction (C) for Pd(0.3)Ce(2)-HMOR catalysts before and after steaming under different conditions: base (♦), st500_05 (■), st500_10 (▲), st500_20 (●), st450_10 (x) and st550_10 (+). Conditions: 1000 ppm NO, 1000 ppm CH_4, 7 vol.% O_2 and GHSV of 40000 h^{-1}.

For st500_05, st500_20 and st450_10, the catalytic performance is quite similar and no significant differences are observed (NO_x and CH_4 conversions are similar, as well as CH_4 selectivity towards SCR). This observation is consistent with the different characterisation results obtained for these catalysts, which revealed no significant changes between them. For st550_10, however, though CH_4 conversion presents similar values to the previously mentioned catalysts, it is observed a significant drop on NO_x conversion, particularly at 500 ºC.

H_2-TPR and DRS UV-Vis techniques showed evidence of significant changes on the Pd and Ce species when steaming treatment is performed with 550 ºC. Surface Ce^{4+} species decrease, likely due to an agglomeration into CeO_2 and Pd species distribution is likely to become affected, which might have an influence in the interaction between Pd and Ce species.

Notwithstanding, a very promising result is obtained when the steaming treatment is performed at 500 ºC with 10 vol.% H_2O (st500_10). Compared to the base catalyst, st500_10 exhibits a NO_x conversion 29% (against 16%) and CH_4 conversion 42% (against 59%), which is translated in a CH_4 selectivity to SCR reaction of 35% (against 14%). H_2-TPR shows that surface Ce^{4+} species increased (1st reduction peak) and the CeO_2 species interacting with palladium species (2nd reduction peak) was kept similar to the one observed for base case. Moreover, FTIR-CO also evidenced an increase of the band ascribed to Ce^{n+} species, together with the increase of the intensity of a band attributed to Pd^{n+} and Ce^{n+} species, likely to be in interaction. Once again, it seems that such interaction between species is important in order to achieve a better catalytic performance.

A redistribution of metal species due to steaming treatment has been previously reported by Ferreira, *et al.* [6] for a Pd/Co-BEA system. In this case, the authors have suggested that one of the reasons for the enhanced catalytic performance observed after the steaming would be the redistribution of cobalt species, with the formation and stabilisation of low-temperature reducible oxo-ions that would play a role in the NO oxidation to NO_2, increasing the global activity.

The quantification of bands of FTIR spectrum in OH groups region (Figure IV-7) revealed that, though a band ascribed to EFAL species become visible from st500_10, it is significantly less intense (compared to the band Si-OH-Al groups) than the equivalent bands for the other steamed catalysts, namely, st500_20 and st550_10. EFAL formation is often associated with loss of crystallinity [14]. However, XRD revealed that base and steamed samples exhibit similar crystallinity, which means that EFAL formation, likely to have occurred due to the steaming treatment, is nor very expressive. In fact, st500_20 exhibits evidence of a significant amount of EFAL species, but it still exhibits the same NO_x CH_4-SCR performance as the base case, which is not the case for st550_10. Hence, one can speculate that when steaming takes place at moderate temperatures (< 500 ºC), EFAL formation is likely to occur due to the removal of Al being compensated by protons. This would explain why st450_10, st500_05 and st500_20 exhibit a NO_x CH_4-SCR performance is similar to the base catalyst.

However, when the steaming takes place at 550 ºC, Al framework species that are being compensated by Pd and Ce species are likely to be in the origin of the EFAL formation observed, which would cause the migration of active metal species to positions less active or even the formation of other species, explaining the loss of activity. It seems, hence, that the application of steaming treatment under conditions neither very soft nor very severe (namely, 500 ºC and 10 vol.% H_2O) is the key to further promote pertinent interactions between Pd and Ce species, without causing formation of EFAL species that will jeopardise the catalytic integrity of the catalyst. Moreover, it is likely that dealumination associated with the formation of such EFAL species causes the opening of small cages (which would explain the increase of the pore volumes), likely to facilitate the access of eventual metal species located there.

IV.3. Steaming position as unitary operation in catalyst preparation

In the previous section, it was shown that by applying a steaming treatment to PdCe-HMOR catalyst it is possible to obtain an enhanced catalytic performance for NO_x CH_4-SCR when considering 500 ºC and 10 vol.% H_2O. This performance is likely to be related to changes in Pd and Ce species, namely, to their interaction. However, it is pertinent to understand if the same treatment applied to monometallic Pd-based catalysts is also observed. Other question that can be raised after observation of the results in the previous section is if, by applying the steaming treatment in different stages of the catalyst preparation (namely, before and between metals introduction), it is possible to produce the same enhancing effect or not. In this section, these points are addressed.

IV.3.1. Monometallic Pd-HMOR system

IV.3.1.1. *Catalyst preparation*

Monometallic Pd-MOR steamed catalyst were prepared according to the scheme presented in Figure IV-10.

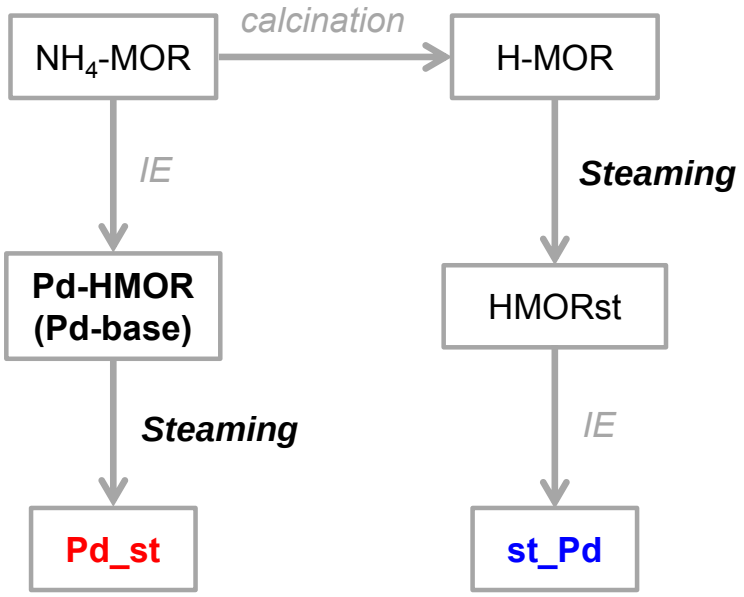

Figure IV-10 – Schematic representation of steamed-monometallic catalysts preparation.

The steaming treatment considered herein was similar to the one described in the previous section. Catalysts were submitted to a thermal treatment, consisting in a calcination procedure under air flow, at 500 ºC (5 ºC/min). Once this temperature was reached, a liquid water flow was fed to the reactor, together in the air flow, corresponding to 10 vol.%, during 3 h. After this period, water flow was stopped and the temperature was kept for an additional hour.

In this study, Pd(0.3)-HMOR is named as Pd-based. Pd_st catalyst was obtained by applying the previously mentioned steaming treatment to Pd(0.3)-HMOR. st_Pd catalyst was obtained by applying the same steaming treatment to a HMOR (obtained after calcination NH_4MOR, 8h, 500 ºC, 5 ºC/min) and, then, by introducing 0.3 wt.% Pd by ion-exchange.

IV.3.1.2. Powder X-ray diffraction (PXRD)

Similar to what was done for Pd(0.3)Ce(2)-HMOR steamed catalysts previously presented in section IV.2.2.1, PXRD patterns were collected for monometallic Pd(0.3)-HMOR steamed catalysts (Figure IV-11).

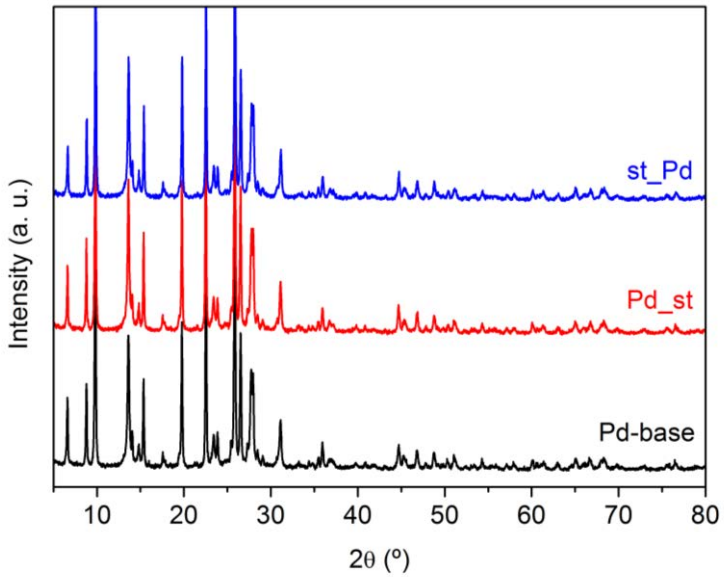

Figure IV-11 – PXRD patterns of Pd(0.3)-HMOR catalysts obtained by performing steaming during different stages of the preparation.

All peaks presented in the diffractograms correspond to MOR structure and no peaks are detected for palladium species, namely, PdO or Pd^0. The crystallinity of each sample was estimated through the integration of diffractograms between 16-30 º. The value obtained for the Pd-base catalyst was assumed to be 100% and it was used as reference in the calculation of the crystallinity of steamed samples (Table IV-5).

Table IV-5 – Crystallinity of Pd(0.3)-HMOR catalysts obtained by performing steaming during different stages of the preparation (reference – Pd-base).

Sample	Crystallinity (%)
Pd_st	95
st_Pd	97

Again in this case, the crystallinity of Pd(0.3)-HMOR steamed samples is higher than 90% (compared to base catalyst) and, consequently, no evidence of structural changes on the catalysts due to steaming are observed by PXRD.

IV.3.1.3. Quantification of acid sites by pyridine-FTIR spectroscopy

Figure IV-12 illustrates the results regarding the quantification of acids sites of HMOR, Pd-base, HMORst and Pd_st, obtained by pyridine adsorption and consecutive thermodesorption, followed by FTIR.

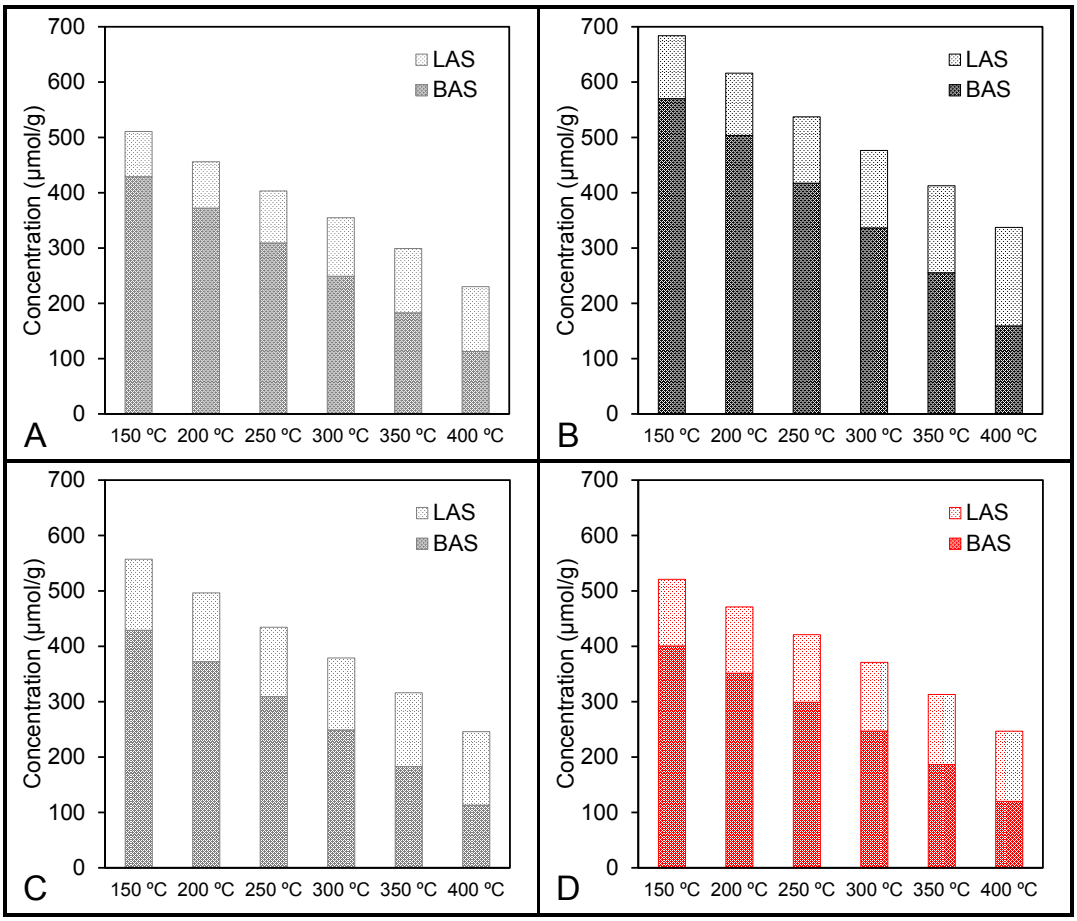

Figure IV-12 – Quantification of acid sites of HMOR (A), Pd-base (B), HMORst (C) and Pd_st by pyridine thermodesorption followed by FTIR.

As it has been previously discussed in Chapter II, section II.4.1.4, the difference in acidity between HMOR and Pd-base (372 *vs*. 503 μmol/g, 200 ºC) is due to the fact that when performing the calcination procedure to obtain HMOR (8h, at 500 ºC), it is likely that part of OH groups were removed in further extent comparing to the calcination of Pd(0.3)-HMOR (1h, at 500 ºC).

By observing the results from HMOR and HMORst (Figure IV-12A and C), it is possible to observed, once again, that the steaming treatment results in a mild loss of BAS (372 *vs*. 322 μmol/g, 200 ºC) and a consequently gain of LAS (84 *vs.* 124 μmol/g, 200 ºC). Similar results are obtained when the steaming treatment is performed in Pd-base in order to obtain Pd_st, where the BAS decrease (503 *vs.* 351 μmol/g, 200 ºC) and LAS increases (113 *vs.* 120 μmol/g, 200 ºC). It is interesting to see that, contrarily to what happens with the metal-free structures, the loss of BAS is far more extensive that the gain in LAS.

IV.3.1.4. Temperature programmed reduction under hydrogen (H_2-TPR)

In Figure IV-13 are presented the H_2-TPR profiles of Pd(0.3)-HMOR catalysts obtained by performing steaming during different stages of the preparation.

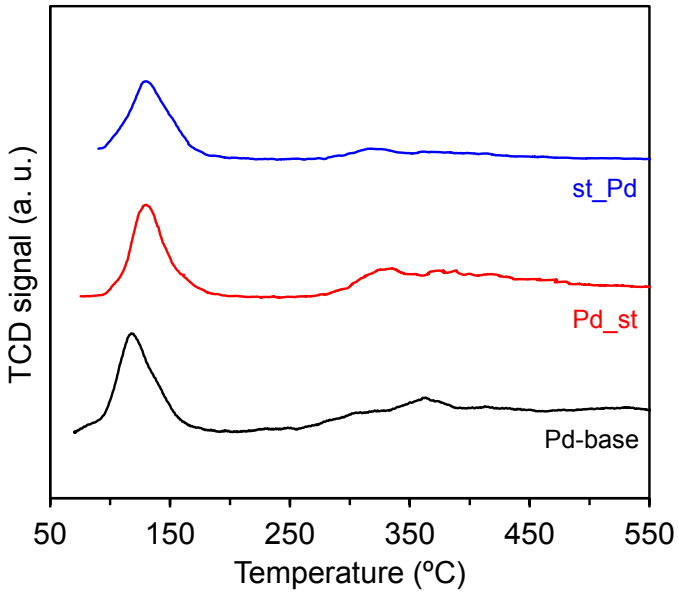

Figure IV-13 – H_2-TPR profile of Pd(0.3)-HMOR catalysts obtained by performing steaming during different stages of the preparation.

All profiles are very similar between them, exhibiting a low reduction peak characteristic from Pd^{2+} ions in exchange positions. Moreover, the quantification of H_2 consumption corresponding to this peak (Table IV-6) resulted in a H_2/Pd ratio of *ca.* 1, suggesting that all palladium is stabilised as this species.

Table IV-6 – Quantification of H_2 consumption by peak integration of H_2-TPR profiles of Pd(0.3)-HMOR catalysts obtained by performing steaming during the preparation.

	T (ºC)	H_2/Pd	µmol H_2 /$g_{catal.}$
Pd-base	70-200	0.9	39
Pd_st	75-200	1.2	33
st_Pd	90-185	1.0	30

Regarding the different Pd^{2+} species distribution (deconvolution of the reduction process in two Gaussian peaks), it is possible to observe that the steamed catalyst present a slightly change in the distribution represented by a higher amount of Pd^{2+} being reduced at lower temperature (Table IV-7). It is also worthy to be mentioned a shift in both reduction temperatures for slightly higher values compared to Pd-base catalyst, which might suggest that Pd species became more stable in the steamed catalysts.

Table IV-7 – Quantification of the relative amount of Pd^{2+} corresponding to both reduction process of Pd(0.3)-HMOR catalysts obtained by performing steaming during different stages of the preparation.

	Gaussian peak 1		Gaussian peak 2	
	T (ºC)	Amount of Pd^{2+}	T (ºC)	Amount of Pd^{2+}
Pd-base	118	69%	141	31%
Pd_st	129	79%	155	21%
st_Pd	129	81%	152	19%

IV.3.1.5. *NO_x CH_4-SCR*

Catalytic test results of Pd-base, Pd_st and st_Pd catalysts in the presence and absence of water in the inlet gas feed are presented in Figure IV-14.

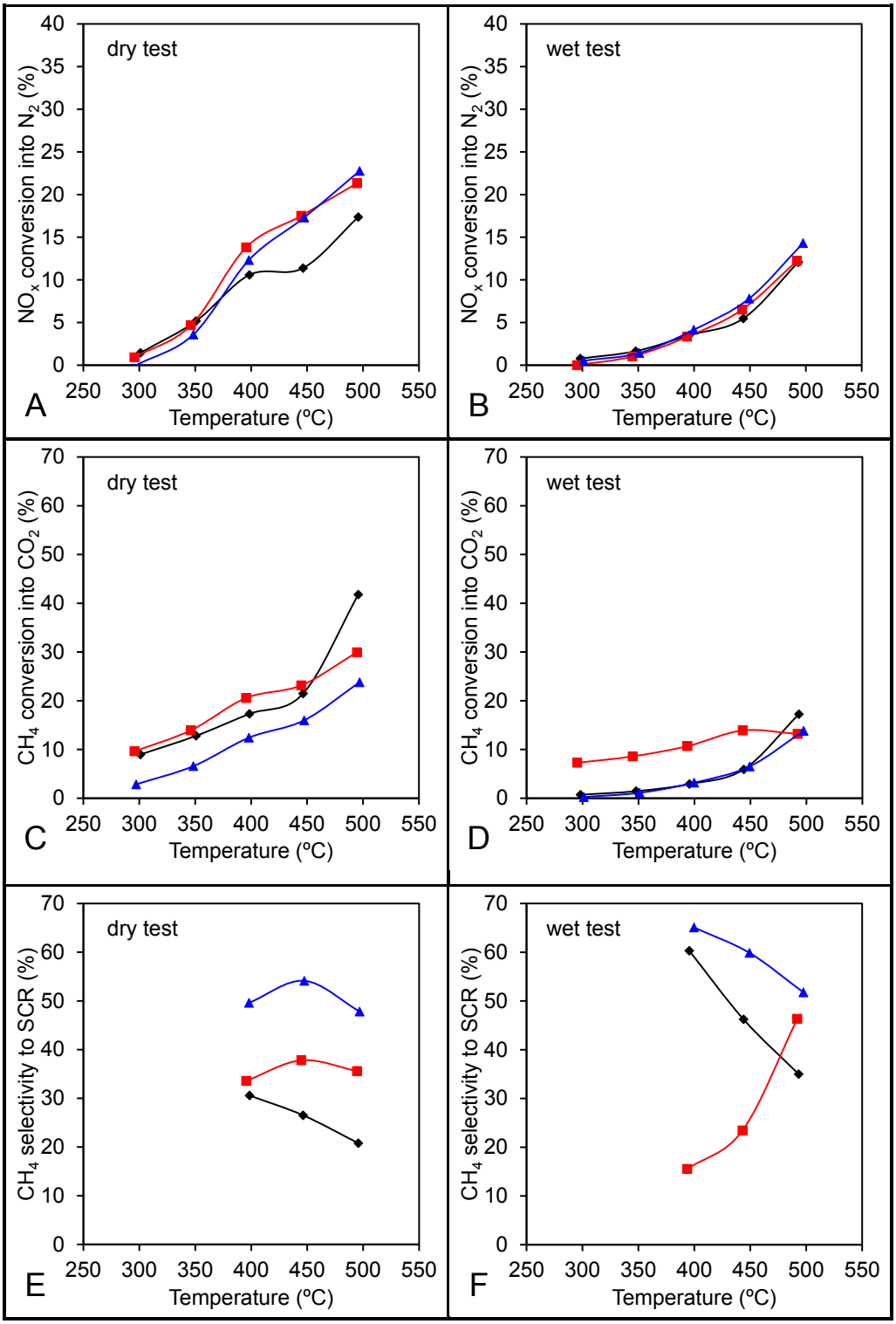

Figure IV-14 – NO_x conversion into N_2 (A,B), CH_4 conversion into CO_2 (B,C) and CH_4 selectivity to NO_x SCR reaction (C,D) for Pd-base (♦), Pd_st (■) and st_Pd (▲). Conditions: 1000 ppm NO, 1000 ppm CH_4, 7 vol.% O_2, 2 (or 0) vol.% H_2O and GHSV of 40000 h^{-1}.

In the absence of water in the inlet gas feed, both steamed catalysts exhibit an enhanced catalytic performance, which is more pronounced at high temperatures. For instance, at 450 ºC, NO_x conversion into N_2 for 11% against 18% for Pd_st and 17% for st_Pd. Moreover, CH_4 selectivity to SCR reaction is significantly higher for the steamed catalysts, when compared to Pd-base.

H_2-TPR revealed that, for both Pd_st and st_Pd, there is a higher quantity of Pd^{2+} ions species that become reduced at lower temperature, when compared to Pd-base, which might be related with the increase NO_x CH_4-SCR performance.

Nevertheless, in the presence of water in the inlet gas feed, all catalysts exhibit practically the same NO_x conversion into N_2, without registry of an enhanced catalytic performance. It should be mentioned, below 450 ºC, that CH_4 selectivity to SCR reaction of Pd_st becomes significantly lower than the one observed for the other two catalysts. However, it should also be mentioned that both NO_x and CH_4 conversion values are significantly low in this range of temperatures (*ca.* 5%), which can influence significantly the interpretation of the results. Notwithstanding, at 500 ºC, CH_4 selectivity values follow the same trend previously observed in the catalytic test in the absence of water, *i.e.* $S_{st\_Pd} > S_{Pd\_st} > S_{Pd\text{-}base}$.

It seems, then, that in the presence of water the eventual enhancing effect on the catalytic performance caused by the steaming treatment becomes buffered by the competitive adsorption of water with the reactants. Hence, it is not likely that the enhanced catalytic effect due to the steaming, observed in the bimetallic formulation (Figure IV-9, base vs. st500_10) is primarily caused by changes in the Pd actives sites.

IV.3.2. Bimetallic PdCe-HMOR system

IV.3.2.1. Catalyst preparation

Figure IV-15 schematises the PdCe-MOR steamed catalysts prepared by performing the steaming treatment in different stages of the catalyst preparation.

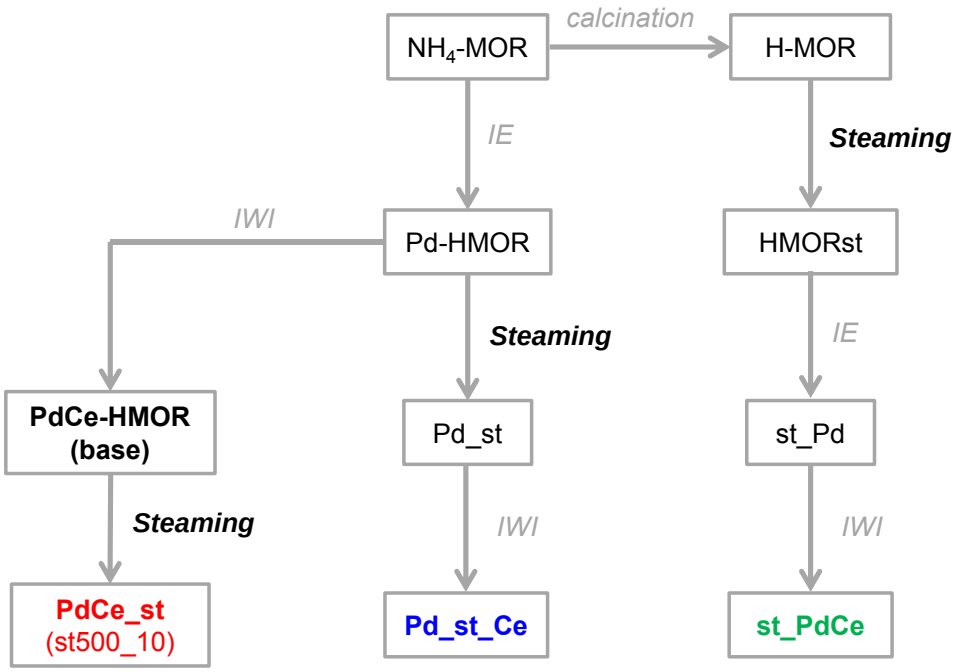

Figure IV-15 – Schematic representation of steamed-bimetallic catalysts preparation.

Once again, the same steaming treatment previous mentioned (section IV.3.1.1) was considered in this case. PdCe_st catalyst is the same one previously named as st500_10. Pd_st_Ce and st_PdCe were obtained from Pd_st and st_Pd, respectively, by adding cerium through incipient wetness impregnation, using the same procedure as for PdCe-HMOR (see Annex C, section C.1.3).

IV.3.2.2. *Powder X-ray diffraction (PXRD)*

PXRD patterns were collected for Pd(0.3)Ce(2)-HMOR steamed catalysts obtained by performing steaming during different stages of the preparation (Figure IV-16).

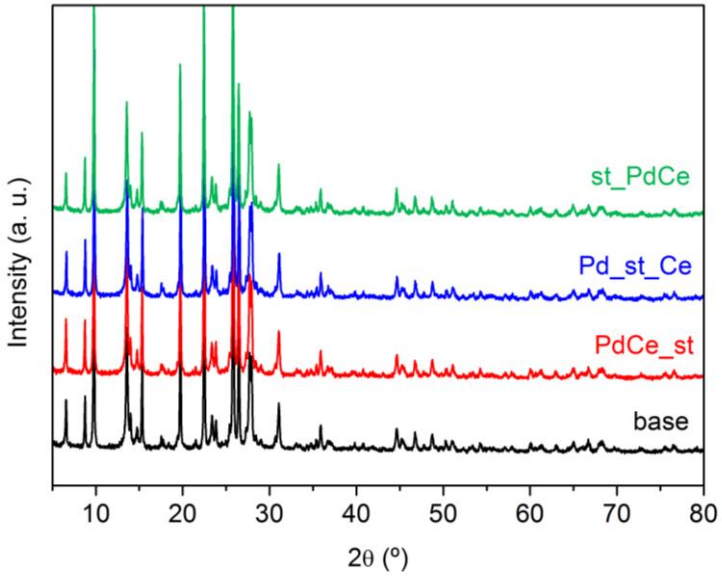

Figure IV-16 – PXRD patterns of Pd(0.3)Ce(2)-HMOR catalysts obtained by performing steaming during different stages of the preparation.

All peaks presented in the diffractograms correspond to MOR structure and no peaks are detected for palladium or cerium species. The crystallinity of each sample was estimated through the integration of diffractograms between 16-30 °. The value obtained for the base catalyst was assumed to be 100% and it was used as reference in the calculation of the crystallinity of steamed samples (Table IV-8).

Table IV-8 – Crystallinity of Pd(0.3)Ce(2)-HMOR catalysts obtained by performing steaming during different stages of the preparation (reference – base).

Sample	Crystallinity (%)
PdCe_st	97
Pd_st_Ce	93
st_PdCe	95

Once again, no significant changes are found between base and steamed catalysts.

IV.3.2.3. Temperature programmed reduction under hydrogen (H_2-TPR)

H_2-TPR profiles of Pd(0.3)Ce(2)-HMOR catalysts obtained by performing the steaming treatment during different stages of the catalyst preparation are presented in Figure IV-17.

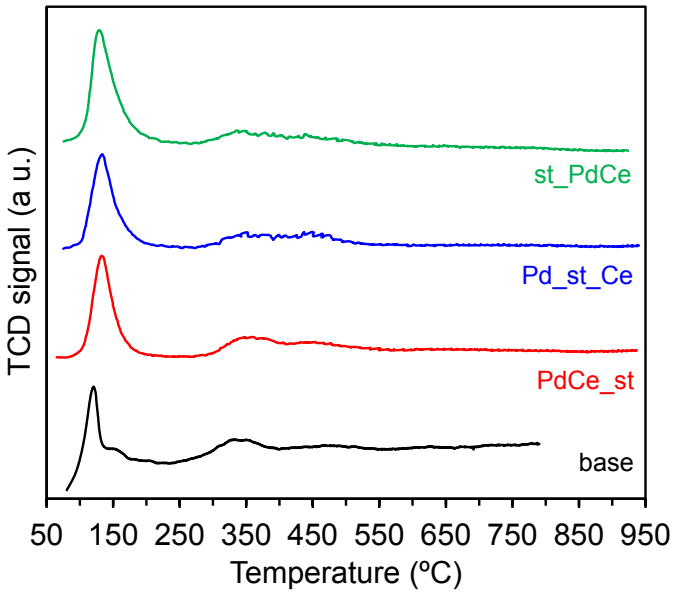

Figure IV-17 – H_2-TPR profile of Pd(0.3)Ce(2)-HMOR catalysts obtained by performing steaming during different stages of the preparation.

All steamed catalyst exhibit a similar catalytic reduction profile, characterised by a reduction process at low temperature (between 80-220 ºC), ascribed to the reduction of Pd^{2+} ions in exchange position and surface Ce^{4+} species, and a reduction process between 240-565 ºC, ascribed to the reduction of CeO_2 species interacting with palladium.

The quantification of H_2 consumption (Table IV-9) reveals that, in general, all steamed catalysts present more surface Ce^{4+} species (higher H_2/Pd ratio at low temperature than base case) and slightly less CeO_2 species in interaction with Pd (lower H_2/Ce ratio at higher temperature), compared to the base catalyst. Moreover, it should be highlighted that st_PdCe is the catalyst that presents the highest differences in H_2 consumption values.

Table IV-9 – Quantification of H_2 consumption by peak integration of H_2-TPR profiles of Pd(0.3)Ce(2)-HMOR catalysts obtained by performing steaming during different stages of the preparation.

	Peak 1			Peak 2		
	T (ºC)	H_2/Pd	µmol H_2 /$g_{catal.}$	T (ºC)	H_2/Ce	µmol H_2 /g_{catal}
base	95-215	1.4	39	240-560	0.27	37
PdCe_st	85-210	2.0	54	275-565	0.24	33
Pd_st_Ce	80-215	2.0	56	275-555	0.20	27
st_PdCe	80-220	2.4	67	275-555	0.17	24

IV.3.2.4. *NO_x CH_4-SCR*

Figure IV-18 illustrates the catalytic test results of Pd(0.3)Ce(2)-HMOR catalysts obtained by performing the steaming treatment during different stages of the catalyst preparation.

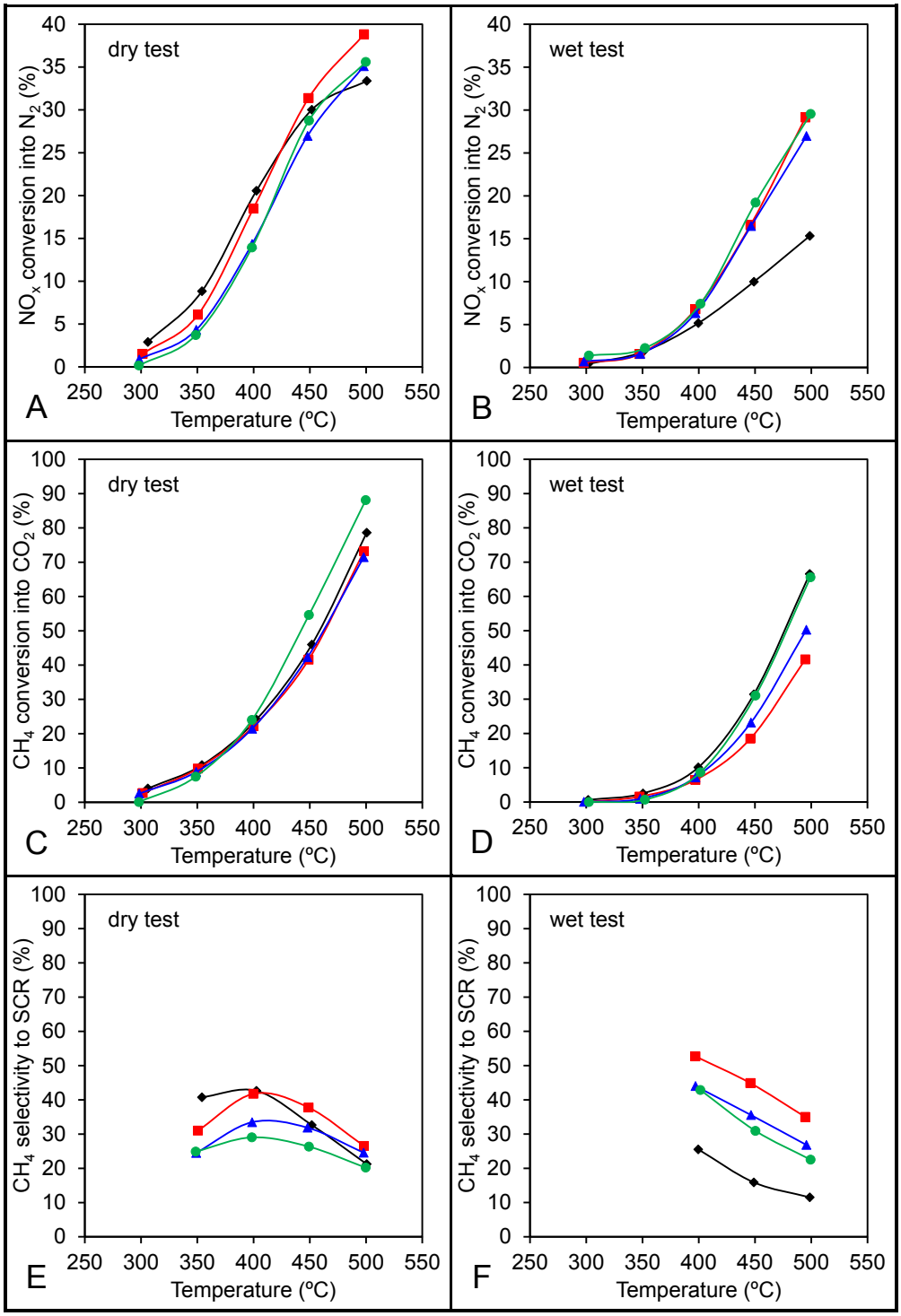

Figure IV-18 – NO_x conversion into N_2 (A,B), CH_4 conversion into CO_2 (B,C) and CH_4 selectivity to NO_x SCR reaction (C,D) for Pd(0.3)Ce(2)-HMOR catalysts obtained by performing steaming during different stages of the preparation: base (♦), PdCe_st (■), Pd_st_Ce (▲) and st_PdCe (●). Conditions: 1000 ppm NO, 1000 ppm CH_4, 7 vol.% O_2, 2 (or 0) vol.% H_2O and GHSV of 40000 h^{-1}.

On one hand, in the absence of water in the inlet feed, all catalyst present similar NO_x conversion values. CH_4 conversion is also similar, except for st_PdCe catalyst, which, at high temperature (>450 ºC) is slightly higher than the others. This catalysts was also the one that exhibits higher amount of surface Ce^{4+} species (see H_2-TPR), which could explain this result since, as it was previously seen for in the previous Chapter II, section II.4.1.8 and Chapter III, section III.2.8, CeO_2 possesses oxidative properties.

On the other hand, when water is present in the inlet gas feed all steamed catalysts exhibit the same NO_x conversion, which is higher than the one observed for the base catalyst. It seems, then, that no matter in which stage of the catalyst preparation the steaming treatment is performed, an enhancing effect is always observed. Previously, in section IV.2 , it has been suggested that the steaming treatment would likely cause changes in the metal species that would favour the NO_x CH_4-SCR reaction. Moreover, it has been propose that the ideal steaming conditions, namely 500 ºC and 10 vol.% H_2O, would be those that would promote such changes in the metal species and, at the same time, would not cause significant changes in the zeolite framework, namely, excessive formation of EFAL species. However, if when the steaming is performed before the metal introduction a similar enhancing effect is also observed, this means it is likely that, instead of a change in the metal species, such modification in the zeolite framework might be responsible for this enhancing effect.

An example of structural effect of MOR zeolite on NO_x CH_4-SCR reaction have been previously reported in literature, namely considering a Pd/Co-MOR system ([15], patent). According to this invention, by using an industrially synthesised “small pores” MOR structure (that absorbs only molecules with kinetic diameter less than 4.4 Å) [16], the authors claimed to obtained a better catalytic performance when compared to formulations based on “large pores” MOR structure (able to adsorb molecules with kinetic diameter of 6.6 Å, namely, benzene). However, the authors do not present an explanation for the observed effect.

In the present case, it is possible that the steaming treatment causes some irregularities in the zeolite framework that may, for instance, promote the adsorption of more reactants (such NO_x), promoting hence the formation of intermediate species. It is also possible that such defects may unblock active sites previously inaccessible to the reactants, such as metal sites stabilised in the small cavities of MOR structure. Nevertheless, these hypothesis lack of more consistent evidences, which were not possible to confirm by the characterisation techniques considered herein.

Notwithstanding, the effect of steaming the formation of other metal species eventually more active for NO_x CH_4-SCR cannot be entirely excluded. In fact, it worthwhile mentioning that, despite all catalyst present similar NO_x conversion values, PdCe_st (in which the steaming was performed once the metals have been previously introduced) is the one that exhibits the lowest CH_4 conversion and, hence, the highest CH_4 selectivity towards SCR reaction. Curiously, from all the steamed catalyst, PdCe_st is also the one the exhibits the higher H_2/Ce ratio regarding the

reduction process, corresponding to CeO_2 species interacting with palladium. This may be seen as another evidence that such species may, indeed, play a crucial role in the NO_x CH_4-SCR reaction.

IV.4. Catalytic performance of steamed catalyst under representative conditions of a real lean-gas engine

In the previous sections, the results obtained considering the steaming treatment of the different PdCe-MOR catalysts showed that when Pd(0.3)Ce(2)-HMOR is submitted to a thermal treatment at 500 ºC, under 10 vol.% H_2O (st500_10 catalyst), the best catalytic performance is achieved, *i. e.*, higher NO_x conversion into N_2 and higher CH_4 selectivity towards SCR reaction. In this section, the representative conditions of exhaust gases from a real heavy duty vehicle's engine (Volvo engine MG9 in lean-gas burn conditions) was considered to assess the catalytic performance of st500_10 and compared to the base catalyst (Pd(0.3)Ce(2)-HMOR before steaming).

The catalytic test conditions considered in this study are summarised in Table IV-10. The range of temperatures considered was 300-700 ºC.

Table IV-10 – Inlet gas feed mixtures corresponding to Volvo engine MG9 exhaust gases (lean-gas burn conditions).

	dry	**wet**
[NO] / ppm	400	400
[CH_4] / ppm	1600	1600
[O_2] / %	7	7
[H_2O] / %	-	2
GHSV / h^{-1}	40000	40000

The steady-state test results for both base and st500_10 catalyst tested under dry and wet conditions are presented Figure IV-19. It is possible to observe that both catalysts exhibit the practically the same NO_x and CH_4 conversion values and, consequently, the same CH_4 selectivity to NO_x SCR reaction. The results reveal that, contrarily to what happened under the test conditions 1000 ppm NO / 1000 ppm CH_4, the enhancing effect due to the steaming treatment is not observed herein.

One possible hypothesis previously proposed in section IV.3.2.4 for this enhancing effect has been the promotion of NO_x adsorption. Since the concentration of NO_x is decrease in the test conditions currently considered, this might explain the absence of promotional effect in the steamed catalysts. A second series of test (dry/wet) was, hence, performed considering the same [NO]/[CH_4] = 4 ratio in the inlet gas feed that represents in the real exhaust gas conditions, but with 1000 ppm NO instead. The results are presented in Figure IV-20.

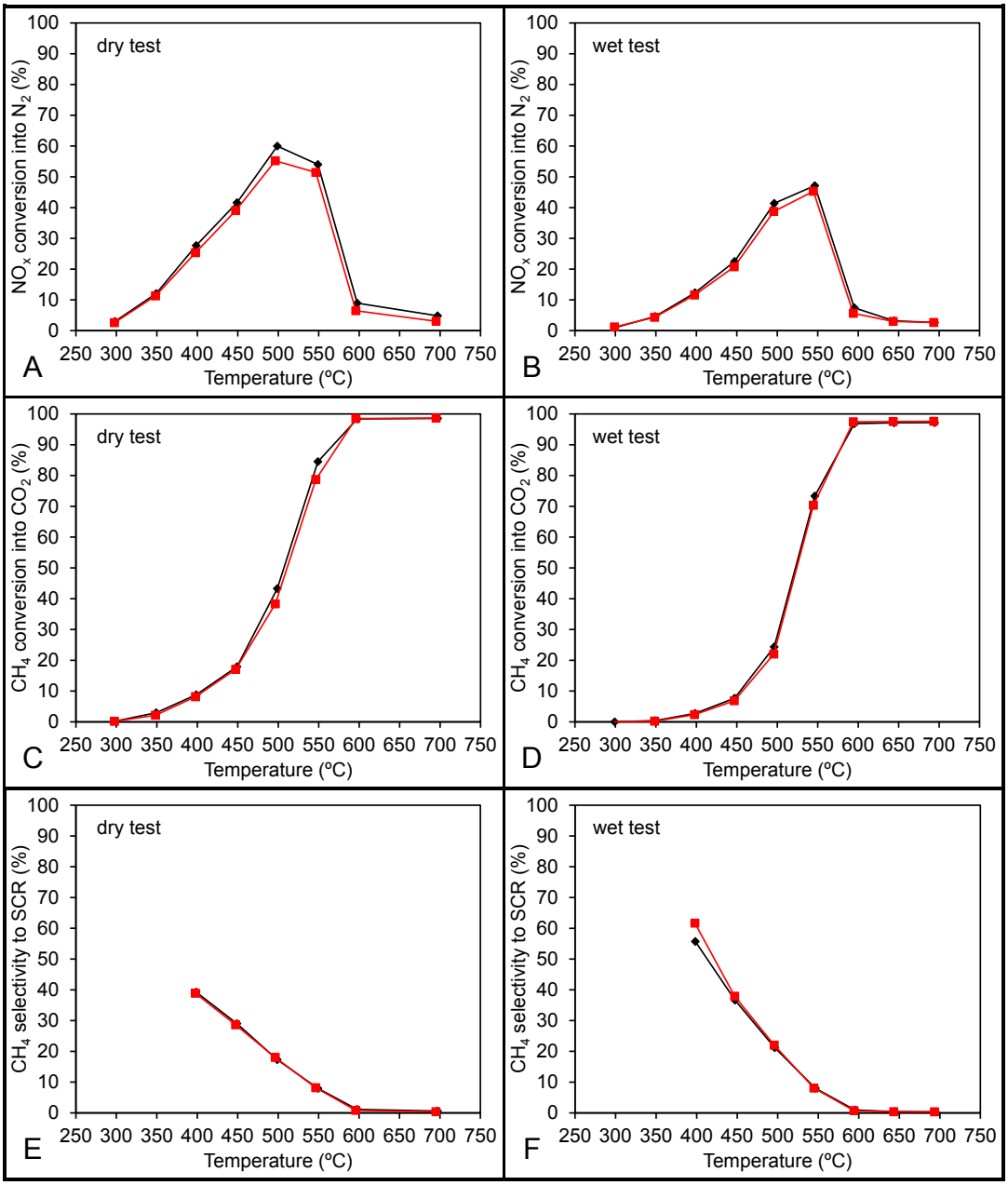

Figure IV-19 – NO_x conversion into N_2 (A,B), CH_4 conversion into CO_2 (B,C) and CH_4 selectivity to NO_x SCR reaction (C,D) for base (♦) and st500_10 (■). Conditions: 400 ppm NO, 1600 ppm CH_4, 7 vol.% O_2, 2 (or 0) vol.% H_2O and GHSV of 40000 h^{-1}.

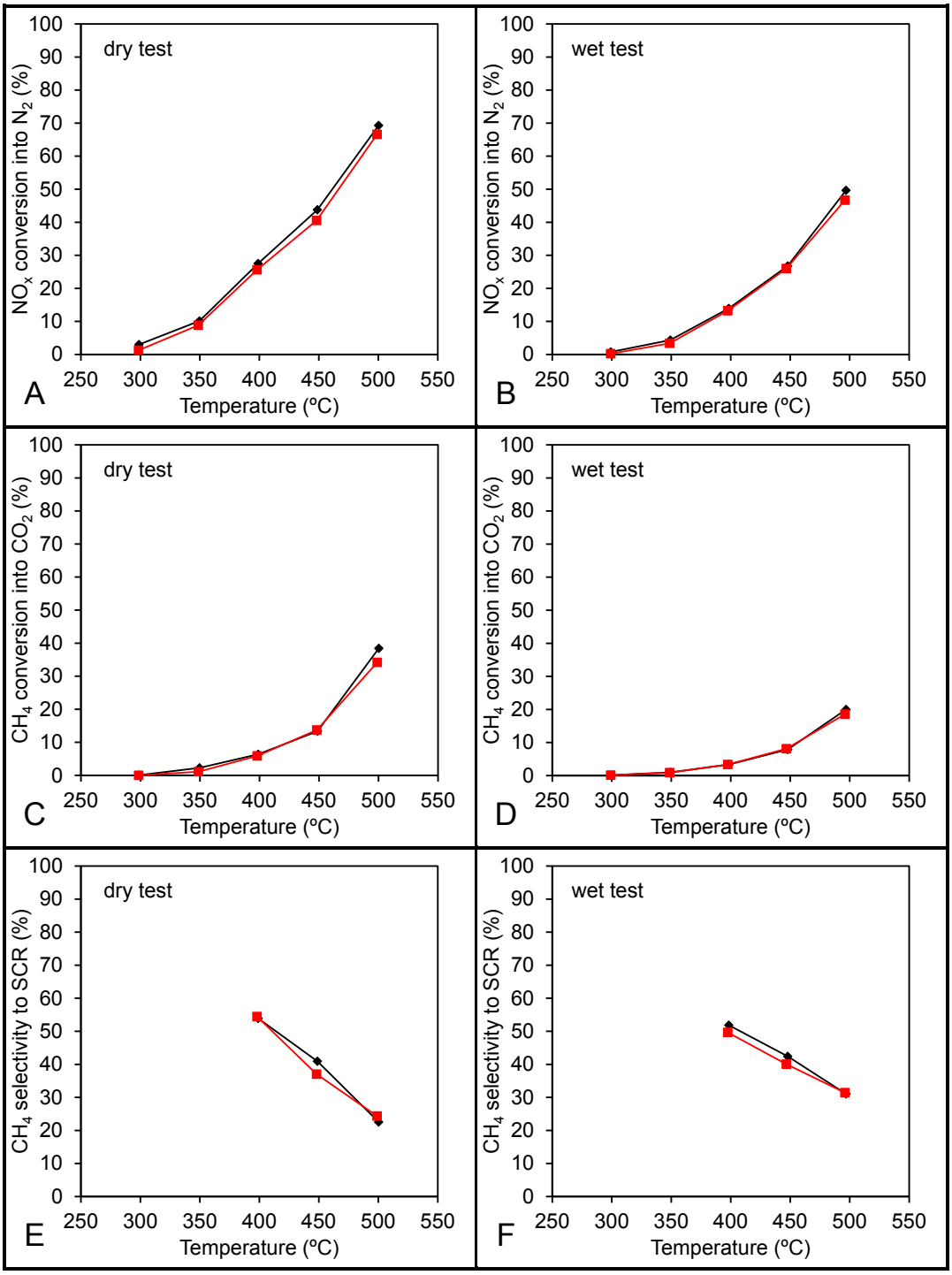

Figure IV-20 – NO_x conversion into N_2 (A,B), CH_4 conversion into CO_2 (B,C) and CH_4 selectivity to NO_x SCR reaction (C,D) for base (♦) and st500_10 (■). Conditions: 1000 ppm NO, 4000 ppm CH_4, 7 vol.% O_2, 2 (or 0) vol.% H_2O and GHSV of 40000 h^{-1}.

Once again, with these conditions, both catalysts present practically the same conversion values and an enhancing effect due to the steaming treatment performed is, once more, not observed. It seems, then, that the catalytic enhancement previously observed only takes places in conditions less favourable for NO_x CH_4-SCR, where less reductant is available (which is the case of 1000 ppm NO, 1000 ppm CH_4).

As it was concluded in the previous section, the characterisation results obtained for both base and steamed catalyst only revealed slight modifications in metal species and even in the zeolite structure. It is possible that, despite being subtle, these modifications may be important, for instance, in the formation of intermediate species which are likely to occur more difficultly when less reductant is available. In situations where a significantly higher amount of methane is in contact with the catalyst (*i.e.* higher partial pressure), one can expect that the formation of R-NO_x and $C_xH_yO_z$ intermediate species (which are believed to the actual intermediate species [17, 18]) is favoured, contributing to the global increase of activity.

Although an improvement in the catalytic performance has not been observed in under representative conditions of a real exhaust gas system, the fact that st500_10 exhibit the same catalytic conversion as the base case is an important result *per se*. Thermal treatments in the presence of water, also known as ageing treatments, are usually considered in literature as a technique to simulate the long-term use of the catalyst [19-21]. In fact, previous results considering Pd/Ce-MOR system [7] showed that after exposing the catalyst to 5 vol.% H_2O (under reaction conditions) an irreversible loss of activity occurred due to the migration of Pd^{2+} (active for NO_x SCR) into PdO particles that favour CH_4 direct combustion. In the steamed catalyst considered in this work this migration does not take place, which explains why st500_10 presents the same conversion as base catalyst. Moreover, this result may be an indication regarding the stability of the catalyst, which one can expect to preserve its catalytic performance under long-term test.

IV.5. Conclusions

The effect of steaming treatment in the catalytic performance of Pd(0.3)Ce(2)-HMOR for NO_x CH_4-SCR was studied. By performing different steaming treatments considering temperatures (450-550 ºC) and water contents in the inlet air feed (5-20 vol.%), it was possible to observe that under 500 ºC and 10 vol.% H_2O, the steamed catalyst (st500_10) exhibits enhanced catalytic performance compared to the base catalyst. Such enhancement is attributed changes in the metal species, namely formation of surface Ce^{4+} species, at the same time that CeO_2 species in interaction in palladium, previously identified in the base catalyst, are kept. The formation of EFAL species was also observed. By considering 500 ºC and 10 vol.% H_2O as steaming conditions, EFAL formation is likely to occur due to the migration of Al sites being compensated by H^+ and not metal cationic species, avoid the loss of dispersion of metal species, in particular, active Pd^{2+} in exchange positions. It is also likely that this mild dealumination gives access to actives species more restrained in the base catalyst, namely metal sites in the small cavities of MOR catalyst.

When steaming treatment is performed at lower temperatures (450 ºC) or with lower water content (5 vol.%), such changes are likely not to occur in the necessary extension. On the contrary, when considering higher temperature or water content, EFAL formation is likely to occur at cost of migration of Al species from zeolite framework which were being coordinate by metal cation, causing undesired changes in the metal species and a significant decrease in the CeO_2 species in interaction with palladium.

The positioning of steaming treatment as operation unit during the preparation of PdCe-MOR catalysts was also assessed, considering the steaming conditions that previously resulted an enhancing effect on Pd(0.3)Ce(2)-HMOR (500 ºC, 10 vol.% H_2O). Firstly, for monometallic Pd-base catalysts, it was observed that independently of considering the steaming treatment before or after the introduction of Pd, both catalysts exhibit similar catalytic performances, equal to Pd(0.3)-HMOR catalyst. Though some changes were observed in the distribution of Pd species, the results show that the enhancing effect previously observed for st500_10 is not likely to be caused by changes in Pd active sites (at least exclusively).

Afterwards, by considering the same steaming treatment on bimetallic formulation, performed before and between metals introduction, it was possible to observe that all bimetallic steamed catalyst exhibit an enhanced catalytic performance. This suggested that structural modifications on the zeolite framework, though subtle, might be behind the enhancing effect observed. One possibility may be the promotion of adsorbed reacts (such as NO_x), which would enhance the formation of intermediary species. Another one could be the unblocking of the zeolite structure that would contribute to an easier access to active metal sites. Notwithstanding, the catalyst that present higher CH_4 selectivity towards SCR reaction was the one were steaming was performed after introduction of both metal species. At the same time, from all bimetallic steamed catalyst, this was the one that presented higher amount of CeO_2 species in interaction with palladium, which reinforces the idea of the importance of these species in the NO_x CH_4-SCR reaction.

Finally, st500_10 catalyst was test under representative conditions of a real exhaust gases of a heavy duty vehicle's engine ([CH_4]/[NO] = 4, when previously was 1) and its catalytic performance was compared with the base (non-steamed) catalyst. Results show that the performance of both catalyst was the same, which suggests when CH_4 is present in large excess compared to NO_x, the enhancing effects due to the steaming treatment become buffered.

IV.6. References

[1] H. Ohtsuka, T. Tabata, Appl. Catal., B, 21 (1999) 133-139.

[2] Z.J. Li, M. Flytzani-Stephanopoulos, Appl. Catal., B, 22 (1999) 35-47.

[3] P. Budi, R.F. Howe, Catal. Today, 38 (1997) 175-179.

[4] J.A.Z. Pieterse, R.W. van den Brink, S. Booneveld, F.A. de Bruijn, in: E. VanSteen, M. Claeys, L.H. Callanan (Eds.) Recent Advances in the Science and Technology of Zeolites and Related Materials, 2004, pp. 2522-2526.

[5] J.A.Z. Pieterse, H. Top, F. Vollink, K. Hoving, R.W. van den Brink, Chem. Eng. J., 120 (2006) 17-23.

[6] A.P. Ferreira, C. Henriques, M.F. Ribeiro, F.R. Ribeiro, Catal. Today, 107–108 (2005) 181-191.

[7] I.O. Costilla, M.D. Sanchez, M. Alicia Volpe, C.E. Gigola, Catal. Today, 172 (2011) 84-89.

[8] G.J. Hutchings, A. Burrows, C. Rhodes, C.J. Kiely, R. McClung, J. Chem. Soc., Faraday Trans., 93 (1997) 3593-3598.

[9] L.F. Isernia, Mater. Res.-Ibero.-Am. J., 16 (2013) 792-802.

[10] D. Pietrogiacomi, M.C. Campa, V. Indovina, J. Phys. Chem. C, 114 (2010) 17812-17818.

[11] I. Salla, T. Montanari, P. Salagre, Y. Cesteros, G. Busca, J. Phys. Chem. B, 109 (2005) 915-922.

[12] K.I. Hadjiivanov, G.N. Vayssilov, Adv. Catal., 47 (2002) 307-511.

[13] G. Leofanti, M. Padovan, G. Tozzola, B. Venturelli, Catal. Today, 41 (1998) 207-219.

[14] J.A.Z. Pieterse, R.W. van den Brink, S. Booneveld, F.A. de Bruijn, Appl. Catal., B, 46 (2003) 239-250.

[15] C. Hamon, O. Le Lamer, J. Saint-Just, Patent, WO15339 (1998).

[16] C. Hamon, Y. Le Goff, Patent, US4910004 (1990).

[17] O. Gorce, F. Baudin, C. Thomas, P. Da Costa, G. Djega-Mariadassou, Appl. Catal., B, 54 (2004) 69-84.

[18] S. Capela, R. Catalao, M.F. Ribeiro, P. Da Costa, G. Djega-Mariadassou, F.R. Ribeiro, C. Henriques, Catal. Today, 137 (2008) 157-161.

[19] C. Descorme, P. Gelin, M. Primet, C. Lecuyer, J. SaintJust, Zeolites: A Refined Tool for Designing Catalytic Sites, 97 (1995) 287-294.

[20] H. Berndt, F.W. Schutze, M. Richter, T. Sowade, W. Grunert, Appl. Catal., B, 40 (2003) 51-67.

[21] D. Wang, Y. Jangjou, Y. Liu, M.K. Sharma, J.Y. Luo, J.H. Li, K. Kamasamudram, W.S. Epling, Appl. Catal., B, 165 (2015) 438-445.

Chapter V. Structured catalysts for automotive applications – A synthetic gas bench study

V.1. Introduction

Though the development of new catalytic formulations, performed at lab-scale, is made considering powder formulations, commercial applications of catalysts for real emission control systems (both for automotive and stationary sources) consider the use of honeycomb monoliths [1, 2]. In particular, for automotive applications, ceramic monoliths made of cordierite ($2MgO.2Al_2O_3.5SiO_2$) are one of the most considered structures for the majority the after-treatment systems, namely, diesel particle filters (DPF) [3], 3-ways catalysts [4], diesel oxidation catalysts (DOC) [5] and selective catalytic reduction with ammonia (NH_3-SCR) [6]. This material is often considered due to its mechanical strength and its low thermal expansion coefficient and its porosity and pore size distribution is suitable to be used for washcoat application and good washcoat adherence [1, 7].

In order to deposit an active catalyst, namely a zeolite-based one, in the walls of honeycomb monoliths, two different methods can be adopted: (i) hydrothermal synthesis, consisting in growing the zeolite particles directly in the monolith walls [8]; (ii) deposition of the zeolite slurry, also known as washcoating [9]. In the case of the latter method, it is possible to firstly perform the deposition of the zeolite in the structure and, then, to introduce the active metal phase, for instance, throughout an ion-exchange procedure similar to the ones performed in the powder formulations [10] or, alternatively, the washcoating procedure can be performed with the final active catalyst formulation. The latter case is the ideal when complex catalysts formulations, containing several metals introduced in the zeolite by different methods, are intended to be used, which is the case of the formulations developed in Chapter II of this work.

Despite the fact that no commercial application is currently available for NO_x selective catalytic reduction systems using methane as reductant (NO_x CH_4-SCR), there are some works reported in literature that consider the use of zeolite-based washcoated monoliths for this application. Zamaro, *et al.* [1] have studied the effect of slurry concentration and use of SiO_2 binder in the preparation of washcoated cordierite monoliths (400 cpsi) considering MOR, MFI and FER zeolites. The authors concluded that the use of MFI led to a more stable washcoat. In the same study, the authors also present the catalytic performance of an In-MFI washcoated monolith and compare it to the powder formulation, which exhibit similar activities. In a later study, the authors also assessed the effect of zeolite slurry concentration and the used of solvents other than water in the preparation of MFI slurries [11].

Boix, *et al*. [9] studied the catalytic performance of Co-MOR washcoated in a cordierite monolith (400 cpsi), assessing the effect of water in the catalytic performance as well the use of cab-o-sil (a commercial SiO_2) as a binder. The authors also compared the use of methane and butane as reductants. In another study conducted by these authors [12], the effect of extra-framework aluminium species on Co-MFI catalysts for NO_x CH_4-SCR was assessed and it was concluded that Al^{3+} and Co^{2+} species in zeolite slurry originate a mixed Co/Al-based oxide after calcination that is inactive for NO_x CH_4-SCR.

In the work presented in this chapter, some parameters regarding the preparation of zeolite slurries were studied, namely, the effect of milling time in the particle size distribution and viscosity. The effect of the zeolite slurry concentration in the total catalyst loading washcoated on the monolith is also assessed. Based in these preliminary study and the data reported in the literature, a washcoating procedure was defined in order to prepare monoliths using Pd(0.3)Ce(2)-HMOR catalyst optimised in Chapter II. Different monoliths with 400 and 600 cpsi were considered in this study. The effect of steaming treatment was also assessed by preparing monoliths washcoated with steamed Pd(0.3)Ce(2)-HMOR (Chapter IV) and also by performing the same steaming treatment on the monoliths after washcoating with Pd(0.3)Ce(2)-HMOR.

V.2. Effect of zeolite slurry properties on the preparation of washcoated monoliths

When preparing structured catalysts throughout washcoating techniques, there are several parameters related to the slurry that influence the washcoat features and that are directly related to the quality of the final monolith to be obtained. Several studies have been performed and documented in literature that describing the effects of such parameters in the preparation of structured catalyst, mostly considering cordierite washcoated with metal oxides catalysts (such as Al_2O_3 [13-15]) but also for zeolite-based washcoated cordierite [1, 11, 16]. These studies may guide in the preparation of structured catalysts.

Nevertheless, it is important to take into account that in order to prepare washcoated monoliths, significant amounts of catalyst are required, compared to the powder formulation. For instance, with about 1 g of starting material (NH_4-MOR), it is possible to obtain enough catalyst for all characterisation techniques and catalytic tests, this last requiring *ca.* 200 mg. For preparing a monolith (with dimension D x L = 1 x 1 in), at least *ca.* 9 g of catalyst are required. Hence, it is important have an idea of the influence of, at least, some parameters, such as particle size distribution, viscosity and zeolite concentration on the slurry. The purpose of this work is not to perform and exhaustive study of the influence of all the parameters that influence the washcoating process for obtaining zeolite-based monoliths but, instead, giving some insights on the effect of, probably, the most relevant zeolite slurry properties that shall be taken into account during the preparation of washcoated monoliths.

To this end, several suspensions were prepared using NH_4MOR powder zeolite (Si/Al = 10, Zeolyst) in order to study the effect of milling time in the particle size distribution and viscosity. The quantification of the total mass loading as a function of the number of immersions during the washcoating process was also determined considering different concentrations of zeolite slurry.

V.2.1. Effect of milling time

According to Mitra and Kunzru [16], in order to have an efficient washcoating process, the zeolite particle sizes should be with the range 2-3 μm. Wet ball milling is an effective method of reducing the particle size, since it allows to keep the crystallinity and surface area of the powder. However, the required milling time may depend on the zeolite considered (namely, its particle size distribution) and also the rotational speed.

The particle size distribution of the zeolite powder (NH_4MOR, Si/Al = 10, Zeolyst) considered in this study is presented in Figure V-1. The average particle size ($\overline{d_p}$), average deviation (σ) and diameter at which 50% of the sample is finer than (d_{50}) is 5.6, 4.3 and 3.3 μm, respectively.

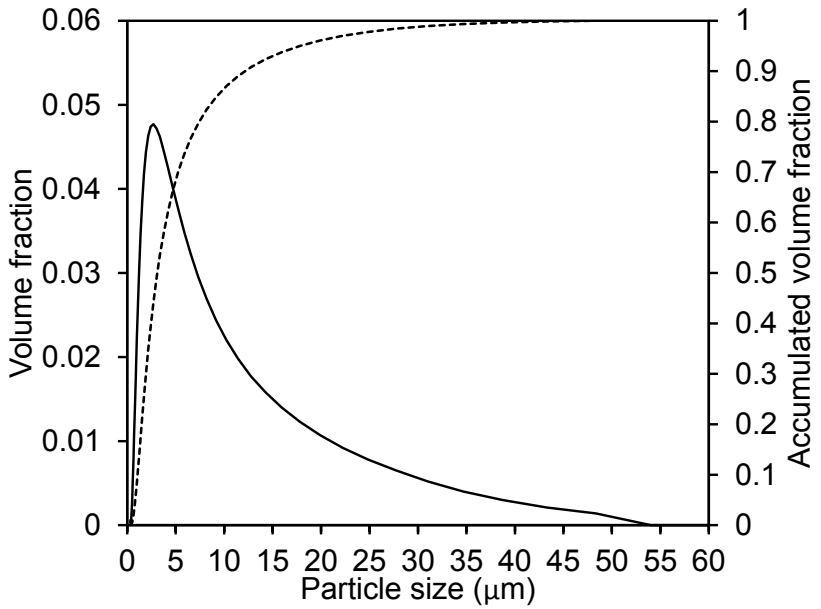

Figure V-1 – Particle size distribution and accumulated volume of NH_4MOR (Si/Al = 10, zeolyst), as received.

A zeolite slurry with 20 wt.% concentration in distilled water was submitted to a wet milling process for 16 h, at a rotational speed of 140 rpm. After 1, 2 and 16 h of milling, measurements of particle size distribution were performed (Figure V-2). Viscosity and pH were also measured (Table V-1).

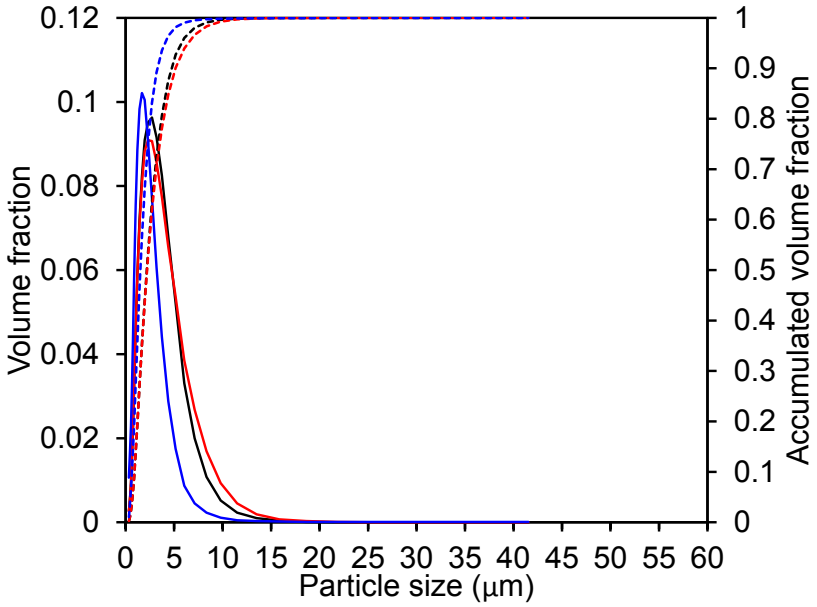

Figure V-2 – Particle size distribution and accumulated volume of NH_4MOR slurries considering different milling times: 1 h (—— ,- - -), 2 h (—— ,- - -) and 16 h (—— ,- - -).

Table V-1 – Average particle diameter ($\overline{d_p}$), respective average deviation (σ), pH and viscosity of NH_4MOR slurries considering different milling times.

Milling time	$\overline{d_p}$ (μm)	σ (μm)	d_{50} (μm)	pH	Viscosity (mPa.s)
1 h	2.8	1.4	2.4	7.44	1.83
2 h	2.9	1.5	2.4	7.83	1.95
16 h	2.0	1.4	1.6	7.83	2.51

The results obtained after 1 and 2 h of milling are very similar, with the averaged particle diameter close to 3 μm (and d_{50} = 2.4 μm). However, after 16h milling, the average particle diameter becomes 2 μm (and d_{50} = 1.6 μm). As expected, viscosity also increases significantly with the increase of milling time to 16 h, which is reasonable since the slurry possesses smaller particles at the end of the process. pH does not vary significantly, and the fact that it is slightly basic can be attributed to an eventual ion-exchange of some NH_4^+ ions compensating Al^- in the zeolite framework.

Since 16 h was the milling time that allowed to obtain the smallest $\overline{d_p}$ (between 2-3 μm – the ideal range to be considered in order to obtain a good quality washcoat [16]) and it is also reported as the time considered for in the preparation of zeolites slurries for other works reported in literature [10], it was decided to consider this time for the preparation of the zeolites slurries in order to obtain the washcoated monoliths presented hereafter.

V.2.2. Concentration of zeolite slurry

The concentration of zeolite slurry will naturally have an influence in the quantity and quality of washcoat deposited in the monoliths. Mitra and Kunzru [16] compared MOR-washcoated catalysts obtained from slurries with 20 and 40% after 4 immersions and observed that with higher concentration, the removal of slurry by blowdown after the immersion resulted in a non-homogeneous coating of the channels. One can also expect that with more concentrated slurries, the number of immersions that will result in the certain mass of washcoat will be smaller.

Commercial catalysts for environmental automotive applications usually consider a mass of catalyst / volume of monolith (m/V) ratio around 150 g/L (this value may depend on the manufacturer but it will be considered as reference for this work). In this work, monoliths used have a cylindrical shape, with 1 in of diameter and 1 in of height, which results in a volume of *ca.* 12.9 cm^3. Assuming the previously mentioned m/V ratio, the mass of catalyst to be deposited would be 1.93 g.

In order to have an idea of how many immersions would be required to achieve the desired mass of washcoat, depending on the zeolite slurry concentration, three slurries with zeolite concentrations of 15, 20 and 30 wt.% were prepared. pH and viscosities of these slurries was registered before the washcoating procedure (Figure V-3).

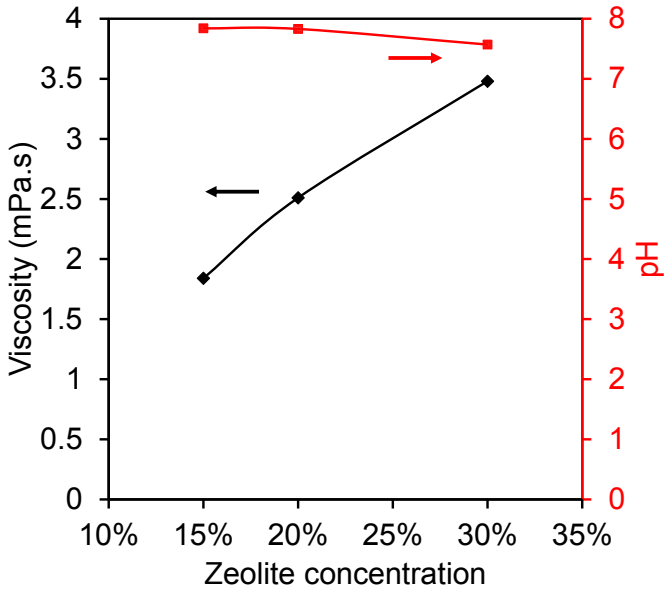

Figure V-3 – Viscosity and pH of NH_4MOR slurries considering zeolite concentrations.

Cordierite honeycomb monoliths (Corning 400 cpsi, $d_{channel}$ = 1.08 mm, t_{wall} = 0.2 mm), containing a cylindrical shape with height and diameter of 1 in, were used as substrates. Fresh monoliths were previously calcined in a muffle (500 ºC, 4 h, 2 ºC/min) in order to clean the monoliths' surface. Then, monoliths' initial masses were registered.

Before starting the washcoating procedure, a mass of colloidal silica (Ludox-HS 40, Sigma-Aldrich) corresponding to 3 wt.% of the total mass of zeolite slurry was added in order to enhance the

mechanical stability and adherence of the washcoat [16]. Then, the procedure started with the immersion of the monolith in the zeolite slurry for 3 min. Afterwards, the monolith was removed from the slurry and the excess slurry was removed by blowing compressed air into the channels. The monolith was then placed in the oven (110 ºC) for 1 h. After this period, the monolith was removed from the oven and 10 min were waited to ensure proper cooling down. The mass of washcoated monolith was then registered. The previously mentioned procedures were repeated until the mass of washcoat was, at least, 1.9 g. Figure V-4 illustrates the total mass loading vs. number of immersions on the different zeolites slurries.

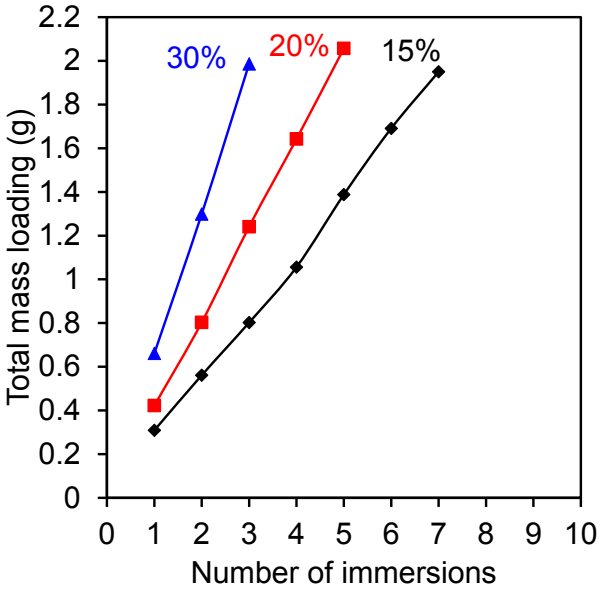

Figure V-4 – Total mass loading *vs.* number of immersions on NH_4MOR slurries considering zeolite concentrations.

It is possible to see that the number of immersions required to obtain 1.9 g of washcoat increases significantly in the dilution of zeolite slurry (3 for 30 %, 5 for 20 % and 7 for 15 %).

An adherence test was also performed on the washcoated monoliths previously mentioned. After the washcoating process, the monoliths were calcined in a muffle (500 ºC, 4 h, 2 ºC/min). The monolith masses were registered before and after calcination procedure and it was verified that no loss of mass occurred due to calcination. The adherence test consisted in submersing the washcoated monoliths in an ultrasonic water bath (37 kHz) for 30 min. Then, the monoliths were dried overnight in the oven (110 ºC). The results showed a loss of mass of 0, 0.3 and 2.3 % for the monoliths obtained from the slurries with 15, 20 and 30 % of zeolite concentration, respectively.

Another important factor to be taken into account in the preparation of the slurry is the mass of catalyst that it will be required. Since all the catalysts were prepared at laboratory scale, the more concentrated the slurry, the higher the number of batches required will be to obtain the powder catalyst. For instance, by considering a total mass of slurry of 45 g (approximately the minimum quantity required to successfully prepare an washcoated monolith - determined empirically), it

would be necessary 6.75, 9 and 13.5 g of catalyst considering 15, 20 and 30% concentration, respectively.

In summary, one can say that by using a slurry with 20% zeolite concentration, a reasonable compromise can be achieved between mass of catalysts required, number of immersions (and, hence, time of preparation) and washcoat adherence. Base on all these factors, it has been decided to consider this concentration for the preparation of the zeolites slurries to obtain the washcoated monoliths presented hereafter.

V.3. Catalytic performance of washcoated monoliths

V.3.1. Catalyst preparation

Cordierite honeycomb monoliths (Corning, 400 cpsi, $d_{channel}$ ≈ 1.09 mm, t_{wall} ≈ 0.2 mm / NGK, 600 cpsi, $d_{channel}$ ≈ 0.96 mm, t_{wall} ≈ 0.1 mm), containing a cylindrical shape with height and diameter of 1 in, were used as substrates.

Four different zeolite slurries of 45 g (20 wt.% of catalyst in distilled water) were prepared by wet ball milling for 16 h, at 140 rpm. Suspensions A and C were prepared by using Pd(0.3)Ce(2)-HMOR catalyst, named as base, and suspensions B and D were prepared by using st500_10 catalyst, obtained after submitting the base catalyst to a steaming treatment at 500 ºC with 10 vol.% H_2O, as described in Chapter IV. pH and viscosity were measured for these slurries (Table V-2), as well as particle size distribution of the catalyst, before and after milling (Figure V-5, Table V-3).

Table V-2 – pH and viscosity of zeolite slurries used to prepared washcoated monoliths.

Slurry	Catalyst	pH	Viscosity (mPa.s)
A	Base	3.31	2.61
B	st500_10	3.77	2.54
C	Base	3.39	2.80
D	st500_10	3.62	2.38

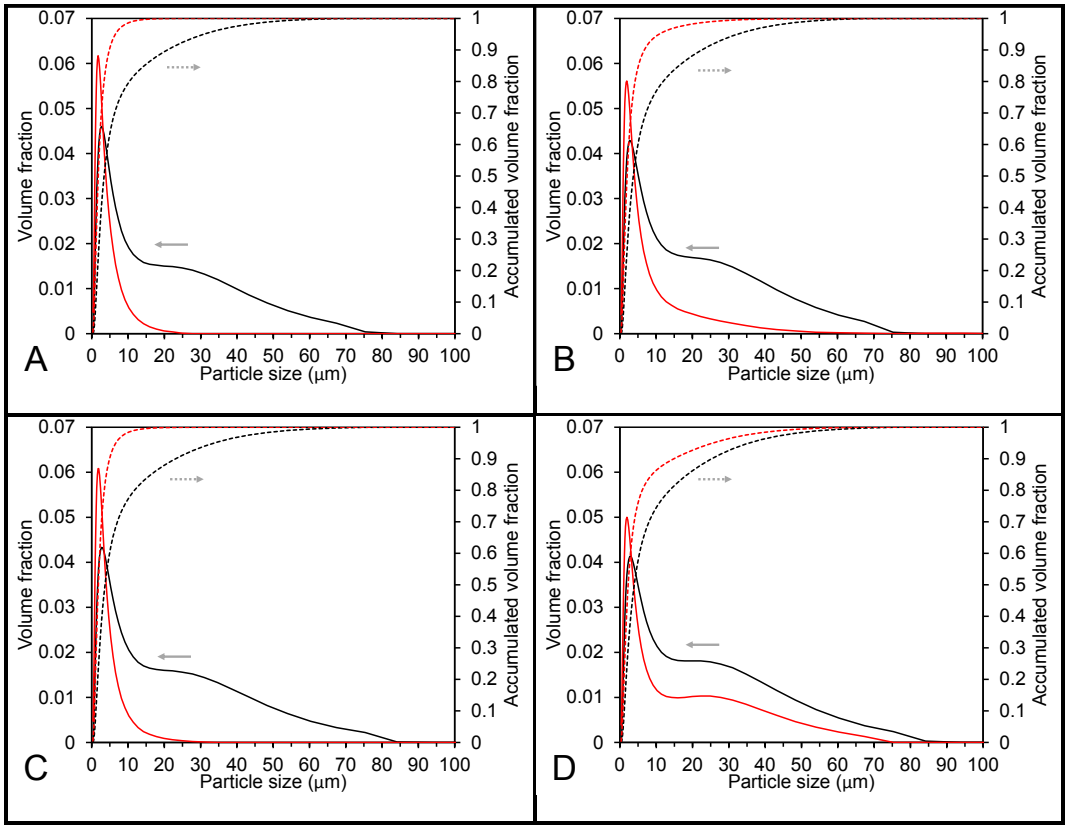

Figure V-5 – Particle size distribution and accumulated volume of zeolite slurries used to prepare zeolite monoliths: powder before milling (black) and after (red).

Table V-3 – Average particle diameter ($\overline{d_p}$) and respective average deviation (σ) of zeolite slurries used to prepared washcoated monoliths.

Slurry	Milling procedure	$\overline{d_p}$ (μm)	σ (μm)	d_{50} (μm)
A	Before milling	8.0	7.3	3.6
	After milling	2.6	1.5	1.9
B	Before milling	8.6	7.8	3.9
	After milling	3.6	2.7	2.1
C	Before milling	8.8	8.1	3.9
	After milling	2.6	1.6	1.9
D	Before milling	9.5	8.8	4.2
	After milling	5.8	5.7	2.4

The crystallinity of the catalysts samples after wet ball milling was assessed by powder X-ray diffraction and compared with the crystallinity of the catalysts before suspension, as described in Chapter II (section II.4.1.5). No loss of crystallinity was observed.

Fresh monoliths were previously calcined in a muffle (500 ºC, 4 h, 2 ºC/min) in order to clean the monoliths surface. Before starting the washcoating procedures, a mass of colloidal silica (Ludox-HS 40, Sigma-Aldrich) corresponding to 3 wt.% of the mass of zeolite slurry. The procedure started with the immersion of the monolith in the zeolite slurry for 3 min. Afterwards, the monolith was removed from the slurry and the excess slurry was removed by blowing compressed air into the channels. The monolith was then placed in the oven (110 ºC) for 1 h. After this period, the monolith was removed from the oven and 10 min were waited to ensure proper cooling down. The mass of washcoated monolith was then registered. The previously mentioned procedures were repeated until the mass of washcoat was *ca.* 1.9 g, which was accomplished after 4 immersions for all monoliths.

Table V-4 summarises the monolith's name, indicating which suspension was used to prepare the respective monoliths, as well as monolith number of cpsi, $m_{catalyst}$ in the washcoat and mass of washcoat per volume of monolith (m/V) ratio.

Table V-4 - pH and viscosity of suspension used to prepared washcoated monoliths.

Monolith name	Suspension	cpsi	$m_{catalyst}$ (g)	m/V (g/L)
base-400	A	400	1.977	154
base-400, aged	A	400	2.072	161
st500_10-400	B	400	1.877	146
base-600	C	600	1.835	143
base, aged-600	C	600	1.973	153
st500_10-600	D	600	1.841	143

V.3.2. Effect of number of cpsi

The influence of the number of cells per square inch (cpsi) in the catalytic performance is assessed herein by comparing the monoliths base-400 and base-600.

V.3.2.1. Scanning electron microscopy (SEM/EDS)

Figure V-6 illustrates SEM images of both base-400 (A, C, E) and base-600 (B, D, F) monoliths along the channels (parallel cut to the channels).

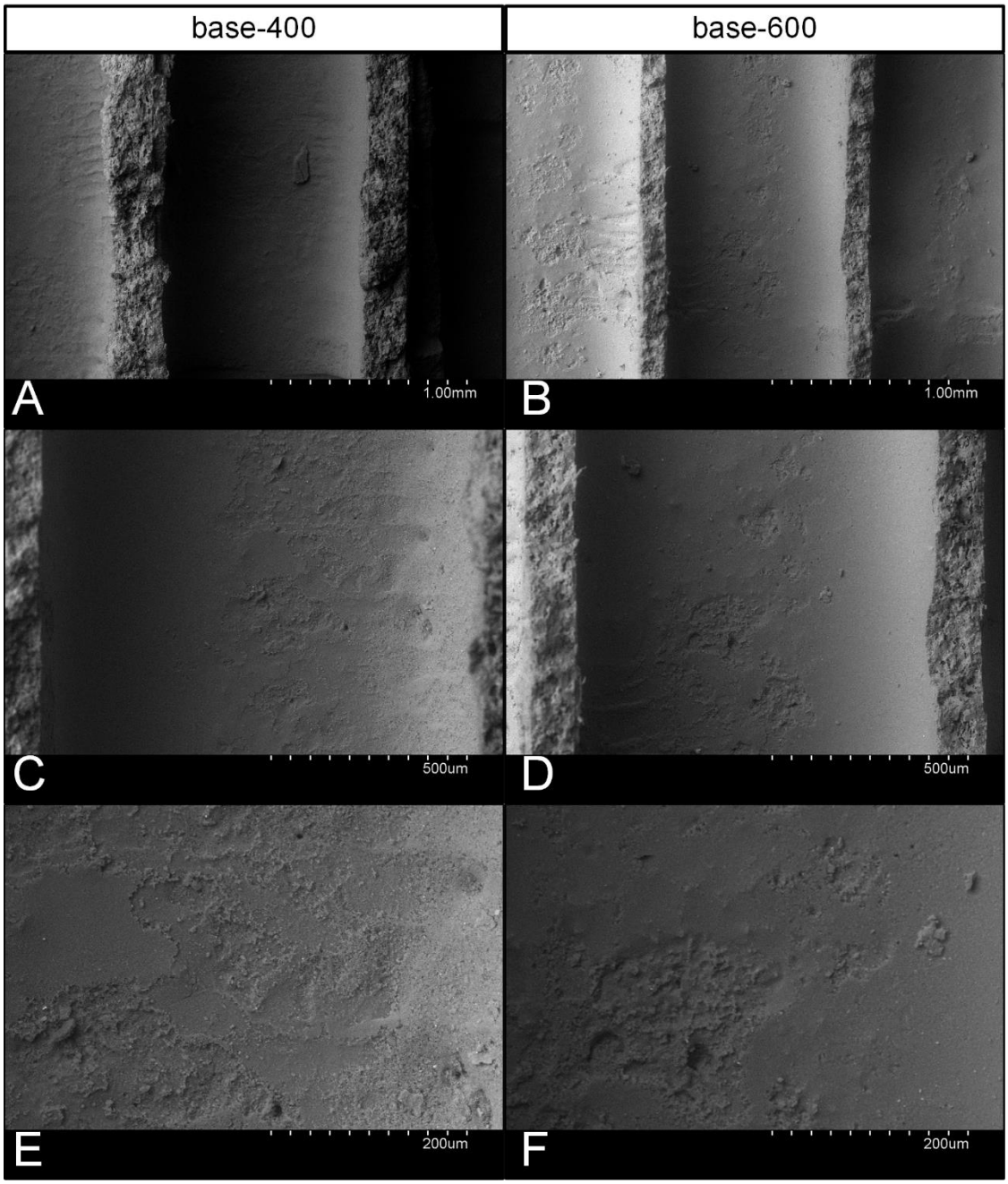

Figure V-6 – SEM images of washcoated monoliths along the channels: base-400 (A, C, E) and base-600 (B, D, F).

From the comparison of the SEM images from base-400 and base-600, one can retain the idea that the washcoat is more homogeneous in the first case, whereas in for base-600 it is possible to observe more textural irregularities.

Energy dispersive X-ray spectroscopy (EDS) analyses were performed to a section of monoliths represented in Figure V-6E and F, in order to obtain the mapping of elements distribution (Mg, Al, Si, Pd and Ce) of both base-400 and base-600 monoliths, respectively. Mg is only present in cordierite whereas Pd and Ce should only be present in washcoat of catalyst. EDS mapping images obtained for base-400 and base-600 monoliths are presented in Figure V-7 and Figure V-8, respectively.

For base-400 monolith (Figure V-7), it is possible to observe that Pd and Ce are well distributed along the image, which seems to indicate that the washcoat is present in practically the entire area of the image recovered. Regarding the Mg mapping image, it is possible to observe that Mg is also well distributed along the image. The fact that this element, belonging to the cordierite, is detected by EDS analysis can be explained due to some penetration of X-ray radiation through the washcoat. It should also be highlighted that, in some regions (namely near the left-downwards corner of Mg mapping image), Mg appear to be more concentrated, which can be an indication of a segment of less thick washcoat, which would allow more radiation to reach cordierite.

For base-600 monolith (Figure V-8), similar conclusions to the ones presented for base-400 monolith can be withdrawn. Notwithstanding, it is worthy to highlight that on Mg mapping image, a more concentrated zone can be observed. This zone is overlapped with what seems to be a crate in the SEM image, which clearly suggests that the washcoat in this region is likely to be thinner.

A qualitative comparison of the images obtain for both monolith, seems to suggest than base-600 monolith contains more irregularities in the washcoat, which may be related to the fact of being thinner for this catalyst.

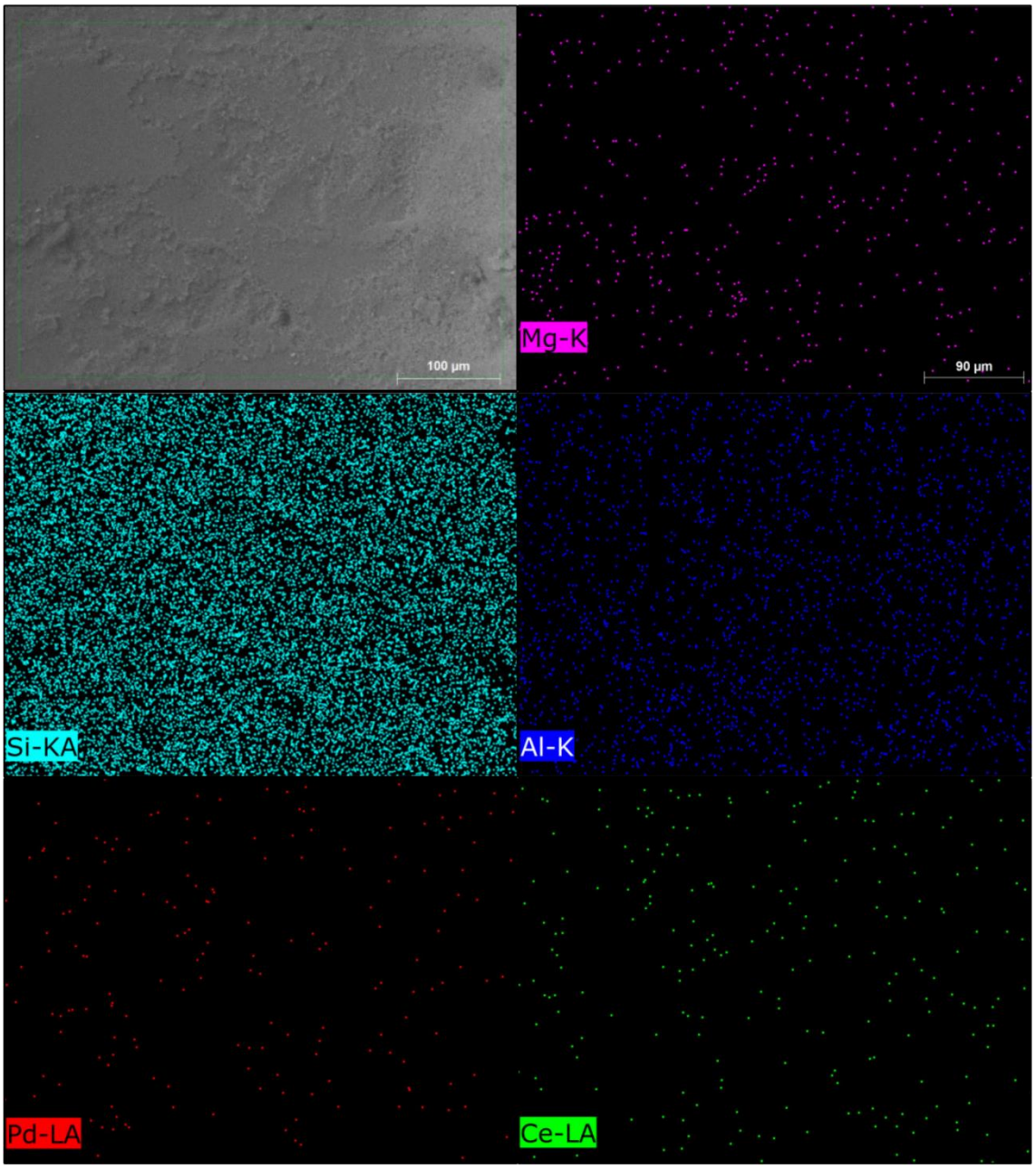

Figure V-7 – EDS mapping from a segment of catalytic layer (Figure V-6E) from washcoated monolith base-400.

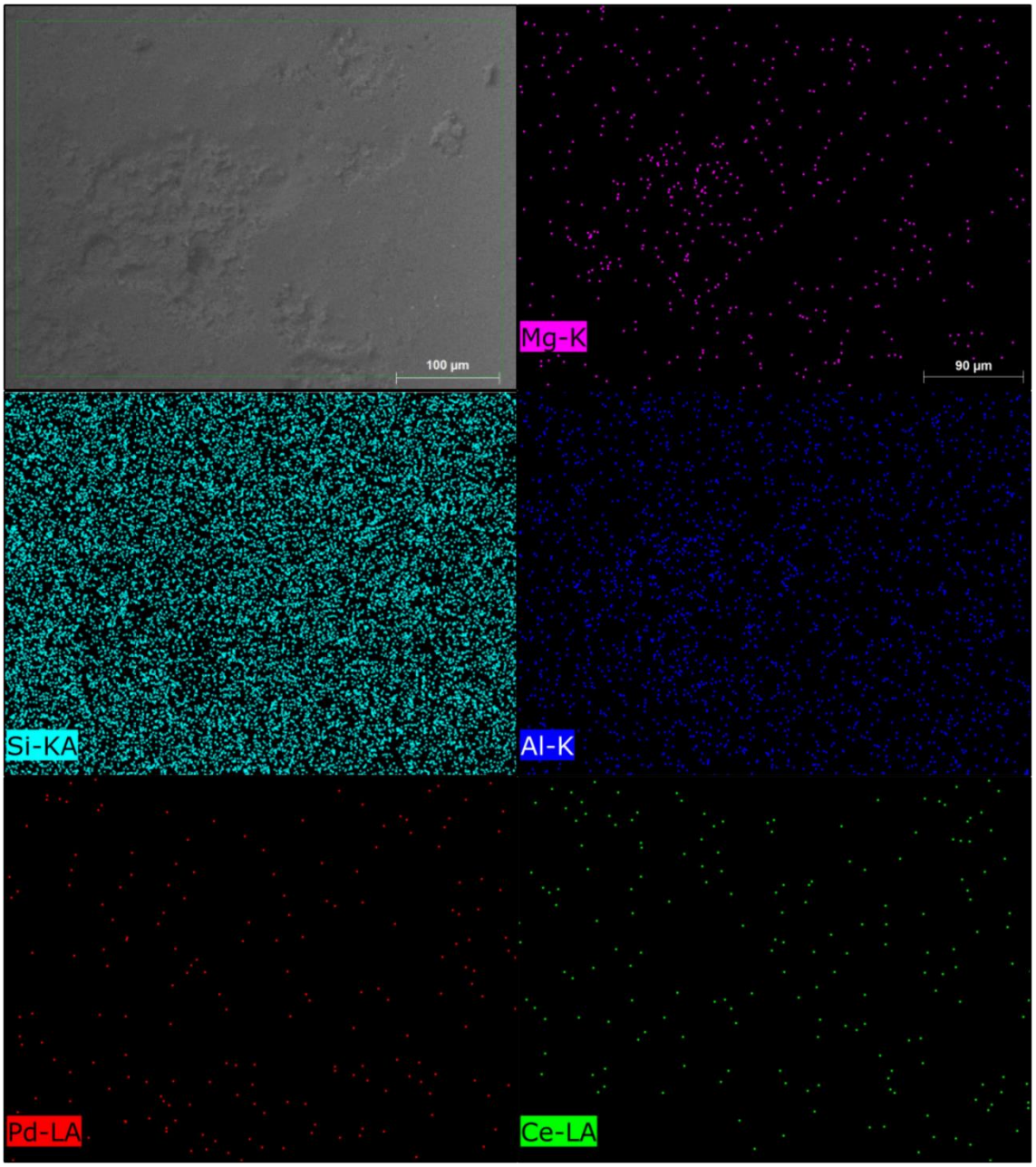

Figure V-8 – EDS mapping from a segment of catalytic layer (Figure V-6D) from washcoated monolith base-600.

Figure V-9 illustrates SEM images of base-400 monolith obtained by performing a transversal cut to the channels.

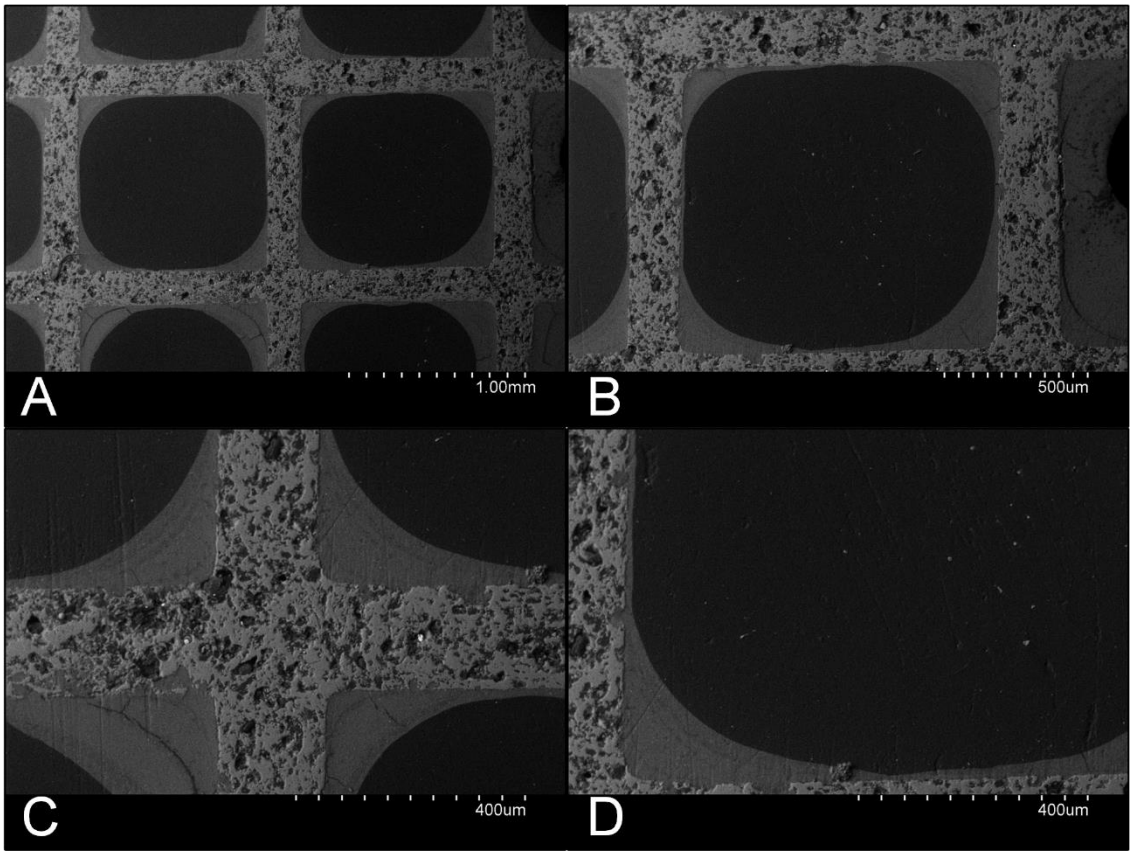

Figure V-9 – SEM images of washcoated monolith base-400: transversal plane.

From SEM analyses, it is possible to observe that washcoat is present in all the channels. Though some of the channels exhibit a washcoat that seems to be homogeneous, it is also possible to observe that some channels exhibit irregularities in the washcoat (Figure V-9A), with some parts resembling fissures (Figure V-9C, left-downwards corner). It is likely that such irregularities may be related to a non-homogenous blowdown of the channels that led to higher accumulation of washcoat in some of the channels. An estimation of the maximum and minimum thickness of the washcoat was obtained considering image Figure V-9D (consisting in a zoom of Figure V-9B), which are, respectively, 152 (at the corner of the monolith) and 13 μm (at the centre).

SEM images of base-600 monolith, obtained by performing a transversal cut to the channels, are presented in Figure V-10. Again for this monolith, it is possible to verify that all channels possess washcoat. Though no irregularities similar to the ones observed for base-400 are seen in the SEM images of base-600, it is possible to observe that some channels clearly exhibit different washcoat thicknesses in the corners, suggesting a non-homogeneous washcoat. Moreover, it is also observable that the washcoat thickness is, in general, lower than the one observed for base-400. An estimation of the maximum and minimum thickness of the washcoat was obtained for base-600

considering image Figure V-10D, which are, respectively, 66 (at the corner of the monolith) and 12 μm (at the centre).

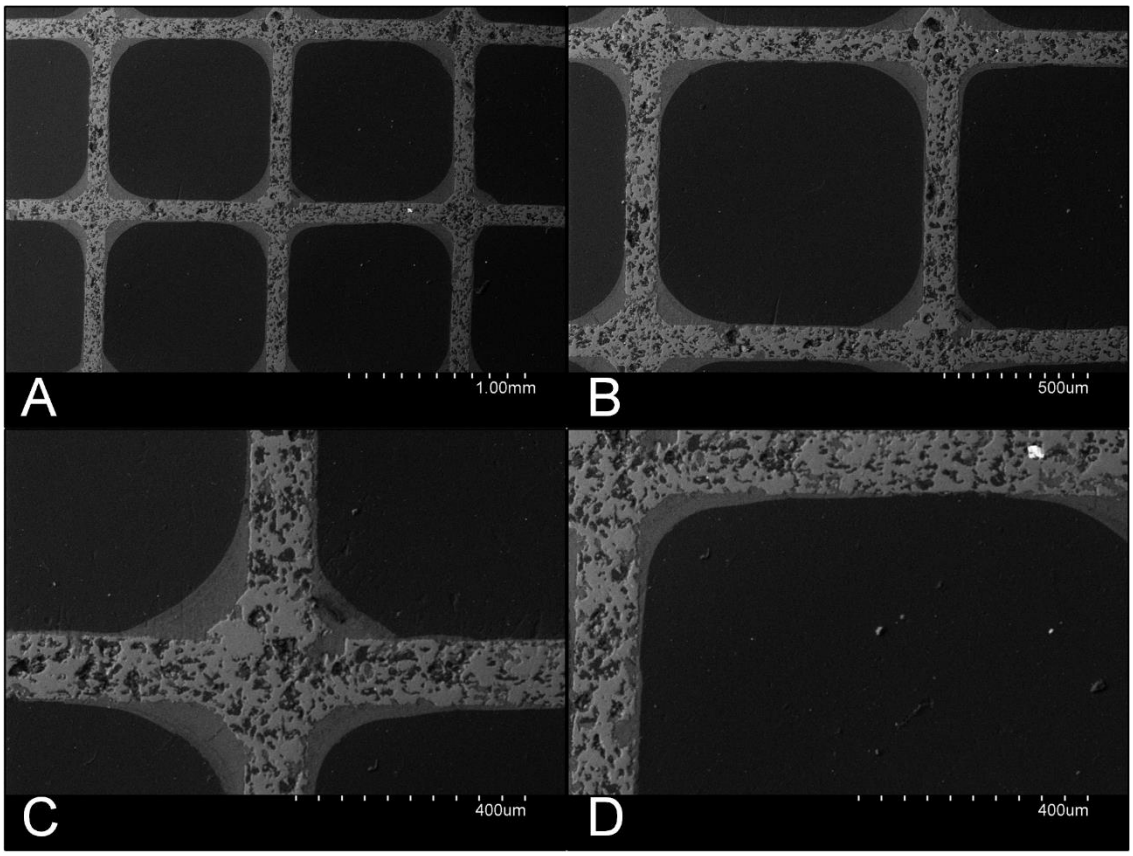

Figure V-10 – SEM images of washcoated monolith base-600: transversal plane.

V.3.2.2. NO_x CH_4-SCR

Monoliths were tested in a synthetic gas bench (temperature-programmed tests, from room temperature to *ca.* 550 ºC), considering an inlet gas feed mixture representative of real exhaust gases of a heavy duty vehicle's engine (Volvo engine MG9 in lean-gas burn conditions) – Further details on the experimental setup are presented in Annex B (section C.3.3). The results are presented in Figure II-21, in the absence of water in the inlet gas feed.

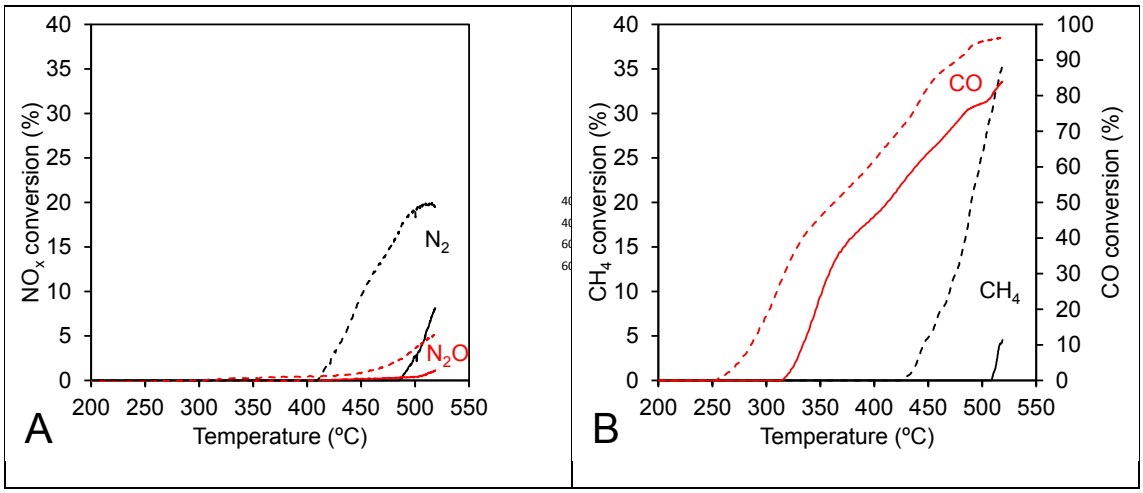

Figure V-11 – NO_x conversion (A) and CH_4 and CO conversion (B) of washcoated monoliths: base-400 (full lines) and base-600 (dashed lines). Conditions: 400 ppm NO, 1600 ppm CH_4, 800 ppm CO, 7% O_2 and GHSV of 40000 h^{-1}.

Results show that, not only the NO_x, CH_4 and CO conversions are always higher for base-600 than base-400, but also that the conversion starts at lower temperatures when considering 600 cpsi. Since both monoliths exhibit different geometries, one cannot exclude that eventual differences in the hydrodynamic flow inside the channels could explain the results observed.

In order to address this issue, two simulations corresponding to a single channel of the monoliths were performed, considering the methodology followed by Ozhan [17], using Gerris Flow solver, a free software program for the solution of the partial deferential equations. Further details on the methodology can be found in Annex H.

The simulations were performed assuming the gases temperature of 520 ºC (approximately the maximum conversion temperature observed), for a channel 1 in (25.4 cm) long. Gas feed properties considered in the simulation are presented in Table V-5 and geometrical of each monolith considered for the simulations is presented in Table V-6.

Table V-5 – Gas feed properties input data considered for the simulation of hydrodynamic flow in base-400 and base-600 monoliths.

T (ºC)	520
Density (kg/m^3)	0.435
Diffusivity NO (m^2/s)	1.243 x 10^{-4}
Diffusivity CH_4 (m^2/s)	1.265 x 10^{-4}
Viscosity (N.s/m^2)	3.599 x 10^{-5}
[NO] (ppm)	400
[CH_4] (ppm)	1600

Table V-6 – Geometrical input data considered for the simulation of hydrodynamic flow in base-400 and base-600 monoliths.

Monolith	$d_{channel}$ (mm)	$v_{channel}$ * (m/s)
base-400	1.09	1.30
base-600	0.96	1.12

* Calculated assuming a flow of 22.83 L/min, corresponding to the volumetric flow of 8.58 L/min of with 400 ppm NO, 1600 ppm CH_4, 800 ppm CO, 7% O_2, N_2 balance, at 25 ºC, which corresponds to the feed mixture in the catalytic test.

Simulation results concerning NO profiles over the channel of both base-400 and base-600 catalysts are exhibited illustrated Figure V-12 and Figure V-13, respectively. For each case, profiles corresponding to three different times (2, 4 and 10 s) are presented. At the later time, the system is already in steady-state. For brevity, only the first 10 mm of the channel are exhibited, since in the rest of the channel the concentration is always zero.

It is important to clarify that the implemented model does not consider the reaction that takes place in the catalyst, since it is assumed that once the reactants touch the wall their concentration becomes zero (i.e. 100 % of conversion). Nevertheless, the purpose of these analysis is only to compare the hydrodynamic flow in the system in both monoliths.

By comparing Figure V-12 and Figure V-13, it is possible to observe that, in both cases, the system converges rapidly to the steady-state and no significant changes are observed between the different times. Moreover, by comparing the simulations obtained after 10 s, it is possible to see that, though some differences are observed in the very beginning of the channels (up to *ca.* 2 mm), the majority of the channel presents a concentration that is zero (dark blue colour) for both configurations.

Figure V-12 – Simulation results for NO concentration profile over the first 10 mm of a single channel of base-400 monolith.

Figure V-13 – Simulation results for NO concentration profile over the first 10 mm of a single channel of base-600 monolith.

NO and CH_4 conversions along the channel (axial distance) are presented in Figure V-14 for base-400 and base-600.

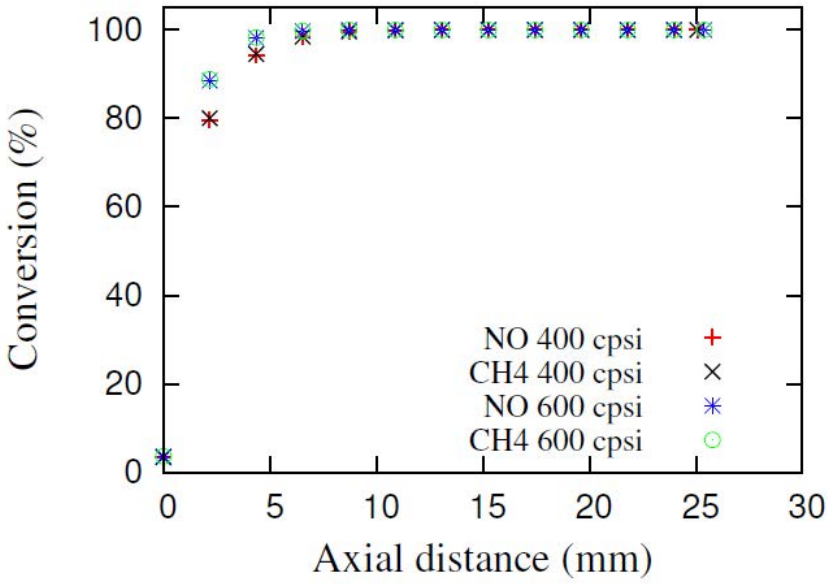

Figure V-14 – NO and CH_4 conversions along the channels of 400 and 600 monoliths, according to the model developed by Ozhan.

Results show that in the first 2 mm of the channel, the conversions are higher for 600 cpsi, *i.e.* a higher percentage (conversion) of the reactants reached the wall of the catalyst. However, after 7 mm, all the reactants have reached the walls and all the profiles become the same. It is then clear that if, at the beginning, some slight differences could be observed due to the hydrodynamic flow in the system, these differences are mitigated and become irrelevant at the end of the channel.

For this reason, one can say that the difference in the hydrodynamic profile due to the different geometries cannot explain, *per se*, the differences in the catalytic performance. In fact, the most reasonable explanation lays on the surface of catalysts that contacts the feed gas. An estimation of the washcoat total surface area for base-400 and base-600 monoliths is presented in Table V-7

Table V-7 – Washcoat surface area estimation for base-400 and base-600 monoliths

Monolith	$d_{channel}$ (mm)	n_{cells} [1]	$t_{washcoat}$ [2] (μm)	$A_{surface,\ total}$ [3] (m^2)
base-400	1.09	314	13	0.0267
base-600	0.96	471	12	0.0352

[1] Considering cylindrical monolith, $D_{monolith}$ = 1 in.

[2] Corresponding to the minimum washcoat thicknesses obtained by SEM.

[3] Considering circular section of each channel with effective diameter = $d_{channel} - 2 \times t_{washcoat}$

According to the estimation performed, the washcoat surface area of base-600 is 32% higher than base-400. It should be mentioned that the previously presented estimations were made considering

that the monolith channels are cylindrical. However, though this approximation may be roughly made for base-400 (see Figure V-9), in the case of base-600 monolith it is clear that the transversal geometry of the channel is somewhere between a square and a circle (see Figure V-10), which means that the actual washcoat surface area is likely to be even higher than the one obtained in estimation performed.

An interesting way of confirm this hypothesis would be to prepare a catalysts with lower or higher number of cpsi (*e.g.* 200 or 900) and verify if some proportionality (for instance linear) would exist between total washcoat surface area and NO_x, CO or CH_4 conversions. Notwithstanding, it is important to highlight that below 400 cpsi, the expected conversions values would be significantly low (namely, below 7 % for NO_x conversion and 5 % for CH_4 conversion – values observed for base-400), which could jeopardise the interpretation of results. Moreover, for commercial automotive applications (*e.g.* heavy duty vehicles) monoliths above 600 cpsi are not considered due to high pressure drops.

Figure V-15 illustrates the catalytic performance of both base-400 and base-600 monoliths tested in the same conditions previously mentioned, but considered 2 vol.% of water in the inlet gas feed.

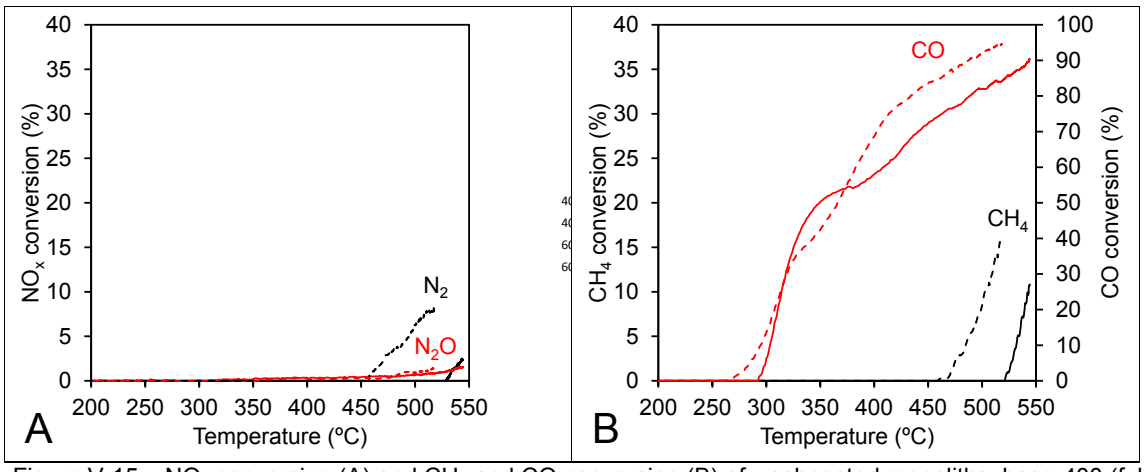

Figure V-15 – NO_x conversion (A) and CH_4 and CO conversion (B) of washcoated monoliths: base-400 (full lines) and base-600 (dashed lines). Conditions: 400 ppm NO, 1600 ppm CH_4, 800 ppm CO, 7% O_2, 2% H_2O and GHSV of 40000 h^{-1}.

Results show that, as expected and already observed in the tests performed with powder formulations, the catalytic performance is drastically affected by the presence of water in the inlet feed. For instance, for base-600, NO_x conversion into N_2 decreases from ca. 20% to 8%. The temperature at which the monoliths start to exhibit some activity for NO_x and CH_4 conversion also decreases. It is worthy to mention that, for CO conversion, the difference in temperatures at which conversions starts is lower and also, in both situations, CO conversion is practically complete above 520 ºC. This is in agreement with the tests performed in the powder formulation.

Finally, it is important to highlight that NO and CH_4 conversion values obtained in the tests with monoliths are considerably lower than the ones obtained with the powder formulations presented in Chapter II (section II.4.1.9). For instance, at 500 ºC, in the absence of water in the inlet gas feed, NO_x conversion into N_2 was 19% against 70%. However, it is important to have present that the geometry of both systems is completely different.

In the powder tests, GHSV is calculated using equation (V-1):

$$\mathrm{GHSV} = \frac{F}{V_{catal}} \tag{V-1}$$

F is the total flow and V_{catal} is the volume of catalytic bed. In this geometry, the gas flow crosses the catalytic bed. However, in the monolith tests, GHSV is calculated according to equation (V-2):

$$\mathrm{GHSV} = \frac{F}{V_{monolith}} \tag{V-2}$$

$V_{monolith}$ is the volume of the monolith, which is a cylinder with diameter and height equal to 1 in – this procedure is the one adopted by industrial catalysts manufacturers and automobile constructors. No matter the washcoat loading (*m*/*V*) considered, if the same flow and monolith dimensions are considered, GHSV remains constant. Moreover, in this geometry, instead of crossing the catalyst, the gas sweeps its surface along the channel without crossing it. It becomes, then, careful must be taken when performing comparisons between the different formulations (powder *vs.* monolith), since they do not have the same physical meaning.

Notwithstanding, it is interesting to see was is the $F/m_{catalyst}$ ratio for both tests. For the powder tests, the total flow was 15 L/h for 0.188 g of catalyst, which results in *ca.* 80 L/(h.g). For the monolith tests, the total flow was 8.58 L/min for 1.93 g of catalysts (mass of washcoat), which results in *ca.* 267 L/(h.g). These numbers shows that, now only the geometry is different, but also that total flow per mass of catalyst in the system is much higher when considering monoliths, which could also contributes to the differences in the conversion values observed.

V.3.3. Effect of steaming treatment

In Chapter IV, it was shown that, by performing a steaming treatment on Pd(0.3)Ce(2)-HMOR at 500 ºC with 10 vol.% H_2O, an enhanced catalytic performance for NO_x CH_4-SCR could be achieved. In this section it is investigated if when considering monolith catalysts, the same behaviour is observed.

To this end, two monoliths were prepared with st500_10 catalyst, using cordierite monoliths with 400 and 600 cpsi, according to the catalyst preparation presented before (section V.3.1), and named as st500_10-400 and st500_10-600, respectively. Moreover, two other monoliths were considered in this study, consisting in base-400 and base-600 monoliths that were submitted to a steaming treatment similar to the one performed to Pd(0.3)Ce(2)-HMOR to obtain st500_10: these catalysts were named as base, aged-400 and based, aged-600, respectively.

Figure IV-10 summarises the preparation of the monoliths considered in this study.

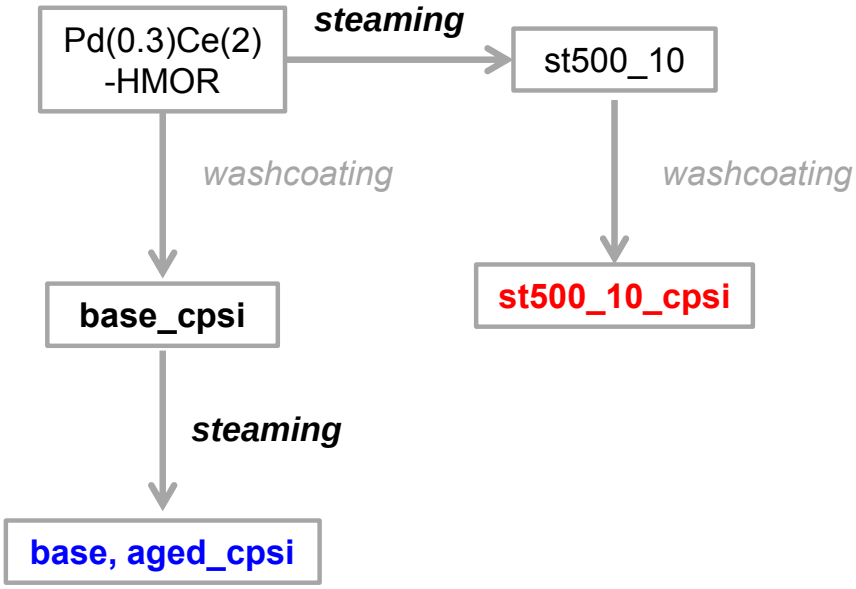

Figure V-16 – Schematic representation of steamed monoliths preparation.

V.3.3.1. Scanning electron microscopy (SEM/EDS)

SEM images of both st500_10-400 and base, aged-400 monoliths are illustrated in Figure V-17 (parallel cut to the channels).

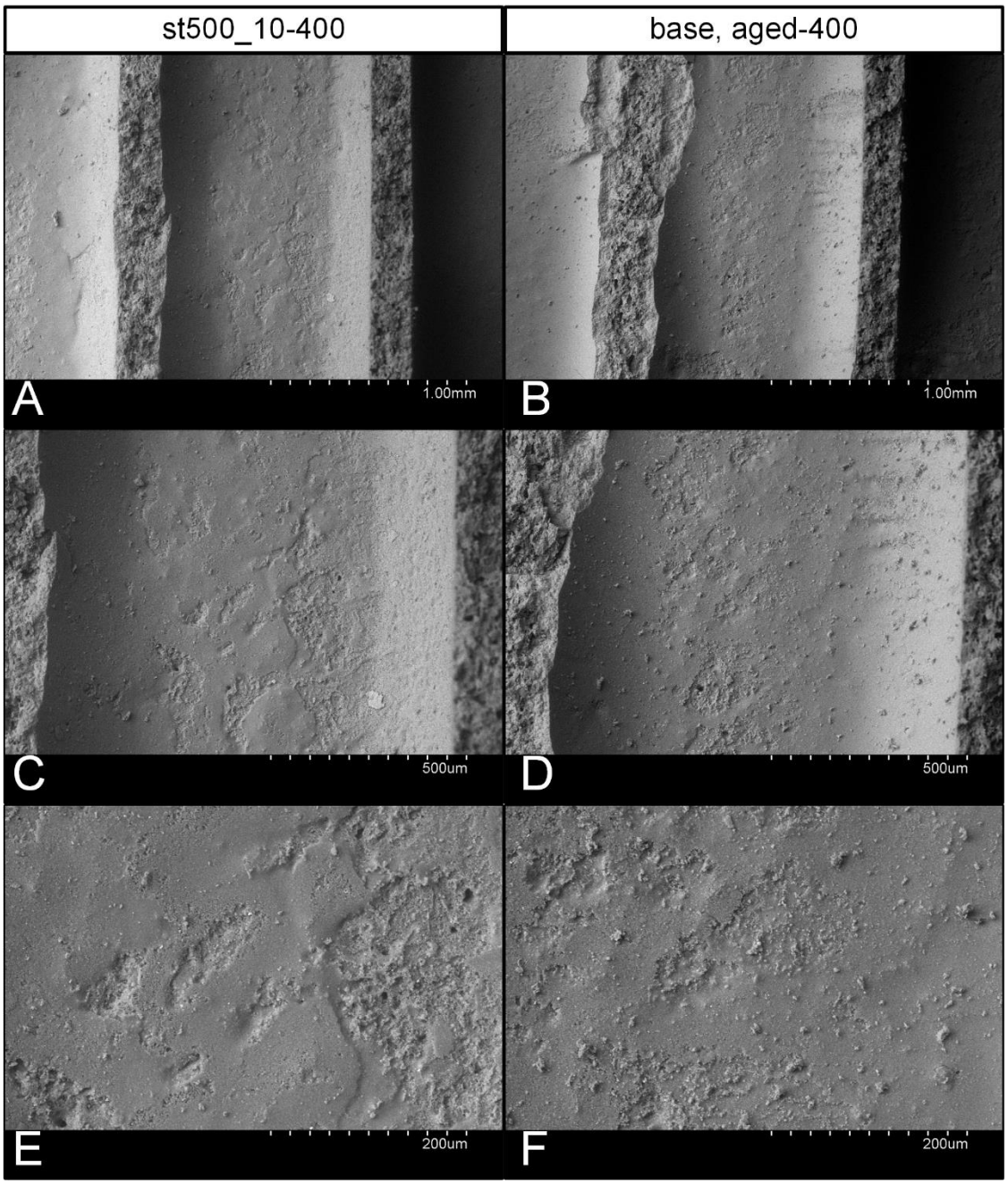

Figure V-17 – SEM images of washcoated monoliths along the channels: st500_10-400 (A, C, E) and base, aged-400 (B, D, F).

When comparing these images to the ones obtained for base-400 monolith (Figure V-9), it resembles that these monoliths exhibit more textural irregularities. Energy-dispersive X-ray (EDS) analyses were also performed to sections of monoliths in Figure V-17E and F (see Annex F, section G.1). The mapping of elements distribution (Mg, Pd and Ce) allows to conclude that, as well as in

base-400 monolith, washcoat is present in practically the entire area of the image recovered for both st500_10-400 and base,aged-400 monoliths.

Figure V-18 exhibits the SEM images of st500_10-400 monolith obtained by performing a transversal cut to the channels. No significant irregularities are observed in the channels of this monolith. Moreover, similar to what has been observed for base-400, all channels exhibit washcoat.

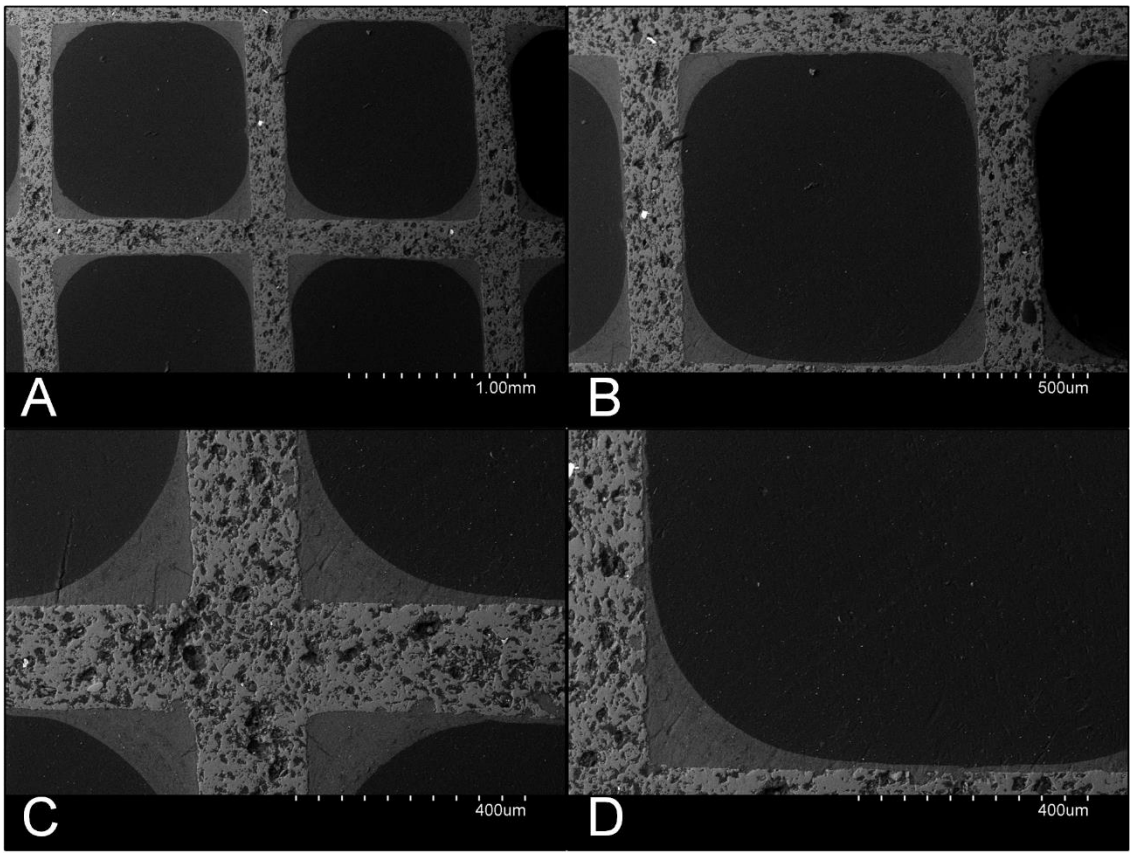

Figure V-18 – SEM images of washcoated monolith st500_10-400: transversal plane.

SEM images of base, aged-400 monolith are shown in Figure V-19 and similar conclusions can be drawn for this monolith. Notwithstanding, it should be mentioned that some irregularities can be observed is some of washcoat segments (see for instance left-upward and right-downward corner of Figure V-19B). Such irregularities may have been caused by the steaming treatment performed on the monolith.

Based on Figure V-18D and Figure V-19D, both maximum and minimum thickness of washcoat were estimated. The results are presented in Table V-8.

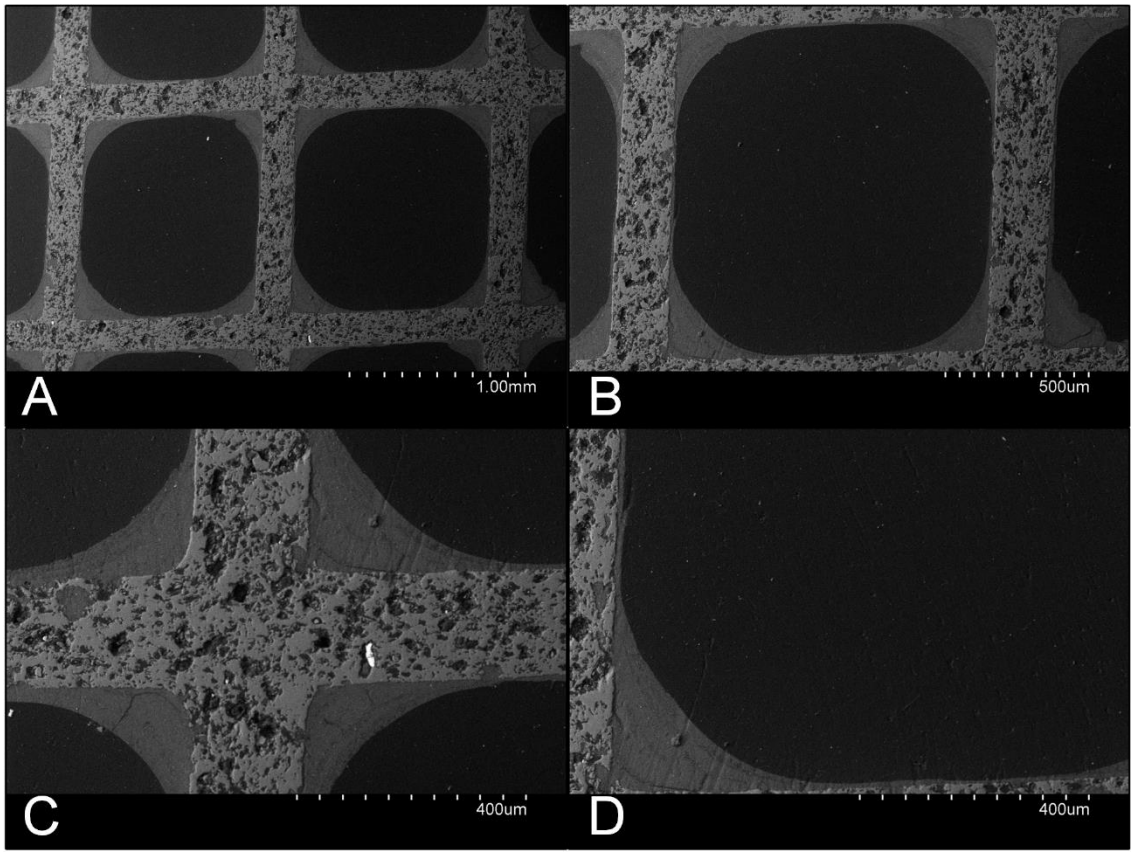

Figure V-19 – SEM images of washcoated monolith base,aged-400: transversal plane.

Table V-8 – Washcoat thicknesses estimation for st500_10-400 and base, aged-400 monoliths.

Monolith	$t_{washcoat,\ min.}$ (μm)	$t_{washcoat,\ max.}$ (μm)
st500_10-400	15	123
base, aged-400	8	180

Figure V-20 illustrates the SEM images of both st500_10-600 and base, aged-600 monoliths (parallel cut to the channels). No significant differences are observed between SEM images of these monoliths and base-600. Moreover, same conclusions already taken regarding EDS analysis and respective Pd, Ce and Mg mapping for base-600 are also valid for this catalyst (see Annex F, section G.2).

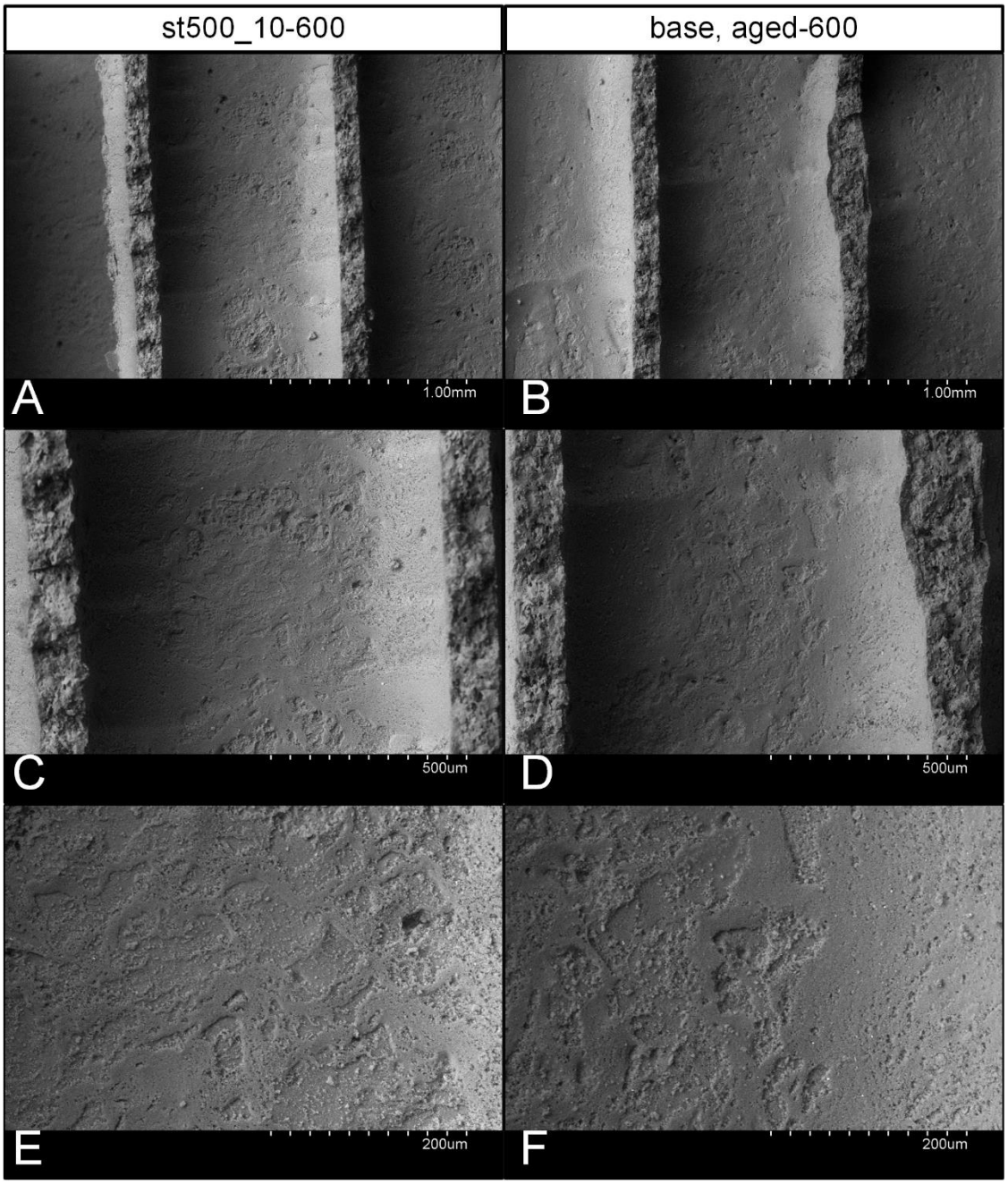

Figure V-20 – SEM images of washcoated monoliths along the channels: st500_10-600 (A, C, E) and base, aged-600 (B, D, F).

SEM images of st500_10-600 monolith, obtained by performing a transversal cut to the channels, are presented in Figure V-21.

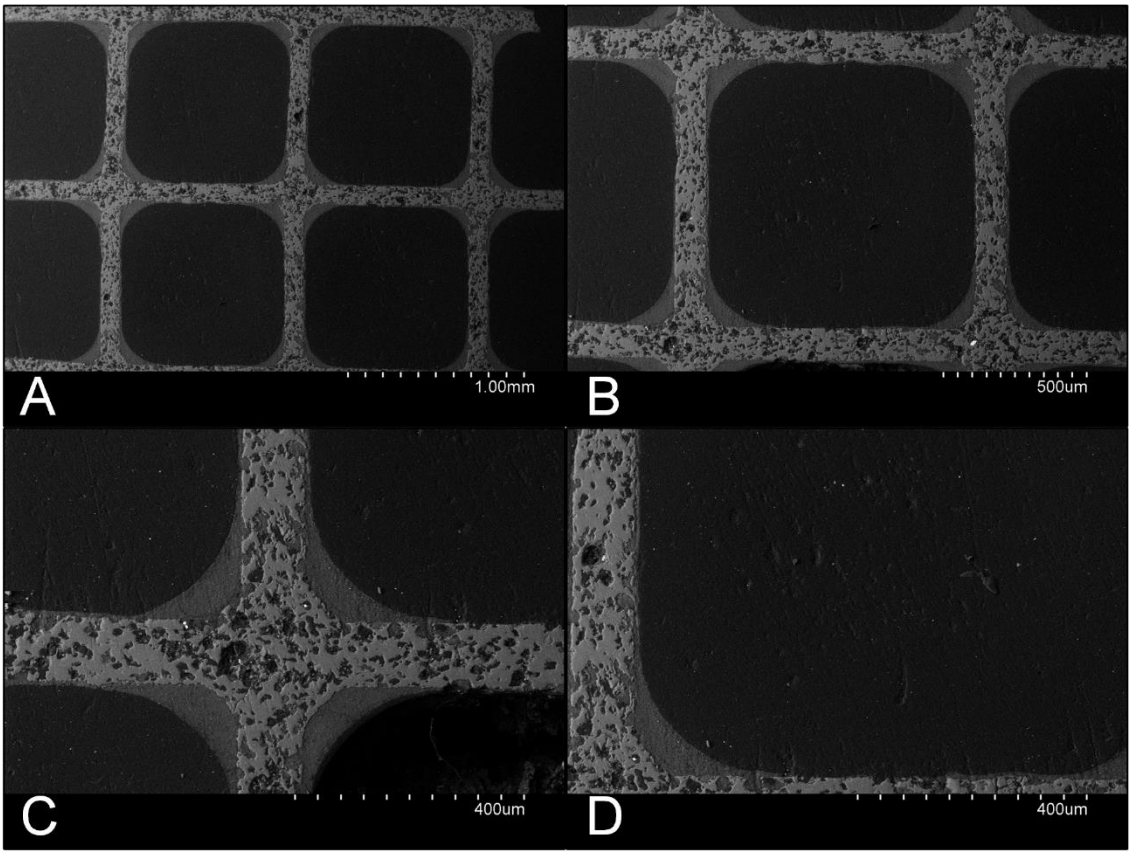

Figure V-21 – SEM images of washcoated monolith st500_10-600: transversal plane.

Once again, all channels observed in the images possess washcoat in the walls. Similarly to what has been observed when comparing base-400 and base-600 monoliths, wall thickness of the washcoat for st500_10-600 is generally smaller than the one of st500_10-400.

Figure V-22 illustrates the SEM images of base, aged-600 monolith, obtained by performing a transversal cut to the channels. Some significant differences are observed when comparing these images with the ones obtained for base-600 and st500_10-600. It is clear that some of the channels possess a washcoat thickness much larger than the one observed for the previous mentioned catalysts. Considering that the same zeolite slurry was used to prepare base-600 and base, aged-600, a reasonable explanation for this may be a deficient blowdown of the slurry excess after immersions during washcoating procedure in the case of base, aged-600. It is also worthy to mention that, similarly to what has been observed for base, aged-400, the monolith also presents irregularities and fissures in the washcoat, which reinforces the idea that steaming treatment damages the washcoats.

Both maximum and minimum washcoat thicknesses were also estimated for st500_10-600 and base, aged-600 monoliths, based on Figure V-21C and Figure V-22D (Table V-9).

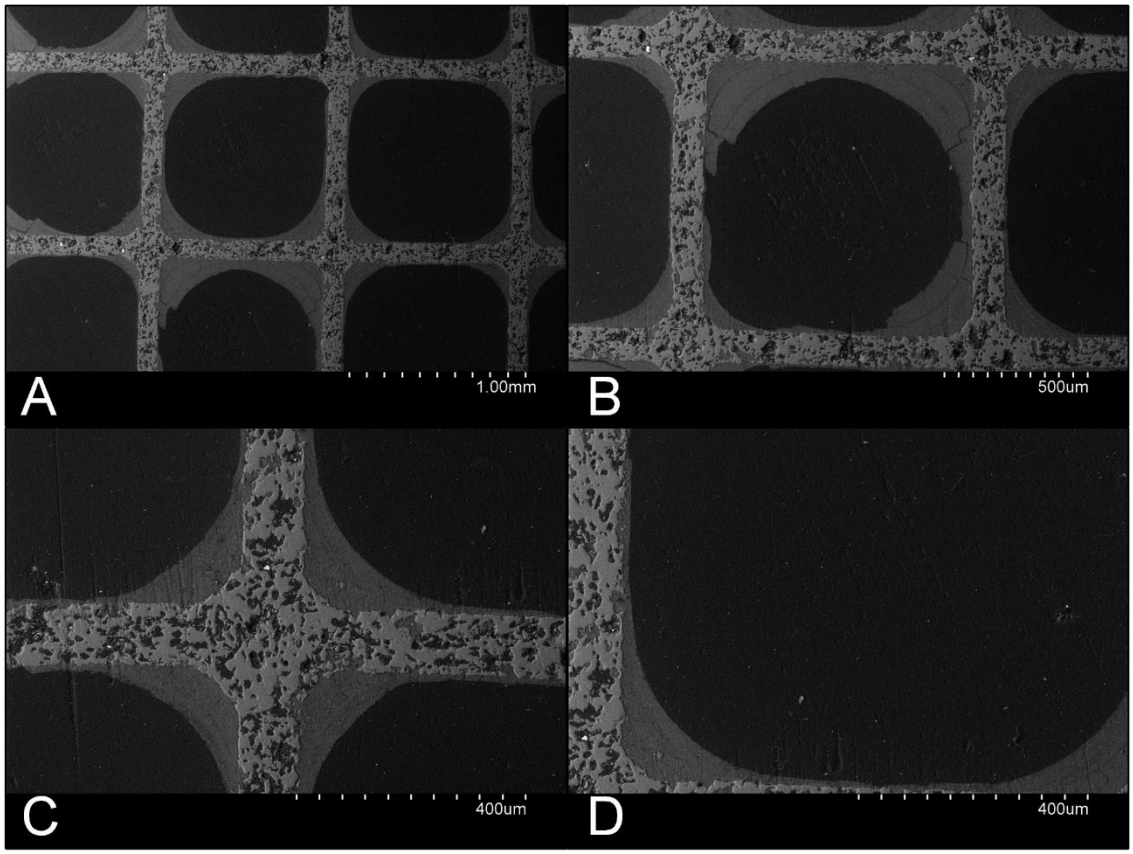

Figure V-22 – SEM images of washcoated monolith base,aged-600: transversal plane.

Table V-9 – Washcoat thicknesses estimation for st500_10-600 and base, aged-600 monoliths.

Monolith	$t_{washcoat,\ min.}$ (μm)	$t_{washcoat,\ max.}$ (μm)
st500_10-600	9	61
base, aged-600	13	100

V.3.3.2. NO_x CH_4-SCR

All monoliths were tested in the same conditions previously described in section V.3.2.2, considering an inlet gas feed mixture representative of real exhaust gases of a heavy duty vehicle's engine (Volvo engine MG9 in lean-gas burn conditions). The results obtained for the tests with base-400, st500_10-400 and base, aged-400, in the absence and presence of water in the inlet gas feed, are compared in Figure V-23 and Figure V-24, respectively.

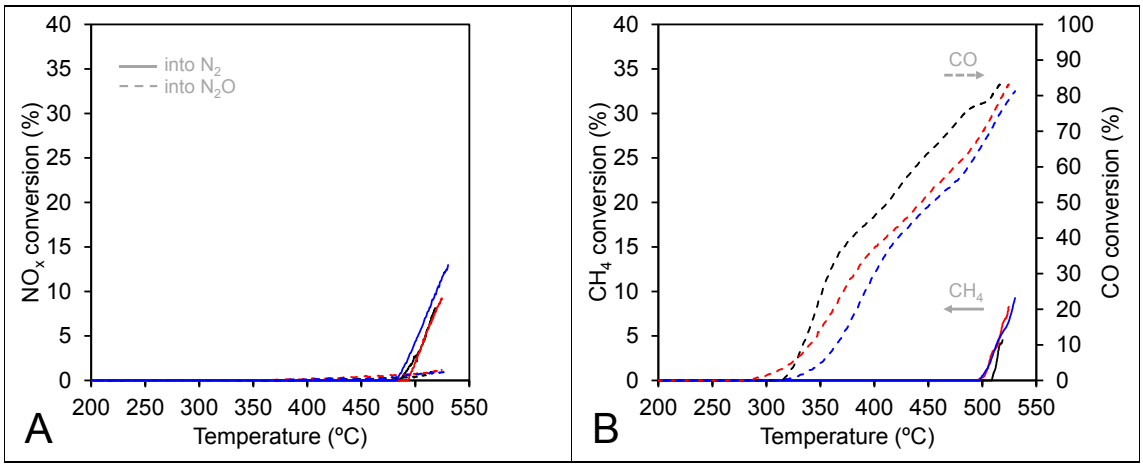

Figure V-23 – NO_x conversion (A) and CH_4 and CO conversion (B) of washcoated monoliths with 400 CPSI: base (black), st500_10 (red) and base, aged (blue). Conditions: 400 ppm NO, 1600 ppm CH_4, 800 ppm CO, 7% O_2 and GHSV of 40000 h^{-1}.

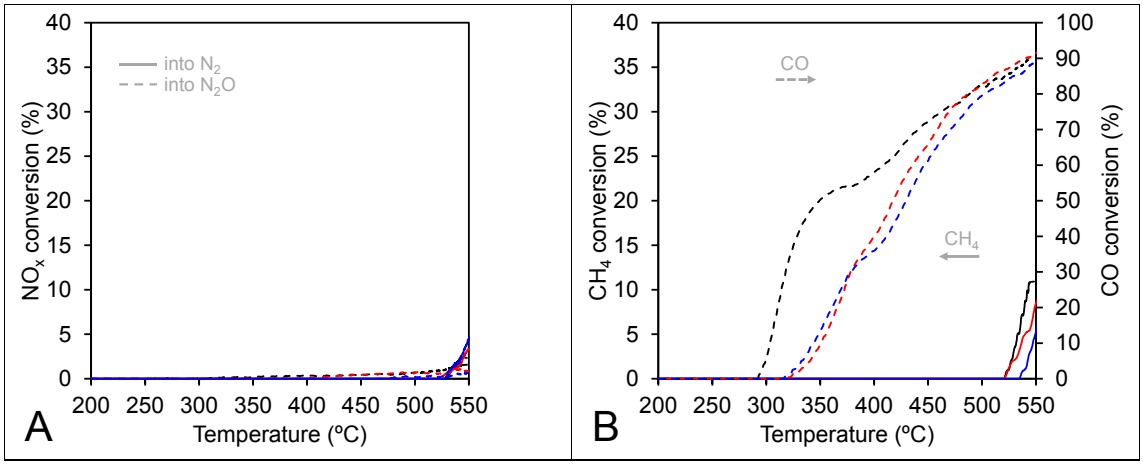

Figure V-24 – NO_x conversion (A) and CH_4 and CO conversion (B) of washcoated monoliths with 400 CPSI: base (black), st500_10 (red) and base, aged monolith (blue). Conditions: 400 ppm NO, 1600 ppm CH_4, 800 ppm CO, 7% O_2, 2% H_2O and GHSV of 40000 h^{-1}.

NO_x and CH_4 conversions values are very similar to all catalysts and no accurate differences can be seen, except for CO conversion which is slightly higher base-400 than for other catalysts. SEM images depicted that washcoat surface of both st500_10-400 and base, aged-400 seemed to be more irregular, which could be synonymous of a worst quality of the washcoat. The fact that such eventual effect only affects CO conversion may be related to the very low conversions of NO_x and CH_4, which may not allow to see the differences.

When the tests were performed in the presence of water in the inlet gas feed, same conclusions are drawn. In this case, the difference between CO conversions becomes even higher between base-400 and the other catalysts, especially at lower temperatures.

Figure V-25 and Figure V-26 illustrates the test results obtained for base-600, st500_10-600 and base, aged-600, in the absence and presence of water in the inlet gas feed, respectively.

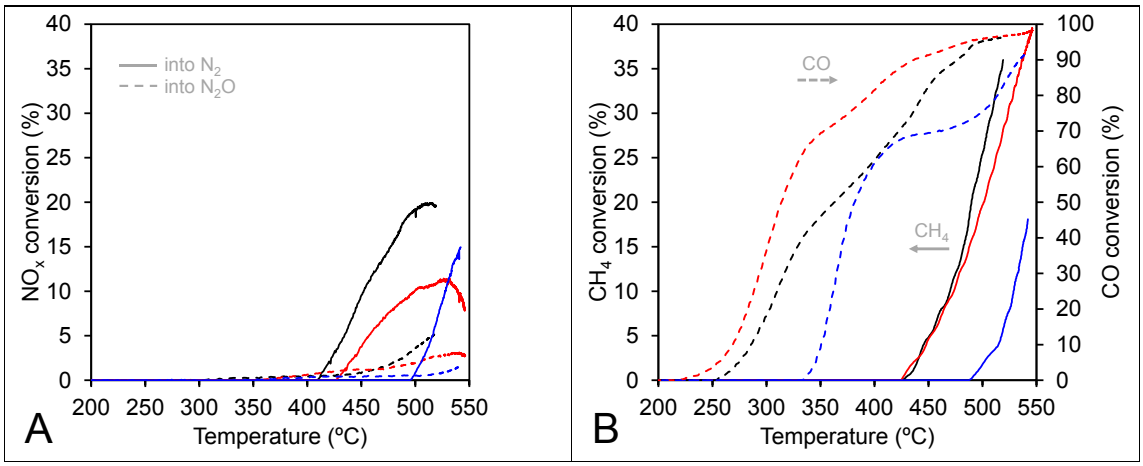

Figure V-25 – NO_x conversion (A) and CH_4 and CO conversion (B) of washcoated monoliths with 600 CPSI: base (black), st500_10 (red) and base, aged monolith (blue). Conditions: 400 ppm NO, 1600 ppm CH_4, 800 ppm CO, 7% O_2 and GHSV of 40000 h^{-1}.

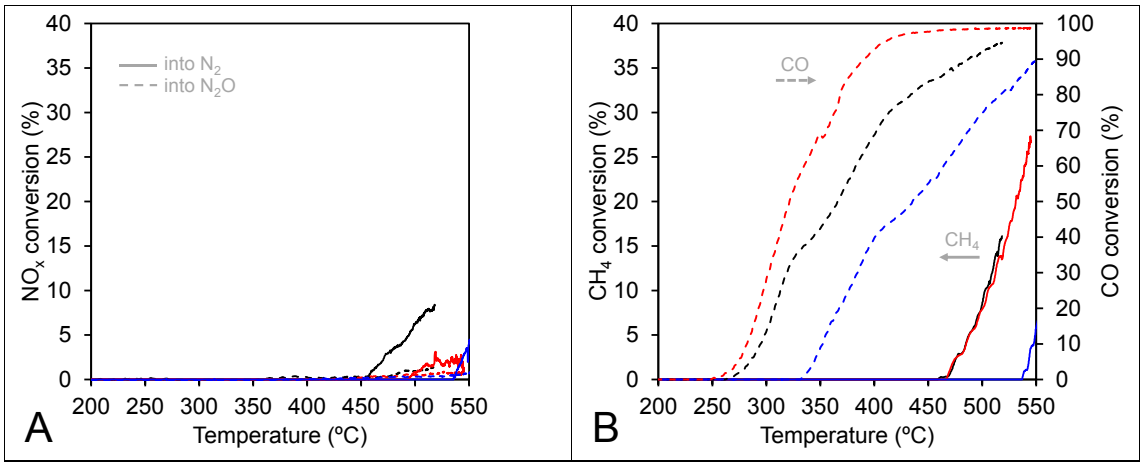

Figure V-26 – NO_x conversion (A) and CH_4 and CO conversion (B) of washcoated monoliths with 600 CPSI: base (black), st500_10 (red) and base, aged monolith (blue). Conditions: 400 ppm NO, 1600 ppm CH_4, 800 ppm CO, 7% O_2, 2% H_2O and GHSV of 40000 h^{-1}.

In this case, significant differences can be observed in the catalytic performance of the three monoliths, with base-600 being the one that allows to achieve higher NO_x conversions into N_2. Base, aged-600 monolith exhibits the worst catalytic performance which can be associated to the partially destruction of the washcoat detected by SEM. Moreover, it is worthy to mention that SEM images of this catalysts revealed very irregular washcoats from channel to channel, which may even means that the washcoating procedure was not correctly performed for this catalyst, in particular, the blowdown of slurry excess after the immersions.

st500_10-600 monolith exhibits lower NO_x and CH_4 conversion values than base-600 monolith. No significant differences in physical structure of the monolith were observe by SEM. However, it should be mentioned that zeolite slurry that gave origin to st500_10-600 (slurry D, Table V-3) possessed an average particle size (5.8 μm) considerably higher than the zeolite slurry that gave origin to base-600 (slurry C, Table V-3 – 2.6 μm). Though no significant changes were observed in the morphology of the washcoats of both monoliths, one cannot exclude an influence of this parameter in the catalytic performance.

Other possible explanation might be the loss of some active species during the washcoating procedure. As it has been previously shown in Chapter IV, by performing the steaming treatment that led to st500_10, the formation of EFAL species due to the steaming treatment is likely to unblock some cavities in the MOR structure, resulting in an easily access of the reactants to metal species eventually contained in such cavities. One cannot exclude the fact that such active species may have easily migrate into the solution during the washcoating procedure due to the unblocking of zeolite structure. Similarly, steaming treatment is likely to favour the formation of surface Ce^{4+} species, which may be eventual more easily washed away during the washcoating procedure. One cannot neither exclude that the washcoating procedure may cause the migration of some Pd and CeO_2 species into the zeolite surface of st500_10 catalyst, eliminating the eventual interaction between Pd^{2+} ions and CeO_2 species that was previously identified as beneficial for NO_x CH_4-SCR reaction. In fact, CO conversion is higher for st500_10-600 monolith, compared to base-600, which may be an evidence of a modification in active species of the catalyst.

V.4. Conclusions

In this chapter, the effect of key parameters on the preparation of structured catalysts, consisting in cordierite monoliths washcoated with zeolites, were studied. The effect of milling time in the preparation of MOR zeolite slurries with 20 wt.% concentration was assessed and it was concluded that, after 16 h of wet milling (at 140 rpm), the average particle size could be reduced from 5.6 μm to 2.0 μm, which is considered within the ideal range (2-3 μm) in order to perform an effective washcoating procedure. The effect of the zeolite concentration in the slurry (15-30 wt.%) was also assessed by measuring the total mass loading of washcoat deposited in the cordierite monolith during the washcoating procedure, after each immersion. It was concluded that, with 20 wt.%, a reasonable compromise could be obtained between the number of immersions required to obtain a given mass loading, the loss of washcoat after adherence test and the required mass of catalyst (prepared at lab-scale) to prepare the monoliths. Based on these studies, it was decided to prepare the monoliths using zeolite slurries with 20 wt.% concentration, obtained after wet ball milling for 16h.

In order to assess the effect of the number of cell per square inch (cpsi) of the monolith in the catalytic performance, two monoliths with 400 and 600 cpsi were washcoated with Pd(0.3)Ce(2)-HMOR catalyst (base). Catalytic test results considering representative conditions of real exhaust gases from a heavy duty vehicle's engine showed that base-600 monolith was the one the exhibited higher NO_x and CH_4 conversions. A simulation of the hydrodynamic flow inside the channels of both base-400 and base-600 revealed that only slight differences in the reactants flows are expected between both monoliths, reason why the discrepancy in the catalytic performance of the monoliths is not likely to be due to hydrodynamic factors. In fact, since the washcoat mass is practically the same in both monoliths, the most plausible explanation lays on the catalyst surface area that contacts the inlet feed gas, which is estimated to be 32% higher in base-600.

Finally, the effect of steaming treatment previously developed in Chapter IV was assessed in the structured catalyst. Monoliths with 400 and 600 cpsi were washcoated with st500_10 catalyst (consisting Pd(0.3)Ce(2)-HMOR submitted to steaming treatment at 500 ºC and 10 vol.%) and also monoliths base-400 and base-600 (washcoated with the base catalyst) were submitted to the same steaming treatment. When comparing the three monoliths with 400 cpsi (base-400, st500_10-400 and base, aged-400), no differences were observed in the NO_x and CH_4 conversions, likely to the very low values registered (maximum conversions of 7% and 5%, respectively).

However, with 600 cpsi, it was possible to verify significant differences in the catalytic performance. Base, aged-600 was the catalyst that exhibited the worst catalytic performance, with lower NO_x, CH_4 and CO conversion values in the entire range of temperatures. This behaviour is likely explained due to the partially destruction of the washcoat that occurred due to the steaming treatment performed in the washcoated monolith. In its turn, st500_10-600 monolith exhibit lower NO_x and CH_4 conversion and higher CO conversion than base-600. It is likely that the beneficial

effects generated in Pd(0.3)Ce(2)-HMOR catalysts due to the steaming treatment of the powder (Chapter IV) were annulled by the washcoating procedure.

V.5. References

[1] J.M. Zamaro, M.A. Ulla, E.E. Miro, Chem. Eng. J., 106 (2005) 25-33.

[2] C.N. Millet, R. Chedotal, P. Da Costa, Appl. Catal., B, 90 (2009) 339-346.

[3] Johnson Matthey, website, What is a Diesel Particulate Filter (DPF)?, http://ect.jmcatalysts.com/Diesel-particulate-filter-DPF-johnson-matthey, accessed in August 2015.

[4] S. Bruehlmann, A.M. Forss, D. Steffen, N.V. Heeb, Environ. Sci. Technol., 39 (2005) 331-338.

[5] L. Lizarraga, S. Souentie, A. Boreave, C. George, B. D'Anna, P. Vernoux, Environ. Sci. Technol., 45 (2011) 10591-10597.

[6] M. Colombo, G. Koltsakis, I. Nova, E. Tronconi, Catal. Today, 188 (2012) 42-52.

[7] J.L. Williams, Catal. Today, 69 (2001) 3-9.

[8] J.M. Zamaro, M.A. Ulla, E.E. Miro, Appl. Catal., A, 314 (2006) 101-113.

[9] A.V. Boix, S.G. Aspromonte, E.E. Miro, Appl. Catal., A, 341 (2008) 26-34.

[10] B. Pereda-Ayo, U. De La Torre, M. Romero-Saez, A. Aranzabal, J.A. Gonzalez-Marcos, J.R. Gonzalez-Velasco, Catal. Today, 216 (2013) 82-89.

[11] J.M. Zamaro, M.A. Ulla, E.E. Miro, Catal. Today, 107-08 (2005) 86-93.

[12] A.V. Boix, E.E. Miro, E.A. Lombardo, J.L.G. Fierro, Catal. Today, 133 (2008) 428-434.

[13] V. Blachou, D. Goula, C. Philippopoulos, Ind. Eng. Chem. Res., 31 (1992) 364-369.

[14] C. Agrafiotis, A. Tsetsekou, J. Mater. Sci., 35 (2000) 951-960.

[15] C. Agrafiotis, A. Tsetsekou, J. Eur. Ceram. Soc., 20 (2000) 825-834.

[16] B. Mitra, D. Kunzru, J. Am. Ceram. Soc., 91 (2008) 64-70.

[17] C. Ozhan, Multi-scale simulation of automotive catalytic converters, PhD Thesis, Université Pierre et Marie Curie - Paris VI, Paris, 2014.

Conclusions and prospects

This work was dedicated to the study and development of zeolite-based catalysts, containing palladium and cerium as active phases, and its application to the selective catalytic reduction of nitrogen oxides, in lean conditions, using methane as reductant (NO_x CH_4-SCR).

The choice of the materials and techniques considered in the development of the catalysts presented in this work was based on an exhaustive literature review that allow not only identify the most promising systems that may lead to successful application at commercial/industrial scale, but also to highlight the main issues still to be addressed in order to fulfil such goal. Typical supports considered in the preparation of active materials for NO_x CH_4-SCR are zeolites and metal oxides. In the case of zeolite-based catalysts, active catalysts can be obtained using MOR, FER and MFI zeolites, by considering the introduction of metal active phases, such as palladium, indium, cobalt and cerium, in particular, when adding two of these metals to the system, which results in enhanced catalytic performance.

Significant advances in the comprehension of Co/zeolite-based catalysts, their active species and respective structure-reactivity relationships, have allowed scientific community to move forward in terms of designing active and selective catalysts for NO_x CH_4-SCR. Notwithstanding, the use of Co as active phase of a catalyst destined to be used in an after-treatment system for pollution abatement of mobile sources is likely to find obstacles from the legal point of view, mainly due to restrictions on the use of this element in catalyst formulations. The use of other systems seems, therefore, inevitable in order to move forward towards the development of a technological solution with potential for industrialisation/commercialisation.

A considerable amount of studies have been dedicated to Pd/zeolite-based catalysts, which also present promising results as potential candidates for NO_x CH_4-SCR catalysts. Moreover, the addition of Ce to Pd/zeolite-based catalysts, in particular considering MOR zeolite as support, has proved to be fruitful in obtaining materials with enhanced catalytic performance. This system was precisely the subject of the study conducted.

PdCe-MOR system was intensively studied in order to identify the nature of metal species stabilised in the zeolite structure and its relevance from the catalytic point of view. Attention was paid to the preparation methods employed, which allow to confirm that ion-exchange (at room temperature) is a suitable method to stabilise palladium as active Pd^{2+} species for NO_x CH_4-SCR. A palladium loading of 0.3 wt.% (between 0.15-0.7 wt.) was proved to be the ideal in order to obtain a selective catalyst, capable of converting NO into N_2 (instead of N_2O). The addition of cerium as co-metal (promoter), even in a small quantity (*ca.* 1%), has proven to be capable of enhancing the catalytic performance of Pd-HMOR, which is attributed to two main factors: *i)* the enhancing of NO_2 formation, which is known to be a first key-step in the NO_x SCR reaction, and *ii)* the promotion of an interaction between Pd^{2+} ions and CeO_2 species, which was shown to contribute to the catalytic performance. However, an ideal balance between Pd and Ce species towards the maximum

catalytic performance is obtained when considering a Ce loading of 2 wt.%. For higher values, CH_4 direct combustion becomes favoured, resulting in a significant decrease of CH_4 selectivity towards NO_x SCR reaction.

The effect of different test conditions in the catalytic performance of the optimised formulation was also assessed. As expected, the increase of reductant in the exhaust gases results in an increase of NO_x conversions. Nevertheless, CH_4 selectivity to NO_x SCR reaction is kept practically constant. It is likely that the increase of this parameter may be the key to further improve the catalytic performance of the catalyst system in study. Also, it was verified that the presence of water in the gas feed inhibits the NO_x CH_4-SCR. Overcoming this obstacle is crucial for the implementation of this type of catalysts as an effective NO_x abatement technology.

The effect of the zeolite structure as catalytic support was also assessed, namely, by considering the preparation of a PdCe-BEA catalyst similar to the formulation optimised for the MOR zeolite (same metal loadings, introduced by the same methods). It has been shown that different Pd and Ce species are stabilised in BEA, namely, PdO and CeO_2 clusters larger than the ones stabilised in PdCe-MOR. These differences are behind the different catalytic performance of PdCe-BEA, which catalytic test results revealed very high NO_x conversions into NO_2 (intermediary step in NO_x SCR reaction) but practically no conversion into N_2. Furthermore, it was verified that, by considering the combination of these two catalysts into a single catalytic system, namely with dual-bed and mixed-bed configurations, a synergic effect between catalysts could be achieved, based on the complementarity of the catalysts from SCR mechanism point of view. It is the first time that similar materials containing different active species based on the same metals are reported to exhibit synergies for NO_x CH_4-SCR.

In this work, it was also shown that by applying a thermal treatment in the presence of water (known as steaming) during the preparation of PdCe-MOR catalysts can lead to materials that exhibits an enhanced catalytic performance, *i. e.*, higher NO_x conversion into N_2 and CH_4 selectivity to NO_x SCR reaction. This only happens for certain steaming conditions, namely, when considering 500 ºC and 10 vol.% H_2O in the gas feed. Results evidence that, at these conditions, mild dealumination of the zeolite structure takes place without jeopardising the active metal species stabilised in the catalyst, namely, Pd^{2+} ions and CeO_2 species interacting with Pd species. It is like that such dealumination process results in the opening of small cages in the zeolite structure where active species are stabilised, becoming in this way more accessible to the reactants.

Finally, a study regarding the scale-up of the optimised PdCe-MOR powder formulation in a honeycomb-monolith structured catalyst was conducted. A preliminary work regarding the effect of milling time and concentration of zeolite slurry, allow to establish a washcoating procedure that proved to be suitable for obtaining washcoated monoliths, namely by considering 16 h of milling time and 20 wt.% of zeolite. The study of the effect of monolith geometry (*i.e.* cpsi - number of cells/in^2) showed that the use of monoliths with 600 cpsi results in considerably higher NO_x conversions when compared to monoliths with 400 cpsi. No significant differences were identified

in the hydrodynamic flow of both channels and, since both monoliths possessed the same mass of catalyst, the explanation for this resulted is likely to be the surface area of washcoat exposed to the passage of gas feed. Nevertheless, independently of the geometry considered, water presence in the gas feed revealed to have, once more, a significant impact on the catalytic performance due to its inhibiting effect.

The effect of steaming treatment was also assessed in the structured catalysts and it was concluded that the enhancing effect associated to the steaming treatment performed during the preparation of the catalysts is no longer observed after washcoating the monoliths with the steamed catalyst. No structural differences were observed in the washcoat of monoliths obtained with steamed and non-steamed powder and a possible explanation for the absence of an enhanced performance might be the elimination of important species during the washcoating procedure, namely, CeO_2 interacting with Pd species. The monoliths washcoated with the non-steamed catalyst were also submitted to a treatment similar to the steaming (ageing), which caused partial destruction of the washcoat, leading to a worst catalytic performance.

The work conducted allowed to move forward towards the understanding and the elucidation of several aspects of NO_x CH_4-SCR reaction over PdCe/zeolite-based catalyst. However, it also raises new important questions to which answers are still to be unveiled.

The role of interacting Ce/Pd species is not entirely clear. It is possible that one of its roles might be the formation of intermediary active compounds involved in the NO_x SCR reaction. For instance, when considering CH_4 as reductant, species such as formaldehyde and methanol have been identified as possible intermediaries in the reaction. A mechanistic study, namely considering *operando* infrared experiments, focused on the identification of potential intermediary species might contribute to answer this question. The further understanding of the reaction mechanism over PdCe/zeolite-based catalysts may open new doors in the designing of this type of catalysts, in particular, the increasing of CH_4 selectivity to NO_x SCR reaction, which has been previously identified as a key point in the improvement of the catalytic performance.

Strategies to overcome the inhibiting effect of water in the NO_x CH_4-SCR reaction are also to be considered as future research work to push forward this technology. Possible strategies may involve the deposition of a hydrophobic layer capable of limiting water adsorption in the metal active sites, leaving them vacant for the reactants. Some works in the literature, though few, points out the use of some techniques, such as chemical vapour deposition of silica, as a possible strategy to retard the water adsorption in the external surface of zeolites.

A detailed study of the variables involved in the multi-bed configuration is also important to ensure the feasibility of this approach as a possible solution in the design of active catalytic systems. For instance, the effect of the masses of both catalysts is crucial to further understand which catalyst is conditioning the most the global performance. It would be also important to consider different layer configurations in order to help to identify additional active sites that might be present in the catalysts (*e.g.* by putting the gas firstly in contact with MOR and then with BEA).

Further characterisation of the steamed and non-steamed materials may also lead to a better understanding of the reasons behind the enhanced effect verified after applying the steaming treatment under certain conditions. For instance, nuclear magnetic resonance of ^{27}Al and ^{1}H may bring important insights on the differences between these catalysts that might explain the enhanced catalytic behaviour. Moreover, though it was not observed by the different techniques applied in this work, significant modifications in the active metal species (Pd/Ce) due to the steaming cannot be entirely excluded. The application of more powerful techniques, namely quick extended X-ray absorption fine structure (EXAFS) spectroscopy, could be enlightening. This technique has the particularity of being possible to be executed *in operando*, which means that it could be applied during the steaming treatment in order to try to identify possible modifications in metal species.

Finally, the scale-up of the PdCe-MOR catalysts considered in this study into honeycomb-monolith structured catalyst is a field with still large potential to be explored. The optimisation of the washcoating technique may be performed in order to achieve more regular and homogenous washcoat layers in the monolith channels. Possible strategies for achieving this goal may involve studies of many different parameters in the quality of the washcoat, namely, the effect of viscosity, the influence of the amount and type of binder, the nature of the solvent used in the suspension, among others. Moreover, analogous strategies to the ones identify as pertinent for enhancing the catalytic performance of powder formulation may also be considered. In particular, the use of dual-layer catalysts obtained by washcoating different active catalysts (such as PdCe-MOR and PdCe-BEA). The washcoating of a hydrophobic layer to retard the water adsorption may also be worthwhile exploring.

Annexes

Annex A. Methodology adopted for the literature review

The adopted methodology to perform this literature review was mainly based on research articles produced by scientific community. In the *Web of Knowledge* database, a search by topic using several combinations of keywords was conducted at the beginning of this thesis, in order to describe the state-of-art concerning the topic in study. This search was last updated at June 2015. The words “methane AND SCR” leaded to 440 results and “methane AND deNOx” leaded to 31 results. A more refined search was made by performing an additional search, using the combination “zeolite AND methane AND SCR” (leading to 264 results).

Based on the tittles and abstracts of the obtained results from these searches, a selection of the most relevant articles was analysed in detail and considered in this literature review, *i. e.*, the articles that explicitly consider/describe/illustrate/explain the catalytic behaviour of a given system for SCR of NO_x with methane. Some references included in those articles (which were not detected in the previous mentioned searches) were also analysed and considered in this work.

A review of patents regarding the NO_x CH_4-SCR technology in lean conditions was also considered. This review was accomplished through the use of *smart searc*h tool available in *Espacenet* website (from European Patent Office) [1]. Two searches considering the combination of words “deNOx AND zeolite” and “NOx AND catalyst AND methane” were conducted, leading to 27 and 73 results, respectively. The tittle and abstract of the patent results were analysed, which allowed the exclusion of some results. The others were quickly analysed, in a first phase, in order to retain the gist of each document.

In a second phase, a special attention was paid to the articles concerning palladium-based catalysts, which were analysed in more detail.

In total 159 articles were considered in this review, which were categorised according to Table A-1. Also, 6 patents were considered in this study.

Table A-1 – Total number of articles from literature considered in this study.

Category catalysts	Number of articles
Monometallic zeolites (palladium)	25
Monometallic zeolites (other metals)	55
Monometallic non-zeolites	22
Sub total	*102*
Bimetallic zeolites (Pd and other than cobalt)	8
Bimetallic zeolites (other metals’ combination)	37
Bimetallic non-zeolites	12
Sub total	*57*
TOTAL	159

Annex B. Catalytic performance data of bimetallic zeolite-based catalysts

Table B-1 – Detailed data regarding operating conditions, catalyst composition and maximum conversion of bimetallic zeolite catalysts analysed.

Notes

a. Values of conversion inside brackets represent different cycles after addition/removal of water;
b. RE stands for *Rare Earth* (particular rare earth is not specified);
c. *n.a.* stands for *not available*, meaning that information is not explicit in the reference.

Ref.	Structure	Si/Al	M1	wt.	M2	wt.	GHSV h^{-1}	Flowrate mL/min	[NO] ppm	[CH_4] ppm	[O_2] %	[H_2O] %	Window of Conversion (ºC)				Maximum NO conversion data				
													dry		wet		T	NO		CH_4	
													min	max	min	max	ºC	dry	wet	dry	wet
[2]	Pt-Pd -MOR	7	Pd	0.4%	Pt	0.4%	30000	100	1000	2000	6%	10%	-	-	-	-	500	40%	-	100%	-
[3]	Co-Pd -MOR	6	Co	6.28%	Pd	0.15%	30000	100	1000	2700	6%	8%	-	-	475	550	550	-	-	60%	90%
[4]	Co-Pd -MOR	10	Pd	0.40%	Co	2.20%	10000	-	500	2500	5%	10%	-	-	400	490	450	-	-	60%	100%
[5]	Ce-Pd -MOR	10	Pd	0.4%	Ce	2-4%	17000	-	245	881	6.4%	11.3%	-	-	-	-	385	-	60%	-	21%
[6]	RE-Pd -MOR	12	Pd	0.3%	RE	1%	-	-	500	2500	5%	5%	-	-	-	-	390	-	56%	-	10%
[7]	Pd-In -MOR	6.7	In	In/Al = 1/6	Pd	0.50%	30000	100	4000	4000	2%	-	400	400	-	-	400	55%	-	47%	-
[8]	Ce-Pd -MOR	5	Pd	0.2%	Ce	2%	33000	220	1010	3300	4.1%	5%	400	650	450	650	550	90% (75%)	75%	100% (85%)	90%

Ref.	Structure	Si/Al	M1	wt.	M2	wt.	GHSV h^{-1}	Flowrate mL/min	[NO] ppm	[CH_4] ppm	[O_2] %	[H_2O] %	Window of Conversion (ºC)				Maximum NO conversion data				
													dry		wet		T	NO		CH_4	
													min	max	min	max	ºC	dry	wet	dry	wet
[9]	Pd-In -MOR	6.7	In	6.8%	Pd	0.50%	15000	-	4000	4000	2%	-	-	-	-	-	400	41%	-	31%	-
[10]	Fe-In -MOR	10	Fe	n.a.	In	n.a.	20000	-	1000	1000	2%	2%	450	550	-	-	500	57%	27%	40%	17%
[11]	Pt-Co -MOR	5.9	Pt	0.39%	Co	2.87%	6500	-	1000	1000	2%	-	475	550	-	-	500	80% (76%)	60%	92% (100%)	92%
[12]	Co-La -MOR	6.5	Co	1.69%	La	1.22%	7500	-	1000	1000	2%	10%	-	-	-	-	500	-	40%	-	70%
[13]	Co-Pd -MFI	13	Pd	0.40%	Co	2.30%	10000	-	500	2500	5%	-	380	500	-	-	390	98%	-	-	-
[14]	Co-Pd -MFI	20.2	Co	3.30%	Pd	0.40%	-	100	100	2000	10%	10%	350	500	375	500	400	90%	85%	-	-
[4]	Co-Pd -MFI	12	Pd	0.40%	Co	2.30%	10000	-	500	2500	5%	10%	-	-	400	490	450	-	-	90%	76%
[15]	In-Ir -MFI	11.9	In	4%	Ir	1%	36000	100	1000	1000	10%	-	350	450	-	-	450	90%	-	90%	-
[16]	In-Fe -MFI	12.5	In	5%	Fe_2O_3	20%	3600	60	2500	2000	4%	3.3%	400	650	-	-	500	100%	91%	75%	92%
[17]	Ce-In -MFI	14	Ce	2%	In	2%	24000	120	1000	1000	10%	5%	375	550	520	550	550	85%	60%	100%	50%
[18]	In-Ce -MFI	14	In	7%	Ce	9%	30000	220	1000	1000	2%	-	450	600	-	-	500	92%	-	-	-
[19]	Co-In -MFI	33	In	1.70%	Co	0.34%	30000	100	4000	4000	2%	-	400	550	-	-	500	85%	-	70%	-

Ref.	Structure	Si/Al	M1	wt.	M2	wt.	GHSV h^{-1}	Flowrate mL/min	[NO] ppm	[CH_4] ppm	[O_2] %	[H_2O] %	Window of Conversion (ºC)				Maximum NO conversion data				
													dry		wet		T	NO		CH_4	
													min	max	min	max	ºC	dry	wet	dry	wet
[20]	Zn-Co -MFI	12.5	Co	2%	Zn	2%	3600	48	2500	2000	2%	-	450	550	-	-	500	55%	-	50%	-
[21]	Ag-Co -MFI	-	Co	3%	Ag	3%	6000	100	1000	5000	2%	2%	350	600	-	-	500	98%	58%	66%	-
[22]	Ce-Ag -MFI	14.05	Ce	Ce/Al =0.08	Ag	Ag/Al = 0.78	7500	-	5000	5000	2.5%	-	475	650	-	-	500	80%	-	80%	-
[4]	Co-Pd -FER	9	Pd	0.35%	Co	2.20%	10000	-	500	2500	5%	10%	-	-	460	490	490	-	-	58%	92%
[23]	Co-Pd -FER	9	Co	2.20%	Pd	0.15%	45000	250	1000	2000	5%	2%	-	-	-	-	500	48%	35%	68%	48%
[24]	Pt-In -FER	8.8	Pt	0.50%	In	0.52%	-	150	1000	1000	2%	2%	450 (400)	550 (550)	450	450	500	82% (70%)	42%	100% (100)	65%
[25]	In-Co -FER	8.8	Co	2.13%	In	3.28%	10000	-	1000	2000	4%	0.25% (dry) 2.5% (wet)	300	500	-	-	450	98%	85%	95%	-
[26]	Mn-Co -FER	8.4	Mn	0.14%	Co	4.66%	30000	-	1000 (+100 NO_2)	1000	2.5%	1%	500	500	-	-	500	51% (50%) (45%)	30% (30%) (30%)	-	-
[4]	Co-Pd -BEA	11	Pd	0.40%	Co	2.20%	10000	-	500	2500	5%	10%	-	-	470	490	490	-	-	65%	25%
[27]	Co-Pd -BEA	12.5	Co	2%	Pd	0.15%	45000	250	1000	2000	5%	2%	-	-	-	-	550	32%	-	35%	-
[28]	Co-Pd -BEA	1000	Pd	0.15%	Co	3%	40000	250	150	1500	7%	-	480	480	-	-	480	55%	-	34%	-

Annex C. Experimental Part

C.1. Catalysts Preparation

The catalysts used in this work were prepared from the following starting materials:

- Mordenite zeolite with Si/Al = 10, provided by Zeolyst International, (CBV21A, lot nr 22001N00067), in the ammonia form (NH_4MOR);
- β zeolite with Si/Al = 12.5 provided by Zeolyst International, (CP814E, lot nr 2493-65), in the ammonia form (NH_4BEA);

C.1.1. HMOR and HBEA

HMOR was obtained by calcination of NH_4MOR under dry air flow (4 $L.h^{-1}.g^{-1}$) at a heating rate of 5 ºC/min until 200 ºC, and kept at this temperature for 1 h. Then, temperature was raised until 500 ºC/min (heating rate of 5 ºC/min) and kept at this temperature for 8 h.

The same procedure was followed to obtain H-BEA from NH_4-BEA.

C.1.2. Pd-based catalysts

In the standard procedure considered in this work to prepare Pd-based catalyst, the catalysts were prepared by ion-exchange at room temperature, for 24h, with a volume of solution/mass of catalyst ratio of 50 mL/g. For each catalyst, the solution was prepared by weighting the required mass of $Pd(NH_3)_4(NO_3)_2$ solution (Aldrich, 99.99% purity, aqueous, 10 wt.%) corresponding to the desired mass of palladium to be introduced in the zeolite support (typically, 6 g of starting material). Distillate water was then added to the solution to complete 50 mL/g. This final solution was added drop wise to the support, under vigorous mixing.

After the exchange, catalysts were centrifuged for 5 min at 6000 rpm to separate the solid phase from the remaining liquid. Afterwards, a sequence of three washing cycles, consisting in adding distillate water and centrifuge for 5 min at 6000 rpm, was performed. Catalysts were then dried in the oven, overnight, at 90 ºC.

The catalysts were calcined under dry air flow (4 $L.h^{-1}.g^{-1}$) at a heating rate of 1 ºC/min until 200 ºC, and kept at this temperature for 1h. Then, temperature was raised until 500 ºC/min (heating rate of 1 ºC/min) and kept at this temperature for 1 h.

Pd(0.3)-HMOR(IE80) considered in Chapter II Chapter IIwas obtained following the same procedure previously described, but considering ion-exchange at 80 ºC (instead room temperature) and heating rate of 0.5 ºC/min (instead 1 ºC/min).

Pd(0.3)-HMOR(IWI) was prepared by introducing Pd by incipient wetness impregnation (IWI) technique. The required $Pd(NH_3)_4(NO_3)_2$ solution (Aldrich, 99.99% purity, aqueous, 10 wt.%) was weighted and added to the quantity of distillate water volume corresponding to the pore volume of the structure. Then, this solution was added drop wise to the structure. The catalyst was then dried in the oven over night at 90ºC and calcination was performed according to the procedure previously described in the standard procedure.

C.1.3. Ce-based catalysts

Ce-based catalysts were prepared by introducing cerium through incipient wetness impregnation technique. A $Ce(NO_3)_3$ solution was prepared by weighting necessary mass of $Ce(NO_3)_3.6H_2O$ salt (Fluka, 99% purity), corresponding to the desired loading of Ce to be introduced, and dissolving it into a water volume equivalent to the pore volume of the catalyst to be impregnated. The solution was then added drop wise to the catalyst.

After impregnation, the catalyst was dried in the oven, overnight, at 90 ºC. Afterwards, the catalyst was calcined under dry air flow (4 $L.h^{-1}.g^{-1}$) at a heating rate of 5 ºC/min until 200 ºC, and kept at this temperature for 1 h, then temperature was raised until 500 ºC/min (heating rate 5 ºC/min) and kept at this temperature for 8 h.

For the catalysts were cerium was introduced by mechanical mixture and co-grinding with cerium oxide, the cerium precursor used was CeO_2(IV) powder (Aldrich, 99.9% purity).

C.1.4. Fe-based catalysts

Fe-based catalysts were prepared considering the same procedure previously described for Ce-based catalysts (incipient wetness impregnation technique), but instead of a Ce precursor salt, a $Fe(NO_3)_3.9H_2O$ salt (Aldrich, 99,99% purity) was used.

For the catalysts were iron was introduced by mechanical mixture and co-grinding with ion oxide, the ion precursor used was Fe_2O_3 powder (Sigma-Aldrich, 99% purity).

C.1.5. Monolith-based structured catalysts

Cordierite honeycomb monoliths (Corning, 400 cpsi, $d_{channel} \approx 1.09$ mm, $t_{wall} \approx 0.2$ mm / NGK, 600 cpsi, $d_{channel} \approx 0.96$ mm, $t_{wall} \approx 0.1$ mm), containing a cylindrical shape with height and diameter of 1 in, were used as substrates.

Typically, 45 mg of a zeolite slurries (20 wt.% of catalyst in distilled water) was prepared by wet ball milling for 16 h, at 140 rpm, performed in a *Fritsch Planetary Micro Mill PULVERISETTE 7 premium*, equipped with two grinding bowl with capacity for 80 mL each (with 28 balls of zirconia, 10 mm diameter). For each slurry, pH and viscosity were measured for these slurries, as well as particle size distribution.

Fresh monoliths were previously calcined in a muffle (500 ºC, 4 h, 2 ºC/min) in order to clean the monoliths surface. Before starting the washcoating procedures, a mass of colloidal silica (Ludox-HS 40, Sigma-Aldrich) corresponding to 3 wt.% of the mass of zeolite slurry. The procedure started with the immersion of the monolith in the zeolite slurry for 3 min. Afterwards, the monolith was removed from the slurry and the excess slurry was removed by blowing compressed air into the channels. The monolith was then placed in the oven (110 ºC) for 1 h. After this period, the monolith was removed from the oven and 10 min were waited to ensure proper cooling down. The mass of washcoated monolith was then registered. The previously mentioned procedures were repeated until the mass of washcoat was *ca.* 1.9 g, which was accomplished after 4 immersions for all monoliths.

C.2. Catalysts characterisation

C.2.1. Inductively coupled plasma - optical emission spectrometry (ICP-OES)

ICP-OES analyses were performed in *Laboratório Central de Análises* – LCA (UA, Aveiro), following an internal procedure based on ISO 11885.

C.2.2. Powder X-ray diffraction (XRD)

XRD was performed on a Bruker D8 Advance diffractometer equipped with a graphite monochromator in order to obtain Cu-K_α radiation. For the pattern collection, a step size of 0.02 º (2θ) and a step time of 12 s were considered. Previously calcined samples were placed in the well of a glass sample holder and pressed using a microscope slide, in order to smooth the sample surface.

Identification of the different crystalline phases was performed by comparing the collected XRD with those on PDF-2 Release 2005 database of the International Centre for Diffraction Data (ICDD). XRD analyses were performed in *Centro de Química Estrutural* – CQE (IST, Lisbon).

C.2.3. Temperature-programmed reduction under hydrogen (H_2-TPR)

Temperature-programmed reduction under hydrogen (H_2-TPR) was performed by contacting a catalyst sample (*ca.* 100 mg) with a mixture of H_2 (5 vol.%)/Ar and heating it until 900 ºC using a ramp of 7.5 ºC/min. Hydrogen consumption was measured with a thermal conductivity detector. Water was removed in a dry ice-cooled trap before the detector. A schematic representation of the H_2-TPR plant used in this work is presented in Figure C-1.

H_2-TPR analyses were performed in *CATHPRO / Centro de Química Estrutural* – CQE (IST, Lisbon).

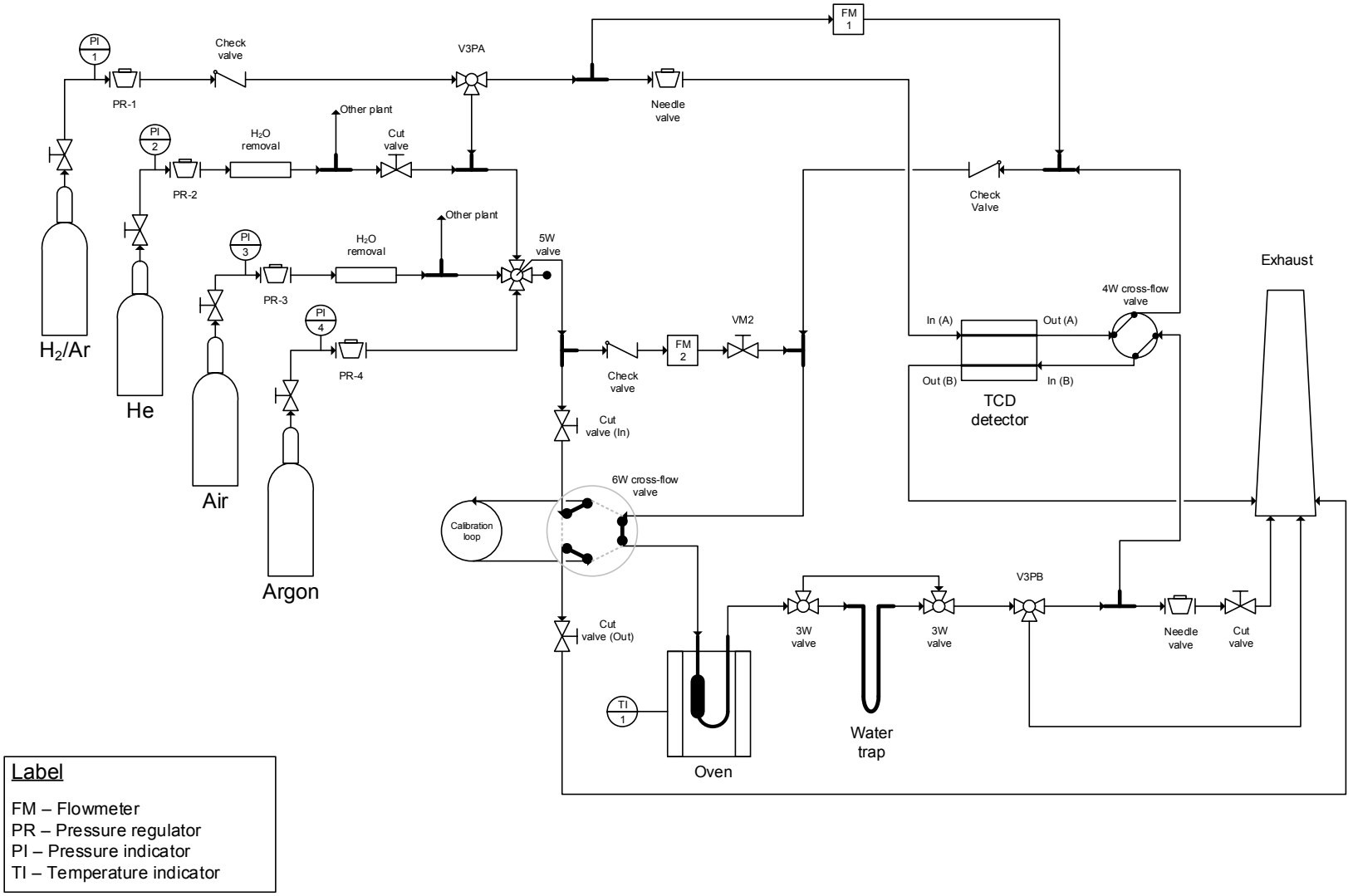

Figure C-1 – Schematic representation of H_2-TPR plant available at CATHPRO/CQE (IST, Lisbon).

C.2.4. Diffuse reflectance UV-Vis spectroscopy (DRS UV-vis)

Diffuse reflectance spectra in the UV-Vis range (DRS UV-Vis) were collected on a *Varian Cary 5000 UV-Vis-NIR* spectrophotometer equipped with a *Praying Mantis* accessory. Spectra were collected at room temperature, using calcined samples (range 200-800 nm, scan rate - 600 nm/min, data interval - 1 nm, SBW - 4 nm). Reflectance spectra were converted into the Schuster-Kubelka-Munk (SKM) function, F(R), calculated at each wavelength using equation (C-1).

$$F(R) = \frac{(1-R)^2}{2R} \qquad \text{(C-1)}$$

R is the ratio of the intensity of the light reflected by the sample to the one reflected by a standard. In order to minimise the effect of zeolite framework absorption, the standard considered was a parent free-metal zeolite of the samples analyses (HMOR for MOR-based catalysts and HBEA for BEA-based catalysts).

DRS UV-Vis analyses were performed in *CATHPRO / Centro de Química Estrutural* – CQE (IST, Lisbon).

Figure C-2 – Picture of *Praying Mantis* accessory coupled in *Varian Cary 5000 UV-Vis-NIR* spectrophotometer available at CATHPRO/CQE (IST, Lisbon).

C.2.5. Infrared spectroscopy using probe molecules (FTIR)

Spectra were collected with a Nicolet 6700 FTIR spectrometer (400-4000 cm^{-1}, 128 scans, 4 cm^{-1} resolution). In all the analyses performed with the different catalysts, self-supporting wafers of catalyst (*ca.* 10 mg/cm^2) were submitted to a pre-treatment (activation), consisting in heating up to 400 ºC at 3 ºC/min, then holding for 30 min, inside a vacuum cell ($P < 10^{-4}$ Pa, equipped with CaF_2 windows) attached to the vacuum line.

Two different probe molecules were considered in this work: carbon monoxide (CO) in order to characterise the metal active phase and pyridine in order to characterise the acidity of the catalysts.

When using CO, after pre-treatment, wafers were reduced at 400 ºC, for 1 h, under 100 torr of H_2. After reduction, the cell was evacuated for 10 min to $P < 10^{-5}$ torr. The wafers were then cooled down to room temperature and a spectrum was collected prior to CO adsorption. Next, 5 torr of CO was introduced into the cell and a spectrum was obtained. The CO gas phase spectrum was collected. All spectra presented were obtained after subtracting CO gas phase and the activated sample (after reduction) contributions, and they were normalised at the same weight/surface wafer ratio.

For the analyses focused on acidity characterisation, after pre-treatment, wafers were cooled down to room temperature and a spectrum was collected prior to pyridine adsorption. Next, 1 torr of pyridine was introduced into the cell and the temperature was raised to 150 ºC and kept for 30 min in order to ensure proper diffusion of pyridine through the catalyst. Afterwards, the cell was evacuated for 10 min to $P < 10^{-5}$ torr and a spectrum was collected at room temperature. Then, the wafer was heated at 50 ºC, for 10 min and afterwards, another spectrum was collected. The same procedure was adopted until 400 ºC, with spectra collected every 50 ºC. Before each spectrum of the catalyst, a background spectrum was always collected.

Figure C-3, Figure C-4 and Figure C-5 illustrate the experimental apparatus used for the FTIR characterisations considered in this work, which was conducted in *Laboratoire Catalyse et Spectroscopie* – LCS (ENSICAN, Caen).

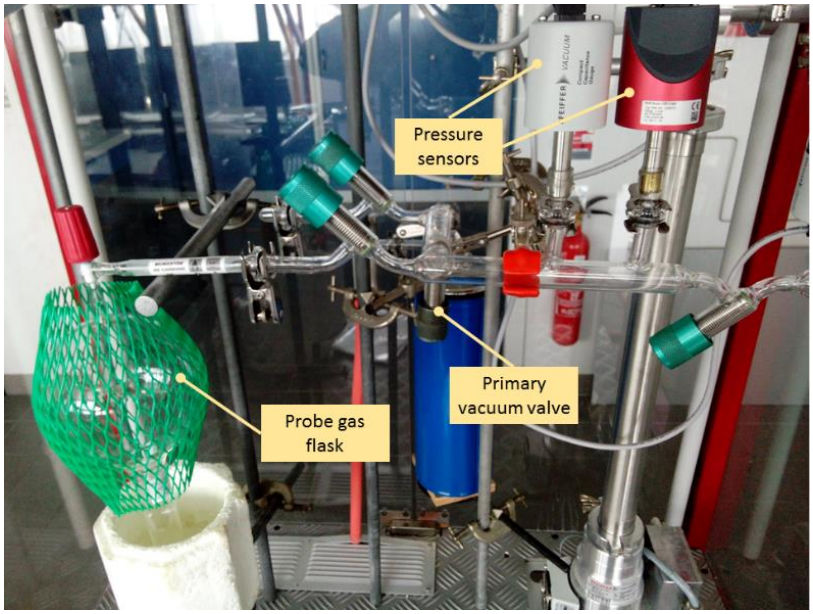

Figure C-3 – Picture of experimental setup for infrared spectroscopy available at LCS (ENSICAEN, Caen) – view of the probe gas flask.

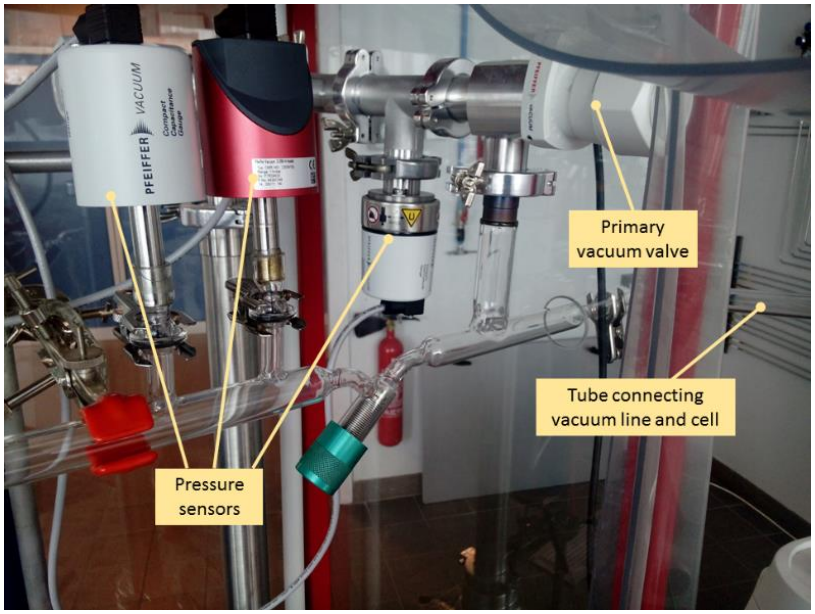

Figure C-4 – Picture of experimental setup for infrared spectroscopy available at LCS (ENSICAEN, Caen) – view of the secondary vacuum line.

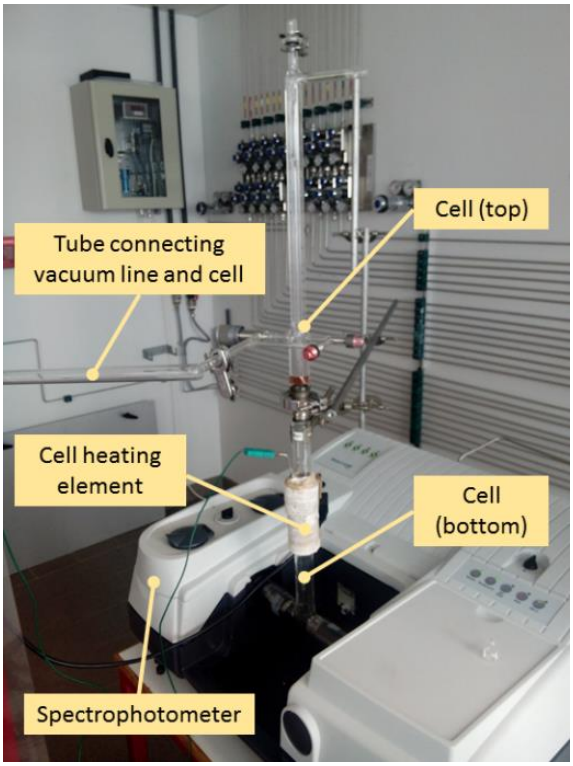

Figure C-5 – Picture of experimental setup for infrared spectroscopy available at LCS (ENSICAEN, Caen) – view of cell and spectrophotometer.

C.2.6. Transmission electron microscopy (TEM/EDS)

Transmission electron microscopy (TEM) was performed on a *JEOL JEM 2010* microscope (LaB6 cannon) operating at 200 kV. Prior to TEM, samples were crushed and then dispersed with ethanol on a carbon-coated copper TEM grid. Energy-dispersive X-ray spectroscopy (EDS) was also performed (probe PGT-Bruker). TEM/EDS analyses were performed in *SIARE* (UPMC, Paris).

C.2.7. Scanning electron microscopy (SEM/EDS)

Scanning electron microscopy (SEM) of the washcoated monoliths was performed on a Hitachi S-3400 N microscope. Images along the channels were collected by performing a transversal cut in the monoliths and by perform SEM directly on the sample. For the collection of images transversal to the channels, an additional preparation was performed. Firstly, monoliths were cut through a transversal plane. Then, channels were filled with an epoxide resin. Once the resin was dried, the surface of the monolith was polished.

SEM/EDS analyses were performed in *Instituto de Carboquímica* - ICB (CSIC, Zaragoza).

C.2.8. N_2 adsorption/desorption

Nitrogen adsorption/desorption measurements were carried out at -196 ºC in a Micromeritics ASAP 2010 apparatus. Before the N_2 adsorption, the catalyst sample was degassed under vacuum at 90 ºC for 1 h and then at 350 ºC for 4h. The total pore volume was calculated from the adsorbed quantity of nitrogen for a relative pressure P/P_0 of 0.97. The micropore volume ($V_{p,micro}$) and external surface area (S_{ext}) were determined using the *t*-plot method and considering the reference isotherm Harkins-Jura [29]. The mesopore volume ($V_{p,meso}$) was calculated by the difference between the total pore volume and the micropore volume. Surface area obtained by Brunauer-Emmett-Teller (BET) theory is also obtained (S_{BET}).

N_2 adsorption/desorption analyses were performed in *CATHPRO / Centro de Química Estrutural* – CQE (IST, Lisbon).

C.2.9. Characterisation of zeolite slurries used in the preparation of monolith-based structured catalysts

Measurements of pH, viscosity and particle size distribution were performed in order to support the preparation of monolith-based structured catalysts.

pH of the zeolite slurries was measured using a *Mettler Toledo Education line* pH meter, equipped with an *Inlab® Expert Pro* probe adequate for suspensions. Before each series of measurements, the pH meter was calibrated using two buffer solutions of the three available, with different pH (10, 7 and 2, from Reagecon – products nr 1040525CTT, 1070525 CTT and 1100525CTT, respectively).

Viscosity of the zeolite slurries was measured using a *AND SV-10* vibro viscometer, using 10 mL of suspension.

Particle size distribution was measured using a laser particle sizer *Fritsch Analysette 22 compact*. Measurements were performed in full-range mode (0.3-300 μm). For each sample, a background was collected (with mechanical mixer and ultrasounds on). Then, the measurement was collected twice for each sample, in order to verify repeatability of the measurements. At the end of each measurement, the dispersion chamber was cleaned.

The characterisation techniques for zeolite slurries herein described were performed in *Institut Jean Le Rond d'Alembert* - IJLRDA (UPMC, Saint-Cyr).

C.3. Catalytic tests

The catalytic tests considered in this work were performed in three different deNO$_x$ plants, two for powders and one for monoliths. All powder catalysts were tested in CATHPRO's deNOx plant (IST, Lisbon) except the ones performed in representative conditions of real exhaust gases, which were performed in IJLRDA's deNOx plant (UPMC, Saint-Cyr). Monoliths were tested in the IJLRDA's synthetic gas bench (UPMC, Saint-Cyr).

C.3.1. CATHPRO's deNO$_x$ plant (powder catalysts)

Schematic representation of CATHPRO's deNO$_x$ plant is presented in Figure C-7. The reactional mixture is obtained by feeding the desired gases through the streams 1 (Ar), 2 (CH_4), 3 (H_2), 4 (O_2) and 5 (NO), which flow are controlled by mass flowmeters (*Brooks Series 5850E*). Stream 1 is divided in streams 6 (used to perform pre-treatment of the catalyst, before test) and stream 7, is divided in stream 8 (that feeds the saturator when tests are to be performed with liquid reactants and water) and stream 10 that balances the reactional mixture. Stream 10 joins stream 11 (consisting in H_2 or CH_4 coming from the streams 2 and 3, respectively), resulting in stream 12, which is combined with stream 4 and results in stream 13. This latter is then combined with stream 9 (from saturator) and stream 15 (consisting in NO or an additional gas that can be added by stream 14 if desired), resulting in stream 16, which can be directed to the reactor (stream 18) or by-passed this one (stream 17). Figure C-6 illustrates the 4W cross-flow valves operation.

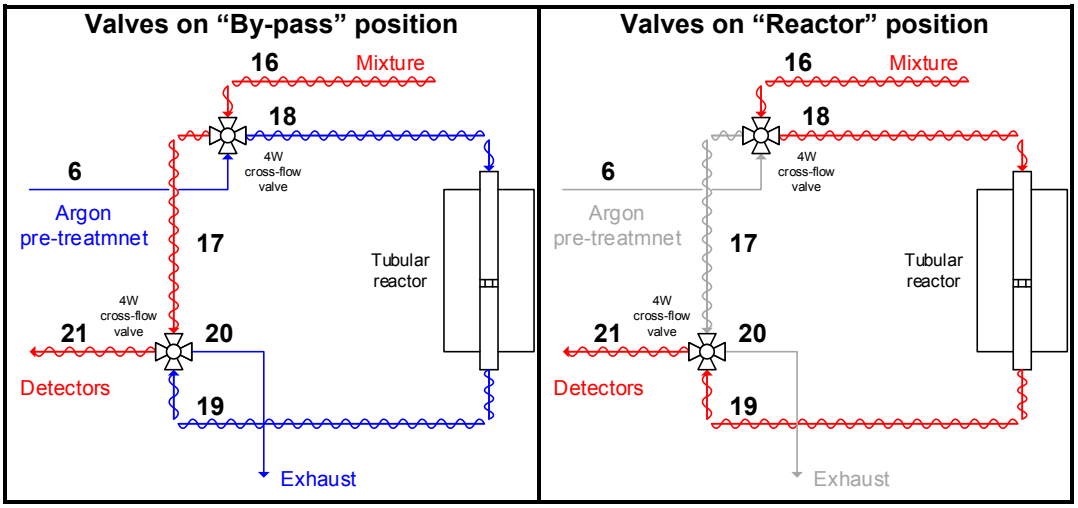

Figure C-6 – Schematic representation of 4W cross-flow valves operation.

The reactors used in this plant were Pyrex tubular reactors, 50 cm long and with internal diameter of 2 cm, containing a porous quartz filter (porous type nr. 3) approximately in the middle, where the powder is retained.

Stream 20 conducts the reactor's outflow gas to the exhaust system during pre-treatment stage and it is not used during the reaction. Stream 21 is divided in stream 22, which feeds part of the

mixture to the MS and then goes to the exhaust (stream 23), and stream 24. This stream passes in a hydrophobic membrane (*Permapure*, model MD-110-72F-4) that removes all the water from the gases by using an air flow that passes in the outside of the membrane, in counter flow. Stream 25 goes then to $CO/CO_2/N_2O$ detector, which is afterwards redirected to CH_4 analyser (stream 26). Part of this stream is then sent to NO/NO_2 analyser (stream 29/30) and the remaining goes to the exhaust (stream 28). When no gases are passing in the plant, air is fed to the NO/NO_2 analyser.

Table C-1 summarises the gases currently available in CATHPRO's $deNO_x$ plant and Table C-2 summarises the detectors installed in the plant.

Table C-1 – List of gases used in CATHPRO's $deNO_x$ plant.

Compound	Bottle (*Ar Líquido*)
NO	NO (1%) / Ar
CH_4	CH_4 (5%) / Ar
O_2	Alphagaz 2
Ar	Alphagaz 1
H_2	Alphagaz 1

Table C-2 – List of gases used in CATHPRO's $deNO_x$ plant.

Compound	Detector
NO/NO_2	*Thermo 42C*, chemiluminescence analyser
$CO/CO_2/N_2O$	*ABB EL 3020*, infrared analyser
CH_4	*ABB EL 3020*, infrared analyser
Several	Pfeiffer Vacuum GSD 301, mass spectrometer

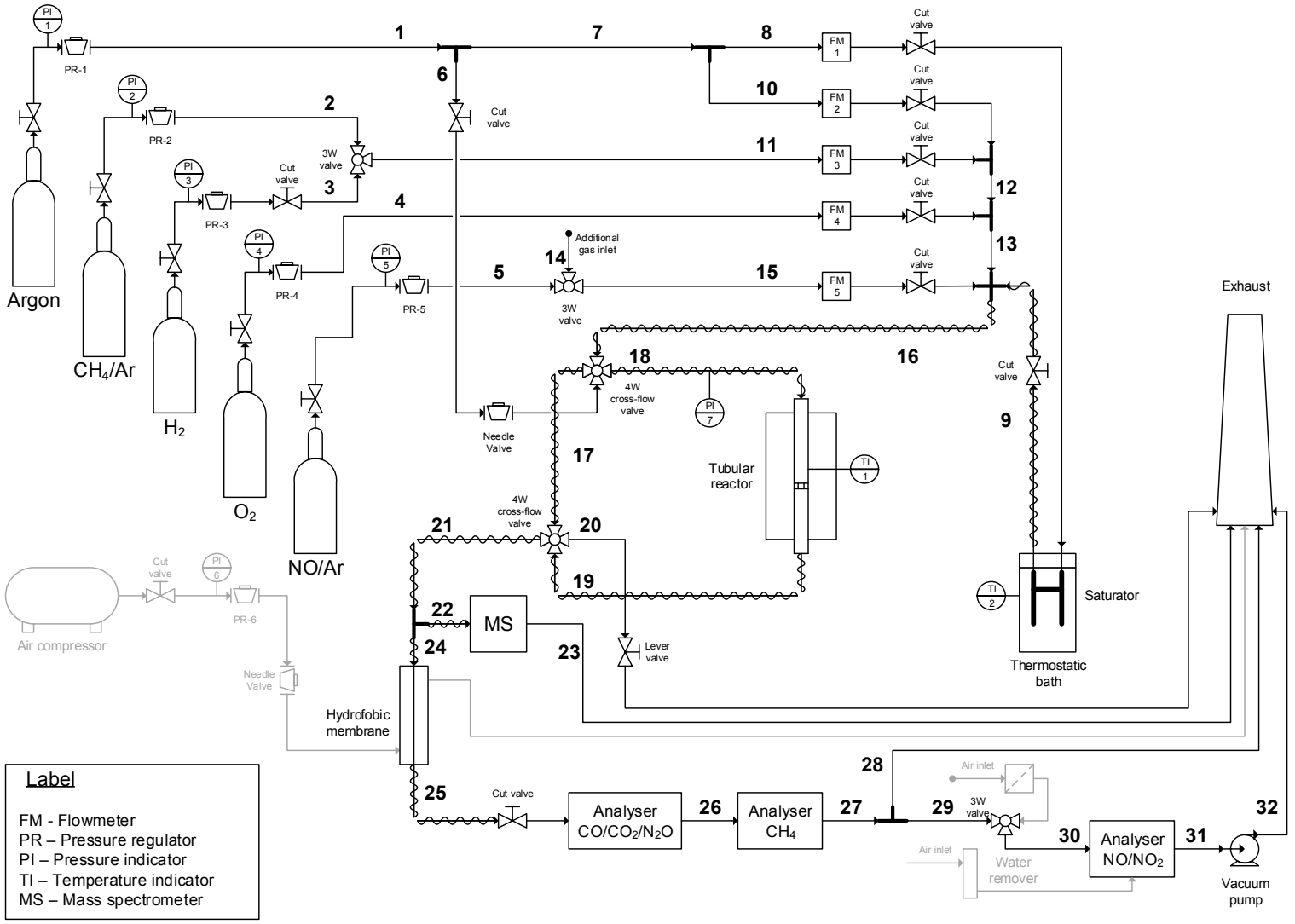

Figure C-7 – Schematic representation of deNO$_x$ plant available at CATHPRO/CQE (IST, Lisbon).

Table C-3 – List of standard m/Z values considered to follow the different compounds, containing the different relative intensities.

m/Z / compound	H_2	CH_4	H_2O	HCN	CO	CO_2	NO	NO_2	N_2	NH_3	N_2O	HCHO	CH_3OH	O2	-NCO	CH_3NO	CH_3NO_2	Ar
2	100																	
14		20					8	11	14	2	14		2			8	8	
15		90					2			8			12			34	48	
16		100			2	10	1	23		80	5			22		5	6	
17			22							100			0,5				1	
18			100										1				1	
20																		20
26				17												2	2	
27				100												13	11	
28				2	100	10			100		11	25	5			21	8	
29												100	45			5	12	
30							100	100			32	58	7			100	100	
31													100			1	2	
32													75	100			1	
40																		100
42															-	5	2	
44						100					100					10	5	
45											1					70	7	
46								38								8	38	
61																	58	

Note:

Relative intensities were obtained from website http://webbook.nist.gov/chemistry/ (accessed in June 2012).

C.3.2. IJLRDA's deNO$_x$ plant (powder catalysts)

Schematic representation of CATHPRO's deNO$_x$ plant is presented in Figure C-10. The reactional mixture is obtained by feeding the desired gases through the streams 1 (CH_4), 2 (O_2), 3 (CO), 4 (CO and H_2) and 7 (Ar), which flow are controlled by mass flowmeters (*Brooks Series 5850E*) 1 to 5, respectively. These streams are fed to an inline inox steel mixer prepared to receive up to 10 different streams that can be combined in a single outlet flow (5 of those inlets are closed). The 3W valve connected to streams 3, 4 and 5 allows the use of CO or CO/H_2 mixture.

Stream 7 (Ar) is divided in streams 8, 9, 10 and 11. When performing test without liquid feed (water or hydrocarbons), Ar feed can be assured by stream 10, with the 4W cross-flow valve connected to this stream in "by-pass" position, meaning that Ar will not be fed to the saturator inside the thermostatic bath 1 (designed to introduce water in the system). For tests with water in the inlet gas feed, this 4W valve is changed to "saturator" position, which will result in the saturation of stream 10, corresponding to part of Ar feed to the system. The remaining Ar feed required to balance the reactional mixture is then feed by stream 11. For liquid hydrocarbons, stream 9 can be saturated by passing in the saturator inside thermostatic bath 2. Stream 8 assures Ar flow for the catalyst pre-treatment and it is fed directly to the 6W cross-flow valve.

Stream 12 becoming from the inline mixer is directed to a 3W valve. This valve is used to perform the flowmeters' calibration. Stream 13, containing the gases previously mixed, joins stream 15 that comes from the water saturator (thermostatic bath 1), resulting in stream 14 that is joined ahead with stream 16 from the hydrocarbons saturator (thermostatic bath 2). The cross element responsible for the conjunction of streams 13, 14 and 15 stills possesses an entry (which is currently closed) that can be used to add an additional stream if necessary (for instance, in case a third saturator is to be installed).

The 6W cross-flow valve is fed by three inlet streams (8 – Ar pre-treatment; 17 – reactional mixture; 19 – reactor's outlet flow) and is connected to three outlet streams (18 – reactor's inlet flow; 20 – line towards detectors; 28 – line towards extraction). Its operation mode is illustrated in Figure C-8. Depending on the position of 6W valve, stream 17 that contains the reactional mixture can be directed to the reactor through stream 18 – "Reactor" position – or can by-pass the reactor directly to detectors through stream 20 – "By-pass" position. Likewise, depending on the 6W valve position, stream 8 can feed Ar pre-treatment directly to the reactor throughout stream 18 – "By-pass" position – or directly to the exhaust – "Reactor" position. Stream 20 receives the reactional mixture (stream 17) – "By pass" position – or the reactor's outlet flow (stream 19) – "Reactor" position.

The reactors used in this plant were Pyrex U-shape reactors, 23 cm long and with internal diameter of 2 cm in the reactional chamber, where a porous quartz filter (porous type nr. 3) retains the catalyst.

Stream 20 is divided in streams 21 and 22. The latter goes to the detectors, including FID (for hydrocarbons) in parallel with three other detectors in series: two infrared detectors for CO/CO_2 and N_2O and a chemiluminescence detector for NO/NO_2. When the mass spectrometer is to be used, the cut valve in stream 21 shall be opened allowing a fraction of the gas to reach the MS. The remaining gas goes to stream 22, which is connected to a 4W cross-flow valve. When the detectors are being used, gas go to stream 23, passing through the detectors and ending in the exhaust (stream 24). If the detectors are not to be used (for instance, in cases where only the MS is required), gases from stream 22 go directly to the exhaust (stream 26). In this case, stream 25 assures that the detectors receive continuously gas flow even when are not being used, namely, atmospheric air (stream 25), avoiding depression in the lines that could jeopardise the equipment.

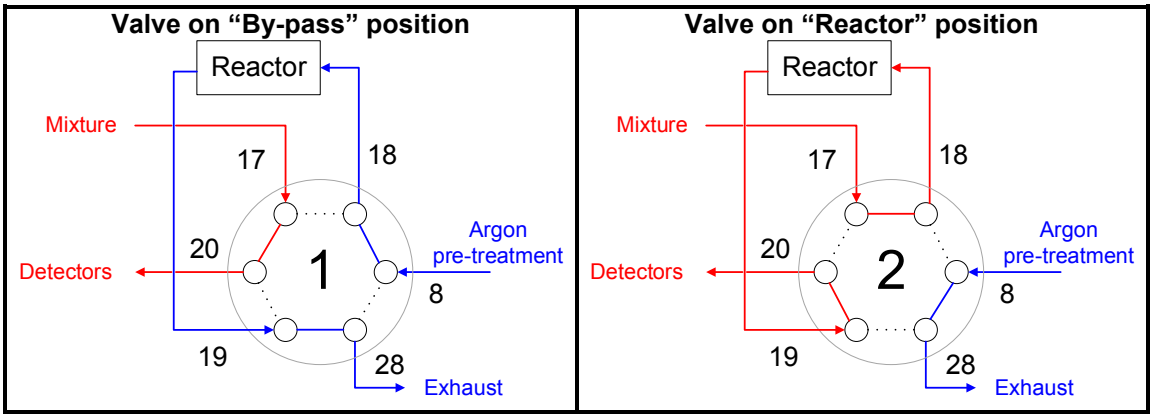

Figure C-8 – Schematic representation of 6W cross-flow valves operation.

Table C-4 summarises the gases currently available in IJLRDA's $deNO_x$ plant and Table C-5 summarises the detectors installed in the plant. A frontal view of the plant is exhibited in Figure C-9.

Table C-4 – List of gases used in IJLRDA's $deNO_x$ plant.

Compound	Bottle (*Air Liquide*)
NO	NO (1%) / Ar
CH_4	CH_4 (1.5%) / Ar
CO	CO (1%) / Ar
CO/H_2	CO (3%) / H_2 (2%) / Ar
O_2	Alphagaz 1
Ar	Alphagaz 1

Table C-5 – List of gases used in IJLRDA's $deNO_x$ plant.

Compound	Detector
NO/NO_2	*Eco Physics CLD 700 AL*, chemiluminescence analyser
CO/CO_2	*Siemens Ultramat 9*, infrared analyser
N_2O	*Siemens Ultramat 9*, infrared analyser
HC	*Siemens FIDAMAT 5E*, flame ionisation detector (FID)
Several	Pfeiffer Vacuum GSD 301 C, mass spectrometer (MS)

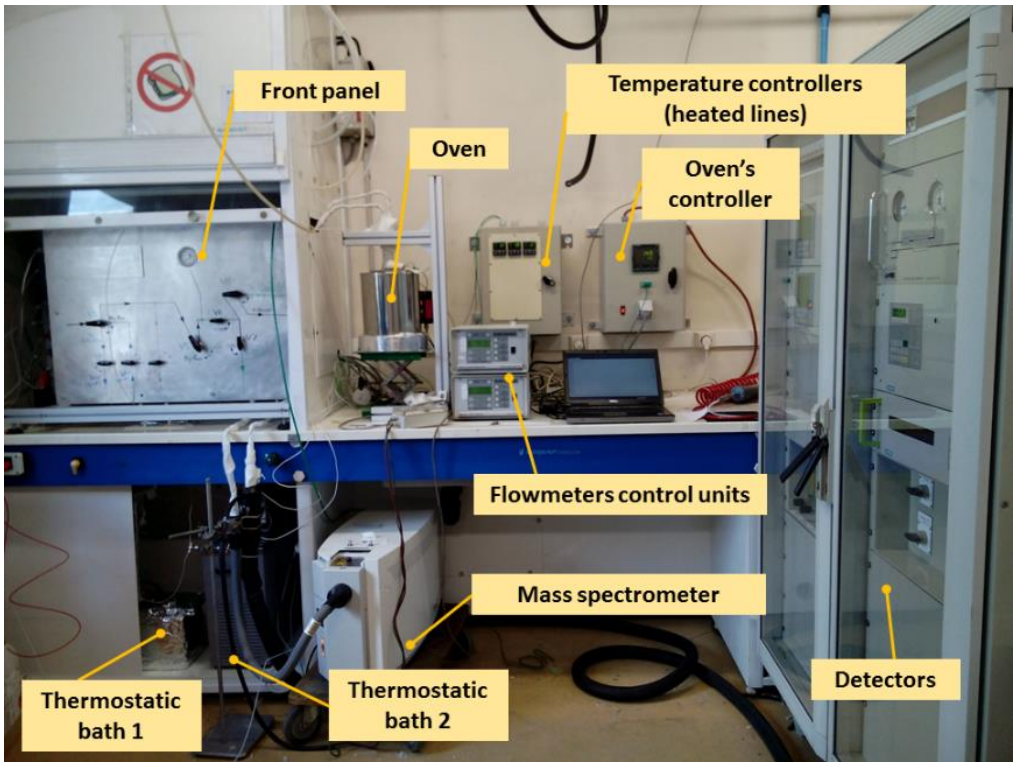

Figure C-9 – Picture of $deNO_x$ plant for powder catalysts available at IJLRDA (UPMC, Saint-Cyr).

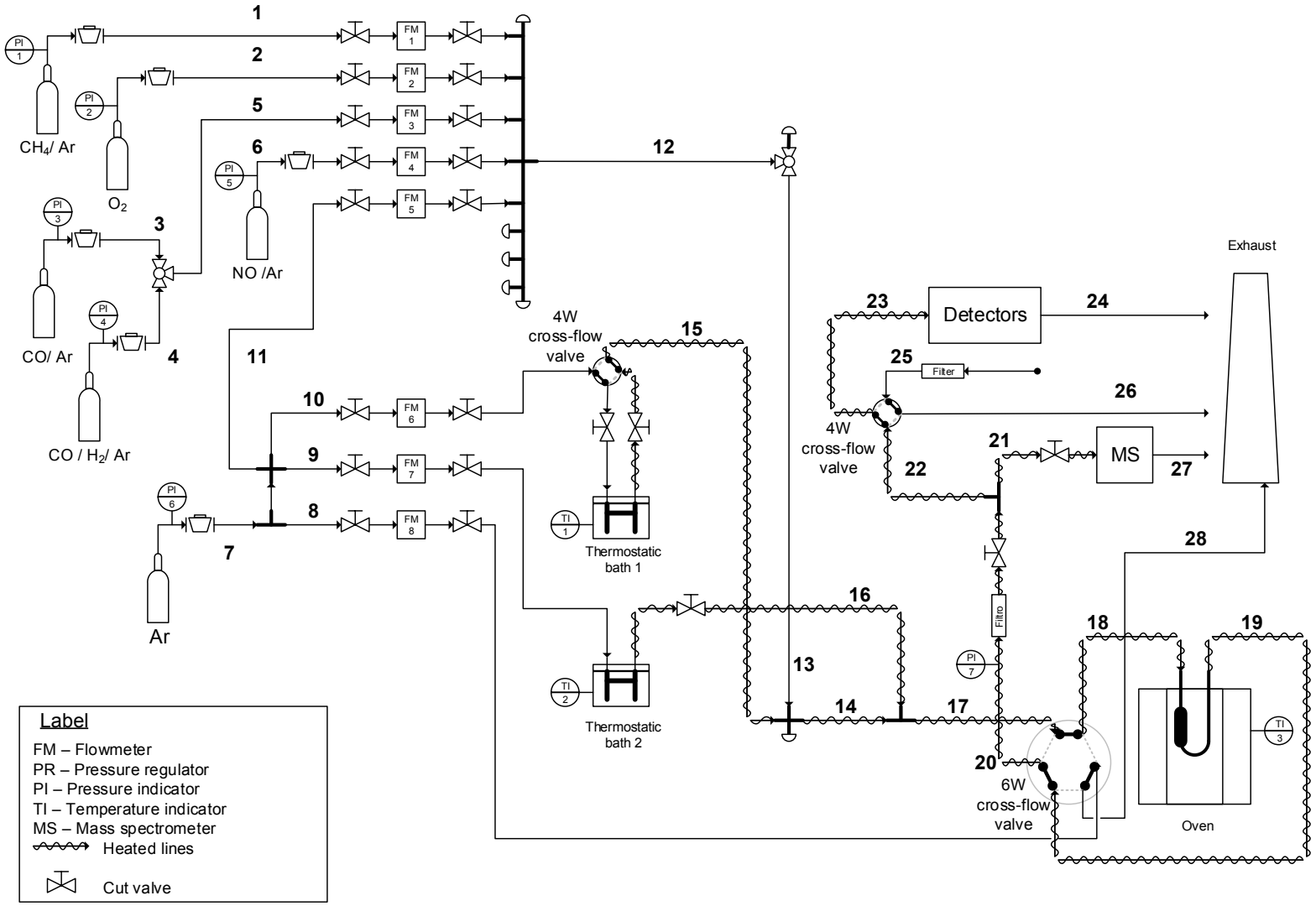

Figure C-10 – Schematic representation of deNO$_x$ plant available at IJLRDA (UPMC, Saint-Cyr).

C.3.3. IJLRDA's synthetic gas bench plant (monolith catalysts)

The schematic representation of the IJLRDA's synthetic gas bench (SGB) plant is presented in Figure C-13. The reactional mixture is obtained by feeding the desired gases through the streams 1 (CO), 2 (C_3H_6), 3 (O_2), 4 (NO), 5 (NO_2), 6 (CO_2) and 7 (N_2), which flows are controlled by mass flowmeters (*Brooks*) 1 to 7, respectively. These streams are fed to an inline inox steel mixer prepared to receive up to 11 different streams that can be combined in a single outlet flow (four of these inlets are closed). The stream resulting from the combination of all gases (stream 9) enters the evaporator, in where liquid water can also be fed and vaporised (stream 8). The resulting stream 10 is then redirected to a 3-way valve which allows to by-pass the reactor (streams 16), or it is redirected to the pre-heater and then reactor (streams 11, 13, 14 and 15), resulting in stream 17. The pre-heater ensures a proper heating of the mixture before entering the reactor and avoids situations where the temperatures upstream and downstream the monolith (registered by temperature indicators TI 4 and 5, respectively) are very different. This configuration is required due to significantly higher gas flow, compared to the laboratory plants for powders (typically, 8.5 L/min in SGB plant against 15 L/h in deNO_x plants for powders).

This one can be directly sent to the exhaust (for instance, during a pre-treatment procedure) using stream 18 or sent to the detectors (stream 19) , going afterwards to the exhaust (stream 20).

Figure C-11 illustrates the operation of the two 3W valves that allows to send the gas mixture to the reactor or to by-pass it. The by-pass configuration is used to record the initial concentration of the gas feed, prior to the test.

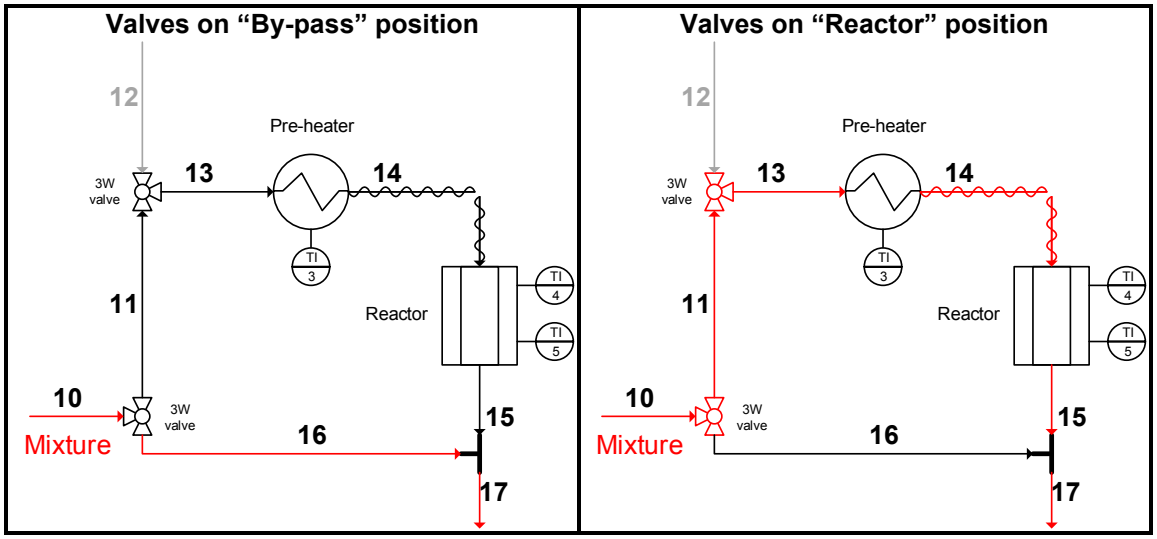

Figure C-11 – Schematic representation of the two 3W valves operation in IJLRDA's SGB plant.

Contrarily to the other gas plants (powder catalysts), it is not possible to perform the stabilisation of the inlet feed mixture during while performing a pre-treatment. In case a pre-treatment is intended to be performed in the monolith, the "reactor" position needs to be adopted and the pre-treatment gas needs to be fed using the same line also used for the reactional mixture.

The system is also equipped with a compressed air line that allows to cool down the pre-heater and reactor faster (see Figure C-12).

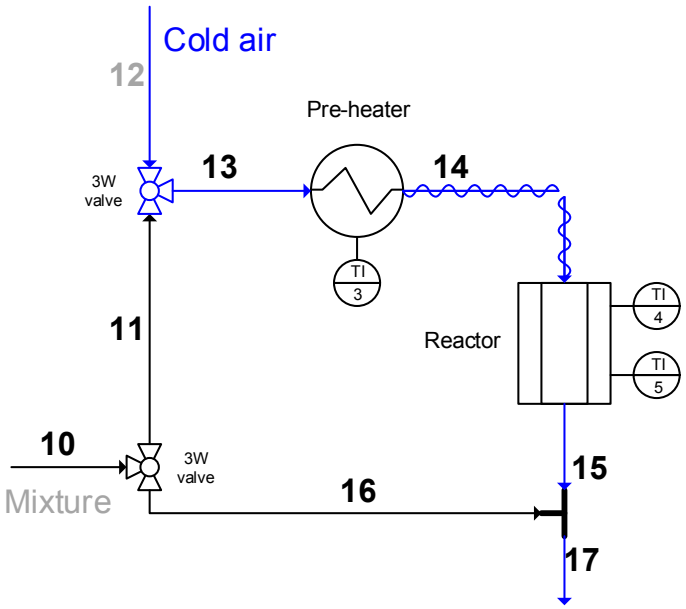

Figure C-12 – Schematic representation of IJLRDA's SGB plant during cooling down with compressed air.

Table C-6 summarises the gases currently available in IJLRDA's SGB plant and Table C-7 summarises the detectors installed in the plant.

Table C-6 – List of gases used in IJLRDA's SGB plant.

Compound	Bottle (*Air Liquide*)
NO	NO (8000 ppm) / N_2
NO_2	NO (8000 ppm) / N_2
CH_4	CH_4 (1%) / N_2
C_3H_6	C_3H_6 (5%) / N_2
CO	CO (3500 ppm) / N_2
CO_2	Alphagaz 1
H_2	Alphagaz 1
O_2	Alphagaz 1
N_2	Alphagaz 1

Table C-7 – List of gases used in IJLRDA's SGB plant.

Compound	Detector
NO/NO_2	*Environnment SA TOPAZE 32M*, chemiluminescence analyser
$CO/CO_2/ N_2O/O2$	*Environnment SA MIR 2M*, infrared analyser
HC	*Environnment SA GRAPHITE 52M*, flame ionisation detector (FID)

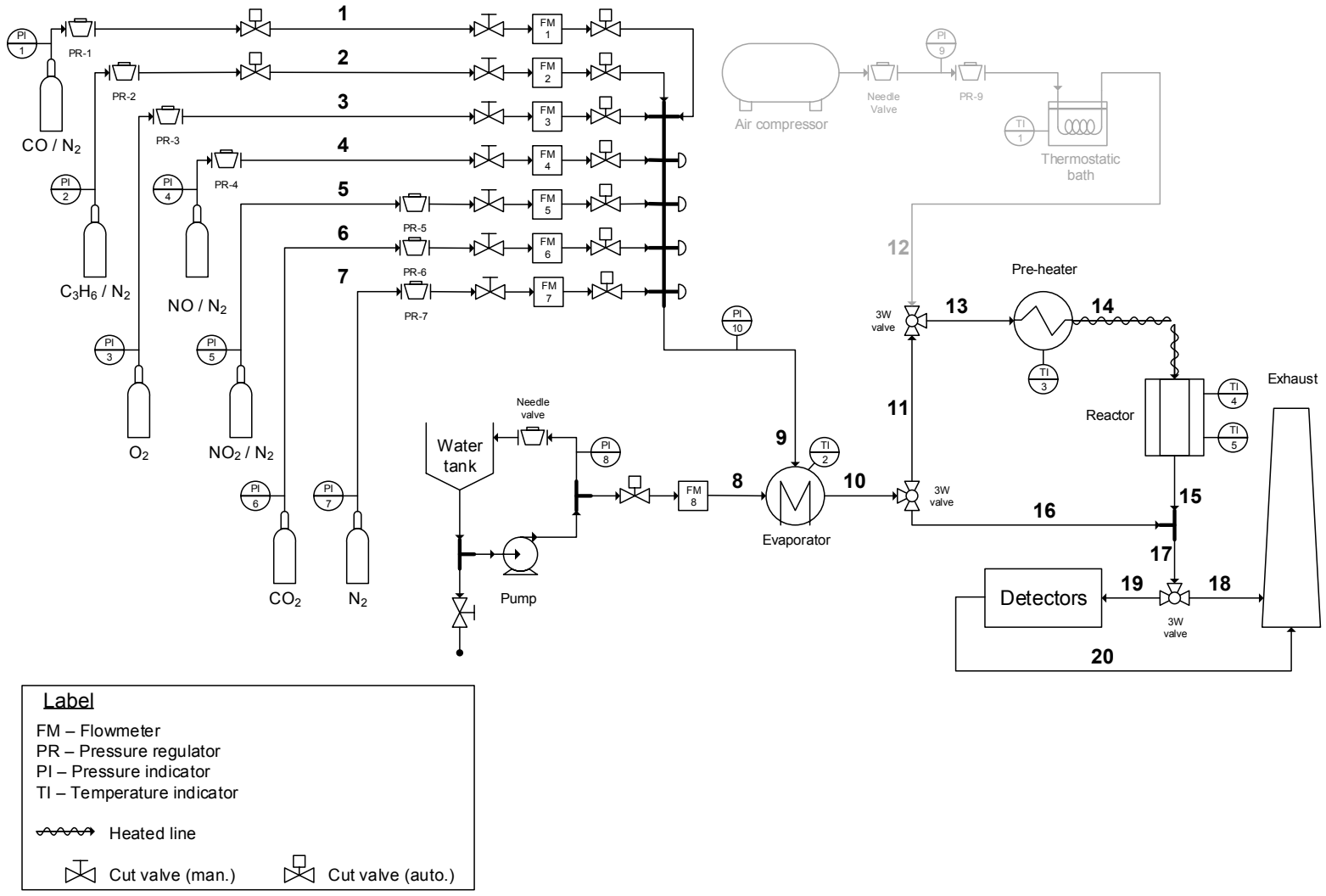

Figure C-13 – Schematic representation of synthetic gas bench (SGB) plant available at IJLRDA (UPMC, Saint-Cyr).

C.3.4. Catalytic test procedure for steady-state tests (powder catalysts)

The procedure described herein was the procedure adopted when both deNO$_x$ plants (at CATHPRO and IJLRDA) were used for tests considering powder formulations.

Catalytic tests were performed using a mass of catalyst (m_{catal}) of *ca.* 190 mg of catalyst (dry basis) corresponding to a gas hourly space velocity (GHSV) of 40000 h^{-1}, which was calculated considering a total gas flow (F) of 15 L/h and apparent density of the catalyst (d_{catal}) of 0.5 g/mL (measured for HMOR), according the equation (C-2).

$$\mathrm{GHSV} = \frac{F.\,d_{catal}}{m_{catal}} \qquad \text{(C-2)}$$

Before the reaction, a pre-treatment was performed in order to clean the catalysts' surface, consisting in heating the catalyst under argon flow (15 L/h), from room temperature to 500 ºC (5 ºC/min) and keeping this temperature for 1 h. Then, the reactor was cooled to 300 ºC. Meanwhile, the reaction mixture was stabilised in a reactor by-pass. Once stable, the reaction mixture was fed to the reactor. When the steady state was reached, the temperature was raised 50 ºC and the procedure was repeated until 500 ºC. Once stable, the temperature was decreased for 300 ºC and kept until steady-state was reached (returning-point temperature). Afterwards, the mixture was put in by-pass to the reactor and the signals were recorded (second by-pass point) at the same time that the reactor was cooled down under flowing argon, until room temperature.

For each temperature *T*, NO$_x$ conversion into N$_2$ was obtained using equation (C-3), CH$_4$ conversion into CO$_2$ was obtained using equation (C-4) and CH$_4$ selectivity to SCR reaction was obtained using equation (C-5).

$$x_{NO_x\,\mathrm{into}\,N_2,T}(\%) = \left(1 - \frac{n_{NO,T} + n_{NO_2,T} + 2\,n_{N_2O,T}}{n_{NO,0} + n_{NO_2,0}}\right) \times 100\% \qquad \text{(C-3)}$$

$$x_{CH_4\,into\,CO_2,T}(\%) = \frac{n_{CO_2,T}}{n_{CH_4,0}} \times 100\% \qquad \text{(C-4)}$$

$$S_{CH_4\,to\,SCR,T}(\%) = \frac{n_{CH_4\,for\,SCR,T}}{n_{CH_4\,converted,T}} = \frac{1}{2}\frac{n_{NO,0} + n_{NO_2,0} - (n_{NO,T} + n_{NO_2,T} + 2\,n_{N_2O,T})}{n_{CH_4,0} - (n_{CO_2,T} + n_{CO,T})} \times 100\% \qquad \text{(C-5)}$$

0 represents the initial condition (by-pass mixture) before starting the reaction.

C.3.5. Catalytic test procedure for temperature-programmed tests (powder catalysts)

The procedure described herein was the procedure adopted when both deNO$_x$ plants (at CATHPRO and IJLRDA) were used for tests considering powder formulations.

Catalytic tests were performed using a mass of catalyst (m_{catal}) of *ca.* 190 mg of catalyst (dry basis) corresponding to a gas hourly space velocity (GHSV) of 40000 h^{-1}, which was calculated considering a total gas flow (F) of 15 L/h and apparent density of the catalyst (d_{catal}) of 0.5 g/mL (measured for HMOR), according the equation (C-6).

$$\mathrm{GHSV} = \frac{F.d_{catal}}{m_{catal}} \qquad \text{(C-6)}$$

Before the reaction, a pre-treatment was performed in order to clean the catalysts' surface, consisting in heating the catalyst under argon flow (15 L/h), from room temperature to 500 ºC (5 ºC/min) and keeping this temperature for 1 h. Then, the reactor was cooled to room temperature. Meanwhile, the reaction mixture was stabilised in a reactor by-pass. Once stable, the reaction mixture was fed to the reactor and a heating ramp of 10 ºC/min was applied until 500 ºC/min. This temperature kept until the steady state was reached. Afterwards, the mixture was put in by-pass to the reactor and the signals were recorded (second by-pass point), at the same time that the reactor was cooled down under flowing argon, until room temperature.

C.3.6. Catalytic test procedure for temperature-programmed tests (monolith catalysts)

The procedure described herein was the procedure adopted when SGB plant was used for tests considering monolith formulations.

Catalytic tests were performed using a cylindrical monolith with same height and diameter (1 in), previously washcoated catalyst, according to the procedure described in Chapter V. A gas hourly space velocity (GHSV) of 40000 h^{-1} was considered, which was calculated assuming a total gas flow (F) of 8.58 L/min and volume of catalyst (V_{catal}) of 12.9 mL, according the equation (C-7).

$$\mathrm{GHSV} = \frac{F}{V_{catal}} \qquad \text{(C-7)}$$

First, the reaction mixture was stabilised in a reactor by-pass. Once stable, the reaction mixture was fed to the reactor and a heating ramp of 10 ºC/min was applied until 550 ºC/min, in both reactor and pre-heater. Once the final temperature was reached, the mixture was put in by-pass to the reactor and the signals were recorded (second by-pass point). After the by-pass, the pre-heater and reactor were cooled down using compressed air until room temperature.

Annex D. Validation of Experimental Methodologies

In this annex are presented the results considered for the validation of the catalytic test performed in this work (repeatability and reproducibility), as well as the catalyst preparation procedure (repeatability).

D.1. Repeatability of steady-state catalytic tests

In order to evaluate the repeatability of the steady-state catalytic tests considered in this work, two different samples of the batch of Pd(0.5)-HMOR catalysts were test for NO_x CH_4-SCR, under the standard conditions considered in this work, following the protocol described in Annex A (section C.3.4) for steady-state catalytic test, performed in the CATHPRO's deNO_x plant (IST, Lisbon). The results are illustrated in Figure D-1.

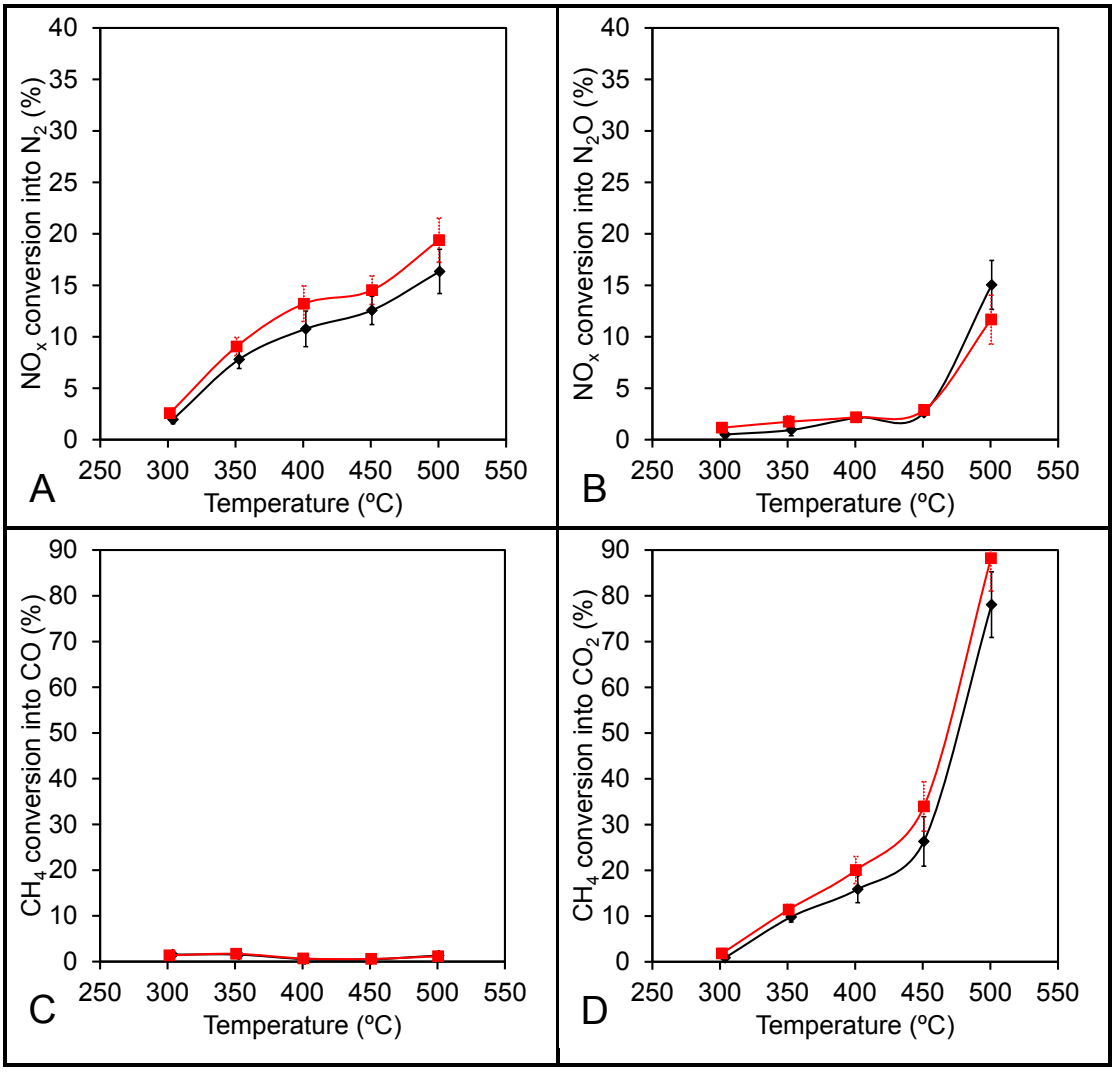

Figure D-1 – NO_x conversion into N_2 (A) and N_2O (B) and CH_4 conversion into CO (C) and CO_2 (D) for two different samples of Pd(0.5)-HMOR from the same batch. Conditions: 1000 ppm NO, 1000 ppm CH_4, 7% O_2 and GHSV of 40000 h^{-1}.

For each temperature, the absolute standard deviation for the NO_x conversion into N_2 and N_2O and CH_4 conversion into CO and CO_2 registered in the two tests was calculated. The values are presented in Table D-1.

Table D-1 – Absolute standard deviation of NO_x and CH_4 conversions for Pd(0.5)-HMOR.

T (ºC)	NO_x conv. into N_2 (%)	NO_x conv. into N_2O (%)	CH_4 conv. into CO (%)	CH_4 conv. into CO_2 (%)
300	0	0	0	1
350	1	1	0	1
400	2	0	0	3
450	1	0	0	5
500	2	2	0	7

The standard deviation for NO_x conversion is (both to N_2 and N_2O) exhibit very low value (below 3%), which means that the test results are reproducible. Notwithstanding, CH_4 conversion, namely into CO_2, exhibits higher standard deviations between the three tests.

The same procedure was used considering two different sample of the same batch of Pd(0.3)Ce(10)-HMOR. The results are presented in Figure D-2 and the absolute standard deviations for NO_x and CH_4 conversions are listed in Table D-2.

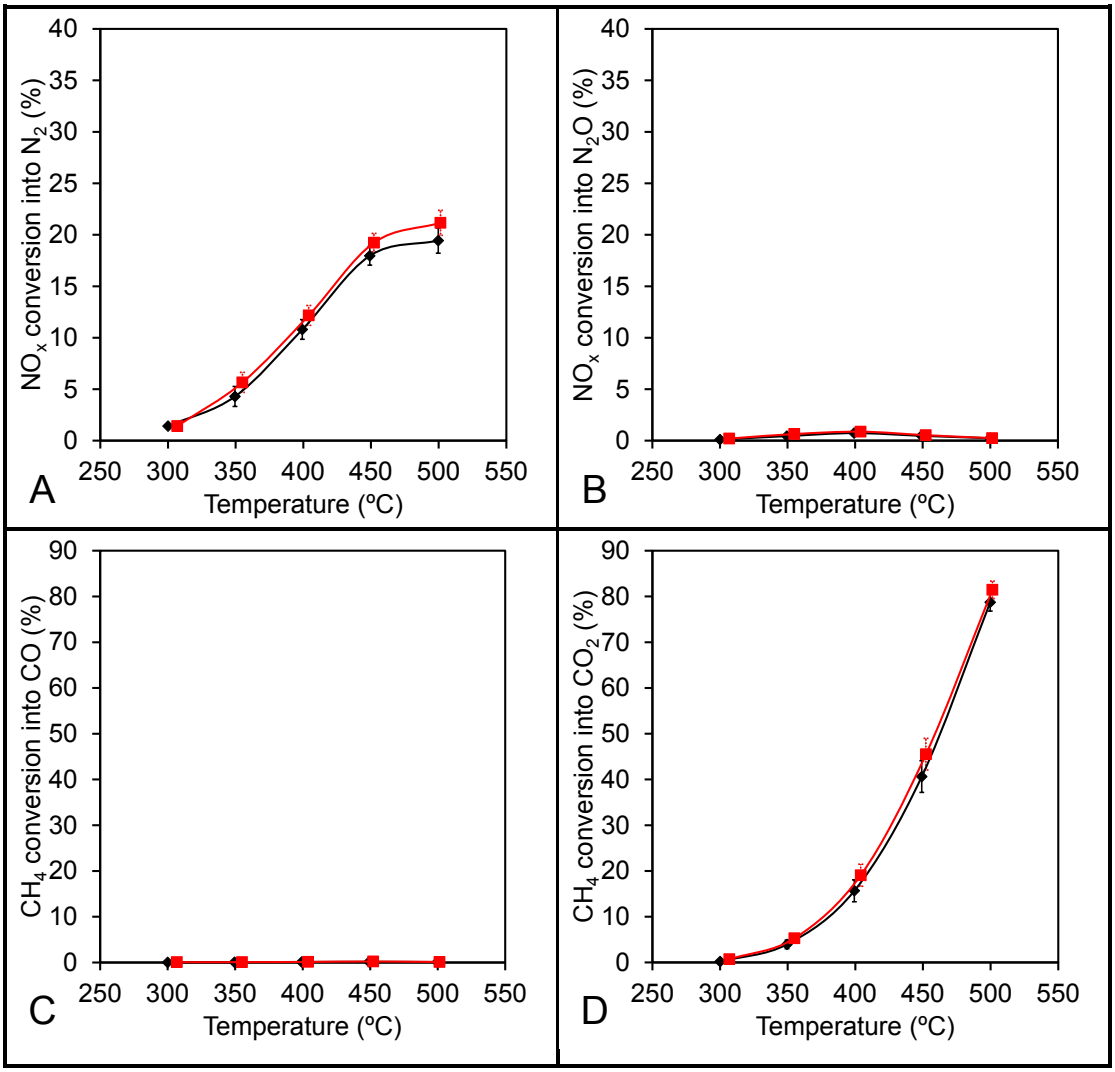

Figure D-2 – NO_x conversion into N_2 (A) and N_2O (B) and CH_4 conversion into CO (C) and CO_2 (D) for two different samples of Pd(0.3)Ce(10)-HMOR from the same batch. Conditions: 1000 ppm NO, 1000 ppm CH_4, 7% O_2 and GHSV of 40000 h^{-1}.

Table D-2 – Absolute standard deviation of NO_x and CH_4 conversions for Pd(0.3)Ce(10)-HMOR.

T (ºC)	NO_x conv. into N_2 (%)	NO_x conv. into N_2O (%)	CH_4 conv. into CO (%)	CH_4 conv. into CO_2 (%)
300	0	0	0	0
350	1	0	0	1
400	1	0	0	2
450	1	0	0	3
500	1	0	0	2

D.2. Repeatability of catalyst preparation of PdCe-HMOR catalysts

In order to assess the repeatability of the catalyst preparation, three different batches of Pd(0.3)Ce(2)-HMOR catalysts were prepared by introduction 0.3 wt.% Pd by ion-exchange (standard procedure, Annex A, section C.1.2) and, then, 2 wt.% Ce by incipient wetness impregnation (Annex A, section C.1.3). Samples of the three batches were tests under the standard conditions considered in this work, following the protocol described in Annex A (section C.3.4). The results are illustrated in Figure D-3.

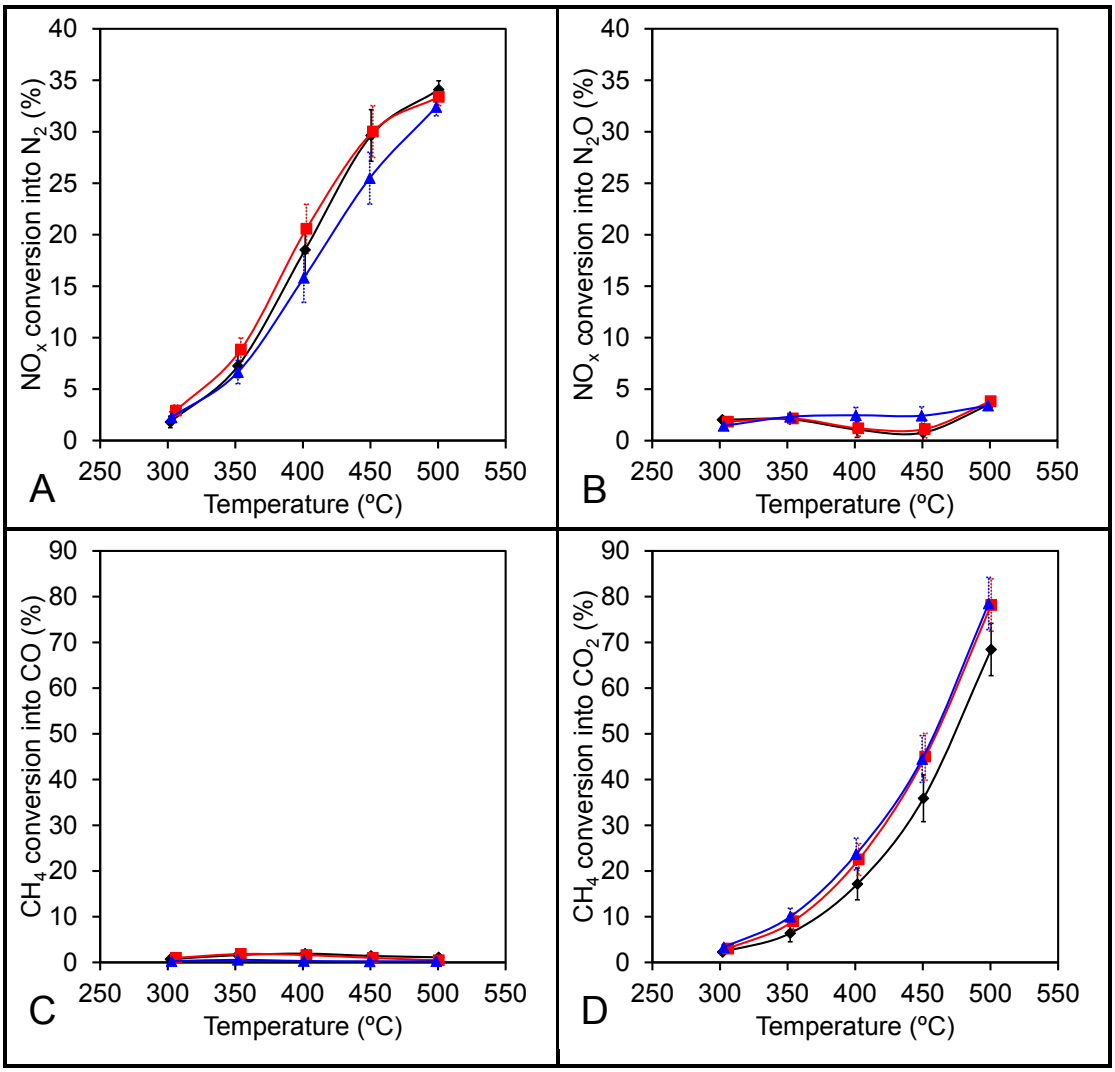

Figure D-3 – NO_x conversion into N_2 (A) and N_2O (B) and CH_4 conversion into CO (C) and CO_2 (D) for samples of Pd(0.3)Ce(2)-HMOR from three different batches. Conditions: 1000 ppm NO, 1000 ppm CH_4, 7% O_2, 2 vol.% H_2O and GHSV of 40000 h^{-1}.

For each temperature, the absolute standard deviation for the NO_x conversion into N_2 and N_2O and CH_4 conversion into CO and CO_2 registered in the two tests was calculated. The values are presented in Table D-3.

Table D-3 – Absolute standard deviation of NO_x and CH_4 conversions for Pd(0.3)Ce(2)-HMOR from three different batches.

T (ºC)	NO_x conv. into N_2 (%)	NO_x conv. into N_2O (%)	CH_4 conv. into CO (%)	CH_4 conv. into CO_2 (%)
300	1	0	0	1
350	1	0	1	2
400	2	1	1	3
450	3	1	1	5
500	1	0	0	6

It is possible to see observe that these values are in line with the standard deviations obtained for the catalytic tests using the same catalyst. Hence, one can conclude that the catalyst preparation procedure is repeatable.

D.3. Reproducibility of steady-state catalytic tests

In these work, two different deNO$_x$ plants for powder formulations were used: CATHPRO's deNO$_x$ plant and IJLRDA's deNO$_x$ plant (see Annex A, sections C.3.1 and C.3.2, respectively). The majority of the catalytic test were performed in CATHPRO's deNO$_x$ plant and only the studies involved mixtures considering CO in the mixture (*i.e.* the ones representative of real exhaust gas conditions) were performed in IJLRDA's deNO$_x$ plant. In order to evaluate the reproducibility of the steady-state catalytic tests results obtained in both plants, Pd(0.3)Ce(2)-HMOR catalyst was tested according to procedure following the protocol described in Annex A (section C.3.4). The results are illustrated in Figure D-4 (N_2O and CO formation are negligible).

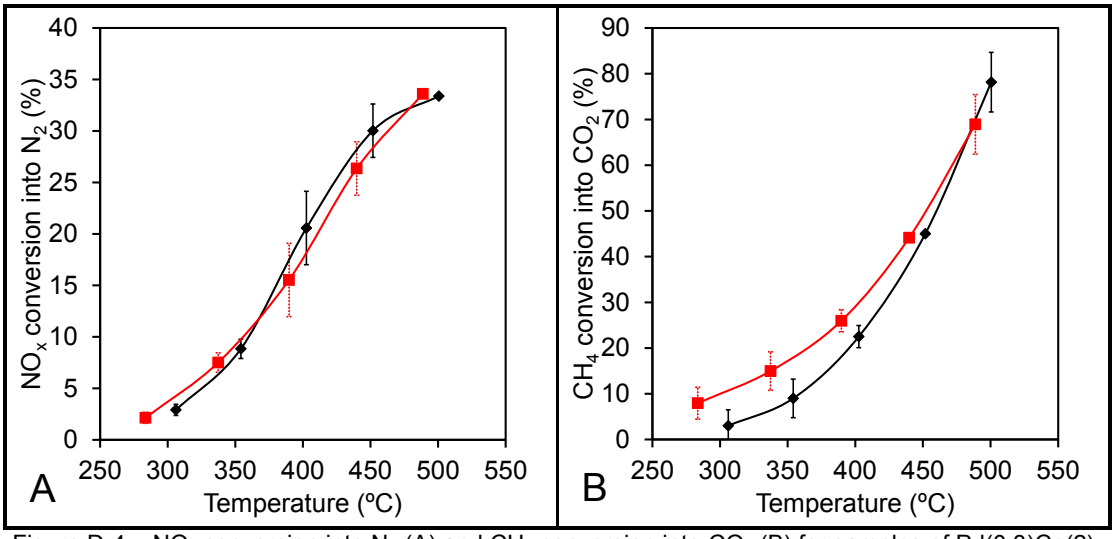

Figure D-4 – NO_x conversion into N_2 (A) and CH_4 conversion into CO_2 (B) for samples of Pd(0.3)Ce(2)-HMOR tested in both deNOx plants: CATHPRO (♦) and IJLRDA (■). Conditions: 1000 ppm NO, 1000 ppm CH_4, 7% O_2 and GHSV of 40000 h^{-1}.

For each temperature, the absolute standard deviation for the NO_x conversion into N_2 and CH_4 conversion into CO_2 registered in the two tests was calculated. The values are presented in Table D-3.

Table D-4 – Absolute standard deviation of NO_x and CH_4 conversions for Pd(0.3)Ce(2)-HMOR tested in both CATHPRO's and IJLRDA's deNO$_x$ plant.

T (ºC)	NO_x conv. into N_2 (%)	CH_4 conv. into CO_2 (%)
300	1	3
350	1	4
400	4	2
450	3	1
500	0	7

It is possible to see observe that these values are in line with the standard deviations obtained for checking the repeatability of the steady-state catalytic tests (see section D.1). Hence, one can conclude that the catalytic tests results obtained in the different plants are reproducible.

Annex E. Calculation of apparent activation energy of NO_x CH_4-SCR on Pd(0.3)Ce(2)-HMOR

The apparent activation energy (E_a) depends is dependent on the reaction conditions considered and the catalyst. In this work, E_a was calculated for Pd(0.3)Ce(2)-HMOR, considering the reaction conditions 1000 ppm NO, 1000 ppm CH_4 and 7% O_2. NO CH_4-SCR reaction is given by equation (C-2).

$$2\,\mathrm{NO} + \mathrm{CH_4} + 2\,\mathrm{O_2} \rightarrow \mathrm{N_2} + CO_2 + 2\,\mathrm{H_2}O \qquad \text{(E-1)}$$

Kinetic equation for the reaction is given by equation (E-2).

$$\mathrm{r} = \mathrm{k} C_{NO}^{\alpha} C_{CH_4}^{\beta} C_{O_2}^{\gamma} \qquad \text{(E-2)}$$

k is the kinetic constant and α, β and γ are the reaction constants of NO, CH_4 and O_2, respectively. These parameters are not known and, hence, the reaction rate (r) cannot be determined. Nevertheless, the initial reaction rate (r_0) can be estimated experimentally by obtaining the NO conversion for the different contact times close to zero. In this case, r_0 corresponds to the slope of the line tangent to the conversion curve that passes in the plot's origin.

The reaction performed was at three different temperatures (350, 400 and 450 ºC), considering three different contact times, corresponding to gas hourly space velocities (GHSV) of 40000, 100000 and 150000 h^{-1}. The results are presented in Figure C-12.

For the initial time, the kinetic equation (E-2) can be expressed by (E-3).

$$\mathrm{r}_0 = \mathrm{k}_0 \exp\left(-\frac{E_a}{RT}\right) C_{NO,0}^{\alpha} C_{CH_4,0}^{\beta} C_{O_2,0}^{\gamma} \qquad \text{(E-3)}$$

By applying logarithm to both terms of the equation, one can obtain an expression of log r_0 as a function of $1/T$ (equation (E-4)).

$$\log \mathrm{r}_0 = -\frac{E_a}{R}\frac{1}{T} + \log\left(\mathrm{k}_0 C_{NO,0}^{\alpha} C_{CH_4,0}^{\beta} C_{O_2,0}^{\gamma}\right) \qquad \text{(E-4)}$$

R (8.3145 J/(mol.K)) is the perfect gas constant and T is the temperature. The term $\log\left(\mathrm{k}_0 C_{NO,0}^{\alpha} C_{CH_4,0}^{\beta} C_{O_2,0}^{\gamma}\right)$ is a constant and, hence, a linear correlation can be obtained for log (r_0) as a function of $1/T$. Table E-1 contains the values of log (r_0) and $1/T$ used in the determination of E_a, obtained by linear regression (Figure E-2)

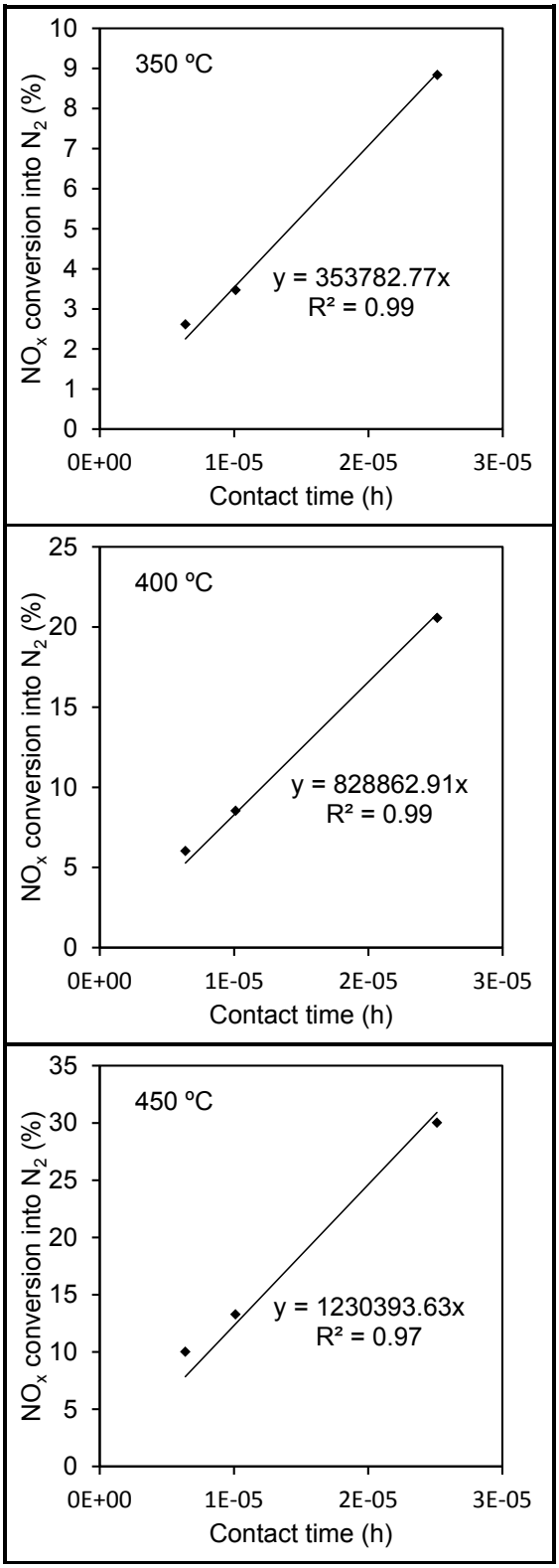

Figure E-1 – NO_x conversion into N_2 over Pd(0.3)Ce-HMOR considering different temperatures and GHSV. Conditions: 1000 ppm NO, 1000 ppm CH_4 and 7% O_2.

Table E-1 – log (r_0) and 1/T values used in the calculation of E_a.

T (ºC)	r_0	1/T (K^{-1})	log (r_0)
350	353783	0.001605	5.55
400	828863	0.001486	5.92
450	1230394	0.001383	6.09

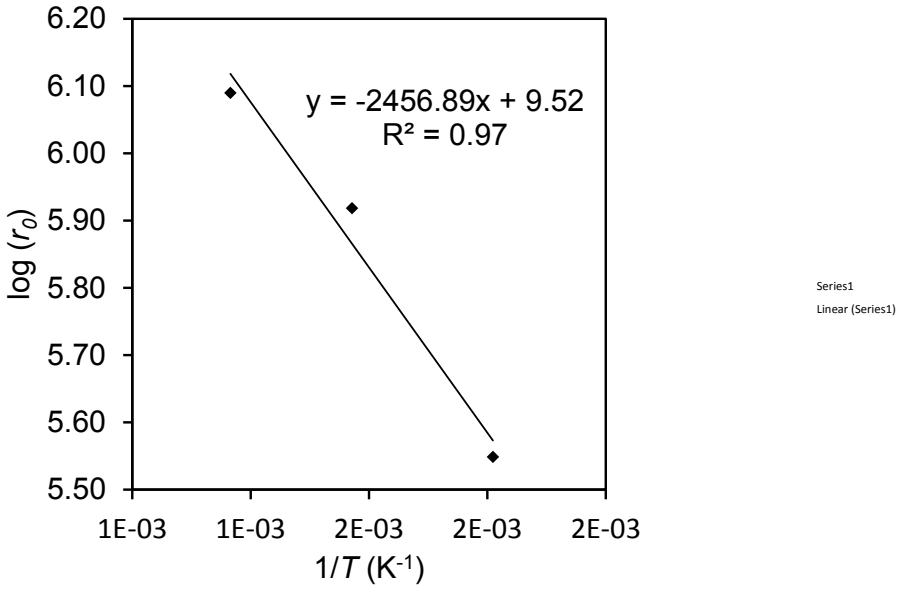

Figure E-2 – log(r_0) *vs.* 1/T and respective linear regression.

E_a activation for the reaction over Pd(0.3)Ce(2)-HMOR is obtained from equation (E-5).

$$-\frac{E_a}{R} = -2456.89 \Leftrightarrow E_a \approx 20.4\ kJ/mol \qquad \text{(E-5)}$$

This value has the same order of magnitude of apparent activation energy reported in the literature for NO reduction over an zeolite-based catalysts, for instance, In-MFI (10 kJ/mol) [30].

Annex F. Further results on transmission electron microscopy (TEM/EDS)

In this annex, further results of TEM/EDS obtained for MOR and BEA series catalysts are presented.

F.1. MOR series

F.1.1. Catalyst Pd(0.3)-HMOR

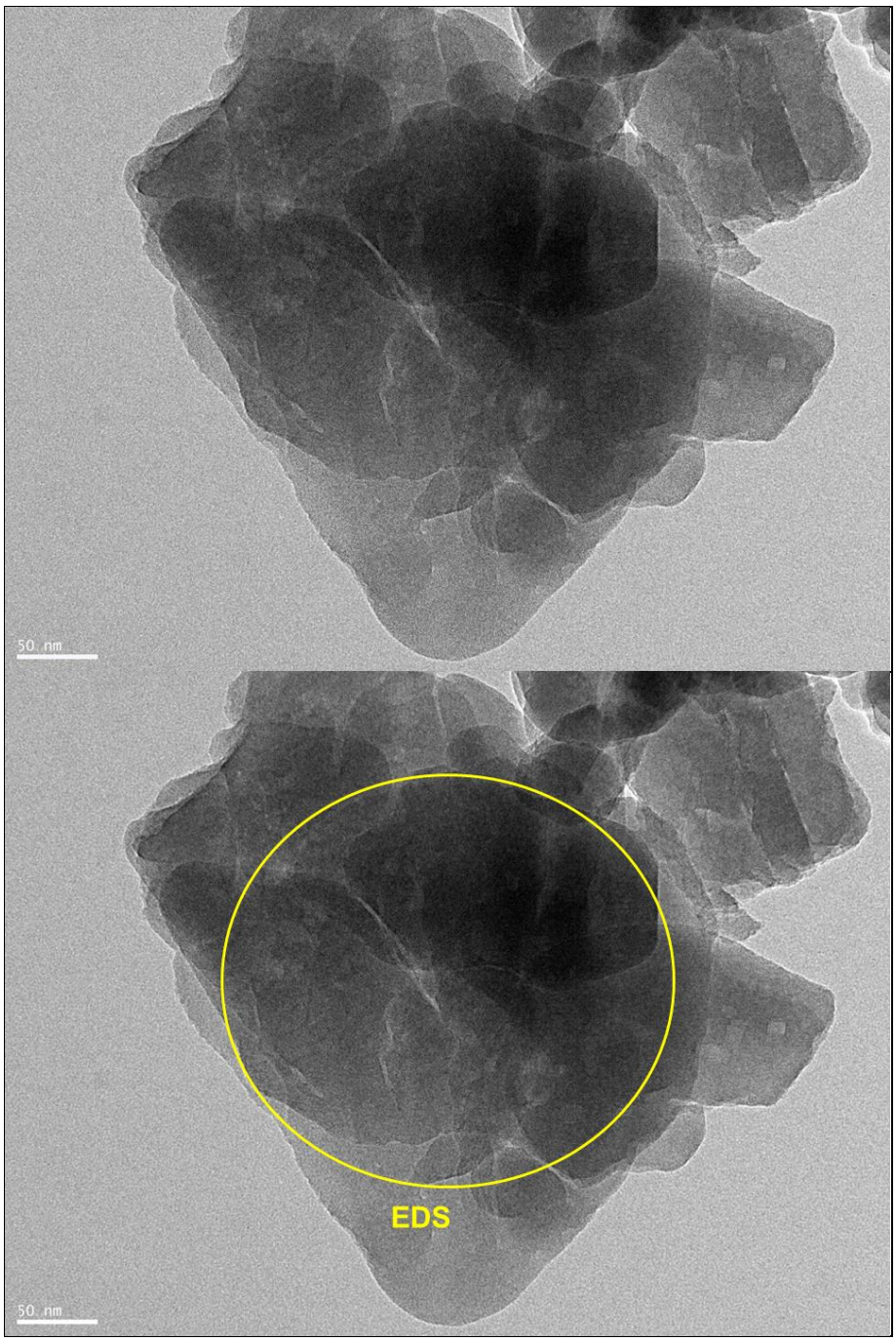

Figure F-1 – TEM image of Pd(0.3)-HMOR, highlighting the region where EDS was performed.

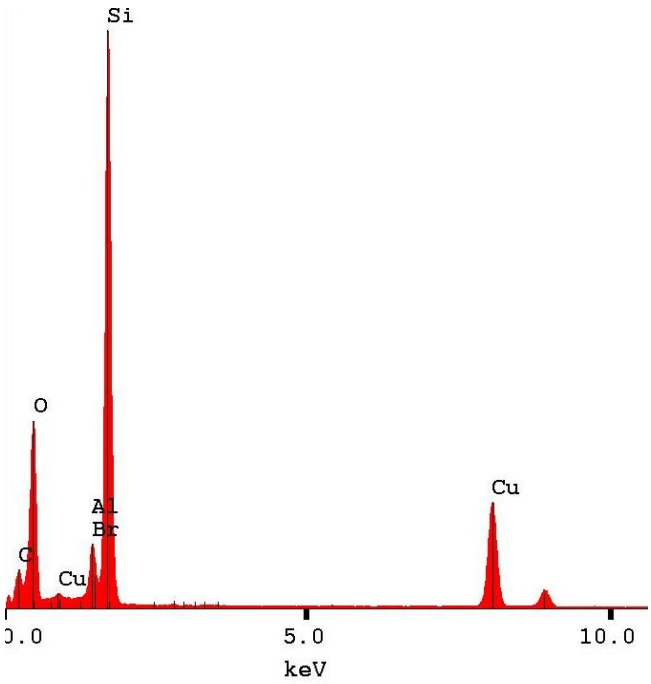

Figure F-2 – EDS spectrum of Pd(0.3)-HMOR corresponding to region highlighted in Figure F-1.

F.1.2. Catalyst Pd(0.3)Ce(2)-HMOR

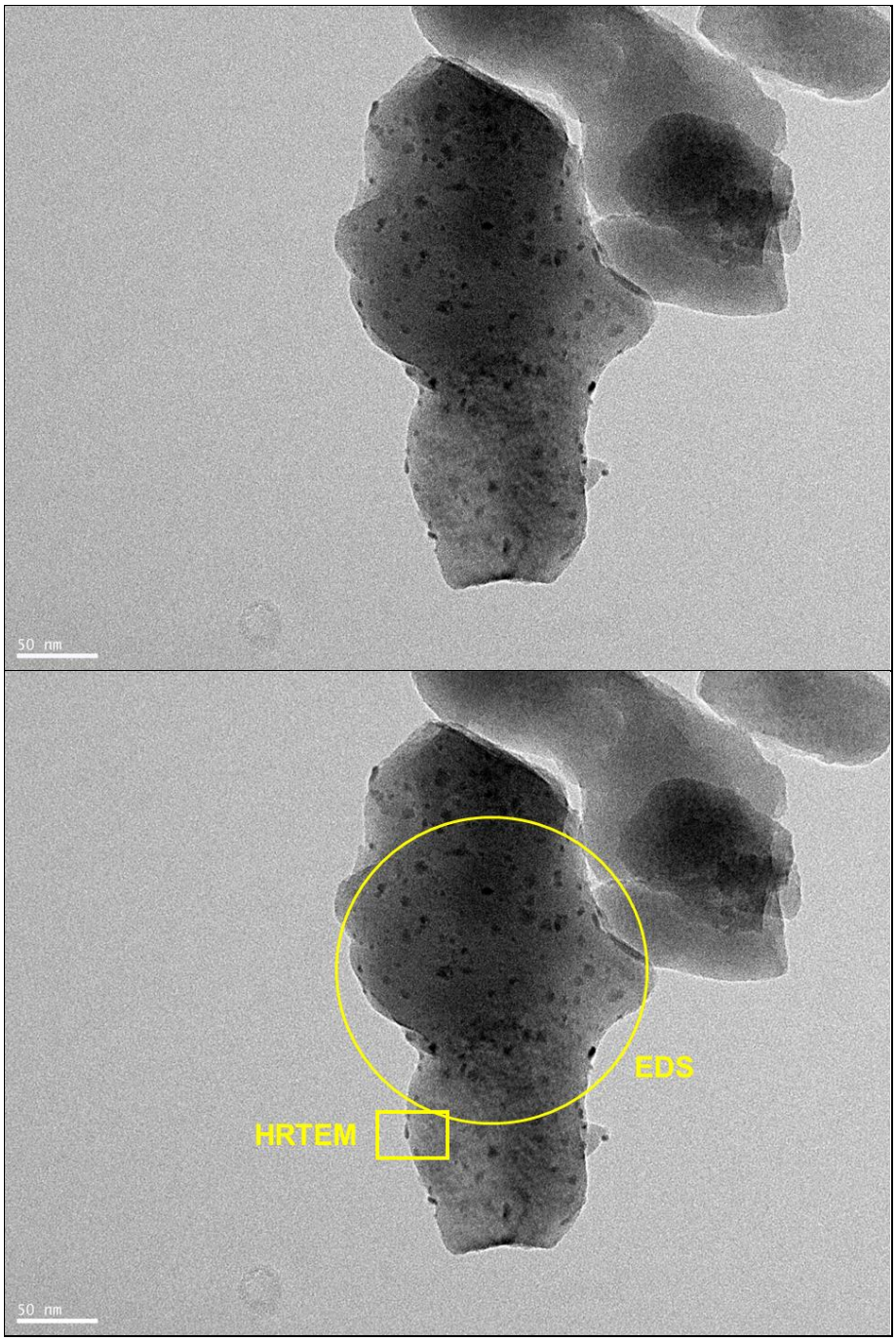

Figure F-3 – TEM image of Pd(0.3)Ce(2)-HMOR, highlighting the regions where EDS and HRTEM were performed.

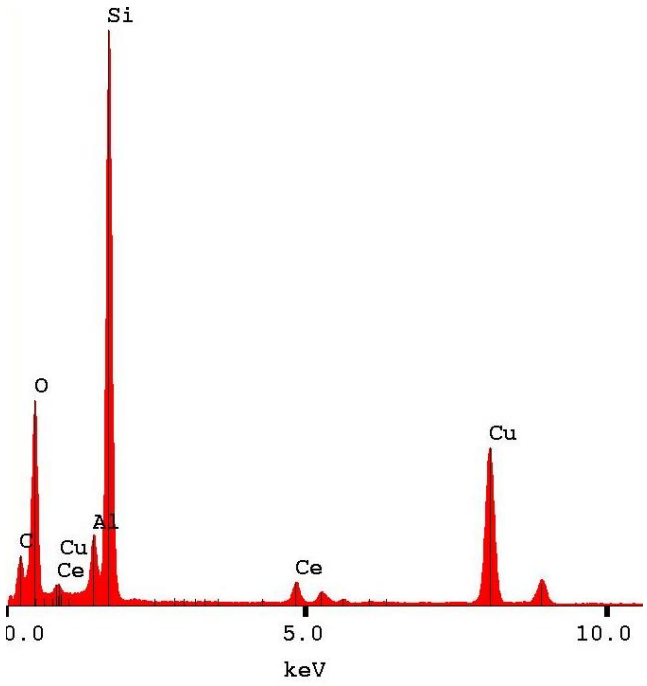

Figure F-4 – EDS spectrum of Pd(0.3)Ce(2)-HMOR corresponding to region highlighted in Figure F-3.

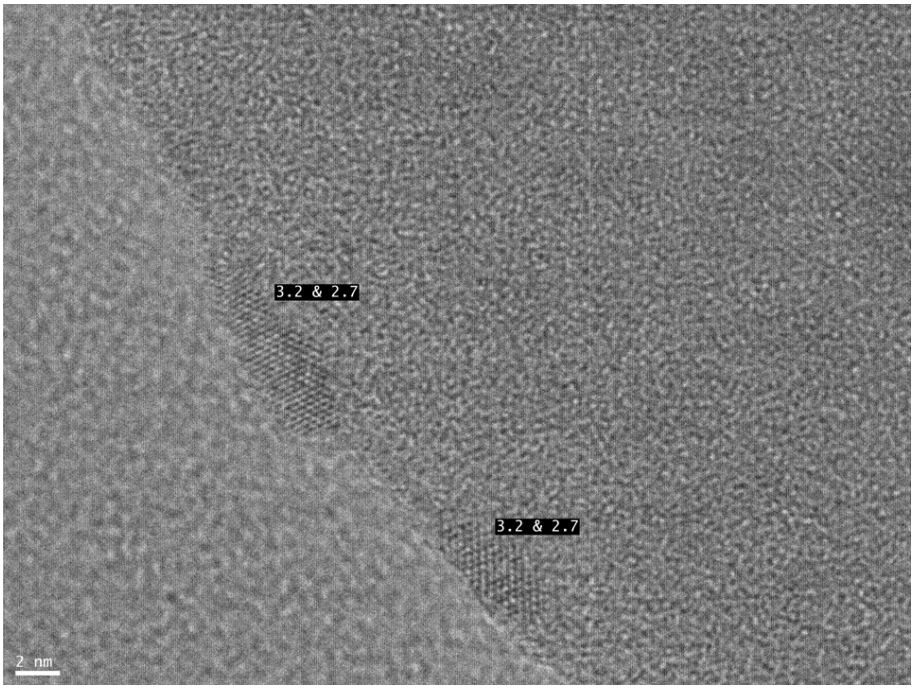

Figure F-5 – HRTEM image of Pd(0.3)Ce(2)-HMOR corresponding to the region highlighted in Figure F-3.

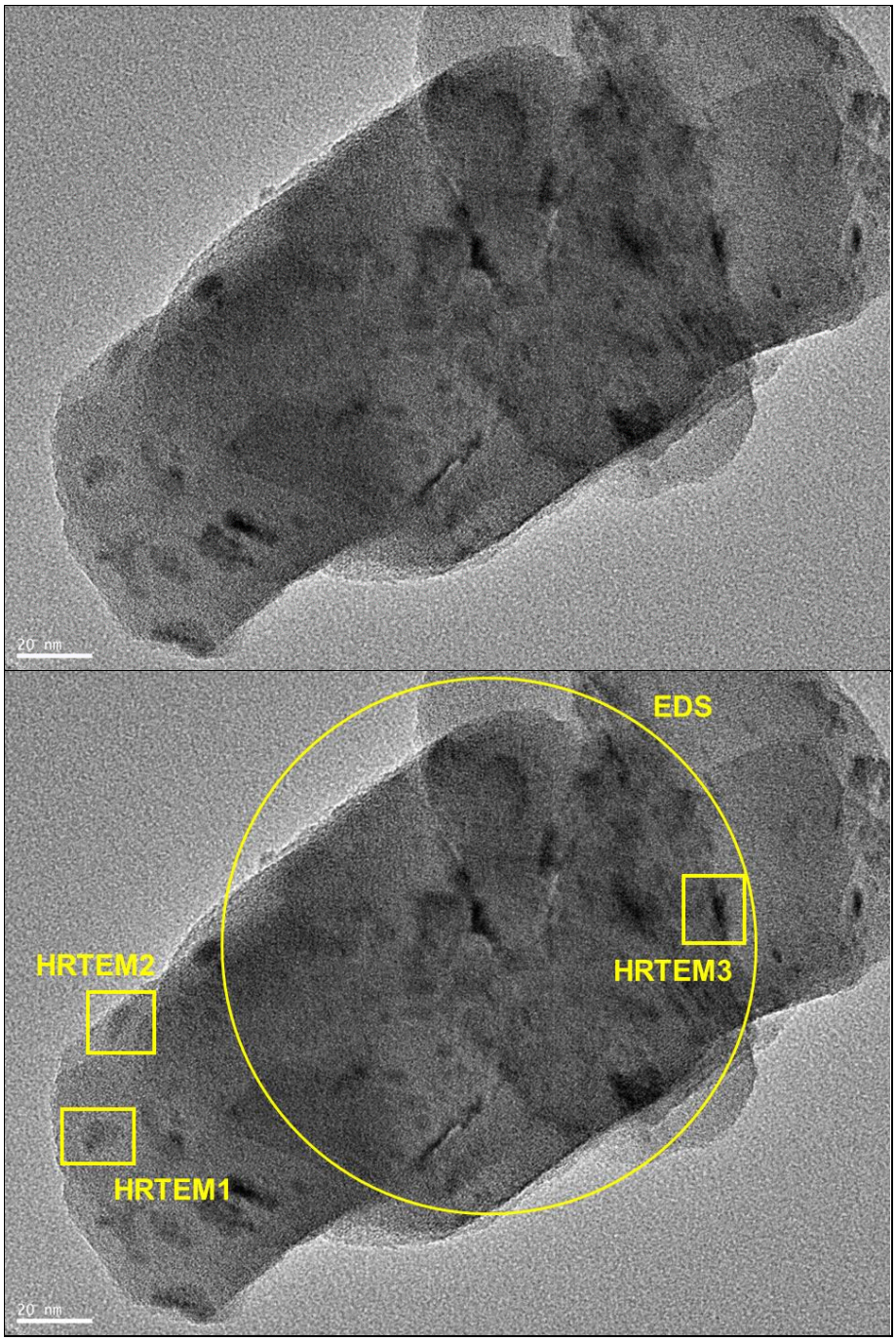

Figure F-6 – Another TEM image of Pd(0.3)Ce(2)-HMOR, highlighting the regions where EDS and HRTEM were.

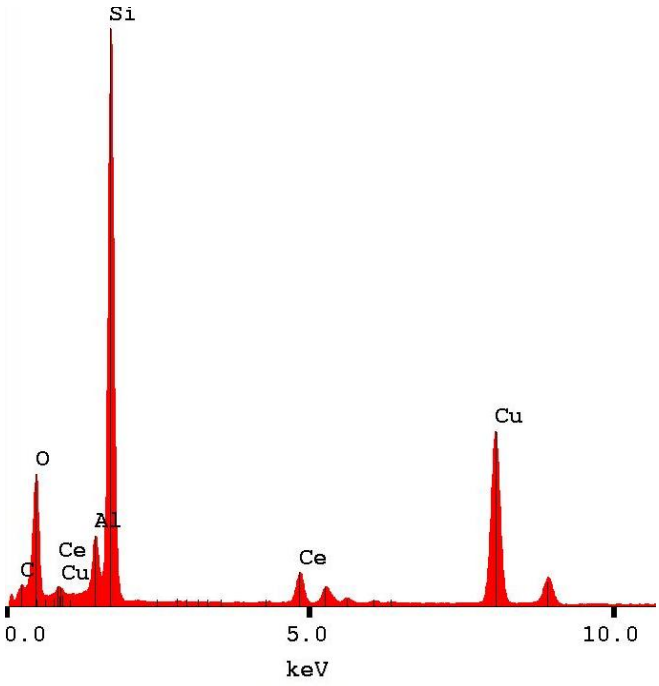

Figure F-7 – EDS spectrum of Pd(0.3)Ce(2)-HMOR corresponding to region highlighted in Figure F-6.

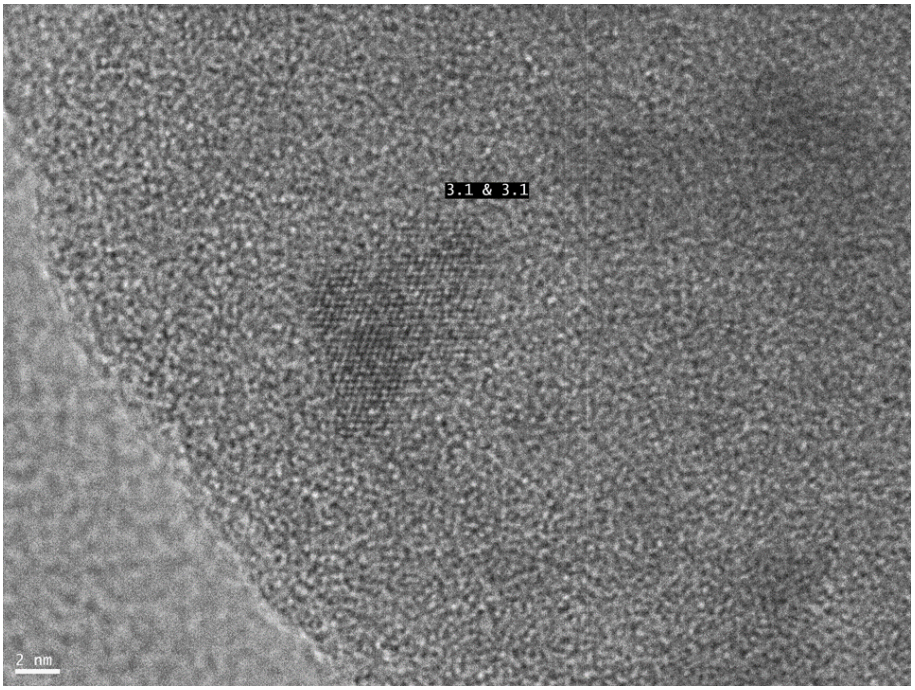

Figure F-8 – HRTEM image of Pd(0.3)Ce(2)-HMOR corresponding to the region highlighted in Figure F-6 (HRTEM1).

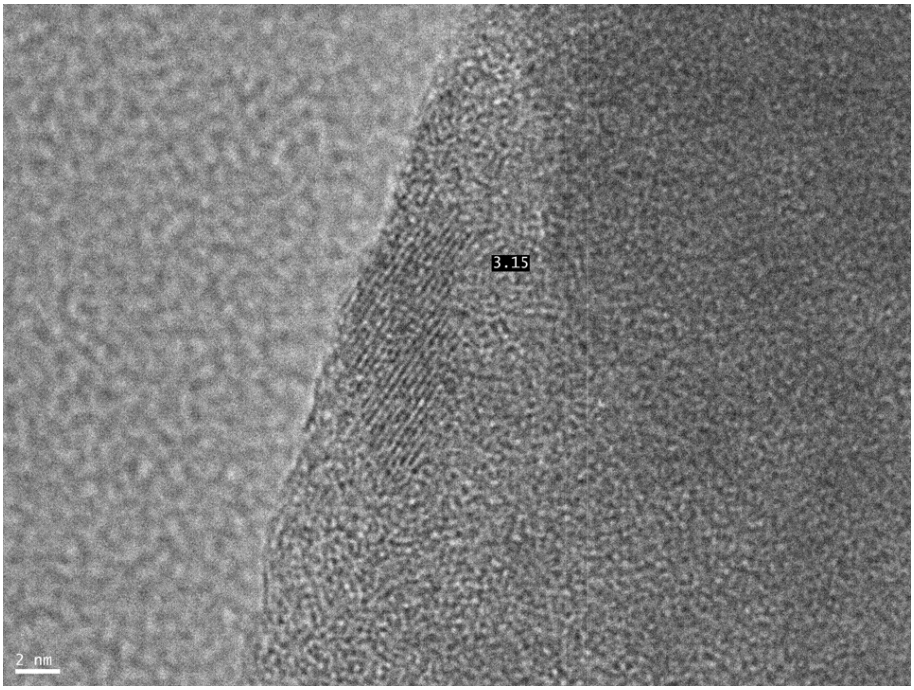

Figure F-9 – HRTEM image of Pd(0.3)Ce(2)-HMOR corresponding to the region highlighted in Figure F-6 (HRTEM2).

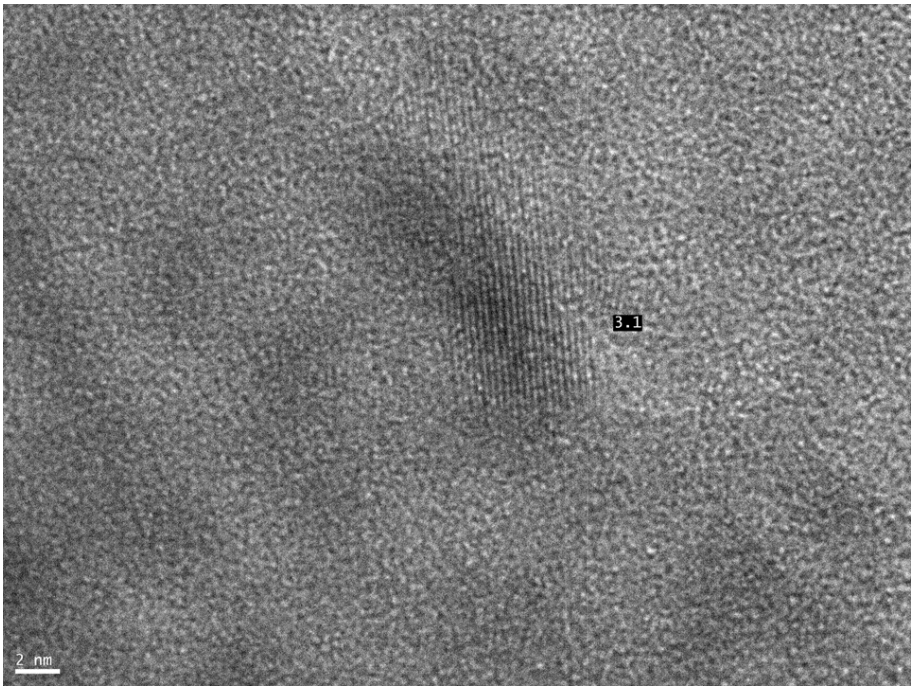

Figure F-10 – HRTEM image of Pd(0.3)Ce(2)-HMOR corresponding to the region highlighted in Figure F-6 (HRTEM3).

F.2. BEA series

F.2.1. Catalyst Pd(0.3) -HBEA

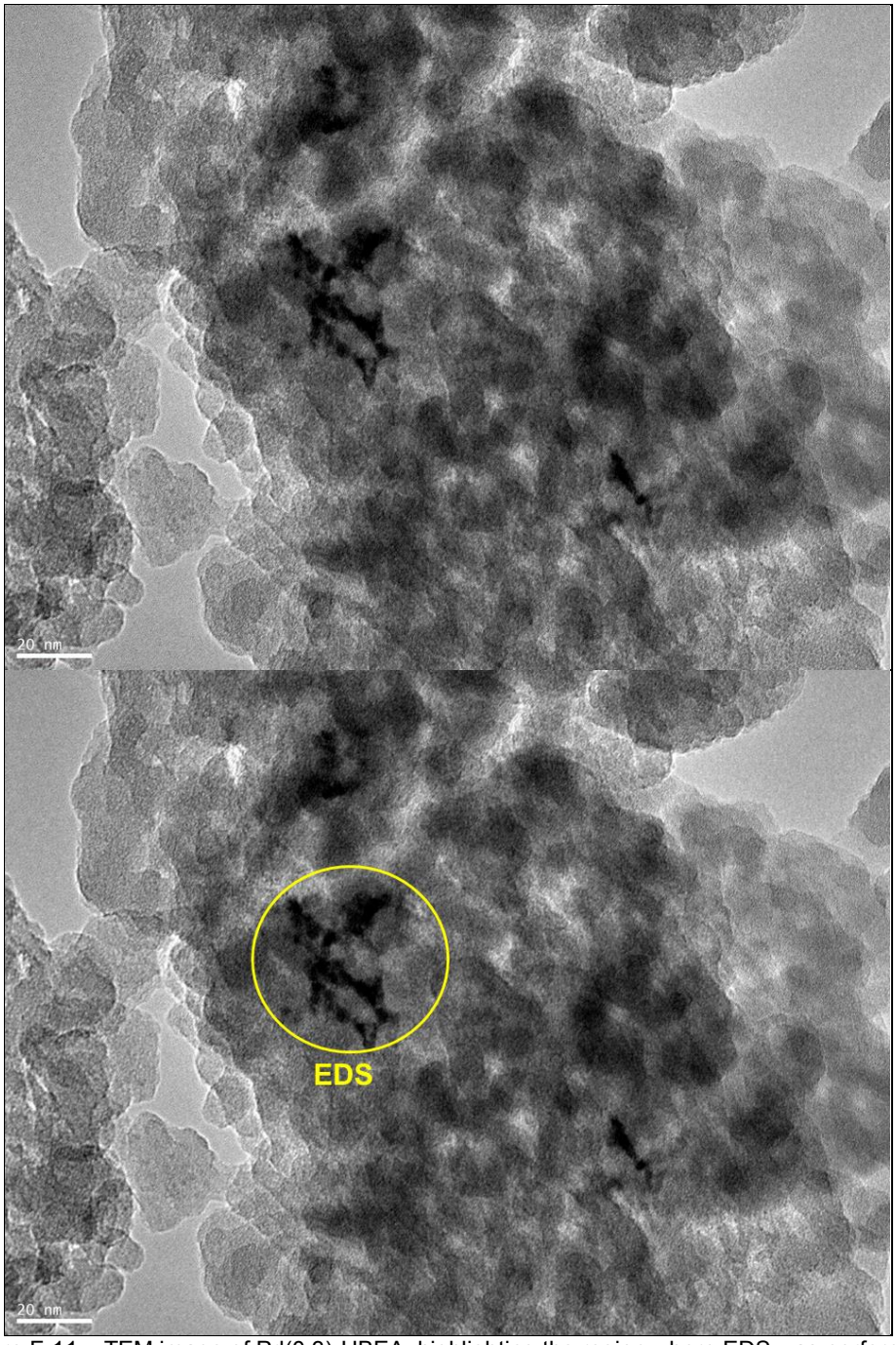

Figure F-11 – TEM image of Pd(0.3)-HBEA, highlighting the region where EDS was performed.

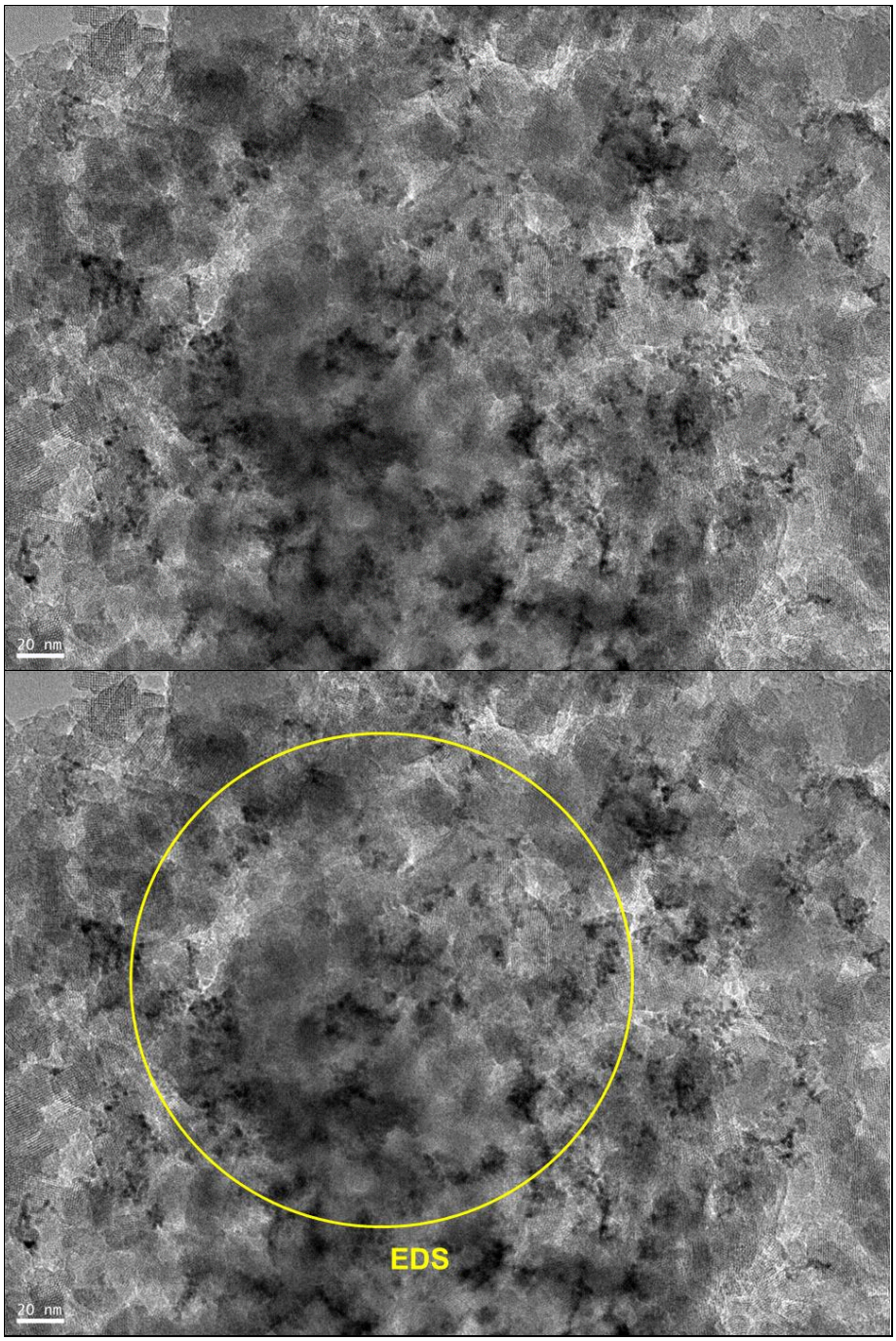

Figure F-12 – Another TEM image of Pd(0.3)-HBEA, highlighting the region where EDS was performed.

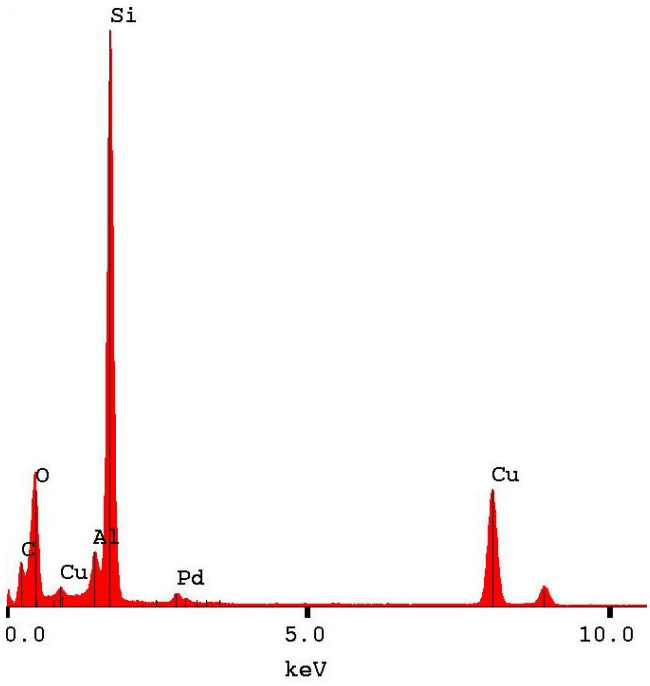

Figure F-13 – EDS spectrum of Pd(0.3)-HBEA corresponding to region highlighted in Figure F-11.

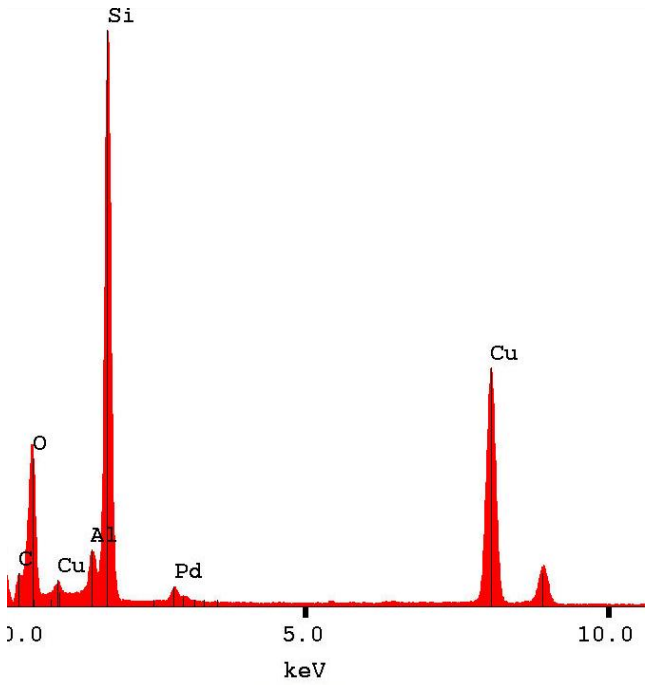

Figure F-14 – EDS spectrum of Pd(0.3)-HBEA corresponding to region highlighted in Figure F-12.

F.2.2. Catalyst Pd(0.3)Ce(2)-HBEA

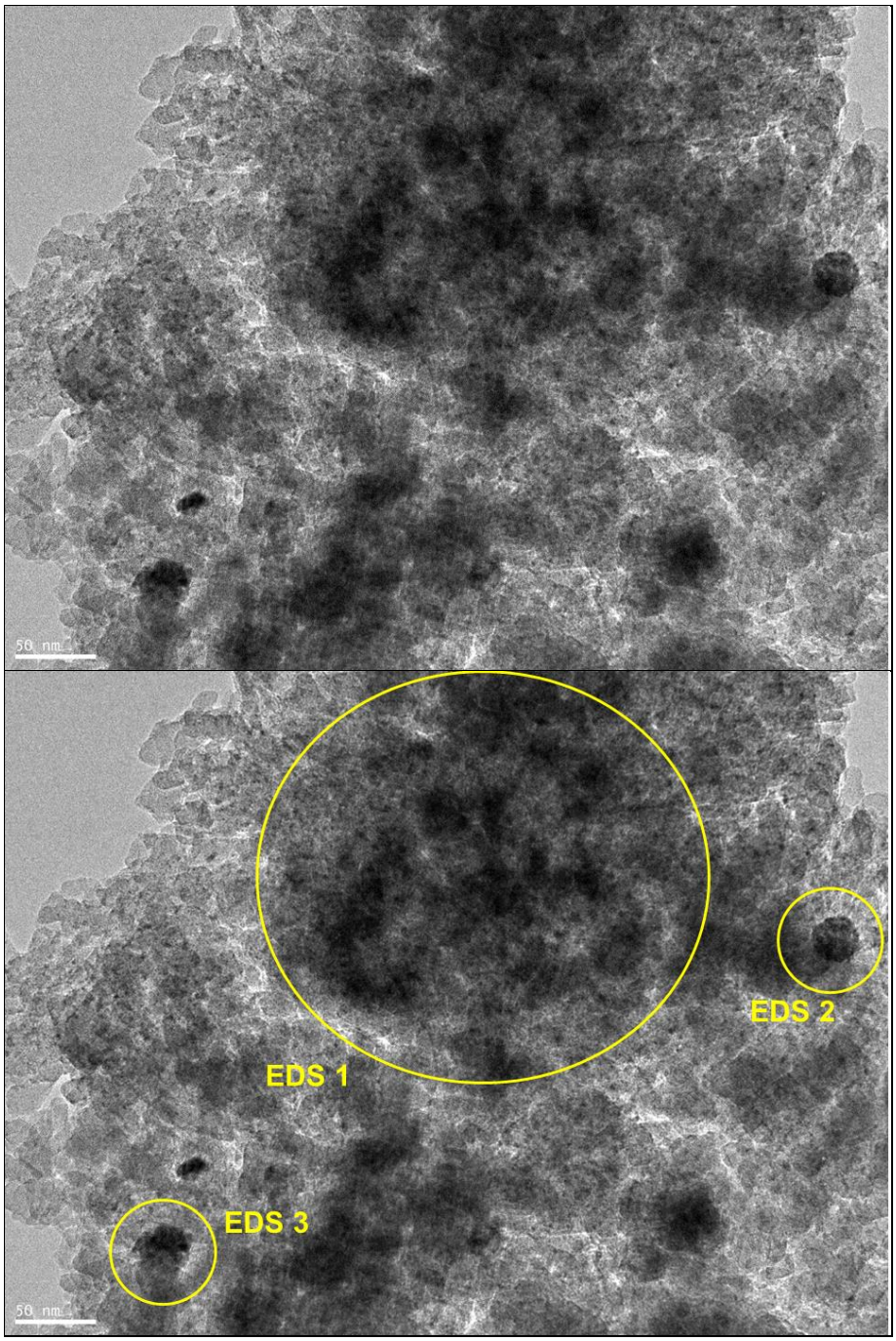

Figure F-15 – TEM image of Pd(0.3)Ce(2)-HBEA, highlighting the regions where EDS was performed.

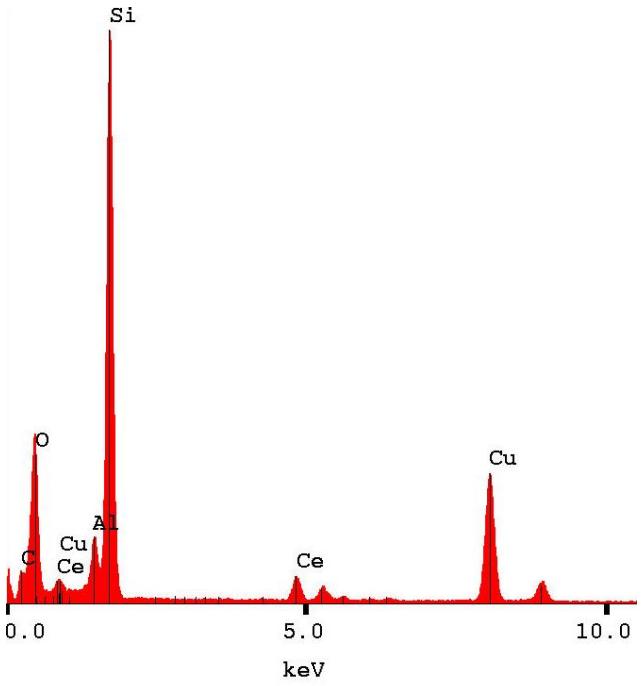

Figure F-16 – EDS spectrum of Pd(0.3)Ce(2)-HBEA corresponding to region highlighted in Figure F-15 (EDS1).

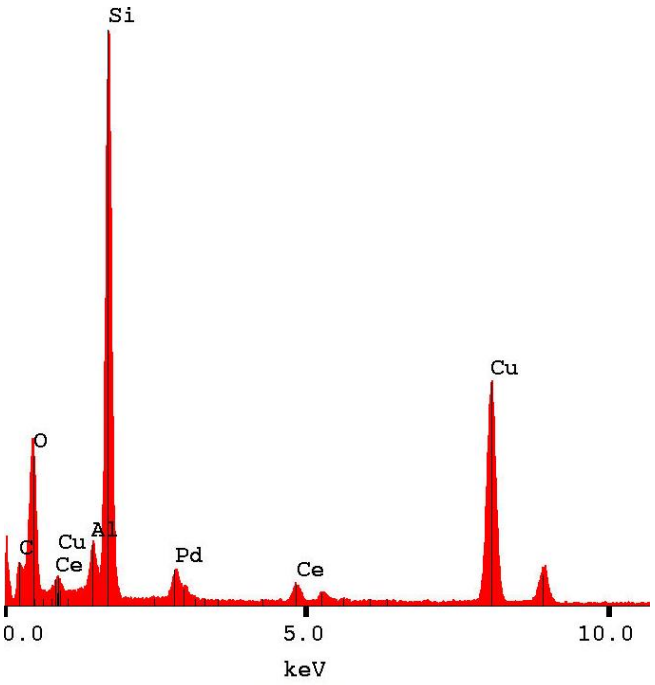

Figure F-17 – EDS spectrum of Pd(0.3)Ce(2)-HBEA corresponding to region highlighted in Figure F-15 (EDS2).

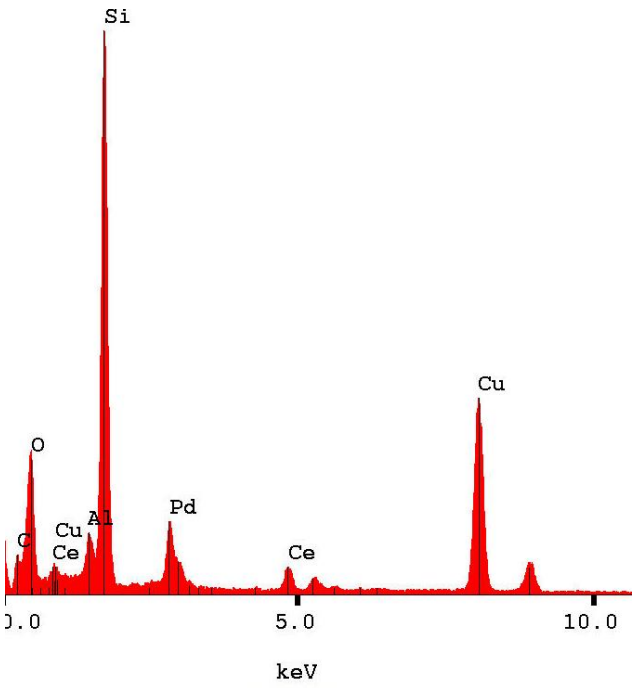

Figure F-18 – EDS spectrum of Pd(0.3)Ce(2)-HBEA corresponding to region highlighted in Figure F-15 (EDS3).

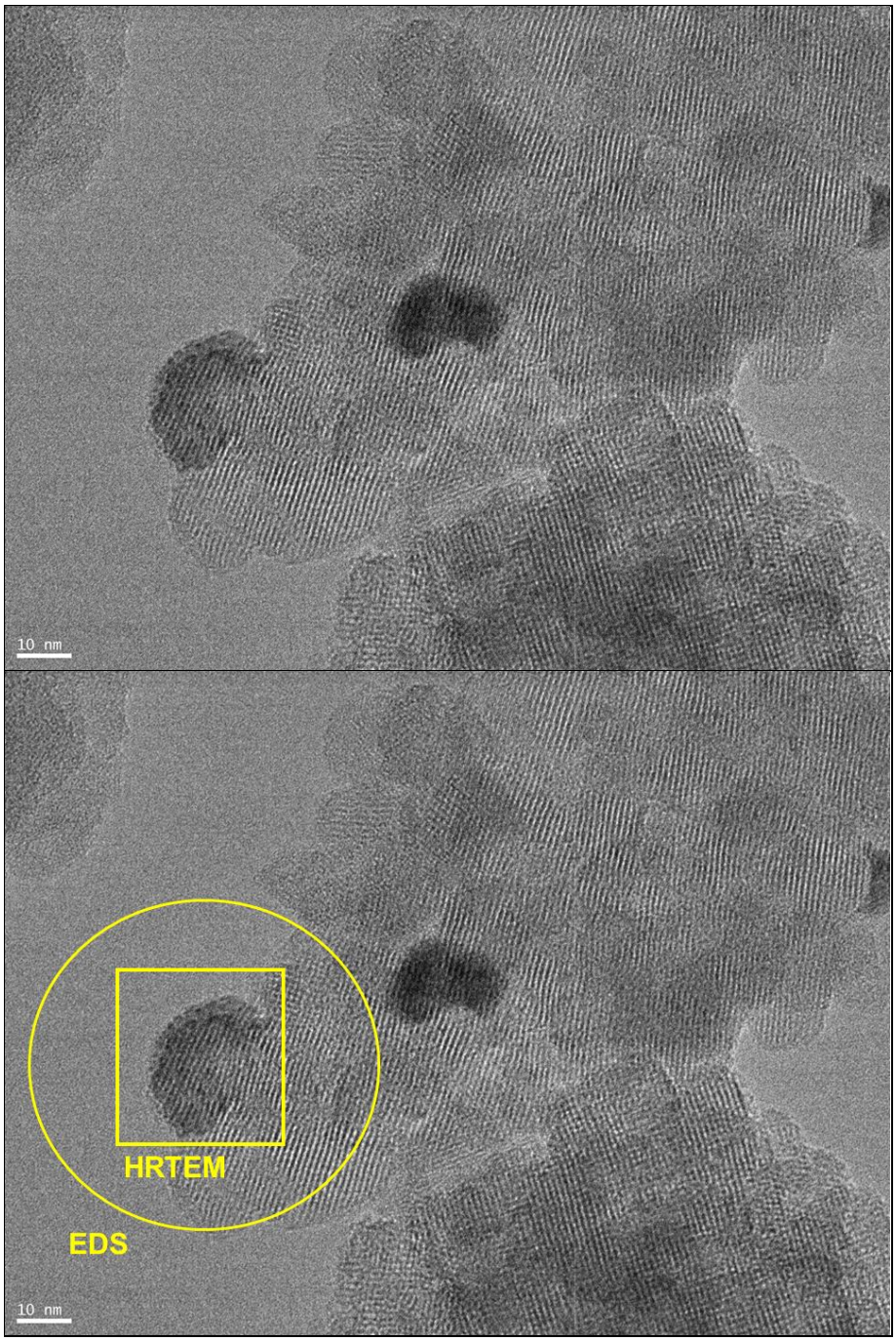

Figure F-19 – Another TEM image of Pd(0.3)Ce(2)-HBEA, highlighting the regions where EDS and HRTEM were performed.

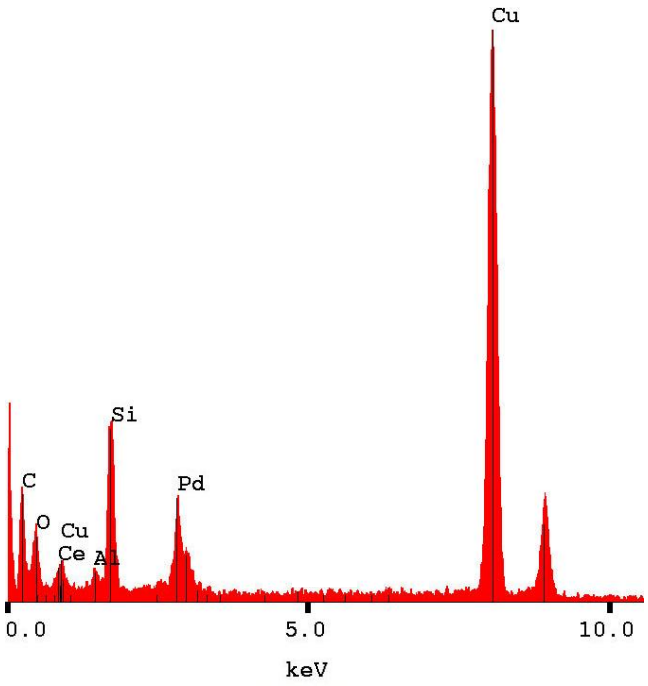

Figure F-20 – EDS spectrum of Pd(0.3)Ce(2)-HBEA corresponding to region highlighted in Figure F-19.

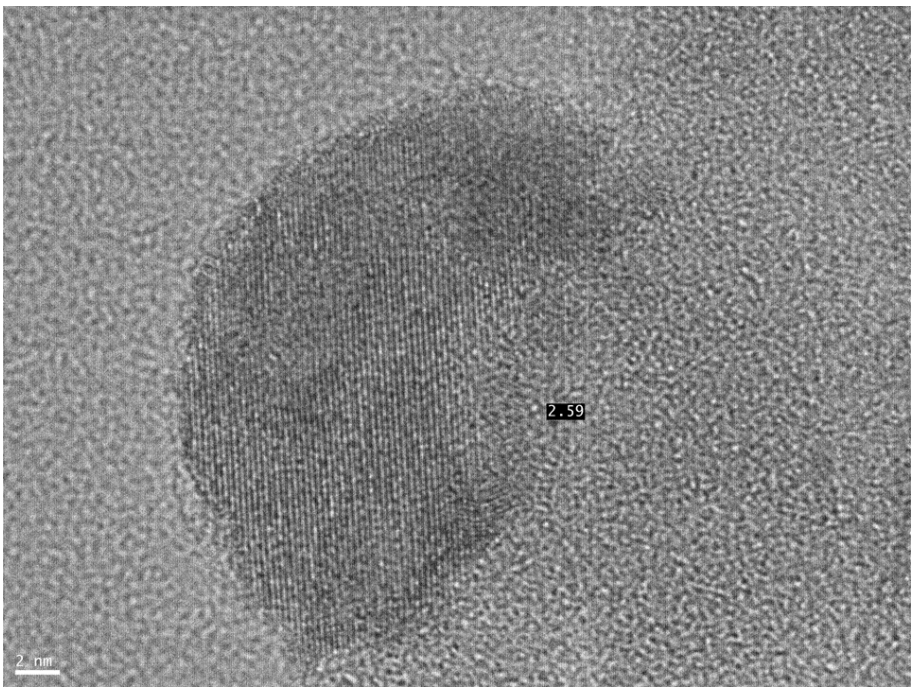

Figure F-21 – HRTEM image of Pd(0.3)Ce(2)-HBEA corresponding to the region highlighted in Figure F-19.

Annex G. Further results on scanning electron microscopy (SEM/EDS)

In this annex, further results of SEM/EDS obtained for washcoated monolith catalysts are presented.

G.1. 400 cpsi

G.1.1. st500_10-400

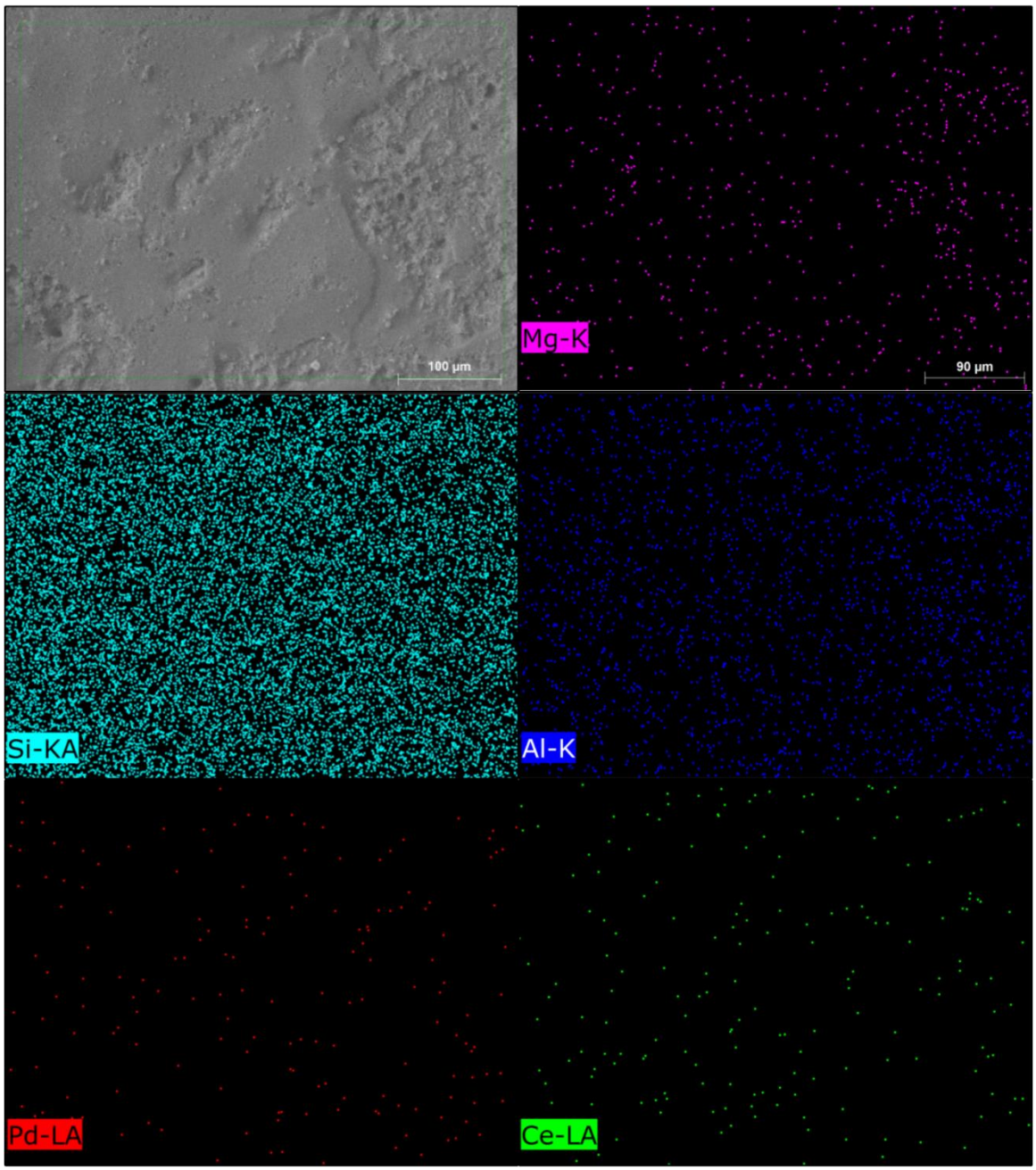

Figure G-1 – EDS mapping from a segment of catalytic layer (Figure V-17E, page 228) from washcoated monolith st500_10-400.

G.1.2. base, aged-400

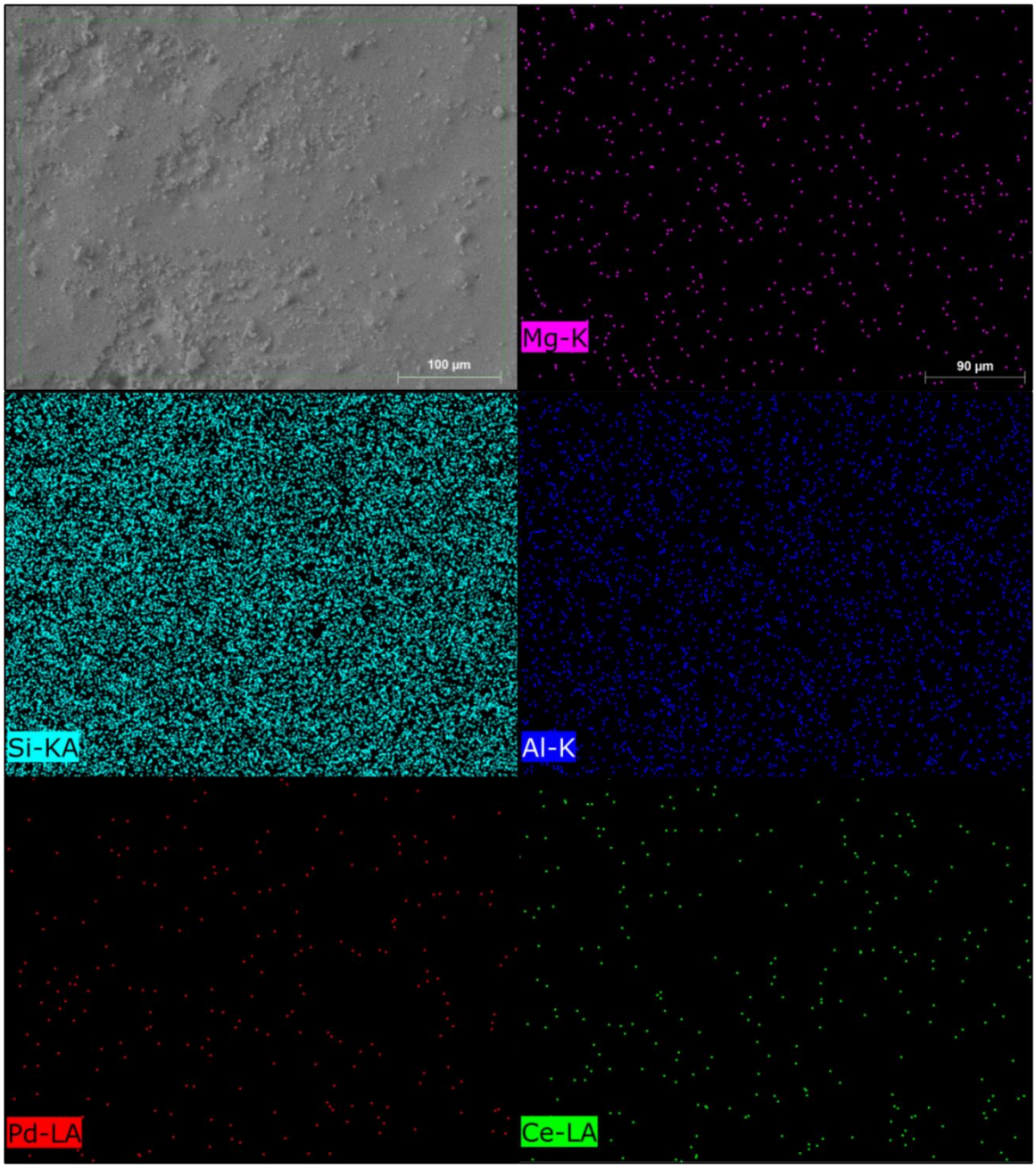

Figure G-2 – EDS mapping from a segment of catalytic layer (Figure V-17F, page 228) from washcoated monolith base, aged-400.

G.2. 600 cpsi

G.2.1. st500_10-600

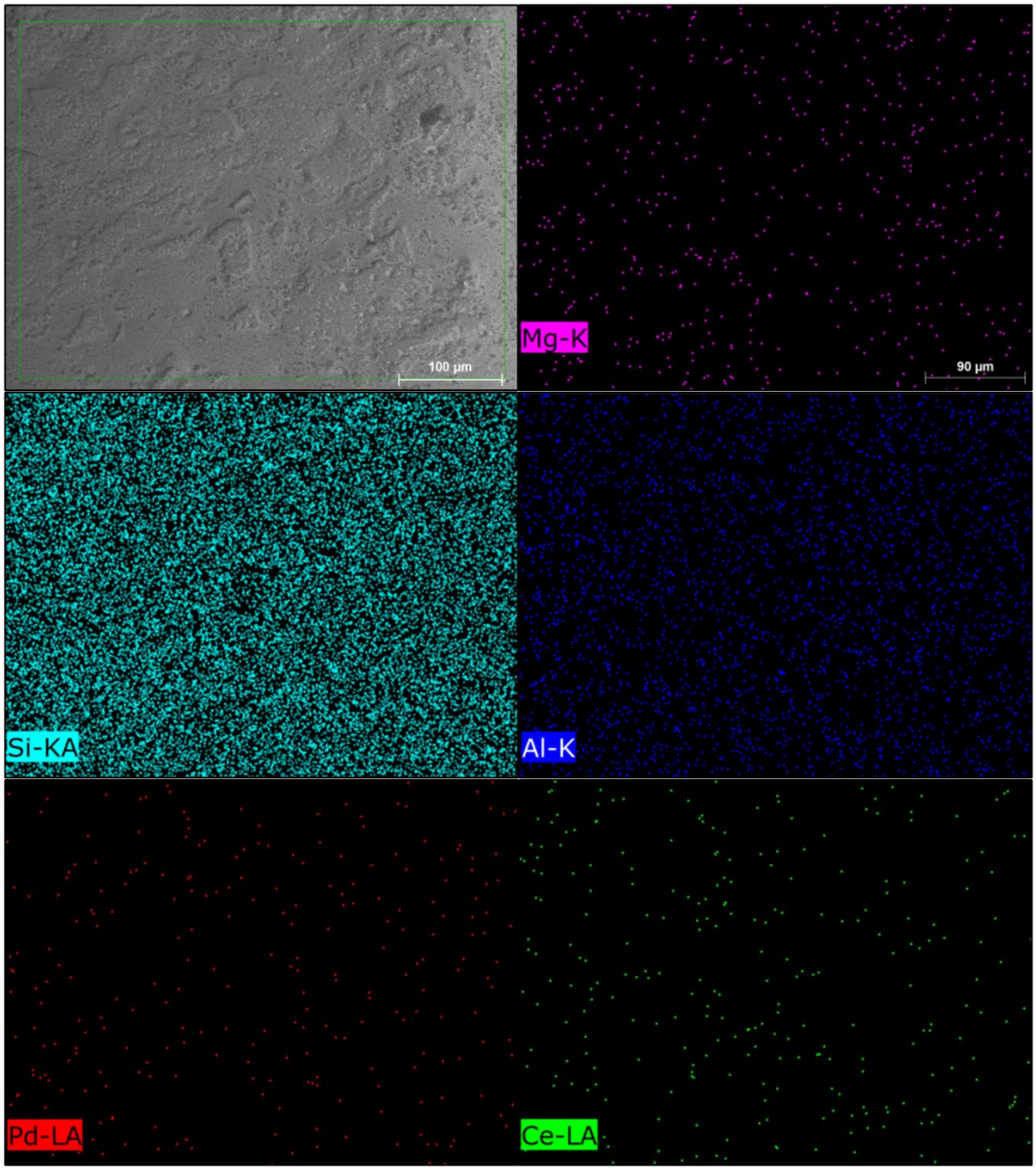

Figure G-3 – EDS mapping from a segment of catalytic layer (Figure V-20E, page 231) from washcoated monolith st500_10-600.

G.2.2. base, aged-600

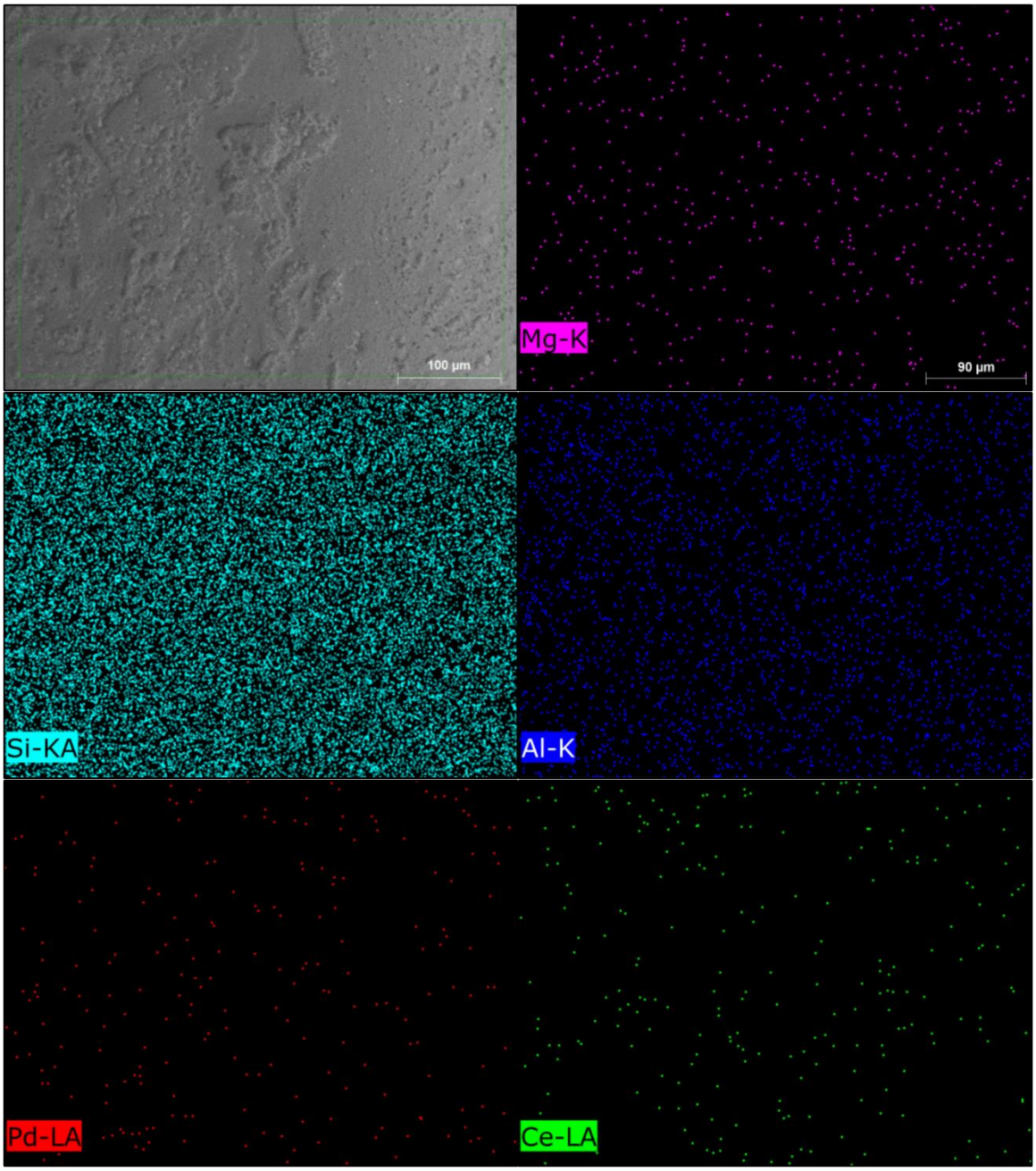

Figure G-4 – EDS mapping from a segment of catalytic layer (Figure V-20F, page 231) from washcoated monolith base, aged-600.

Annex H. Model for flow simulation inside of monolith channels

H.1. Methodology

Single channel 2D simulations, corresponding to the monoliths prepared with 400 and 600 cpsi, were performed by adopting the methodology followed by Ozhan [31] using Gerris Flow solver, a free software program for the solution of the partial deferential equations. According to the methodology proposed [31], the gas feed was assumed to be an incompressible fluid, which is an assumption widely used for the simulation of the in catalytic converters due to the fact that Mach number is smaller than 0.05, acoustic waves have a negligible impact, the variation in pressure is lower than 10% of total absolute pressure.

The implement model considers the governing equations (C-3) and (C-4) and (C-5).

$$\nabla . \mathrm{u} = 0 \tag{H-1}$$

$$\rho\left(\frac{\partial u}{\partial t} + u.\nabla.\mathrm{u}\right) = -\nabla \mathrm{p} + \mu\nabla^2\mathrm{u} + \mathrm{S} \tag{H-2}$$

t is the time, u is the velocity, ρ is the fluid density p is the pressure, μ is the viscosity and S is the momentum source term.

Additionally, *N*-1 transport equations, where *N* is the number of components present in the system were also consider (equation (C-5)).

$$\frac{\partial C_i}{\partial t} = \nabla . (\mathrm{D}\nabla \mathrm{c}_i) - \nabla . (\mathrm{uc}_i) + R_i \tag{H-3}$$

c_i is the concentration of component i, D is the diffusion coefficient and R_i is the reaction rate.

These three equations are solved by imposing proper boundary conditions. In the inlet, velocity is assumed to be known and, at the outlet, classical outflow boundary conditions are applied (Dirichlet boundary condition for pressure and Neumann boundary condition for the normal velocity). At the walls, the velocity is imposed to be zero.

The conversion process in catalytic converters is a heterogeneous reaction where the transformation of hazardous exhaust gases occurs at the monolith catalytic walls. This leads to a concentration gradient near the wall, which requires a high resolution in this region, increasing the computational cost. One of the interesting characteristic of the solver is the capability to perform dynamic Adaptive Mesh Refinement (AMR) using quadtree meshes. Hence, this method was applied in order to well capture concentration boundary layer near the catalytic walls, by decreasing the computational cost. The accuracy and efficiency of the code and the AMR solution has demonstrated by Ozhan [31].

H.2. Input data considered in the simulations

The data representing the simulation scenarios considered in Chapter V (Table V-5 and Table V-6) was use in order to obtain the non-dimensional variables that are, indeed, the input data considered for the simulations performed. These values are presented in Table C-2

Table H-1 – Gas feed properties input data considered for the simulation of hydrodynamic flow in base-400 and base-600 monoliths.

	400 cpsi	600 cpsi
$\frac{\bar{u}}{u_c}$	1.0	1.0
$\frac{\nu}{u_c l_c}$	0.058	0.076
$\frac{D_{NO}}{u_c l_c}$	0.088	0.116
$\frac{D_{CH_4}}{u_c l_c}$	0.089	0.118
x_{NO}	0.0004	0.0004
x_{CH_4}	0.0016	0.0016

$\bar{u}$ is the uniform velocity profile imposed at the inlet of the channel, u_c is the characteristic velocity of the problem (chosen to be the average velocity in the channel), l_c is the characteristic length of the problem (chosen to be the length of the channel), ν kinematic viscosity of the gas, D_{NO} is the molecular diffusivity of NO in the gas, D_{CH_4} is the molecular diffusivity of CH_4 in the gas, x_{NO} is the molar fraction of NO in the gas and $x_{CH_4}$is the molar fraction of CH_4 in the gas.

References from annexes

[1] European Patent Office, website, Espacenet, http://worldwide.espacenet.com/?locale=en_EP, accessed in 22/06/2015.

[2] C.M. de Correa, F. Córdoba C, F. Bustamante L, in: F.V.M.S.M. Avelino Corma, G.F. José Luis (Eds.) Stud. Surf. Sci. Catal., Elsevier, 2000, 130, 1469-1474.

[3] F. Bustamante, F. Cordoba, M. Yates, C.M. de Correa, Appl. Catal., A, 234 (2002) 127-136.

[4] J.A.Z. Pieterse, R.W. van den Brink, S. Booneveld, F.A. de Bruijn, Appl. Catal., B, 46 (2003) 239-250.

[5] J.A.Z. Pieterse, R.W. van den Brink, S. Booneveld, F.A. de Bruijn, in: E. VanSteen, M. Claeys, L.H. Callanan (Eds.) Recent Advances in the Science and Technology of Zeolites and Related Materials, 2004, pp. 2522-2526.

[6] J.A.Z. Pieterse, H. Top, F. Vollink, K. Hoving, R.W. van den Brink, Chem. Eng. J., 120 (2006) 17-23.

[7] F. Lonyi, H.E. Solt, J. Valyon, H. Decolatti, L.B. Gutierrez, E. Miro, Appl. Catal., B, 100 (2010) 133-142.

[8] I.O. Costilla, M.D. Sanchez, M. Alicia Volpe, C.E. Gigola, Catal. Today, 172 (2011) 84-89.

[9] H. Decolatti, H. Solt, F. Lonyi, J. Valyon, E. Miro, L. Gutierrez, Catal. Today, 172 (2011) 124-131.

[10] R. Serra, M.J. Vecchietti, E. Miro, A. Boix, Catal. Today, 133 (2008) 480-486.

[11] L. Gutierrez, A. Boix, J.O. Petunchi, J. Catal., 179 (1998) 179-191.

[12] L. Gutierrez, E.A. Lombardo, Appl. Catal., A, 360 (2009) 107-119.

[13] J.A.Z. Pieterse, R.W. van den Brink, S. Booneveld, F.A. de Bruijn, Appl. Catal., B, 39 (2002) 167-179.

[14] M. Ogura, Y. Sugiura, M. Hayashi, E. Kikuchi, Catal. Lett., 42 (1996) 185-189.

[15] M. Ogura, M. Hayashi, E. Kikuchi, Catal. Today, 42 (1998) 159-166.

[16] X.D. Wang, T. Zhang, X.Y. Sun, W. Guan, D.B. Liang, L.W. Lin, Appl. Catal., B, 24 (2000) 169-173.

[17] H. Berndt, F.W. Schutze, M. Richter, T. Sowade, W. Grunert, Appl. Catal., B, 40 (2003) 51-67.

[18] T. Sowade, T. Liese, C. Schmidt, F.W. Schutze, X. Yu, H. Berndt, W. Grunert, J. Catal., 225 (2004) 105-115.

[19] F. Lonyi, H.E. Solt, J. Valyon, A. Boix, L.B. Gutierrez, J. Mol. Catal. A: Chem., 345 (2011) 75-80.

[20] L.L. Ren, T. Zhang, D.B. Liang, C.H. Xu, J.W. Tang, L.W. Lin, Appl. Catal., B, 35 (2002) 317-321.

[21] X. Chen, A. Zhu, C.T. Au, C. Shi, Catal. Lett., 141 (2011) 207-212.

[22] Z.J. Li, M. Flytzani-Stephanopoulos, Appl. Catal., A, 165 (1997) 15-34.

[23] A.P. Ferreira, S. Capela, P. Da Costa, C. Henriques, M.F. Ribeiro, F.R. Ribeiro, Catal. Today, 119 (2007) 156-165.

[24] J.M. Ramallo-Lopez, F.G. Requejo, L.B. Gutierrez, E.E. Miro, Appl. Catal., B, 29 (2001) 35-46.

[25] A. Kubacka, J. Janas, B. Sulikowski, Appl. Catal., B, 69 (2006) 43-48.

[26] P. Ciambelli, D. Sannino, E. Palo, A. Ruggiero, Top. Catal., 42-43 (2007) 177-181.

[27] A.P. Ferreira, C. Henriques, M.F. Ribeiro, F.R. Ribeiro, Catal. Today, 107–108 (2005) 181-191.

[28] A. Rodrigues, P. da Costa, C. Methivier, S. Dzwigaj, Catal. Today, 176 (2011) 72-76.

[29] G. Leofanti, M. Padovan, G. Tozzola, B. Venturelli, Catal. Today, 41 (1998) 207-219.

[30] T. Sowade, E.W. Schutze, H. Berndt, W. Grunert, Chem. Eng. Technol., 27 (2004) 1277-1289.

[31] C. Ozhan, Multi-scale simulation of automotive catalytic converters, PhD Thesis, Université Pierre et Marie Curie - Paris VI, Paris, 2014.